The Design Modelling of PEEK Composite for Bone Implants

Submitted by

Bankole Ibrahim Oladapo

(P17243433)

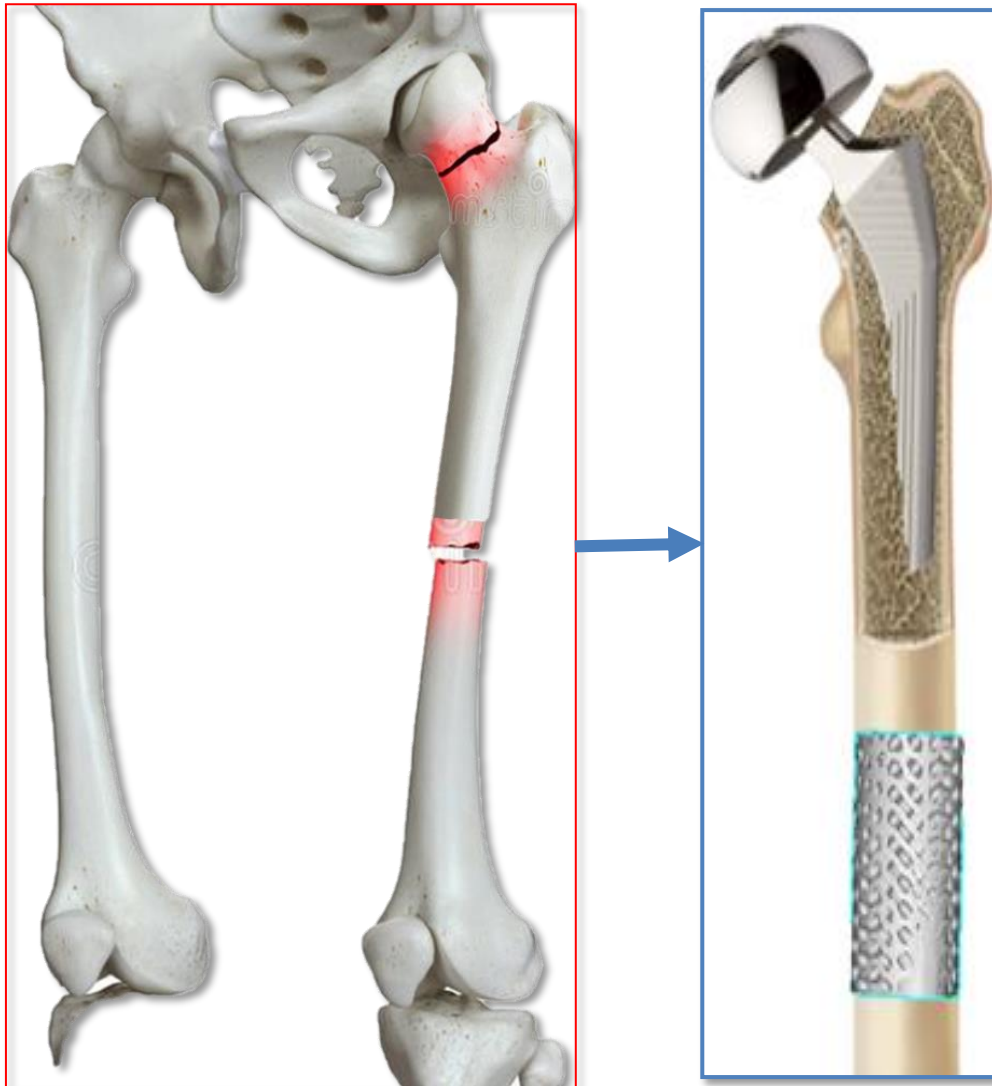For the award of the degree of

Doctor of Philosophy

School of Engineering and Sustainable Development

De Montfort University, Leicester, United Kingdom

Supervisors: Dr S. Abolfazl Zahedi

Dr Seng Chong

September 2022

Novel Design Modelling of Hip Bone and Femur Implants

Dedicate to every helper of My Life.

Acknowledgements

First and foremost, I thank God, the Almighty, for giving me the strength and patience to carry on this project and blessing me with many great people who have been my most significant personal and professional life.

My sincere gratitude and appreciations go to my supervisor, **Dr S. Abolfazl Zahedi**, for giving me the honour of working with him and for his unwavering support, encouragement, and guidance throughout my work. I am grateful to Dr Seng Chong for his help and support. Thank you, Dr Sikiru O. Ismail of the University of Hertfordshire, for your continued mentoring, support and distance supervisor; thank you for allowing God to use you for the success of this thesis.

Big thank you to my lovely wife, Kemi Oladapo, for your support and my two beautiful daughters, Wealth and Olivia.

Thanks to all my friends and Family

Author Declaration

I declare that, except where explicit reference is made to the contribution of others, this thesis is the result of my work and has not been submitted for any other degree at the De Montfort University, Leicester, UK, or any other institution.

Bankole I Oladapo

Table Contents

List of Tables

List of Figure

Abstract

This research study shows the enhancing biocompatibility and structural integrity of Hip and Femur Implants through PEEK Composite and FDM Techniques. Examines using polyether-ether-ketone (PEEK) materials for improved bone implantation. While PEEK materials offer benefits such as non-toxicity, high strength, and toughness, they often fall short in replicating natural bone strength and biological properties. Addressing these limitations, this study presents the development and application of functional PEEK composites in designing and manufacturing hip and femur bone implants that closely emulate natural bone structures. By adopting fused deposition modelling (FDM) techniques, and have developed porous hip and femur bone implants with homogenization lattice structures. The PEEK was enhanced through extrusion, spraying and coating deposition methods, incorporating biocomposites like calcium hydroxyapatite (cHAp)/reduced graphene oxide (rGO) to boost the material's performance. This novel approach also involves creating a novel lattice structure to mimic the bone structure within the composite for a more realistic bone implant. The research encompasses extensive testing, including compressive and tensile tests on PEEK and its composites, comparing these with simulated outcomes. The implants, comprising varying composite aggregates (up to 30% weight), were 3D-printed and assessed using scanning electron microscopy (SEM) and energy-dispersive X-ray spectroscopy (EDXS). The biocompatibility of these PEEK composites was verified through in-vitro cell cytotoxicity experiments, revealing a marked improvement in cell adhesion and overall properties. The cells produced PEEK composites quicker than pure PEEK materials was observed. Adding cHAp and rGO significantly boosted the material's mechanical strengths to match those of a hip bone. The elastic modulus, anisotropy, and cell properties were also investigated, resulting in a PEEK-hydroxyapatite (HAp) composite with micropores and nanostructures, promoting bioactivity, controlled configuration distribution, and cell growth. In conclusion, this thesis not only elucidates the potential of PEEK composites in facilitating hip and femur bone implantation but also paves the way for developing more biocompatible materials. This will undeniably benefit hip and femur implantation's scientific and industries.

Keywords: Bone implant; PEEK; cHAp; Biocompatible; Hip implant; rGO; Bioactivity;

List of Abbreviations

3D	Three dimensional
AM	Additive manufacturing
AR	Aspect Ratio
BCCO	Body Centre Cubbic Octahedron
BMD	Bone mineral density
CAD	Computer-Aided Design
CFR-PEEK	Carbon-fiber reinforced polyetheretherketone
Cr_2O_3	Chromium (III) oxyhydroxide
DMA	Dynamic Mechanical Analysis
DMEM	Dulbecco's modified eagle's medium
DSC	Differential Scanning Calorimetry
E	Young's modulus
E_c	Modulus of the composite
EDXS	Dispersive X-ray spectroscopy
ED	Energy Density
FCCO	Face Center Cubic Octahedron,
FDM	Fused deposition modelling
FEA	Finite Element Analysis
HAp	Hydroxyapatite
cHAp	Calcium Hydroxyapatite
HT	High Temperature

HT-LS	High-Temperature Laser Sintering
LS	Laser Sintering
MSC	Mesenchymal stem cells
NAS	Nutrient Agar solution
NiTi	Nickel-titanium
OCC	Octahedron-cross cell,
OCP	Octacalcium phosphates
P	Applied pressure
PA	Polyamide
PAEK	Poly Aryl Ether Ketone
PBS	Phosphate-buffered saline
PCL	Polycaprolactone
PE	Poly(ethylene)
PEEK	Poly Ether Ether Ketone
PEK	Poly Ether Ketone
PLA	Polylactic acid
PMMA	Poly(methyl methacrylate)
SBF	Simulated body fluid
rGO	Reduced Graphene oxide
SEM	Scanning Electron Microscopy
STL	Standard Tessellation Language
TGA	Thermo-Gravimetrical Analysis

TCP   Tricalcium phosphate

TOC   Truncated octahedron Cell,

UHMWPE   Ultra-high molecular weight polyethene

List of Symbols

The mainly used symbols and abbreviations used in the thesis are listed below.

E   Young's Modulus (MPa or GPa)

ρ Density (g/cm^3)

$\Delta\rho$ Change in apparent density of bone (g/cm^3)

A (ρ)   Internal free surface area

a (ρ)   Internal free surface area per unit volume

Wt%   Weight percentage

ε Strain

σ Stress

υ Piosson Ratio

Chapter 1
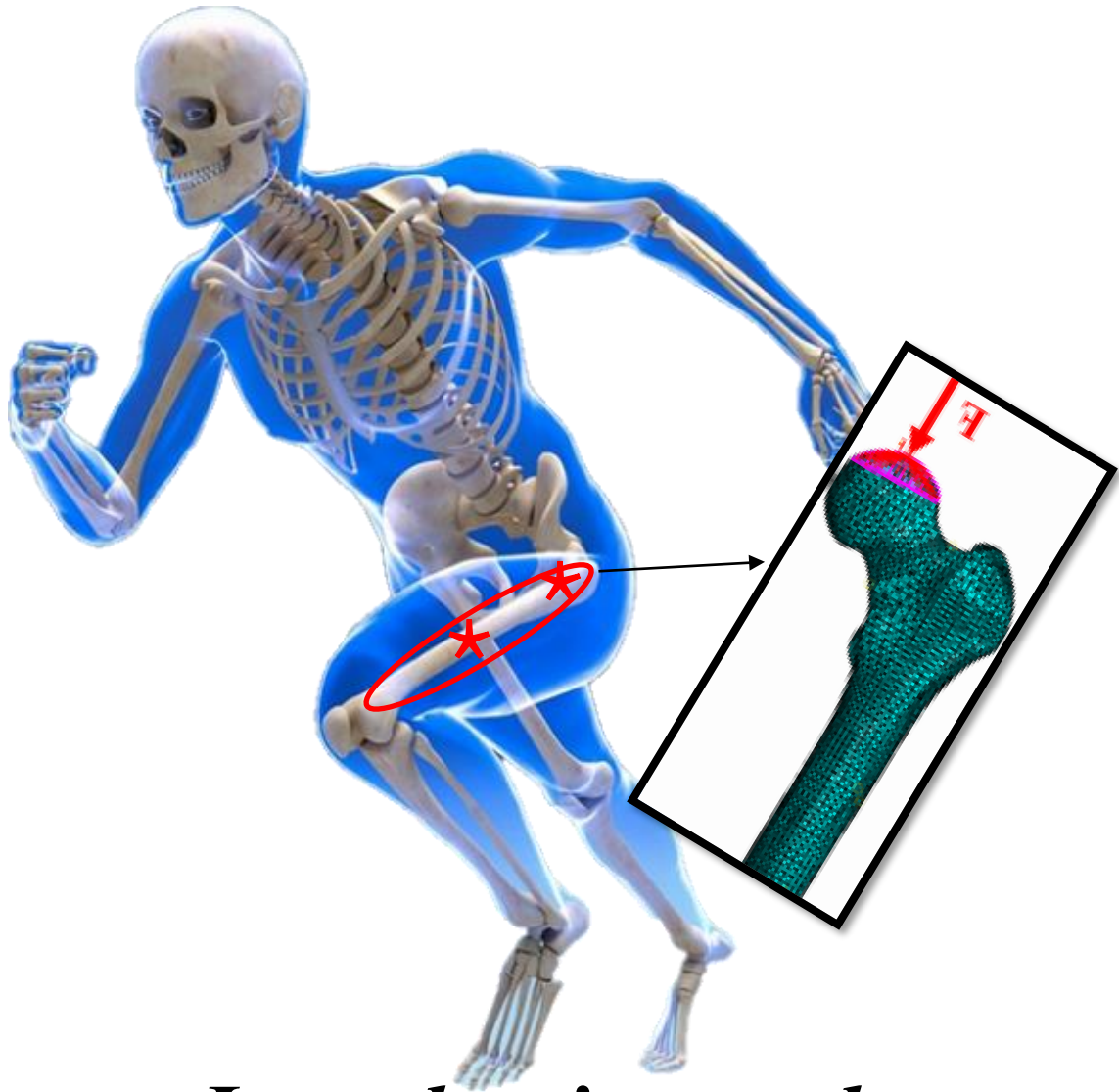
Introduction and background of PEEK composite bone implant

CHAPTER ONE

1.0.   INTRODUCTION

1.1.   Background to the research

This chapter presents the research background of designing and fabricating hip and femur medical implants. The significance of the study, the key goals and objectives, the extent of the research, the importance (justification), the repercussions, the knowledge additions (research innovation), and the form of a condensed thesis are all covered. It is well acknowledged that 3D printing and additive manufacturing (AM) is transforming industrial processes. There are many challenges in AM competing with specific established traditional techniques, which are still considered sluggish. 3D printing for mass production requires time, rendering it unsuitable for many industries [1,2]. However, the medical sector is very interested in this implant technology since it may develop customised treatments for each patient. Physicians use about 7.5 billion distinct morphologies for medical 3D printing of bone, thus becoming a viable option for creating a custom-made implant to suit patient requirements [3]. According to Allied industry research, the medical 3D printing market will reach about $17 billion in 2020 [4]. The possibilities of increasing the medical industry market can be attributed to 3D printing technology customisation capabilities. Additive Manufacturing of prostheses and implants that improve surgical outcomes or medical devices that simplify delicate transactions, such as surgical guides or other visual aids [4,5].

Technological and health advancements have enhanced people's quality of life by extending the average life expectancy to 69.8 years. Millions of people worldwide are plagued by degenerative and inflammatory diseases of the bones and joints caused by it [5]. These issues cause over half of all chronic illnesses affecting persons over 50 in developed countries. Europe's senior population (over 65) has risen in the last decade [6]. According to official estimates, the elderly will account for about 26% of the population in 2030, increasing to 29% in 2060 [7]. Between 2015 and 2060, the number of individuals over 80 will double, from 614,000 to 1,421,000 [8,9]. These findings are concerning because, in addition to the problems mentioned previously, this age group has

a high prevalence of bone fractures, low back pain, and other musculoskeletal problems that require resolution with permanent, temporary, or biodegradable biomaterials.

Orthopaedics aims to implant biomaterials into the human body to fulfil biological tasks. Additionally, when required, it entails replacing or mending various tissues, such as bone and cartilage, directing bone healing, as shown in Figure 1.1. There are presently critical orthopaedic needs for bone replacement, joint repair, and regeneration. Immense biomaterials have been improved over the last 60 years, with three distinct generations emerging. The first generation encompasses materials used in wood and metal for bone repair and support. Titanium and other alloys are used in the second generation of implant materials with selective laser melting (SLM) production. Materials designed to elicit specific biological reactions at the molecular level are now in their third generation [10,11]. These groups must be understood conceptually since each reflects a development in the needs and characteristics of the materials. Figure 1.1 shows that around 1.2 million wheelchair users in the UK are due to bone defects. Two-thirds of them are regular users. Approximately 160,000 total hip and knee replacement procedures are performed in England and Wales yearly. Hip and knee replacements are performed in over 400 facilities. The market for orthopaedic implants is expected to grow by $10.09 billion between 2021 and 2025, according to [12,13]. This result implies that research and development efforts focus on first or second-generation biomaterials based on their characteristics. New-generation materials do not always necessitate abolishing those already in use.

Proportion population using mobility device
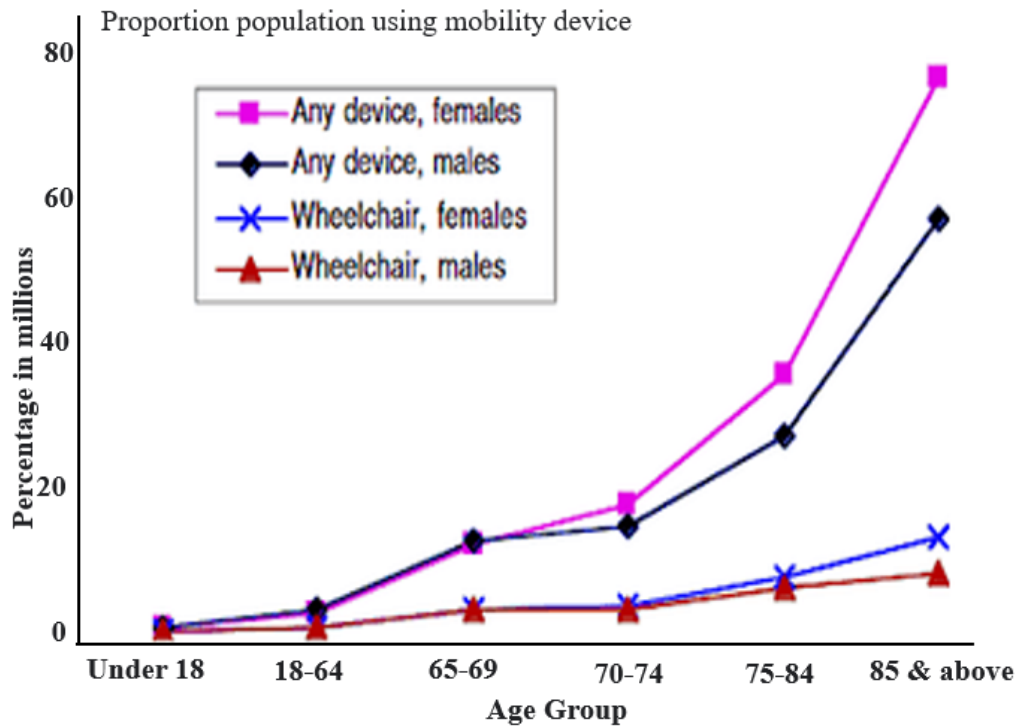
Figure 1.1 Background and motivation-problem in a bone defect brings about this research on bone defects and the proportion of the population using mobility and device [14, 15].

Furthermore, because the human body is very corrosive, prospective materials are subjected to stringent requirements. As a result, the first generation of biomaterials was made from readily available industrial materials that were required to be as inert as possible to prevent corrosion and the release of ions and particles after implantation. Mechanical characteristics are also critical in determining whether materials are suitable for implant production. Another urgent need is the notion of biocompatibility when coupled with standardised *in-vitro* and *in-vivo* testing, which enables the assessment of synthetic materials' biological behaviour. The sole criterion for synthetic materials was a good mix of physical characteristics corresponding to the restored tissue while eliciting a minimum harmful reaction from the host. Due to their static nature, these were classified as first-generation biomaterials [15,16].

The second generation of biomaterials was introduced between 1980 and 2000. It was distinguished by developing bioactive materials capable of interacting with biological systems. This result enhances biological responsiveness and tissue connection while also increasing the ability of bioabsorbable materials to degrade gradually. Materials' contact or impact on cells to drive or activate them to fulfil tasks and behaviours is referred to as

27

bioactivity. Mineralisation fortifies the connection between bone tissue and the implant. It is one of the most widely used techniques for increasing bioactivity in bone healing and fixing applications. Figure 1.2 depicts the current materials used in the production of hip implants and the current growth in polymer usage for an implant which shows a continuous growth over the years when compared with other materials [17,18].
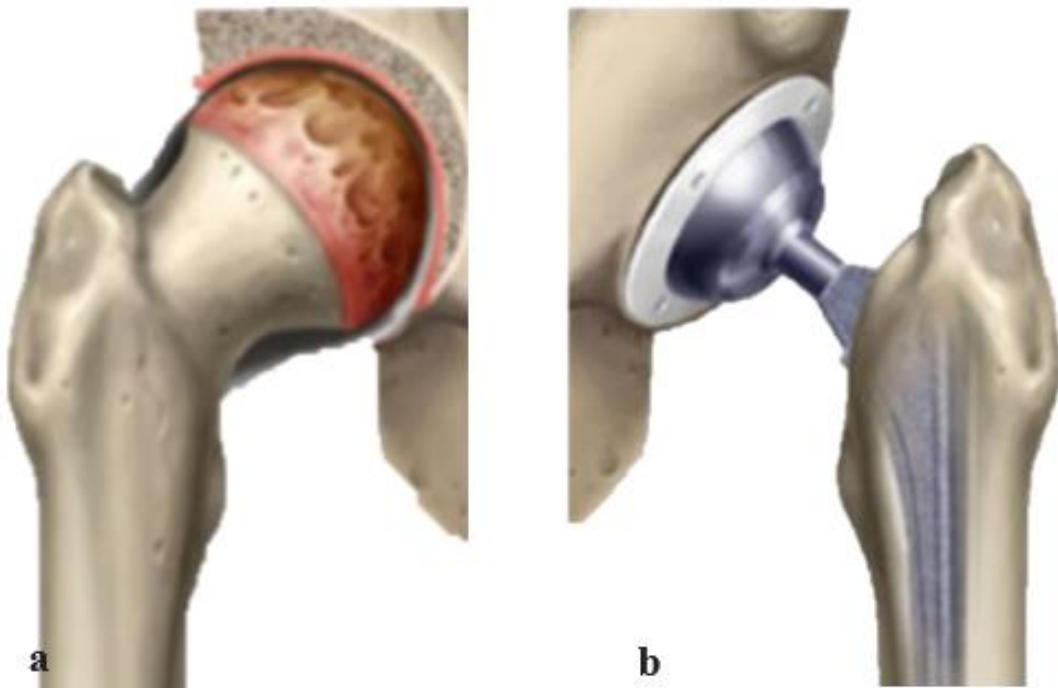
Figure 1.2 Human femur bone, depicting (a) a diseased hip bone that needs replacement and (b) a present model of a hip bone implant with metal [19,20].

The characteristics of these materials must be compatible with their capacity to communicate with and promote cellular activity and behaviour. This generation involves developing temporary 3D porous structures that encourage cell invasion, proliferation, and surfaces functionalised with peptide sequences that imitate extracellular matrix components to elicit biological responses. Tissue engineering is a growing field that may provide viable tissue and graft transplantation alternatives. Tissue engineering entails manipulating cells, which is not an easy task and is a significant shortcoming when considering the widespread usage of this method in a hospital setting. Despite this, tissue engineering is a promising technique that offers many new opportunities for research and study in regenerative medicine [20,21].

Stainless steel alloys were the first metal in orthopaedics throughout the twentieth century. It was about the 1940s when titanium and titanium alloys were first produced commercially [22]. A new class of memory alloys, nickel-titanium (NiTi) shaped, emerged in the 1960s. Their remarkable mechanical properties looked to open a whole new field of application to limited allergenicity and its applicability. This develops an oxide layer of highly adhering, self-repairing, and corrosion-resistant chromium (III) oxyhydroxide (Cr_2O_3) on the surface. Stainless steel is frequently utilised in temporary trauma devices like fracture plates and screws because of its cheap availability and secure processing. Due to the better mechanical and corrosion characteristics of titanium (Ti) and cobalt-chromium (Co-Cr) based alloys, their application in orthopaedic joint prostheses is limited because of the stiffness and significant weight and lack of inadequate biocompatibility [23].

The first generation's most widely used ceramic biomaterials include alumina and other porous ceramics, with alumina being the most common. As a result of its low friction and wear coefficients, alumina has been extensively utilised for over two decades. However, it has an extremely high modulus of elasticity, measuring 380 GPa [24]. Alumina acetabular cup is a spongy bone substitute that produces significant mechanical stress issues in older individuals with osteoporosis, ultimately leading to degeneration. In particular, the leftover monomer can potentially enter the bloodstream and cause an embolism. In some situations, the stiffness difference between a metallic prosthesis and the bone can produce stress, leading to cracks and the release of particles, which can induce an inflammatory reaction when they touch the surrounding tissues.

Polyether-ether-ketone (PEEK) and ultrahigh molecular weight polyethene (UHMWPE) are especially appealing for orthopaedic applications [25]. Examples include acetabular coating cups in total hip arthroplasties and total hip replacements. Tibial implants are used as a spacer to replace the artificial knee arthroplasties. PEEK materials are excellent alternatives for medical applications due to their unique features, which include excellent impact resistance and high toughness while preserving biocompatibility. On the other hand, wear occurs, and debris produces unfavourable consequences. Bioactive interfaces, which trigger a particular biological reaction, are becoming more critical in creating second-generation biomaterials [26,27]. Figure 1.3 shows the fracture stages healing of a scaffold implant through the healing and degradation of biomaterials
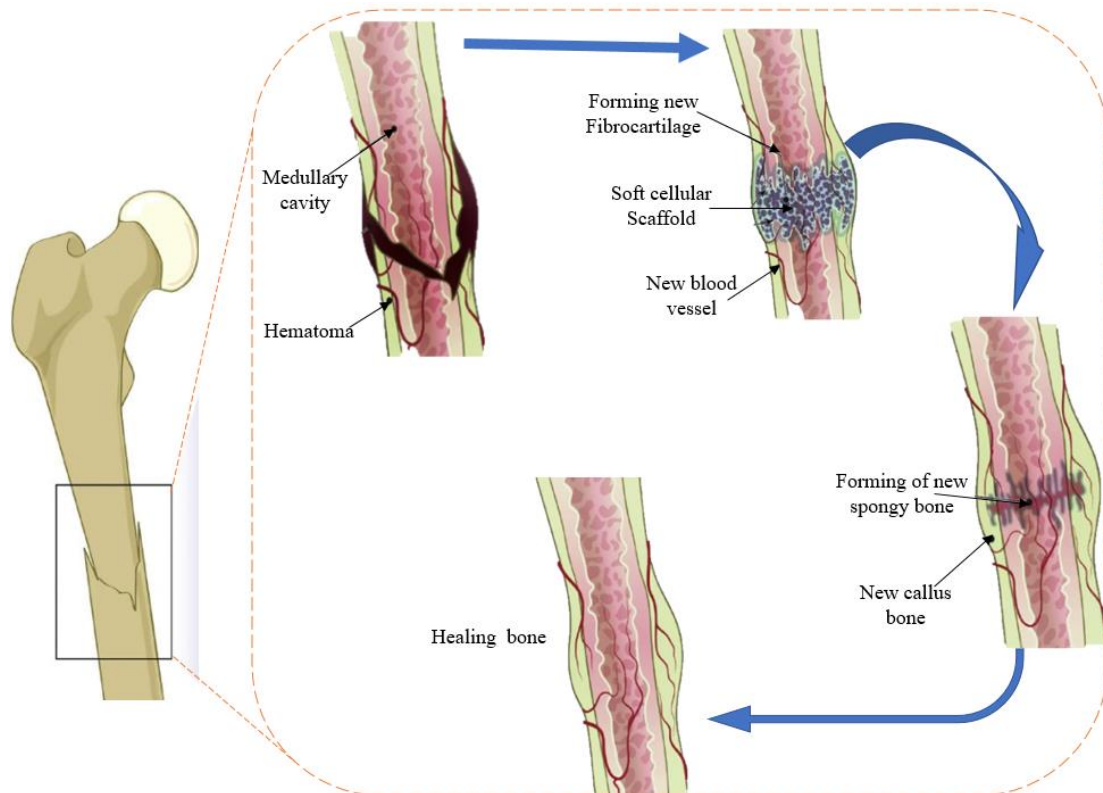
Figure 1.3 Stages of secondary fracture healing [28,29].

The PEEK is a semicrystalline, straight-chain polyaromatic polymer that exhibits excellent mechanical strength and chemical resistance [25]. For this reason, about two decades ago, its use as a biomaterial for orthopaedic, traumatological, and spinal implants began to be investigated. One of the most studied strategies currently involves producing polymeric composites and nanocomposites in polymers used as biomaterials. The latter are composite materials in which the reinforcement has at least one dimension on the nanometre scale, usually below 100 nm. Including particles, nanoparticles, or fibres in polymers, carbon fibres and nanotubes, hydroxyapatite particles, and nanoparticles, in general, increase the materials' strength and modulus and reduce the deformation at the break. In orthopaedic applications, polymeric composites have become extensive due to the production capacity of low-density materials, high performance, and mechanical properties comparable to bone tissue [29,30].

Hydroxyapatite (HAp) is an inorganic mineral found in the composition of bones and teeth. In addition to having osteoconductive characteristics, it can be manufactured synthetically. This material stimulates new bone tissue development on the implant from

its muscles, making the prosthesis more stable. It results in a substantial rise in the material's elastic modulus and improves its performance. On the other hand, composites significantly impact their tensile strength and toughness. It is known that modest concentrations of inorganic nanometric particles of 3 to 5%, combined with polymeric matrix, may offer the same characteristics and advantages as traditional composites, with 20-30% reinforcement. Scientific data from [29-31] suggests that a biomaterial substrate generated by nanoscale components is superior biologically. As a result, nanostructured components are regarded as potentially valuable biomaterials [31,32]. On the other hand, the availability of powders containing particles of the nanometric scale is still restricted. In the next section, the introduction of product types suitable for PEEK and its composites, such as cHAp and rGO will be discussed, in addition to the extrusion process.

1.2. Extrusion process

PEEK is a high-performance semicrystalline engineering thermoplastic which is a material that becomes plastic on heating and hardens on cooling and can repeat these processes and retain its properties. PEEK belongs to the poly (aryl-ether-ketones) PAEK class, which is distinguished by the presence of benzene rings linked by oxygen (ether) and carbonyls (ketone). Its glass transition temperature is approximately 143ºC, and the crystalline melting temperature is about 334ºC. This result implies a high performance at high temperatures and processing temperatures of 355-380ºC. Despite the high processing temperatures, PEEK is easily moulded using traditional processing techniques such as extrusion and injection moulding. PEEK can reach maximum crystallinity values between 30% and 35%. After extrusion, the material can also be machined in the chosen format. However, PEEK became the top contender for high-performance thermoplastics to replace metal implants, particularly in the orthopaedic field, as Force-bearing implants in the late 1990s. After repeated heating, the material proved healthy and maintained its high mechanical properties [7,33].

1.2.1. PEEK for bone implants

The need for bone implants has skyrocketed in recent years, owing primarily to congenital and late-life illnesses and diseases. The hip and femur, placed in the area where the therapy is to be done, are options for alleviating or eliminating the effects of these disorders. PEEK is a polymer utilised as a raw material in producing orthopaedic

implants. This polymer has good mechanical qualities, is biocompatible, and possesses features like those found in human bones. In terms of elasticity coefficients, it is almost identical to the original implant, suggesting a higher functional efficiency. The usage of PEEK has grown significantly in recent years to about 1.5 million kilograms in a year[32,33].

1.2.2. Motivation for study

As previously stated, over 190,000 total hip, femur, and knee replacement procedures are performed yearly in England and Wales alone. Hip and femur replacements are performed in over 400 facilities. Titanium and other metal are the primary materials used in implants; however, they are heavier, more expensive than polymer-based materials, and difficult to process through fused deposition modelling (FDM) [31,32]. Titanium is difficult to machine and process into the different bone implants and mimics bone structure through lattice structure. PEEK is a good material recently introduced into bone-implant, which is easy to machine when compared with titanium and other metal and not relatively expensive. The demand for this polymer grew due to the interest in developing hip prostheses and fracture fixation plates to make the biomaterial closer to the rigidity of human bones[34]. However, doubts and concerns about PEEK's high performance and better compatibility are questionable for a hip implant.

In the cortical bone, the elasticity module is approximately 18 GPa. Without adding other elements that can modify its properties, PEEK has an elasticity modulus between 3 to 4 GPa, which can be improved if a composite is added. It is observed in titanium, another biomaterial used, at approximately 110 GPa, which is too heavy and stiff for the body. PEEK properties can be manipulated using physical, chemical, and mechanical processing methods, combining changes in surface properties to improve their applicability and functionality in bone implants to the maximum [35–37]. However, biocompatibility is needed to reduce toxicity, increase the bioactivities with body tissue, and increase the strength to a higher standard like that of bone. In machinability, PEEK is better to machine than titanium and other metal but not easy to machine compared to other polymers due to the high melting temperature. It is, therefore, advisable to use FDM as a production method in this thesis for the easy operation and manipulation of components compared with other AM processes and to archive accurate expected results-with good tolerance. This will help medical devices and other manufacturing industries

benefit from the design and manufacturing process explained in this work. It will help many implant industries with a selection of materials and design prospects in bone-implant design, especially hip and femur implants. Specifically, the development of prostheses and bone implants has spread globally with the rapid advancement of medicine and all the associated biotechnology. Parallel to this development, this research will benefit from different biocompatible materials that perform structural functions in the human body as implants and prostheses of reinforcements.

1.3. **Statement of problems**

In bone repair, osteogenic biomaterials are critical because they provide the required substrate for cell growth, tissue regeneration and cell proliferation and differentiation while also regulating the activity and function of cells in the bone. The development of bone biomaterials has been prioritised, with particular attention on the resulting issues: (i) emerging ideal biomaterials with an optimal balance of physical and mechanical qualities, (ii) Inducing the purposeful separation of stem cells for artificial-to-biological conversion. PEEK materials have proven to be durable and promising in recent years. However, the PEEK and its family compounds, such as poly-ether-ketone (PEK) and some of their composites, could not support optimum cell proliferation on the surface of the materials due to a lack of good biocompatibility properties. Numerous strategies have been investigated to address the difficulties associated with tissue engineering applications. These methods can be grouped into surface treatments and material modifications. When a material is modified, additives that can change the properties of the matrix are introduced, or the matrix is blended with another polymer. The biocompatibility, mechanical issue, and structural integrity have not been extensively investigated using experimental and computational methodologies. Therefore, this PhD research explores the above limitations of PEEK towards improving their properties for a breakthrough in bone implants. The proposed research method, materials, and solutions are discussed in the next section.

1.4. Proposed research methodology and solutions

This research aims to create a distinctive composite scaffold for an implant using PEEK and two other composites, cHAp and rGO, in various micrometric scale combinations. The objective is to create porous three-dimensional structures with organised

interconnectivity between the pores and appropriate mechanical characteristics. The material selection preparation and the 3D models of the suggested scaffolds are used to modify the scaffold's parameters. Experimental and modelling techniques were used to examine surface treatment and compatibility suggestions. The study and treatment of PEEK's surface structure for bone implants' surface integrity have been suggested based on the introduction of a novel composite. Another coating technique is discussed by immersing the polymer into the composite dissolved in acetone and ethanol, which applies to two distinct extruding machine configurations. To improve and mimic bone-like structure compatibility in the implant is necessary to introduce lattice structures, such as face centre cubic octahedron (FCCO), diamond, primitive and gyroid. They were investigated using microstructural analysis. This needs to be proposed research aim and objective in the next section.

1.5.   The research aims and objectives.

1.5.1.   Aim

This research aims to develop a biomedical PEEK composite for hip and femur implant scaffolds.

1.5.2.   Objectives of the study

The following aim was completed, as described previously, to meet the study's objectives:

i.   Investigate the unique approaches for PEEK composite to manufacture a novel composite.

ii.   Develop and optimise a scaffold with PEEK-cHAp-rGO in different ratios: 1 to 5% for a bone implant.

iii.   Investigate the standard lattices and combination of a distinct lattice with PEEK, cHAp and rGO for a bone implant.

iv.   Design modelling and simulating lattice structures for a hip implant and femur bone.

v.   To characterise the scaffold's in-vitro biocompatibility, conduct mechanical testing, data analysis, and cell culture investigations.

1.5.3. Contributions to knowledge (research novelty)

In this experimental and analytical investigation on developing and analysing a new polymer composite for an implant, a thorough and critical evaluation of the most current composite designs for biomedical implants was undertaken in the introduction section. Following that, the research questions were discussed. The structure and geometry of the lattices, the materials and parametric printing techniques used, and the inherent difficulties that PEEK composites face were all addressed. The interconnectivity impacts of mechanical characteristics that may restrict the samples were also discussed, as are the related problems that face the 3D printing of composites in general and the potential limitations of the models. In addition, the sample's surface roughness and porosity were evaluated for their significance. Surface roughness is more likely to arise in PEEK, cHAp, and rGO material producers due to the well-designed bone shape and a complete understanding of 3D printing conditions. Compared to other materials, this outcome will yield more bone-reinforced composites for an implant. In addition to the different anticipated results from the core experimental and theoretical studies and the literature study contributions, the following contributions were made as this doctoral research progressed.:

- A novel result of PEEK and PLA composite sample ratios on 3D printing for a bone implant was achieved. It is conceivable that the implications include appropriate management of surface roughness impacts but are not restricted. The optimum printing settings and composite samples have been established with pinpoint accuracy in experimental and computational circumstances.

- Thorough experimental research was conducted on PEEK's scanning electron microscope (SEM) and its composites and related calculations. An experimental simulation and analytical study of the lattice structure for bone hip and femur implants on the samples have yielded promising and early findings, which will help to bridge some research gaps.

- The impact of the new polymer composite's printing geometry integrated into PEEK is one of the benefits of this suggested model over the current models in the literature. The other advantage is that it is simpler to implement. In addition, a combination of concentrated and evenly distributed Force conditions will be applied to the samples using experimental and analytical techniques to determine

the effect of the structures. The design model was evaluated with several other models published in the literature. The findings were produced to show the compliant biocompatible bone implant created using the suggested model to mimic the outcomes of a bone hip and femur scaffold.

1.6. Structure of the thesis

The thesis is organised chronologically into the seven distinct chapters listed below. The flow and structure are briefly shown in Figure 1.4.
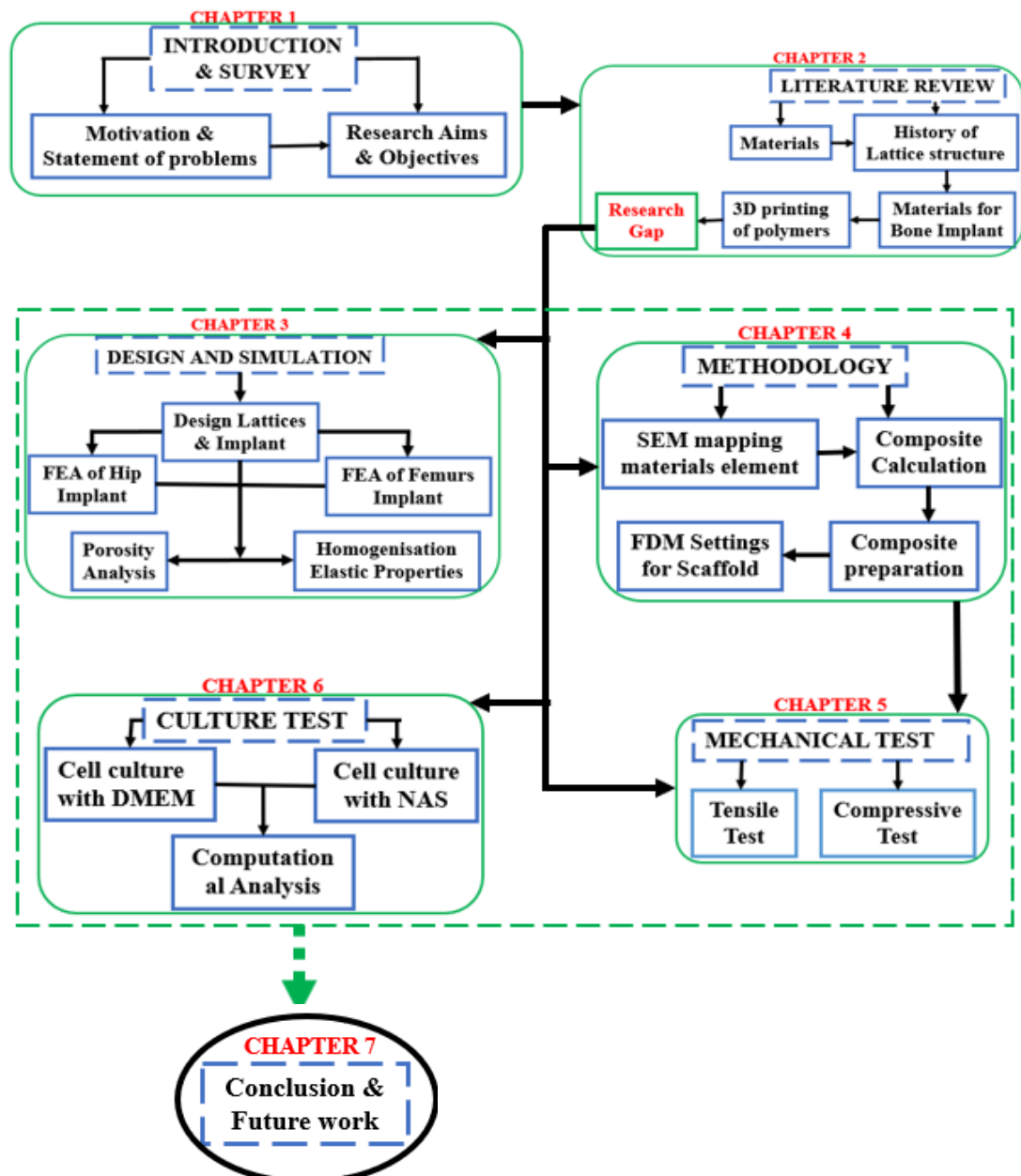
Figure 1.4 Research structure

- Chapter 1: Introduction - This chapter serves as a guide for outlining the work's goals and demonstrating the document's structure.

- Chapter 2: Literature review - This chapter discusses fundamental ideas that help contextualise the findings of the doctorate study. Additionally, it contains a bibliography evaluation of prior studies that addressed similar goals to those addressed in this study. It serves as a reference point for evaluating the acquired findings and conclusions.

- Chapter 3: Materials and Techniques- This chapter discusses the process for producing composite formulations and evaluating the composite materials' characteristics. Additionally, it elucidates the suggested methods for coating the composite samples.

- Chapter 4: Lattices creation - This chapter discusses the design of novel lattice structures relevant to bone structure. Evaluating various composites as additive and implant material is provided and analysed.

- Chapter 5: Characterisation of mechanical strength and AM simulations of bone implants - A sequence of computer experiments was conducted, and the simulation results were presented, evaluated to the accurate results, and thoroughly debated.

- Chapter 6: Microanalysis of structural cells - AM was used to obtain results from sample characterization tests, such as raw materials and structures. Surface roughness, SEM analysis, morphology, and infrared spectroscopy are used to characterise the mechanical properties of the composite material. At the same time, *in-vitro* tests are performed to determine the cell culture and proliferation potential of the composite material's surface porosity. Finally, the development of mesenchymal cells on the structures' surfaces was analysed.

- Chapter 7: Conclusions and future research - The closing comments on the experimental and simulation findings are emphasised. Summarised paths for future studies are also suggested to continue the study presented in this thesis.

- Bibliographies and references: Following the Vancouver Referencing Style, this part includes a list of all resources used in the thesis text, both cited (references) and uncited (bibliographies).

- Dissemination: The study's publications are in indexed journals, respected books/book chapters/encyclopaedias, and regional/international conferences. The

lectures are made at various scientific and academic conferences and activities. Appendices: This section concludes the thesis by including the names and images/figures of other pertinent and supporting documents, codes, and certifications, to name a few, to provide further or clear comprehension of what has been stated or alluded to throughout the thesis.

Chapter 2

Systematic literature reviews on bone implant for research Gap

CHAPTER TWO

2.0. LITERATURE REVIEW

2.1. Introduction

This chapter describes the significant features of tissue engineering, emphasising the manufacture of support structures in the literature for tissue regeneration in terms of manufacturing techniques and materials used. This chapter focuses on the regeneration of bone tissue because of the enormous scope of application of the materials and methods developed in this doctoral thesis in tissue engineering. In this sense, this chapter includes an introduction to the main characteristics of tissue at a biological level and a bibliographic review of the main existing techniques used to search for strategies that allow the tissue to regenerate effectively. It also presents a compilation of the characteristics and main applications of the different materials proposed in the literature as potential supports for bone tissue regeneration and their main limitations. The literature review justifies polycaprolactone as a polymeric base material to formulate the different composites proposed in this work. This section gives an extensive description of the previous results on this material, and its main characteristics were studied and reported.

This study includes a description of the main characteristics of the plant species and a review of the background of aloe extracts in tissue engineering applications. Finally, an evaluation of techniques based on plasma treatment to enhance the bifunctional properties of materials typically used in tissue engineering is included. Plasma treatment offers the possibility of introducing carboxyl and efficient hydroxyl groups on the surface of relatively simple material. Figure 2.1 depicts a flowchart for a literature review categorising composite materials and their production processes of methods used in AM, stating a review of a technique of PEEK, its implants, and their purposes in the medical field. For this reason, this technique was proposed previously for the polymer coating stage and is expected to provide functional groups on the surface of the polycaprolactone capable of interacting with the composite present in the extract[38,39].
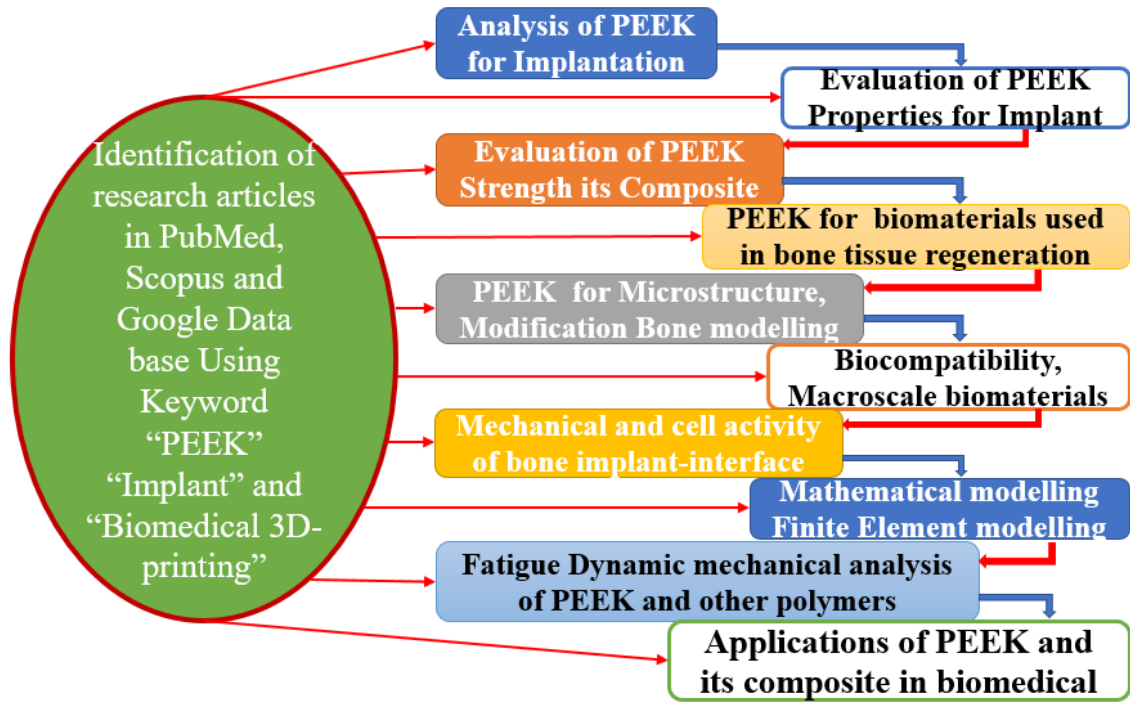
Figure 2.1 Summary literature review of PEEK, its implants, and their applications in the medical field.

The various internal and external mechanical cues that control tissue recovery and the natural processes of bone formation and healing are discussed in this review chapter. The mechanical-biology analysis allows for a more straightforward abstraction of the bone-implant interface, which leads to the development of a mathematical model of bone osseointegration. The following section describes the physiological and biochemical processes that allow new bone growth when the bone implant meets the body. Several mathematical models are reviewed in the literature, including specific tissue-recovery mechanisms, typical bone-bone implant healing, and a condensed mathematical model of implant integration and its mechanical-natural reality [40,41]. The next section critically reviews biocompatibility, a bioactive composite of different materials suitable for the PEEK production of hip and femur implants.

2.2. Biocomposite materials

2.2.1. Biomaterials

A biomaterial is expected to interact with different biological to cure, enhance, or substitute tissue that temporarily performs a specific function. Biomaterials are designed to close touch with tissues and must meet several requirements to retain inherent properties such as biocompatibility. The biomaterial can repair injured tissue. They are divided into natural and synthetic [42–44]. When utilising them in specific applications,

consideration should be given to biocompatibility, mechanical stress, cost, and shape. As the structural components of scaffolds, biomaterials are critical in this setting. Even though these materials have been documented for millennia, practical methods for tissue regeneration are being developed. The categorisation of biomaterials utilised in tissue engineering, and the modification region for this study are shown in Figure 2.2. These techniques include an approach centred on altering the implant surface chemistry and affecting surface bioactivity[40-42]. The bioactivity of PEEK has been reported to be enhanced by wet chemical treatment in several investigations. PEEK surface chemistry changed to PEEK-OH and was subjected to various chemical treatments. The H_2O contact angle of the sample decreased, indicating an increase in the bioactivity of PEEK. Another research discovered that the amine and carboxylic functional groups on the surface of PEEK could increase cell attachment and proliferation. PEEK-OH, generated by wet chemical treatment, were tested for bioactivity using fibronectin (FN) adsorption[42-44].

The results from [43,44] showed that proteins might be adsorbed, where fibronectin is covalently grafted onto PEEK-NCO. According to the findings, the effectiveness of the FN-treated substrate increased $CaCO_2$ cell adhesion and proliferation in the absence of serum in separate research compared with the FN-coated PEEK substrate. The use of wet chemical treatment before enhancing apatite production by immersion in SBF was investigated with PEEK in SBF. The impact of NaOH pre-treatment on apatite formation was investigated [45,46]. The results indicated that the development of apatite coatings, which improved with pre-treatment, was feasible with NaOH. PEEK sulfonate, PEEK with subsequent dip and PEEK with a further drop in acetone. According to Figure 2.2, the research gap is printed in red ink, which is the modification of PEEK by combining cHAp and rGO using the surface modification method of a physical and chemical surface coating.
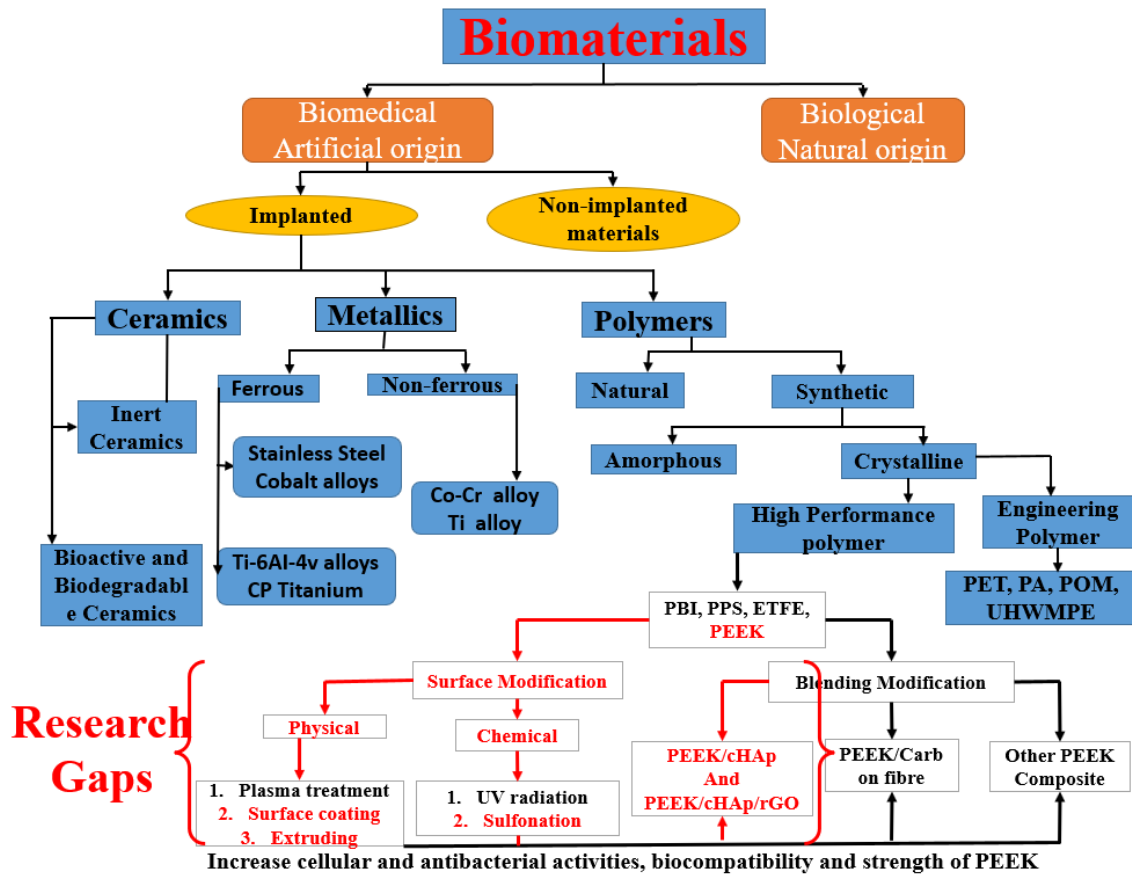
Figure 2.2 Classification of implant biomaterials and modification area for this research and gap.

2.2.2. Bioactive composites

Bioactive composites are compounds of calcium, phosphorus, and silicon dioxide. They are hard solids and osteoinductive since they are bioactive ceramics. This property implies that their union with bone is produced without forming an intermediate fibrous tissue layer. Therefore, they are used in bone defects as filler material and in compact form to create implants. When used as a graft, they form strong bonds with adjacent tissues between 52 and 70 MPa and generally increase union over time. The bioactive composite modulus of elasticity has a value like bone but still presents stress release. Also, the ultra-porosity provides a large bonding surface with the tissue. The ability to be also reabsorbed is advantageous. In tissue engineering, biocomposites that mimic living matter structures match the properties of tissues to be replaced. Metal matrix composite materials can be used for prostheses, with austenitic PEEK, PLA and PCL as a matrix and graphene oxide (GO) or HAp as a reinforcement. These composites have excellent mechanical properties but little adhesion with the bone [47,48]. Hence some coatings solve the compatibility problem. For the replacement of hard tissues, polymer-reinforced

ceramic matrix biocomposites can be an alternative. Simultaneously, the polymer decreases the elastic modulus of the compound to the extent that it approaches that of the actual bone, with the consequent decrease in tensions in the implant-bone joints. The best-known biocomposite is the ultra-high molecular weight polyethene hydroxyapatite compound.

2.2.2.1. Hydroxyapatite

HAp is a biocompatible, bioactive, osteoconductive and absorbable calcium phosphate. The use of calcium phosphates in medicine and dentistry began more than 20 years ago. Its applications include dental implants, percutaneous systems, orthopaedics, maxillofacial surgery, and hip and femur surgery [48,49]. The stability of calcium phosphate ceramics depends on the temperature and water content during processing and the medium in which they are found. Under the body conditions, the only stable calcium phosphates are brushite or dicalcium phosphate for a pH less than 4.5 and HAp for a pH greater than 4.5 [50]. cHAp is a ceramic material formed from tricalcium phosphate of formula $Ca_{10}(PO_4)_6(OH)_2$. Its biocompatibility is very high because its composition is similar to bones, with an almost equal ratio of calcium and phosphorus. Its most prominent property is interacting with bone tissue to stimulate bone growth [1,51,52]. It is obtained by sintering from calcium and phosphate salts of phosphoric acid and calcium hydroxide. It can also be produced using marine coral as a calcium carbonate source and transformed using ammonium phosphate at high pressure and temperature [53,54].

The drawback of this material is its low toughness and mechanical strength of high brittleness. There are also ceramic matrix compounds where a metal is used as reinforcement, improving mechanical properties. In the manufacture of composite biomaterials, it must be considered that each component must be biocompatible with the body's environment and not degrades the interface between the members. Chitosan-based biocomposite scaffolds for bone tissue engineering are shown in Figure 2.3.
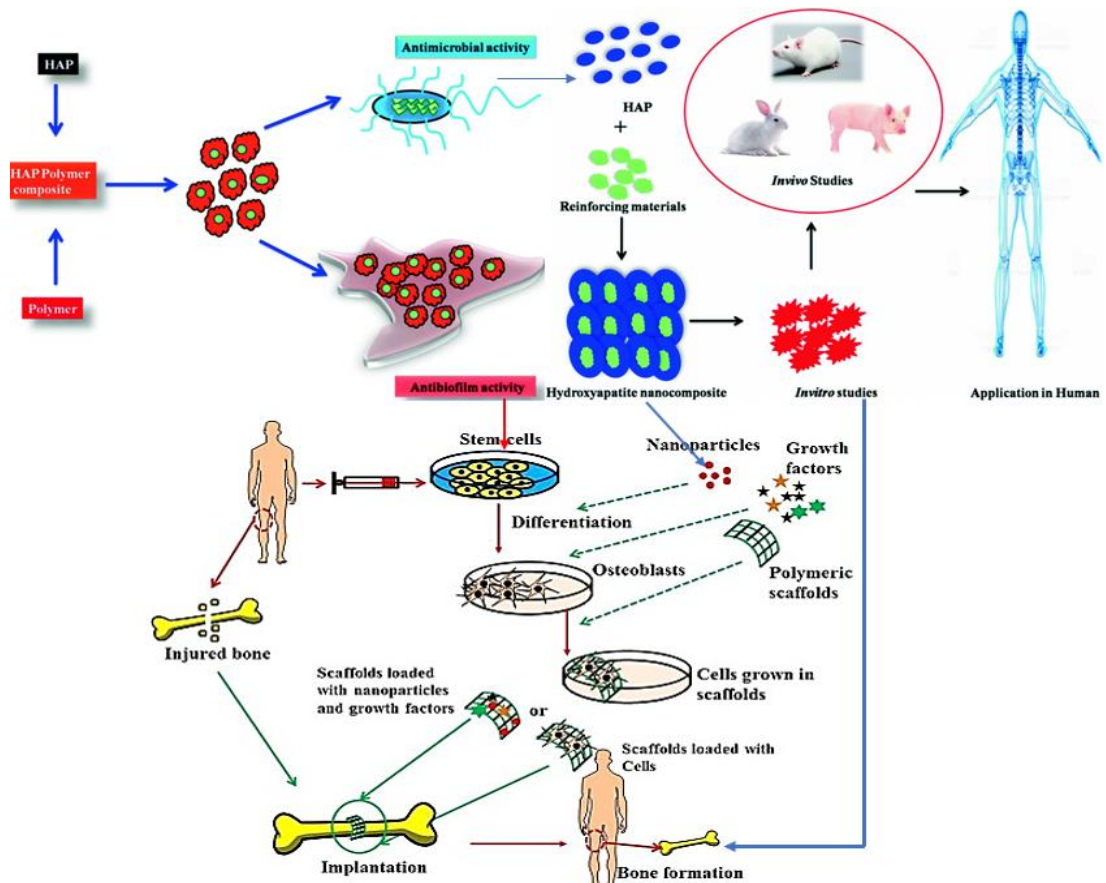
Figure 2.3 Chitosan-based biocomposite scaffolds for bone tissue creation are being used to repair significant measurable bone defects. Cells and biomaterials, or a combination of cells stacked onto biodegradable platforms, are used in these scaffolds. [55,57].

These scaffolds, which contain cells and biomaterials or a combination of cells packed onto biodegradable programs, address fundamentally measurable bone defects. Increased bone cell penetration during osteointegration is facilitated by increased porosity; nevertheless, the mechanical properties of the coating are weakened as a result [55,56]. Because of this subject, a delicate balance must be struck to identify the optimum porosity for maximum saturation of bone cells without negatively affecting mechanical properties.

HAp presents in various forms: in concrete blocks, porous solids, or powder. The powders are pressed and sintered at different temperatures, always higher than 100°C and at intervals to obtain the solids. The material properties received depend on these intervals; its modulus of elasticity can vary from 40 to 150 GPa [58]. With these data, it can be observed that the mechanical behaviour of HAp is higher than that of other ceramics, such as alumina. HAp stimulates the interaction between the bone and the

implant, accelerating its growth and integrating the prosthesis. Due to the excellent adhesion, they are coated mainly with PEEK components in femoral stems. The drawback of this coating is that it is used for high-temperature thermal spraying, transforming part of the HAp into a mixture of CaO, tricalcium phosphate and tetra calcium phosphate [59–61]. Therefore, it must undergo a 6-hour steam treatment or maintenance at 600°C to restore HAp, affecting the base metal's properties [62]. Several studies are being conducted to explore the combination of PEEK with certain bioactive elements, which encourage bone development surrounding the implant to enhance the implant's fixation [63,64]. In biomaterials, cHAp has established itself as standard reference material. The structure and chemicals of cHAp are like the mineral portion of bones and teeth [13]. It has outstanding biocompatibility and bioactivity characteristics. Allowing the growth of bone cells, fibroblasts, and osteoblasts does not differentiate it from the bone surface. Its hydrophilicity, which will enable it to be wetted by bodily fluids, does not distinguish it from the bone surface. Despite all the benefits of cHAp, its clinical use is restricted due to its slow biodegradation. In studies conducted over extended periods, it has been shown that cHAp starts to be reabsorbed gradually 4 to 5 years after implantation [63]. Figure 2.4 from the left side shows the cell development of Hap NP forming into the fibre of a polymer matrix, also serving as a drug supplement for the polymer treatment for better compatibility to promote cell growth. After testing in Invitro for cell growth, a lattice scaffold coated in PEEK and cHAp nanoparticles is implanted into the damaged bone. The 3D-printed scaffold with a lattice structure creates an effective bone implant for the damaged bone [6,65,66].
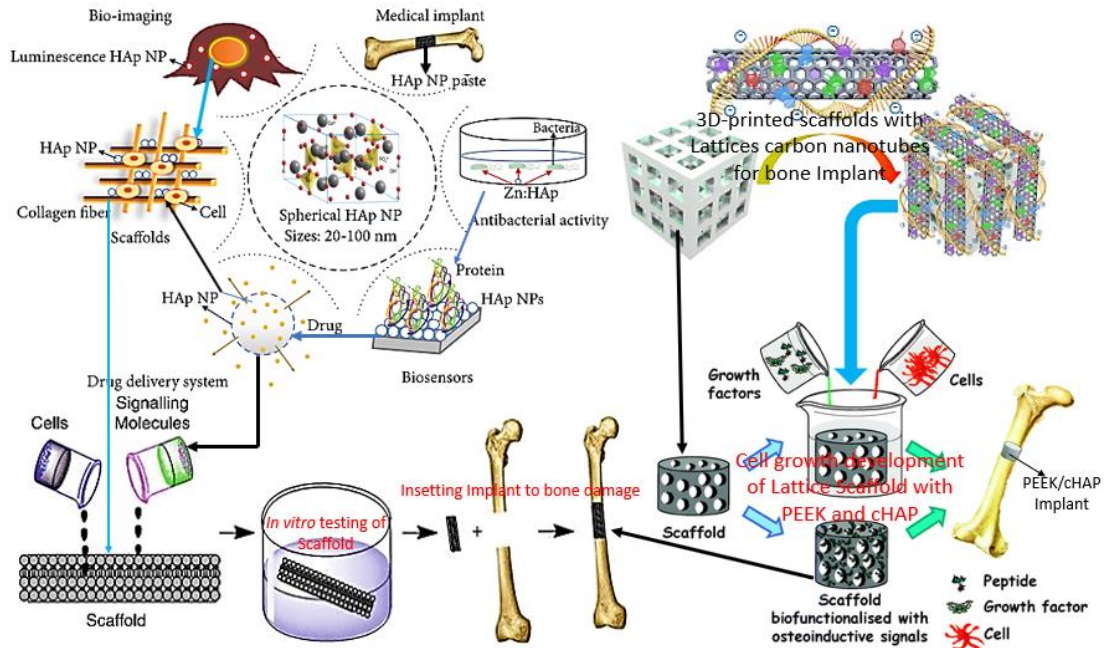
Figure 2.4 depicts the cell growth and development of a PEEK and cHAp nanoparticle-coated lattice scaffold and 3D-printed scaffolds with carbon nanotube lattices to produce an efficient bone-implant bioprinting technique[64,67].

HAp is a natural calcium phosphate and a primary mineral component of bone tissues. Its ceramics $Ca_{10}(PO_4)_6(OH)_2$ have been believed to be highly applicable. Grafts treat various ruined tissues. Its crystallinity ensures a high rate of extensive decomposition when constructed scaffolds, providing their symmetrical shape during tissue self-regeneration [62-64]. There are also bone substitutes for octa calcium phosphates (OCP) and bone regeneration nanocomposites for the tricalcium phosphate (TCP), consisting of calcium phosphate phases with low solubility hydroxyapatite. These are all low-crystallised carbonated cHAp, which began to be used as biomaterials from acknowledging the limitations of the cHAp phase use. Composite materials are shaped by the fraternisation of two or more biomaterials, one of which will be the base. The other will be supporting components, aiming to achieve specific properties for various applications. The mechanical properties of scaffolds are determined by their biocompatibility and the mixture of calcium phosphates and polymers. For bone tissue regeneration, PCL-HAp, PGA-HAp composites, and collagen-chitosan were defined [64,67,67].

2.2.3. **PEEK as a biomaterial**

PEEK column implants have recently gained popularity for treating spinal injuries. The structure of the PEEK molecule is depicted in Figure 2.5. PEEK was first developed as a high-performance thermoplastic to replace metal implants in the late 1990s, following the groundbreaking work of the British company In-vitro[66,67]. Since April 1998, it has been commercially available for this purpose [68,69]. Figure 2.5 also depicts the calcium-based nanomaterials, such as cHAp, frequently used to construct new bone scaffolds on a PEEK surface. Figure 2.5 illustrates a biological macromolecule framework with spinal electrostimulation applied longitudinally through an axial channel[70–72].
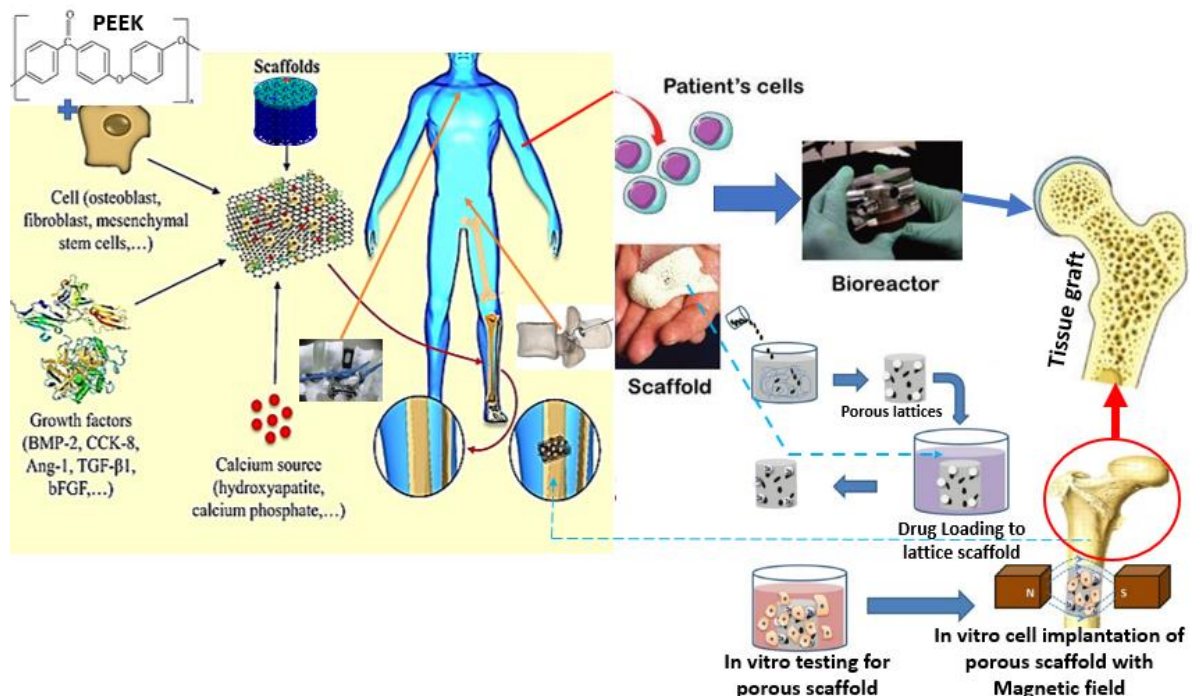
Figure 2.5 PEEK biological cellular structure, electrostimulation leg scaffold with a longitudinal axial channel and electrostimulation spinal scaffold with a longitudinal axial channel [73,74].

2.2.3.1. **PEEK and other polymers for bone implant**

Ceramic materials are excessively fragile to withstand the mechanical stresses of bone tissue grafts. Thus polymers are used either of natural origins, such as collagen or chitosan, or synthetics, such as polylactic acid (PLA). PLA polymers are absorbable. Therefore, the main advantage is eliminating subsequent surgical processes that remove the support structures. Figure 2.6 lists the primary materials used in bone tissue regeneration using tissue engineering techniques. This brief section describes the main

characteristics of each of them. It presents some references that exemplify how they have been used in state-of-the-art. The new bone may develop and penetrate the porous sulfonate layer, demonstrating biological cytocompatibility Ossie integration [75,76]. Table 1 summarises the functional groups deposited in PEEK through wet chemical deposition to improve its bioactivity. When resorbable materials are used, the cell growth rate must be approximately equal to the degradation rate of support materials. The graft replaces the tissue at a reasonable rate since excessively rapid degradation implies a loss in the mechanical properties of the regenerated area. Also, a too-slow process hinders proper cell growth.

On the other hand, some composites take advantage of different materials, especially mixtures of polymers and ceramic materials. Hydroxyapatite polycaprolactone is one of these most common types. However, polymer combinations with additional features are usually made of biofunctional processing products. Hydrogels stand out in biomaterials of a polymeric nature, 3D polymeric matrices capable of retaining a quantity of water, making them very interesting in simulating biological tissues and drug release. The environment provided by the hydrogels makes them suitable for incorporating cells in the medium to effectively support the printing process with the cells contained inside the hydrogel, with the advantage of controlling proliferation at specific sites [77,78]. This type of strategy is known as bioprinting. Polymers that formulate hydrogels are sodium alginate, collagen, chitosan, gelatine, fibrin, and hyaluronic acid.
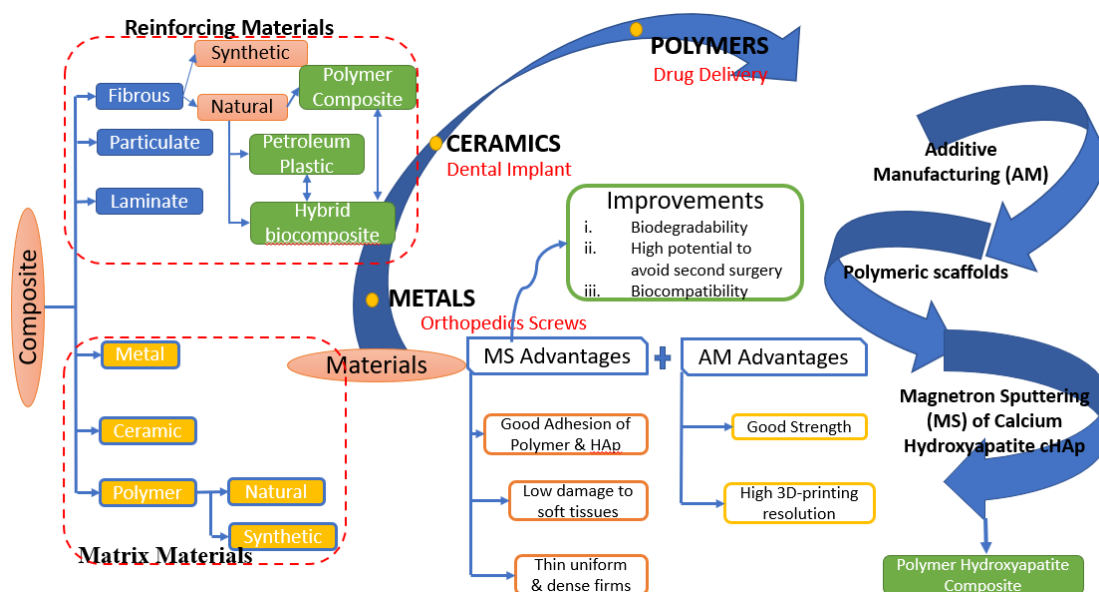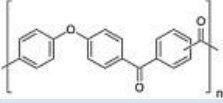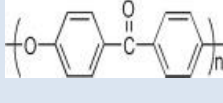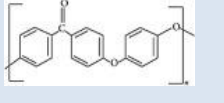
Figure. 2.6 Analysis of biodegradable synthetic polymer composites and cHAp and their sustainability [79,80].

However, despite their outstanding biocompatibility characteristics and capability to provide a favourable environment for cell development, the application of such structures in bone regeneration is constrained by insufficient mechanical stiffness. It is worth highlighting that extensive research is focused on searching for different cross-linking systems capable of increasing the mechanical resistance of hydrogels while maintaining their cytocompatibility. Studies have also focused on developing additive hydrogels to improve structural integrity and mechanical properties. Obtaining printed gelatine structures demonstrated that nanohydroxyapatite in these supports is vital in osteogenic differentiation. They gave it an exciting potential for application in bone regeneration processes [81,81]. One of the primary polymers used in bone regeneration is PEEK. This polymer has many advantages and has been cited by many researchers. This critical review polymer (PEEK) will be discussed in more detail in the next section.

2.2.3.2. Characteristics of PEEK

PEEK can be combined with various additives to produce a variety of composites. A composite material comprises two phases, each retaining its unique physical and biological performances. Glass and carbon fibres were among the first additions utilised to enhance the strength and stiffness of PEEK. PEEK and carbon fibres combine to form an effective user interface that transfers mechanical stresses between the fibres and the polymer matrix. When carbon fibres are combined with PEEK, their length, size, and orientation determine their properties. This composite material is presently being utilised in the hip, femur and joint replacement implants, along with certain additives that improve the material's biomechanical properties. Barium sulphate is an example of an additive having these characteristics. Figure 2.7 shows the flowchart of Amorphous high-performance polymers that are thermoformed, translucent, and used for bone implant through FDM. When combined with PEEK, a radio pacifier improves visibility and contrast in the medical image region, allowing easier radiological management during and after surgery [82,83]. Table 2.1 compares the molecular structures of several kinds of high-performance thermoplastics.

Table 2.1 Comparison of diverse types of high-performance thermoplastics [84, 85].

Properties	Poly-Ether-Ketone-Ketone (PEKK)	Poly-Aryl-Ether-Ketone (PAEK)	Poly-Ether-Ether-Ketone (PEEK)
Chemical structure			
Glass transition temperature (°C)	158	147	143
Processing temperature (°C)	380	330–360	385
Tensile strength (MPa)	145	149	152
Youngs' modulus (GPa)	5.2	4.1	5.2
Biocompatibility	Yes	Yes	Yes
Processability	Medium	Medium	Easy
applications	Automotive, chemical, and aerospace industries	Bearings, piston parts, pumps, and valves	Like PEKK and PAEK, along with biomedical applications.
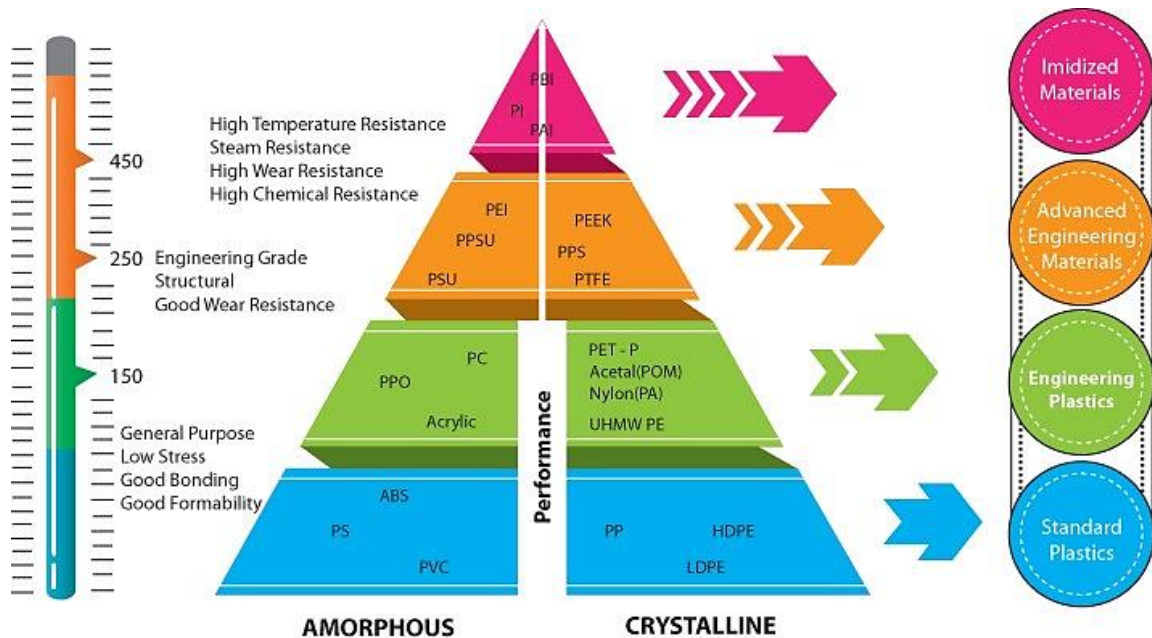
Figure 2.7 Flowchart of amorphous high-performance polymers and thermoformed capable, translucent [85,86]

2.2.3.3. PEEK and its merit

Different metallic implants and PEEK structures benefit from radiolucency benefits, including far more accurate insertion techniques and faster detection of postoperative problems. Biomaterials experts are pleased to have supported the goal to accelerate medical device innovation by providing innovative solutions and funding for research into PEEK. *In-vitro* is a breakthrough technology that utilises implantable polymers

based on high-performance PEEK, such as PEEK-cHAp Enhanced. The work maintains the outstanding compression and compression shear performances observed before. The actions listed in Table 2.2 may benefit PEEK-based biomedical composites and help enhance PEEK quality attributes. Researchers are constantly looking for ways to improve the performance of conventional metallic implants by using PEEK materials as subordinating materials [70,84,86]. Along the way, PEEK developed a reputation as a possible substitute for precious metals. The following table summarises the different actions that may benefit PEEK-based biomedical components.

In contrast to PMMA and composite resins, which exhibited a polymerisation shrinkage of about 2% at 4% and deformed the scaffold from the original expected shape, PEEK does not shrink during the polymerisation process and remains chemically inert. In addition, PEEK exhibits good hardness, stiffness, and strength stability across a broad temperature range [86-88]. In comparison to other thermoplastic materials, this results in less distortion. A polished surface is essential for both its aesthetics and role in the build-up of bacterial plaque, as shown by discovering a clear connection between surface topography and the development of biofilms on surfaces. Furthermore, the result of the biofilm surface of PEEK is comparable to or even less than that of dental materials like titanium zirconium. Due to these promising physical-mechanical properties compared with traditional alloys and ceramic dental materials [22,87,88].

Table 2.2 Methods of improving quality of PEEK characteristics.

Method	Material system	Affected property	Significant outcome	Ref.
Composite fabrication	PEEK-Alumina	Mechanical	Using 60% alumina reinforcement increased the dynamic strength of the resulting composite by 78 %.	[89–91]
	PEEK, Carbon fibres and nano-ZrO2	Mechanical and tribological	The stress concentration at the carbon fibre interface and the shear stress between sliding surfaces were reduced using nano-ZrO2 reinforcement.	[92–94]
	PEEK-HAp	Mechanical	The resulting composite had a significantly higher tensile strength because of the strong interaction between HAp and PEEK.	[35,59,65,73]
	PEEK-inorganic tungsten disulphide-nanoparticles	Mechanical and microscopical	Since it was first developed, 60 % more hardness has been added to the product.	[95,96]

	PEEK-carbon nanotubes	Mechanical and crystalline	PEEK's mechanical characteristics were improved because of the addition of the reinforcement, which also helped to decrease the crystallisation rate.	[97–100]
	PEEK-β-TCP	Biological	The proliferation rates of normal human osteoblast cells' growth on -TCP/PEEK were lower than normal human cells' growth on PEEK.	[54,101]
Blending	PEEK-Polytetrafluoroethylene	Tribological	The usage of polytetrafluoroethylene in PEEK has resulted in a reduction	[94,102,103]
Processing temperature	Injection moulding process	Mechanical and tribological	The hardness of the material rose as the processing temperature increased.	[7,82]
Use of additives	Polyetherimide	Mechanical	The mechanical and processing of PEEK-based products were improved because of the usage of AM.	[104,105]
Sterilisation	–		It has been discovered that steam therapy is more effective than other methods.	[113,114]
Electron beam deposition	Titanium/PEEK	Biological	*PEEK implants with titanium coating have a higher bone-in-contact ratio than implants without the coating, according to in-vivo research.*	[22,106,107]
Plasma immersion ion deposition	–		The therapy that was tried out aided in developing next-generation orthopaedic implants.	[112]
Pre-treatment of PEEK	Piranha solution etching and abrasion followed by chemical treatment, and	Chemical	According to the researchers, PEEK's adhesive qualities were enhanced by using a conjunction.	[108–110]
Plasma treatment	–		Applying plasma to PEEK at atmospheric pressure significantly improved the strength polymer.	[25,37,111]

Polymeric composites have remained generally used in orthopaedic applications. Compared with bone tissue, they are expected to have modest densities, high performances, and mechanical properties. The thermal coating of cHAp is a time-consuming and complicated procedure. Using traditional melt mixing techniques, the dispersion of these particles in a thick polymer matrix is challenging. Biomaterials must remain to perform their functions for increasingly prolonged periods since the population's life expectancy has continuously increased [115,116]. There are many challenges concerning developing polymeric biomaterials, such as superior properties under fatigue, creep, and friction. Thus, this project aimed to produce a PEEK-nHAp

nanocomposite for biomaterial application and study the short traction and impact and prolonged duration fatigue mechanical behaviour, correlating the results obtained with the analysis of dynamic-mechanical thermal and the morphology resulting from the injection moulding of the same. Finally, *in vitro* biocompatibility experiments assessed the biomaterial interaction with the living organism [117,118]. The structure of the material enhances chemical and heat resistance. It has a melting temperature of about 343°C, and its elastic modulus is between 3 and 4GPa.

PEEK is also chemically inert. Since this material has a pearl white or opaque greyish-brown colour, a composite resin coating is also necessary to achieve the ideal aesthetic. Water absorption, polymerisation shrinkage, structural stability, and polishing capacity are the most important characteristics to consider when evaluating the clinical lifespan of dental restorations. Even after a seven-day immersion at 121°C, it has been shown that PEEK absorbs less water than polymethylmethacrylate (PMMA). This brings about the difficulty in producing PEEK with other composites in different AM processes. PEEK is difficult to have with other composite combines. The next section addresses the various methods used in producing PEEK and its composite and the merit and demerit of this manufacturing method.

2.3. Adopted manufacturing techniques for PEEK

The techniques used to manufacture scaffolds must meet requirements that guarantee subsequent elucidation. The proportion accuracy in reproducing the anatomical design is necessary for all products. They should maintain the porosity characteristics, size, interconnectivity, and morphology to ensure regularity in this property for bone cell attachment. The traditional techniques for PEEK and its composite include FDM, union by fibres, phase separation processes, solvent casting, and particulate leaching coagulation of the material from a solution of the same gas [119,120]. Contrary to desirable characteristics, it foams high-pressure processing, hydrocarbon quenching, dry freezing, and combination [119]. These disadvantages include excessive dependence on manual labour, irregular geometric features, especially those related to the porosity of structure, toxic solvents, and design limitations [3,24,121].

On the other hand, AM techniques provide the advantage of granting high design flexibility, which is of great interest when it is intended to obtain specific structures for a

patient. Adding a composite improves the surface of the customised elements by integrating functionalised lacquering, which can enhance interface properties and combine drugs to cure pathologies derived from surgeries, if deemed necessary, by releasing these drugs. However, this grouping method does not provide any information on the principle of layered material processing of the different technologies. The other processing principles to classify AM technologies proposes this classification into seven categories or groups, as presented in Table 2.3. This will need to the next section, where the best manufacturing technic for PEEK is investigated and discussed, which is FDM

Table 2.3 Classification of AM technologies according to the principle of layer processing

Classification	Description of principles	Technologies in used	Ref.
Light curing in Cuba	The liquid photosensitive polymer is selectively cured in a vat by light-activated polymerisation.	Stereolithography (SL) Continuous liquid interface production (CLIP)	[122,123]
Material extrusion	Material is selectively distributed (deposited) through a nozzle or hole.	Fused deposition modelling (FDM)	[124,125]
Material blasting	The building material is deposited in tiny drops.	Polyjet, Multi-jet printing (MJP)	[126,127]
Binder blasting	A liquid binder is to join powdered materials.	Colour jet printing (CJP).	[128–130]
Powder bed fusion	Thermal energy selectively fuses regions of a dust bed.	Laser selective sintering (SLS), Electron beam squeezing (EBM) and among others.	[126,131]
Adding blades	Blades of material are joined (glued) to form an object.	Solids technology, Selective deposition lamination (SDL) Laminated object manufacturing (LOM)	[4,132]
Directed energy deposition (DED)	For the fusion of materials when deposited, thermal energy is used.	Laser-engineered net shaping (LENS) Direct metal deposition (DMD) 3D laser cladding and others.	[3,107,133]

2.4. FDM of PEEK

There are steps to standardise the properties of the biomedical PEEK. This standard specifies how the virgin raw material, pure – without additives, should be made available by the supplier, detailing the requirements and methods to be applied [112]. It also points out that PEEK characteristics can be modified and improved through some processes, including injection, extrusion, and sterilisation, to mention but a few. After making the products, the standard stipulates that validation tests must be carried out to ensure safety

and effectiveness, as agreed among the manufacturer, the consumer, and the responsible regulatory bodies. It also states that these normative references do not cover materials containing dyes, processing aids, other additives, and mixtures of other polymers containing PEEK or recovered materials [7,33]. Table 2.4 presents distinctive properties of forms manufactured from PEEK composite. However, commercial FDM machines require feeding wire-shaped material, a complex operation for many materials used to manufacture scaffolds. They are readily biodegradable, and their processability is not as versatile as thermoplastics commonly used in molten deposition modelling. This technique provides excellent accuracy at a micrometric working scale, repetitively obtaining structures and pore interconnectivity. However, the high-temperature application during the extrusion process can cause a partial degradation of the thermoplastic biodegradable and makes it impossible to introduce many natural polymers and growth factors into the formulation that cannot be processed at high temperatures [54,134]. Therefore, processes based on the extrusion of material solution and those based on deposition in low-temperature conditions have been proposed to ensure the solidification of the material. This thesis has studied introducing complex materials in AM techniques based on extrusion. This process allows greater versatility in the various materials used [86,127,135].

2.4.1. 3D printing of PEEK implants

After an accident has led to a fracture, the best way to quickly regenerate the bone is to have stable and close contact with the bone fragments. The fracture space is more significant than 0.5 mm, and it is advisable to use implants to fix the damaged bone fragments. AM technology has a significant added value, allowing custom implants to be printed and offering faster bone regeneration. In addition to healing the bone faster, operations are more straightforward, and the risk of infection is reduced. Osseointegration is a healing method that involves contacting the bone surface with an implant without additional tissue. Therefore, PEEK implants are recommended for this medical procedure. Indeed, the development of bone cells directly on the PEEK implant is observed after a few weeks. This reaction can lead to permanent bone anchoring, making it easier to heal the bone and reducing the risk of long-term complications.

3D printing allows greater freedom of design and the creation of tailor-made parts. When applied to the medical field, each patient needs implants adapted to their morphology or

healing needs [51,112]. A 3D printer such as Roboze One + 400 Xtreme can make implants faster while reducing material loss. Delivery times are reduced to zero, a significant advantage when dealing with potentially urgent operations and surgeries. As previously elucidated, PEEK has certain advantages in the medical field. Here are some concrete examples of what can be achieved with PEEK material: A cranial accident patient victim underwent an operation to implant a PEEK part, representing 75% of its cranial surface. The piece, printed to measure, allowed the patient to recover. More than 500 patients in the United States could benefit from this procedure each month. Parts printed in PEEK have made it possible to protect satisfied patients from the harmful effects of radiation caused by radiotherapy. Impressions have been implanted between an organ and the radiation to protect the latter from the rays' harmful effects.

The 3D printing is tailor-made; the medical team can precisely protect organs and let the rays pass only over the areas that require intervention. Table 2.4 provides a complete description of the different PEEK biomaterials used for various biomedical applications. Likewise, Table 2.4 compares other high-performance thermoplastic materials that are popular options for 3D printing [51,136,137]. Historically, PEEK was not used for high-speed manufacturing expected to the elevated cost of production—the 3D printing of printable hydroxyapatite (HAp) materials to replace lost bone support tissue.

Table 2.4 PEEK-based biomedical devices are included in this list.

PEEK composite	Processing method	Mechanical & service area	Description
Nano-TiO$_2$/PEEK [37,70,138]	At 400 °C, the powder is mixed, and the compression mould is formed.	The bending modulus is 3.8 GPa,	Because of the use of nano-TiO2 filling, the bioactivity is substantially enhanced.
Nano-HAP/PEEK [35,59,117]	At 380°C, the powder is mixed, and the mould is compressed.	The elastic modulus of 4.6 MPa implants.	Nano-HAp/PEEK composites have been found to enhance cell spreading and osteogenic in-vitro.
HAp embedded PEEK [34,60]	Compression moulding, as well as chemical leaching, are used.	Inter-body spinal fusion.	The resultant material shows great promise for use in spinal implant applications.
PEEK blanks [87,137,139, 140]	After the milling process, the acid coating was performed.	14.45 ± 2.57 MPa. Dental prosthesis.	The mechanical characteristics of PEEK covered with silica were improved.
PEEK [22,141,142]	Using a phosphate-buffered saline	A maximum average Force of 1.92kN.	Soaking did not affect PEEK.

	solution, mould and soak at 400 degrees Celsius.	Orthopaedic.	
Knitted carbon/PEEK [143–145]	Micro-braiding yarn and heat moulding at 380°C are used in this process.	Orthopaedic fixations.	The deformability of knitted composite bone plates was shown to be more significant.
Chitosan/PEEK [37,54,146]	Air plasma modification.	Regenerative medicine.	The antibacterial properties of chitosan were incorporated into the polymer.
PEEK PSIs [126,147,148]	–	Maxillo-facial surgery.	There were no problems because of the substance.
PEEK films [36,103,149]	Processing at 180°C with moulding and NaOH treatment	Ophthalmology.	The growth of the apatite layer on PEEK was very sluggish.
PEEK [150,151]	CNC milling.	Skull bone treatment.	Results encouraged the use of PEEK.

2.4.2. Applications of PEEK and composite

This study's systematic review collects current knowledge on the PEEK of the coating method using cHAp. The gathered data demonstrates that the coating procedure may benefit the characteristics of PEEK. Additionally, the hardness of the PEEK surface influences the penetration of cHAp particles before coating. Increased crystallinity resulted in stiff characters and reduced cHAp particle penetration. The high-temperature coating process changes the crystallinity of the post-process component, resulting in localised deterioration and thermal stresses in the polymer[146-149]. As addressed extensively in this study, the mechanical properties of PEEK are temperature-dependent. Notably, implant cHAp particles may initiate pre-cracks and act as stress concentrators. This study demonstrates that crack propagation is the primary failure mode for PEEK implants during fatigue, occurring between Tg and crystalline fusion temperatures of 143°C and 343°C, respectively, at a temperature of about 37°C. cHAp particles may initiate fracture propagation in PEEK by lowering the stress intensity factor needed for crack development [146,152,153]. The particles' penetration depth, crystallinity, and the stiffness of the resin around the particles are all included as factors. Bone growth around the implant depends on the implant's morphology and the location of the cementation line. Mechanical adhesion phenomena are often ignored, although cell growth and tissue formation directly affect cell attachment. The development of PEEK as a biomedical material implant for bone tissue engineering and general polymeric applications is

depicted in Figure 2.8. Mechanical contraction and activation factors are similar and simplified at the macrostructural level by the viscoelastic properties of the fibrin matrix and new osteoid. The Forcing effects on the implant are negligible when considering a recommended first healing time of three to six months. In addition to the theoretical contribution obtained from a review of previous research [89,127,154,155], these characteristics allow the construction of a preliminary model of the formation and repair processes at the polymeric implant-human tissue interface.

An orthopaedic embed is a medical device that replaces a missing joint or bone and stabilises a fractured bone. The clinical embed is mainly constructed using maintained steel and PEEK for excellence. The plastic layer is designed to resemble a ligament. Interior obsession is an orthopaedic procedure that involves the placement of precise inserts to repair a bone. During the surgical treatment for fractured bones caused by internal preoccupation, the bone parts are first reduced to normal. They are secured in place with the use of internal fixators. Plates, screws, nails, pins, and wires are examples. Knee tendons that are in good condition benefit the joint. Current embedding systems comprehend the common's complexity and faithfully imitate a typical knee movement. For instance, in a healthy knee, the joints stabilise the joint. Where the femur, tibia and fibula meet at the tibia, many implanted planes protect the patient's tendons, some inserted by others. The patella of the kneecap rests against the femur in the front portion of the knee. These bones are connected by tendons, muscles, and ligaments that assist in shaping and adjusting the joint axis [156–158]. Figure 2.9 depicts the method of implanting PEEK composites for medical purposes. Although four bones surround the knee joint, an implant affects the femur, tibia, and patella. Due to the three-part nature of prosthetic knee joints, many tooling companies develop and produce knee joints composed of various metals, plastic, and ceramic.
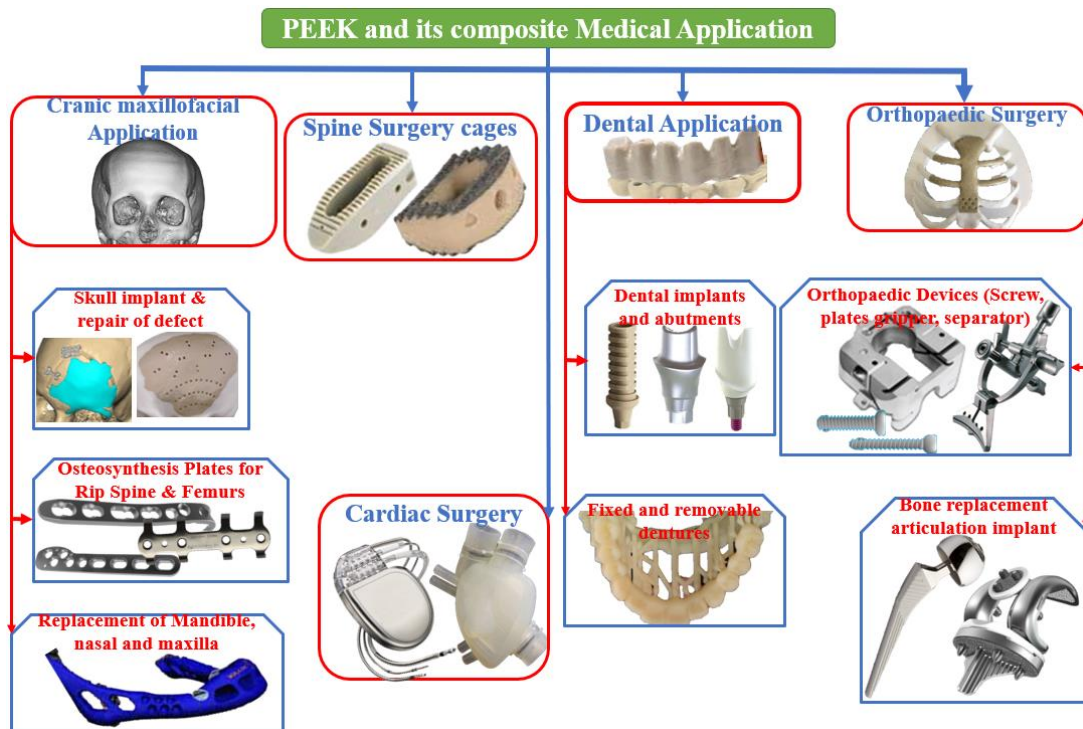
Figure. 2.8 Implantation of PEEK composites in medical applications is being investigated [61,140,159,160].

Implants are intended to either completely replace an organ or significantly enhance the function of one or more organs. As a result, it is completely suited to the patient and their body. When conventional production techniques are used, customisation is time-consuming and costly. In contrast, medical 3D printing comes into play, allowing for customised dental implants. Numerous companies have entered this sector and manufacture bespoke medical devices using 3D technology. 3D printing offers many benefits, including converting a digital 3D model straight to a 3D anatomical model. It is critical to save time by delivering very high precision. Assuming it is worthwhile, this usher in an era of medical device personalisation. 3D anatomical sculptures with complicated geometric forms can also utilise conventional manufacturing methods.
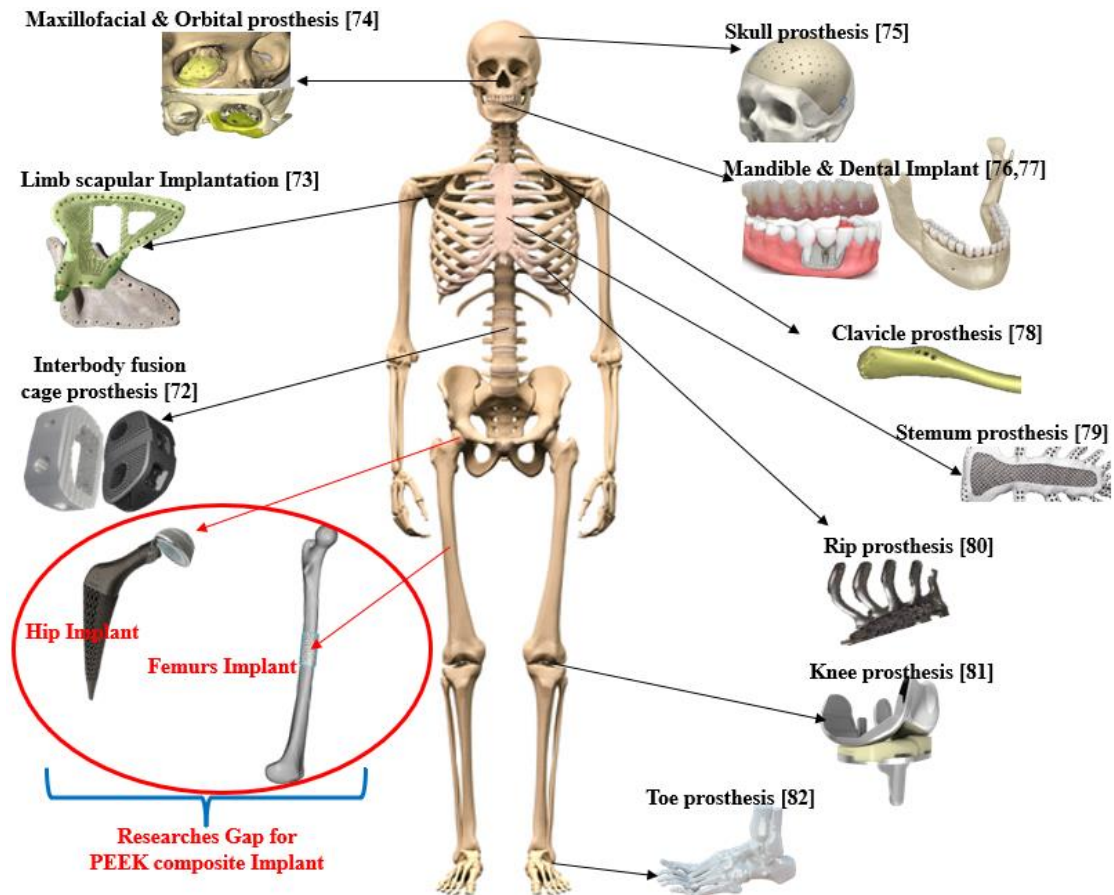
Figure. 2.9 Examples of PEEK implants used in medical orthopaedics, as shown in a schematic diagram [45,64,161,162].

Talking about different types of bone and bone-implant as an application of PEEK and its various composite. There is a need to discuss how to produce both the internal and external structure of a bone and implant to have a good design and geometric design. The next section will review the lattice structures that help mimic the bone structure that makes a struct and good biological structure for cell tissue growth, known as a scaffold.

2.5. Lattice structure

Interest in obtaining as light as possible while maintaining appropriate mechanical properties has generally increased in the transport sector, especially in the automobile and aerospace industries [163]. Some lightweight materials consist of sandwich panels with micro-lattice cores or micro reticules. Due to their broad spectrum of possibilities for future applications, these new structures have been the object of further investigation in the last few years [164,165]. These applications are light structures, micro lattice structure thermal insulators, energy absorbers and explosives protection. Mechanical

61

strengths of these structures depend directly on the relative density (ρ), Ntopology of the rays, formed system and angle. Some studies have established that pyramidal structures provide greater strength.

In Beam Lattice, a lattice represented by a cylindrical or rectangular strut connected and linked together the element in different directions can be avoided. They could cause less similar collapses and not achieve rigidity [164,166,167]. In contrast, they are more sensitive to localised deformations and suffer from localised damage in a specific orientation. Therefore, the proposed study on random structures allows the mechanical properties to be improved in all directions, causing eliminating natural fall plans for a type of general collapse. In addition, the potential for providing such structures is very high, although there are some drawbacks. One of them involves manufacturing. In the maturation process, no effective optimisation method has been established to fabricate structures of this type with given properties. There is also no model to predict a sufficient collapse of the arrangements. The resolution to these minor inconveniences places this material as a great alternative. As far as fabrication is concerned, the most innovative methods are now available in 3D fabrication varieties.

The function of the type of material to be constructed determines 3D fabrication technology. The material selected and the manufacturing process directly influence the properties of the micro-lattice structure [164,168,169]. The element is reasonably used as a lattice structure to apply the micro-reticular materials as a structural unit of some construction. This type of configuration allows a flat surface material to form part of a flat surface. The sandwich-type panel also enables the distribution of features across the structure to benefit from a type of configuration. Some studies have reported the number of variables to manufacture microstructures for metals. Figure 2.10. shows different samples of Lattice cells and fabrication processes applied to bone implants. The sheet TPMS is the soft sheetlike structure used to represent the internal part of bone made of different designs. The skeletal TPMS is also used to generate the internal structure of the bone structure, which is made of a beam structure strengthened with varying radios of curves. However, an extrapolation of polymeric materials was done. Some researchers [170,171] identified four variables to appropriately assign a polymer to the function of its application as required: morphology, cell type, material and manufacturing process.
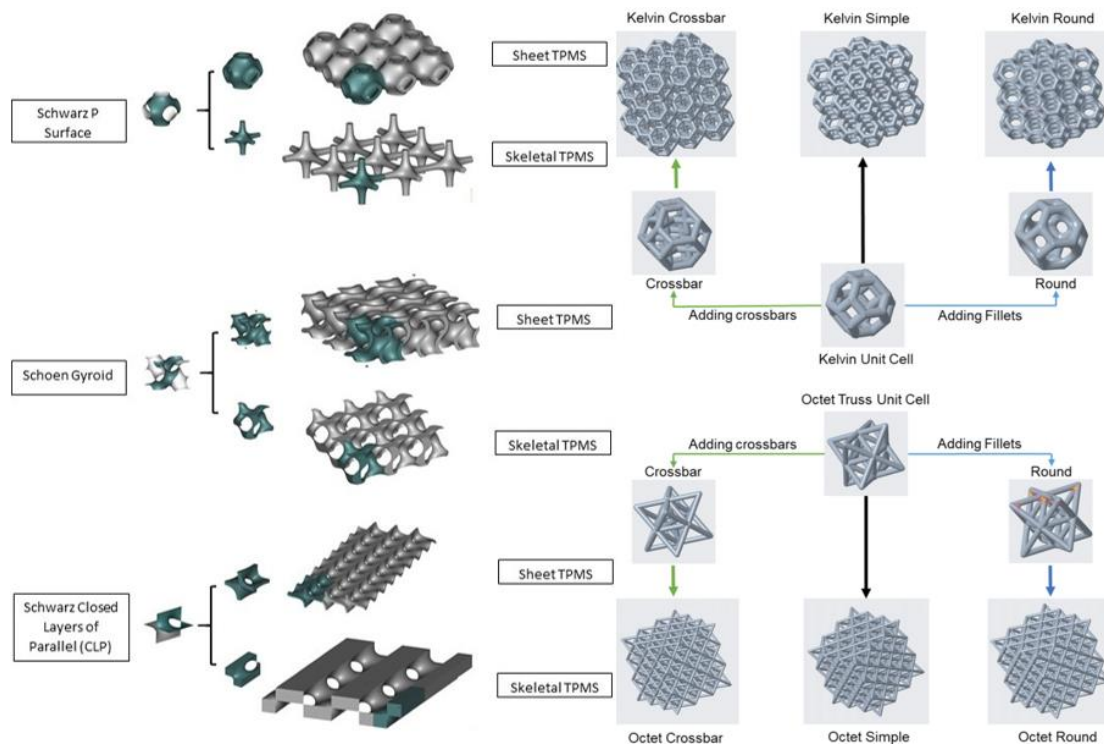
Figure. 2.10. Samples of Lattice cells and Schematic process for implant fabrication [172,173].

2.5.1. Porosity in 3D printing

Various porous metallic materials have assisted the biological fixation of implants throughout the past two decades. Bone ingrowth around and with the porous surfaces is crucial for the effectiveness of cementless implants. As first-generation ingrowth surfaces have given way to developing a new generation of metallic foams with the potential to enhance cementless technology in all orthopaedic parts, porous biomaterials have grown over time [159,174]. The main things that an ideal porous metal should have are biocompatibility, which means that it should support regular cellular activity without harming the host tissue locally or systemically; it should be osteoconductive and osteoinductive. It should be able to cause blood vessels to grow inside or around the implant. Also, it should not make people sick. Size of pores: Scaffolds should have both large and small pores, which must be linked. Microporous and macroporous scaffolds can do better than scaffolds with only one porosity type. Porosity worsens mechanical properties like compressive strength and resistance to corrosion, which is a shame.

2.5.2. Lattice biomimetic of bone structure

Bone tissue is a connective tissue of stable composition that performs supportive and protective functions. It differs from other body tissues in its high inorganic materials and contains mineral salts combined with the organic matrix. The composition of the bone varies according to each person's age, habits and health. The prominent inorganic bones are calcium and phosphate; they form between 60 and 70% of the bone weight and have solid consistency [175,176]. Water is also abundant in living bone; its percentage by weight is up to 25%, and most in the organic matrix. The rest of the bone comprises other substances, such as proteins. The bone mineral is immersed in collagen protein fibres with different orientations. Collagen is the main element of the organic components of bone. Fibres are rigid and flexible; they resist stretching and have little extensibility. Collagen is the main fibrous component of many skeletal structures [177]. Scaffolds must develop the role of mimicking the extracellular medium to guide and favour the cells' adhesion, proliferation, and migration during tissue regeneration. To conveniently fulfil this function, the design and manufacture of scaffolds must comply with the following requirements.

To have interconnected pores of adequate dimensions to favour tissue integration and vascularisation, the blood supply in its implantation *in-vivo*. Therefore, the scaffold's porosity also affects the diffusion of nutrients and gases necessary for cellular respiration. Bones are mainly composed of cortical bone and trabecular bone. The spongy bone occurs in the epiphyses of long bones inside the minor and flat bones [154,167,174]. The spaces among the trabeculae are occupied with red bone marrow. The cortical bone covers the porous, dense structure like ivory. Figure 2.11 shows the anisotropy features of microstructures for bone replacements with porous lattice implants with an application of AM in orthopaedics. A healthy bone structure mimics a lattice structure which helps control the design and develop a structure that is not just random. Producing a redone system like bone will not give appropriate control on the structure for better mechanical strength.
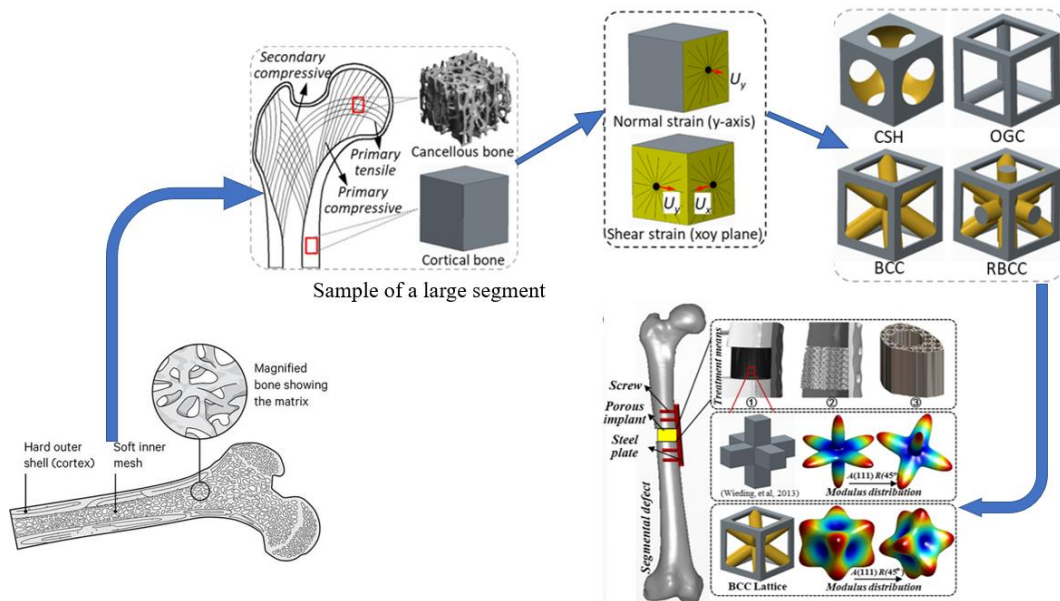
Figure 2.11 Anisotropy features of microstructures for bone replacements with porous lattice implants with an application of AM in orthopaedics and a healthy bone structure mimics a lattice structure [174,178,179].

2.5.3. Homogenisation in lattice design

The geometric boundary method calculates time history and spherical coordinate systems when a program performs homogenisation and returns FEA results on cellular materials. The unit cell's characteristic length is generally considered several degrees lower than the expected length of the component. The homogeneous representation saves computing time when designing dense structures [180,181]. Homogeneous representation is a way of describing a dense network structure without displaying it in the model. Mathematical definitions are stored and used in Creo Simulate to analyse the structural, linear, static, and modal responses. This result translates to less time spent defining the mesh. Homogenisation techniques, reduced model size, faster simulation, and dynamic behaviour of periodic solids can also be verified. Multiscale approaches based on non-asymptotic amplification were established in traditional homogenization to acquire data equal to data continuity on the characteristics and shapes of unit cells. Still, a study of the cell unit is critical to understanding the macro-level mechanical response of the material [48,178,179]. Various analytical methods and numbers have been proposed for the lattice cells in the implant struts, represented by a different colour in Figure 2.12. Also, Figure 2.12 depicts the schematic process of the experimental lattice process of fabricating femur and hip implants.
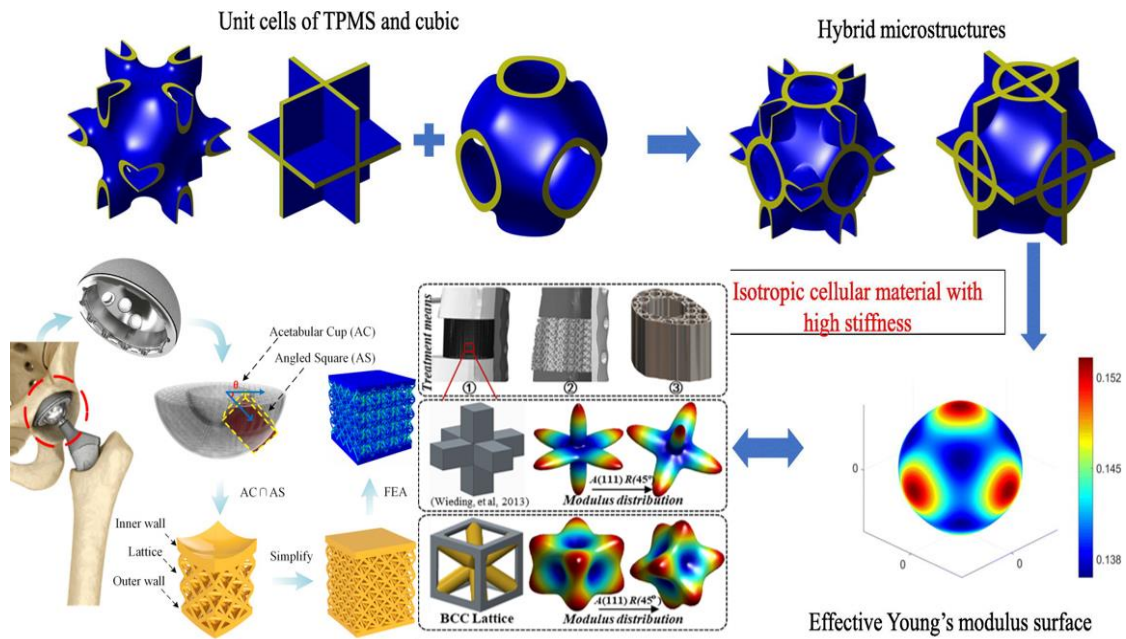
Figure 2.12 Sample acetabular function on an isotropic lattice of a large segment of bone repair with porous scaffold using homogenisation [178,182].

In terms of the practical characteristics of a unit cell, the primary goal is to achieve macro-material properties. Homogenisation often eliminates the need for an in-depth and sometimes impracticable study of the whole cellular microstructure. Matrix-based methods have recently made it feasible to homogenise flat features using Bloch's theorem and the Cauchy-Bore hypothesis materials. The characterisation of cellular materials has benefited from the development of discrete homogenisation methods [65]. A homogeneous property and discrete sum of the equilibrium eigenvalues are turned into a continuous stress-strain relationship. For materials having periodic microstructures, numerical techniques such as the theory of asymptomatic homogenisation have successfully predicted their effective mechanical characteristics. The simulated combined stress response and damage modes were compatible with the experimental findings. The main benefit of anisotropy and homogenisation over other homogenisation methods is that the stress distribution in the unit cell can be precisely calculated and utilised for a thorough study of material strength and damage. Various articles' primary issue in any particular solution method is choosing the most effective homogenisation approach with the lowest computing cost. However, this effort is often accompanied by trade-offs. For example, closed-form equations may rapidly determine mesh materials' functional characteristics [174,183]. However, accuracy problems may emerge if the

microstructure does not match the model's assumptions. This led to discussions and a critical review description of the cell generation process on a scaffold for bone implant in the next section.

2.6. Cell regeneration and growth on a scaffold

As defined by the International Society for bio fabrication in 2016, fabrication can be described as an enabling biological functional product with a structure organised from cells, molecules, and biomaterials such as microtissues of materials and cells through bioprinting and other subsequent automated processes. Artificial biomedical implants have become increasingly complicated because of advancements in manufacturing methods and the development of innovative materials [184,185]. The recent dealing with significant bone abnormalities, the materials utilised in therapy, and potential screening methods are critically reviewed. Materials articles can be grouped into three major groups depending on the materials used to create innovative bone graft alternatives. Polymers are the three categories [49,186]. As previously stated, the bone tissue research community is not particularly concerned with non-biodegradable polymers. However, several non-biodegradable polymer techniques show promising results in surface modification to address future implant infection issues. Many earlier investigations employed Mesenchymal stem cells (MSC) to demonstrate in vitro biocompatibility and functioning of developed materials scaffolds [73,187]. MSCs are selected because they are regarded as the most promising choice for cellular support of implant recovery. They include the in vitro model that closely reflects the natural bone healing process. Their multilineage differentiation and anti-inflammatory behaviour are reasons for this. Although MSC is very straightforward to acquire from a patient's adipose tissue, the cell number separated from the tissue is too low for direct therapeutic usage [188]. As a result, following isolation, stem cells must be grown *in-vivo*. Following the expansion, stem cells with osteoinductive capabilities can be placed on the produced scaffold. These features signal that MSC always develops into osteoblasts, resulting in the scaffold's highest potential initial osteoblast cell population [143,189]. Figure 2.13 shows implantation, demonstrating injection into a bone tissue defect. The distribution's structure, structure, and size influence the structure's mechanical characteristics and migrate cells. Bio-absorbable materials, composed of biodegradable and bioabsorbable materials, are biodegraded by an enzyme attack.
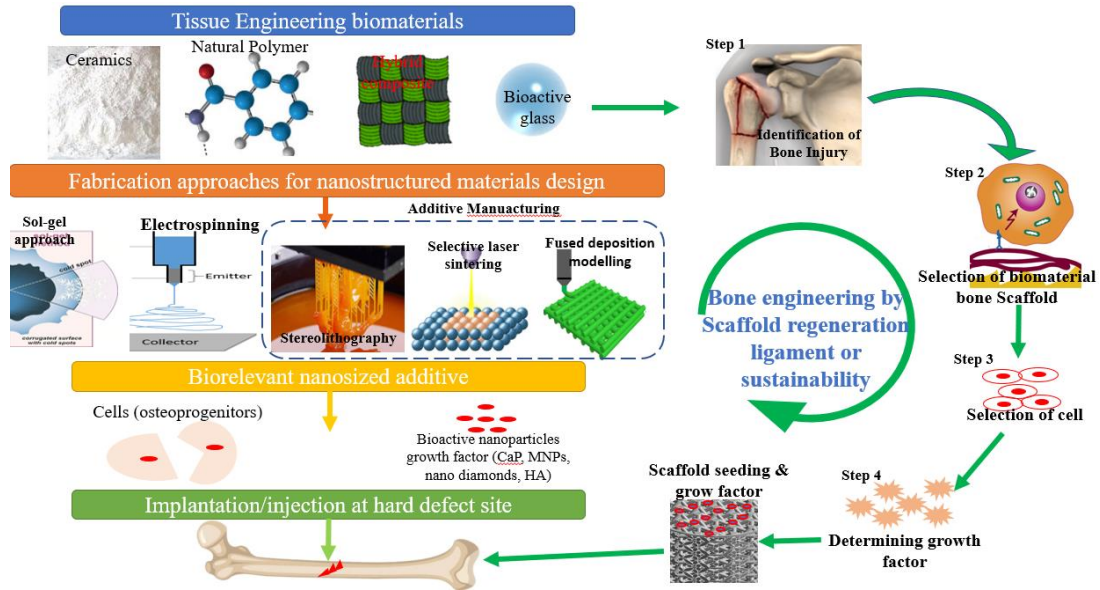
Figure 2.13. Implantation, demonstrating injection into a bone tissue defect.

2.7. Summary

The discovery of innovative materials for fabricating support structures for bone tissue regeneration is a high-priority research topic for developing new therapies for musculoskeletal disorders. Because of the literature review performed in this chapter, it is fair to conclude that, given the complexity of replicating biological tissue, there is a tendency to combine different components to maximise their relative advantages. Modifying the surfaces of structures used as bone regeneration supports is another approach to improving their properties. Surfaces are treated via plasma functionalisation or the application of bioactive coatings. The activation formulation for PEEK-based composites and the surface treatment of PEEK-based composite components were studied in this research. As shown in the present chapter's discussion, this material was selected due to its ability to regenerate bone tissue. Finally, the benefits of the reviews demonstrate the superiority of AM over other conventional manufacturing techniques for porous tissue engineering applications. The activation and surface treatment of PEEK-based composites is investigated in this research due to their shown capacity to repair bone tissue. This research demonstrates the advantages of AM techniques over conventional methods of porous tissue production. The study illuminates many critical aspects of how Hap and PEEK interact to stimulate physiological fluids. These studies will contribute to a better understanding of nanomaterial interactions.

2.8. Research gaps

The hypothesis was that computer modelling and FEA of various lattice to biomimetic bone structures would help understand the strength of the resulting PEEK-matrix composites. There is no report on combining these methods to reduce rGO and bioactive calcium hydroxyapatite (cHAp). A novel porous lattice structure PEE-K composite for hip and femur bone implants with increased biomechanical strength and biomimetic bone structure has not been studied. The mechanical characteristics of these composites for bone implants have not been investigated. This work aims to describe a model of different new lattice PEEK composite reinforced with rGO and cHAp applied to bone implants like hip and femur implants. The objectives of this work were to perform computational analyses on various lattice PEEK composite models that characterise their morphology, structure, and mechanical properties. Moreover, conduct a preliminary investigation into how cells respond to combined modifications of rGO and cHAp in various proportions and the formation of surface macropores.

Chapter 3
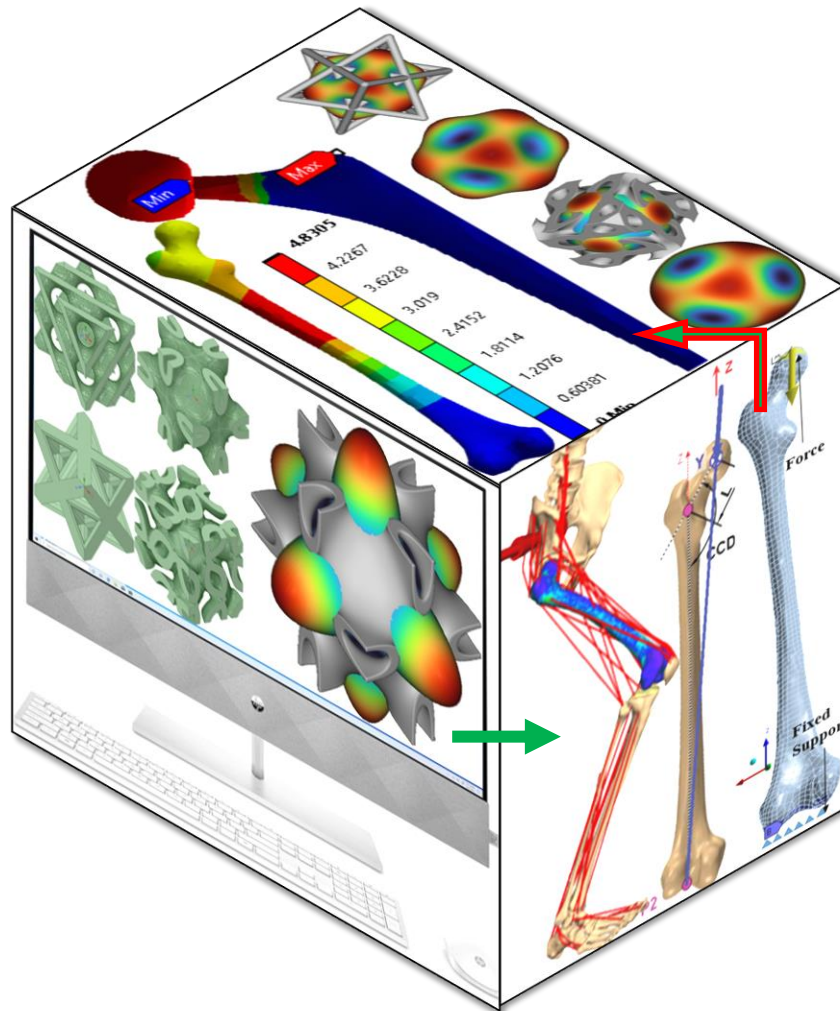
Design lattice structure to mimic bone implant

CHAPTER THREE

3.0. DESIGN AND SIMULATION

3.1. Design lattices cell

Traditional subtraction methods, such as matrix plates, cannot produce complex structures with FDM. In the FDM process, objects are built up layer by layer. As produced via AM, the composites must create ultra-thin 3D designs for macro metric bone implants in length and breadth. These materials exhibit characteristics that are unique and, at times, startling. In this thesis, PEEK pore scaffolds with improved capability and lower weight were designed. After reviewing the literature, ten different lattice structures were selected, and the design unique to this thesis applies to hip and femur implants. These include Octahedron-cross, Octet-Truss, BCC-octahedron and Truncated octahedron. The beam lattices and a combination of different lattice structures to give an optimum design and porosity are used for the study. Also, six formulas, such as gyroid, diamond, primitive, neoviuos, splitp and lidinoin lattice, were selected based on their strength and structure to mimic bone structure for hip and femur implants. The cell design's different lattice structures and pores are compared in Figure 3.1, showing their porosity and cell combination. This results in increased penetrability to body fluids for the Force applied to each cell structure due to the increased penetrability. It is under computer control that the ideal geometry of the final complicated item is developed. 3D printed PEEK filler granules for filament were used, replacing composites 80-150 microns in length and 7 microns in diameter, 2x 2x2mm. A cell of Ø0.4 mm is shown in the porous PEEK-rGO-cHAp design configurations sample model. This study sought to improve understanding and offer simulation guidance by simulating and analysing various grid designs using finite element analysis (FEA) software. Since enhancing the part's homogenised characteristics, the components in the homogenisation process have a cumulative effect. Figure 3.1 presents five selected lattices to compare their porosity, pore size and structure to natural bone and know the easy movement of fluid within the structure. The average measure of the beam's cross-section width and thickness in open-cell specimens is included. Figure 3.1 shows the design of different lattice structures applied to hip and femur bone implants. The idea of selecting these types of lattice start cures is based on the lattice cell's mechanical strength and structural network. Some of these designs

combine lattice structures to make up one for better mechanical strength. This combination of cell structures is unique to this research. It has not been applied to PEEK and composite like cHAP and rGO before except by the author of this research indifferent ratio combination comparison.
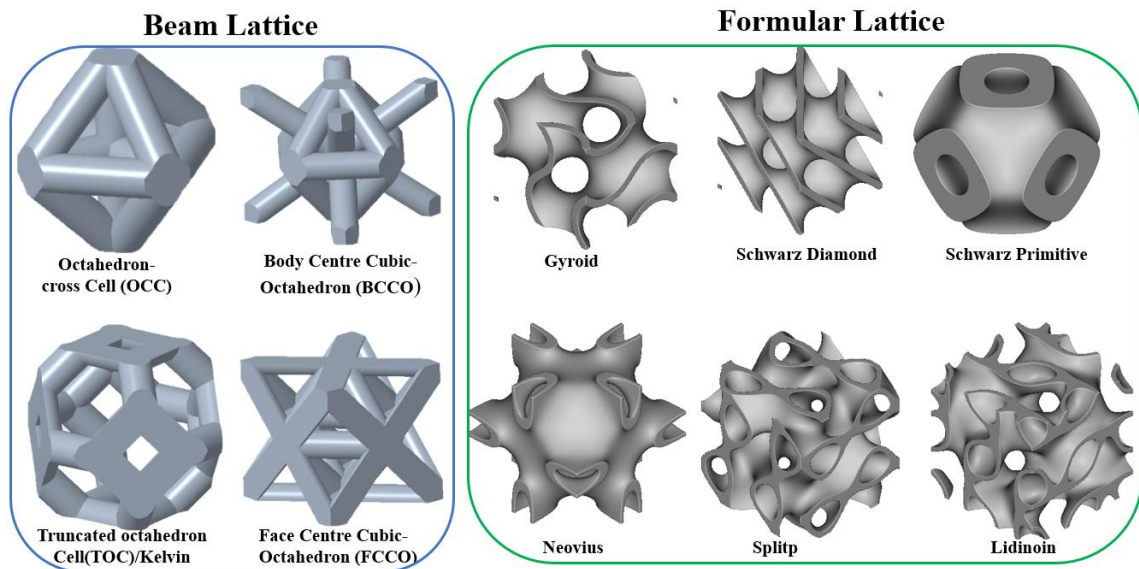
Figure 3.1 Proposed lattice CAD models for bone structures designed for this research.

As shown in Figure 3.2, the probes with an open cell correspond to a micro lattice with a cubic beam repeated periodically. Also, Figure 3.2 shows a section of the five samples from the ten lattice designs. The different beam lattice scaffold increases strut thickness, leading to a difference in porosity. With inclination angles, neither one of the beams is blocked by the other beams in x, y, or z axis. When designing, the near wire was created by considering the same structure as the micro lattice type. The uniqueness of the beams vanishes due to an increase in thickness and is substituted by walls, which maintain the same geometry between the nodes.
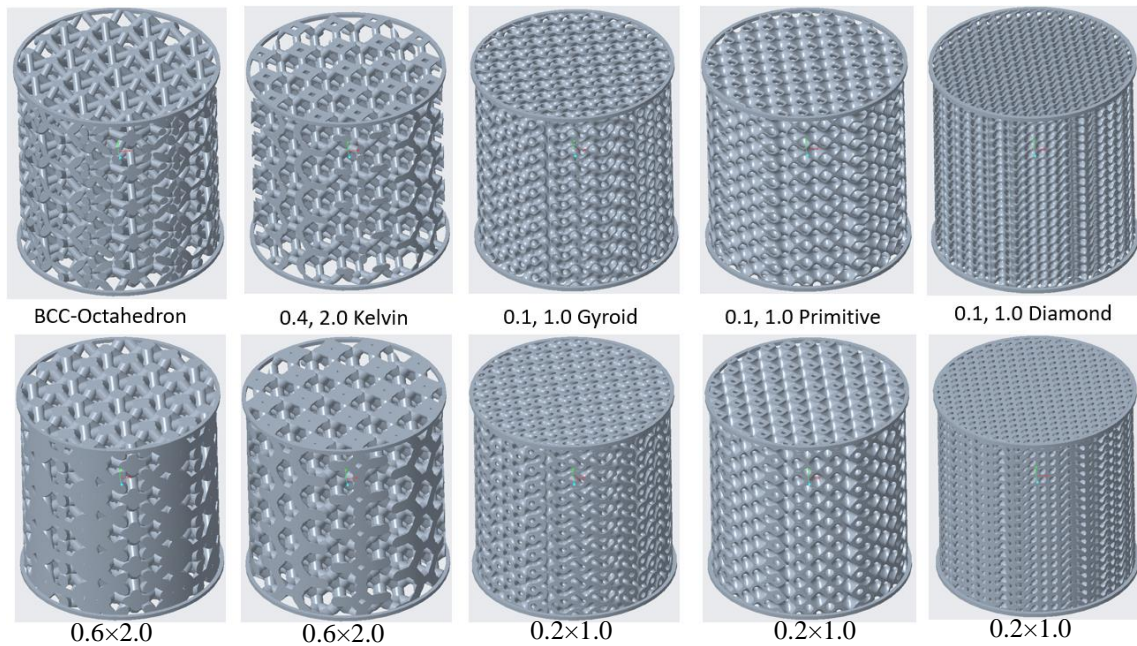
Figure 3.2. Some different beam and formula lattice scaffolds and increases in strut thickness lead to a difference in porosity from the beam lattice structure.

3.2. Lattice Cells Analysis

Lattice cells exhibit unique and often unexpected characteristics in a micrometre-scale for an implant. They form lightweight biocomposites that revert to their original structure when compressed. 3D printing was utilised to create PEEK pores that were more capable and lighter. Figure 3.3 depicts a comparison of 4 lattice holes for the Force to the unit cell of a 2 x 2 x 2 mm of 0.4 mm strut demonstrating displacement and a 10x10 mm model of a scaffold: (a) octet-truss, (b) octahedron that has been truncated, (c) octahedron-cross and (d) octahedron BCC. A novel method for 3D printing bone structures that use a macro cell structure with controlled porosity was developed and modelled. In Figure 3.3, 4 lattices were compared with porous designs, which increased body liquid inflow capacities for the Force to each cell inside the PEEK composite and structural strength with different volumes and affected the porosity.
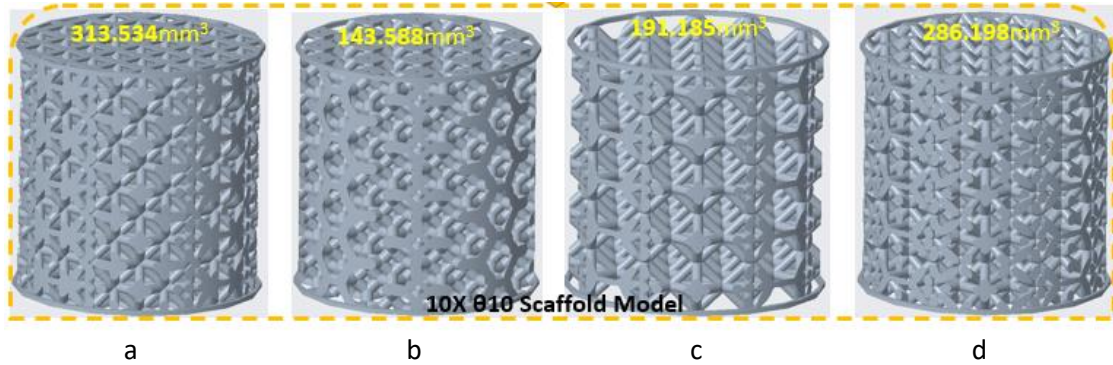
Figure 3.3. Comparison of 4lattice holes with force applied to the unit cell of a 2x2x2mm of 0.4mm strut demonstrating displacement of scaffold (a) Octet-Truss (FCCO) (b) Truncated octahedron (TOC) (c) Octahedron-cross (OCC)(d) BCC-octahedron (BCCO) with different volume and affect the porosity

After reviewing the literature, four lattice structures for FEA analysis, including Octahedron-cross, Truncated octahedron, BCC- octahedron and Octet-Truss, are used to study. These structures are selected based on their mechanical strength and biomimetic design, like the internal structure of bones that can benefit from topology optimisation. Some of the lattice structure is described in Table 3.1 with the corresponding pore size. The comparison of the four pores of the network with the porous lattice design results in increased permeability to body fluids for the force applied to the cell inside the PEEK compound structure due to the increased permeability. The volume and porosity ratios of lattice structures are presented in Table 3.1 [49]

Table 3.1. Designed lattice structure

Samples	Volume (mm³)	Porosity (%)
FCCO	313.534	58.45
TOC	143.588	80.97
OCC	191.185	74.66
BCCO	286.198	62.07

Bones may have an excellent capacity for the same weight and size because of the cell's mechanical strength, shown by its ability to keep its intricate 3D mesh structure after forty optimisation cycles [150]. It is required for transporting body fluids but has insufficient pressure. This new method is critical for mobile phones and medical equipment applications. Because of their lightweight and high mechanical strength capacity, the FCCO, diamond, and scaffold structures for 3D printing with two cells of 0.25 and 0.2 mm for diamond framing were chosen.

The apparent density of the samples after sintering was estimated using Archimedes' method. The model was weighed dry for 15 minutes before being accepted as a saturated water sample. The model was immersed in boiling water to allow air to travel through the opening. On the other hand, the submerged sampling measured water-changing pores. The scaffold equation is used to calculate total porosity (3.1). The relative density of a scaffold can be determined by dividing it by its theoretical density with the lattice density. The ρ_{app} 1.3kgm^{-3} represents the theoretical density of PEEK, whereas R represents the apparent density determined using the technique. Archimedes' principle estimated the sample's apparent density after manufacture. The overall porosity of the scaffold is calculated using Equation (3.3). The relative density can be estimated by dividing the material thickness by the theoretical appearance using Equation 3.1-3.3. The m represents the mass of the scaffold m' Represent the mass before immersing in water.

$$\rho_{app} = \rho_{liq}\left(\frac{m}{m'-m}\right) \tag{3.1}$$

$$Porosity\,(\%) = \left(1 - \frac{\rho_{app}}{\rho_{the}}\right) \times 100 \tag{3.2}$$

$$Relative\ density = \left(\frac{\rho_{app}}{\rho_{the}}\right) \times 100 \tag{3.3}$$

Where ρ_{app} Is the apparent density in the air, ρ_{liq} Is the actual density of the substance in water, ρ_{the} is the density of the scaffold

3.3. FEA of Homogenised stiffness mechanical properties

PTC Creo 8 software was used to create the porous structural design. The porosity was assessed to verify the mathematical model of porosity and geometric parameters and establish its applicability. We tested porosity to verify the mathematical porosity and geometric characteristics model and know whether it could be used in real-world situations. The theoretical and experimental results are shown in Figures 3.4-3.8, as subsequently summarised. Porosity rises, yet the difference between theoretical and CAD-modeled computed values widens. However, the inaccuracy stays at 5% in this instance. Figure 3.4 and 3.5 compares the lattice models t stress and strain graph behaviour of the Octahedron-cross Cell (OCC) Body Centre Cubic-Octahedron (BCCO) model. Figures 3.6 and 3.7 also disrobe comparison of FEA of truncated octahedron cell (TOC)/Kelvin and face centre cubic-octahedron (FCCO). It can be shown from the graph

figure 3.4-3.7 that the strength of the composite increase as the composite percentage increase, which shows a favourable amount of increase in strength, toughness and flexibility.
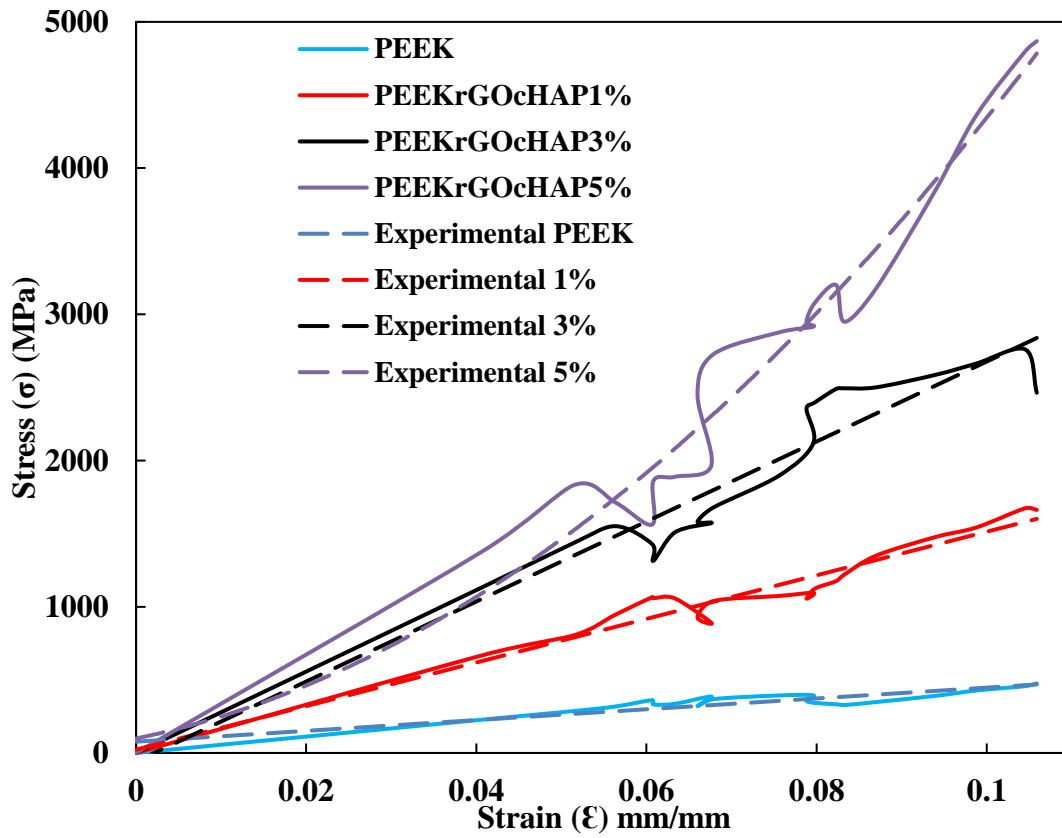
Figure 3.4 Comparison of Octahedron-cross Cell (OCC)
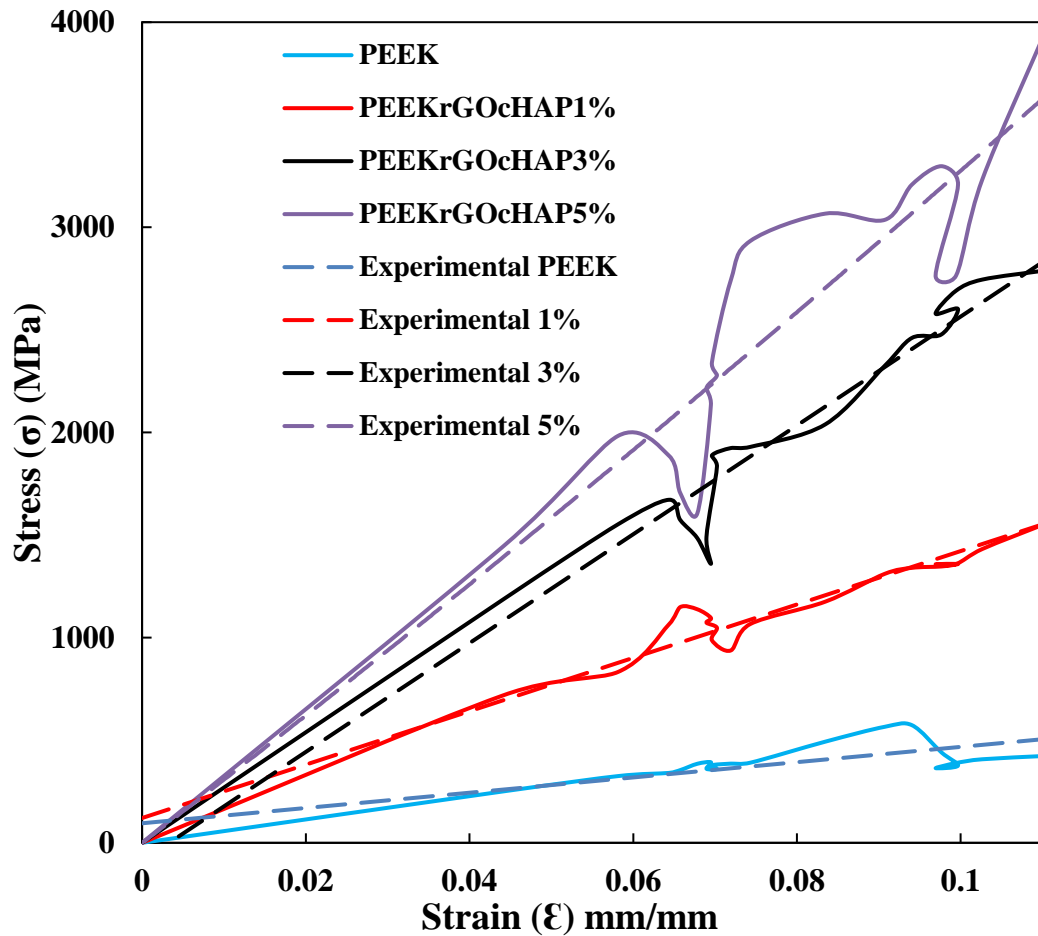
Figure 3.5 Comparison of Body Centre Cubic-Octahedron (BCCO)

At a full domain scale of 14.5 and 375 mm^2, 40 points were found using the one corner area-scale method on the first day, 15.1 and 538 μm^2 on the first day, and 14.3 on the 7th day, shown in Figures 3.6 ad 3.7. Also, a tensile test was performed using a dog-bone structure on several lattice structures as on the composite and post-mechanical strength.
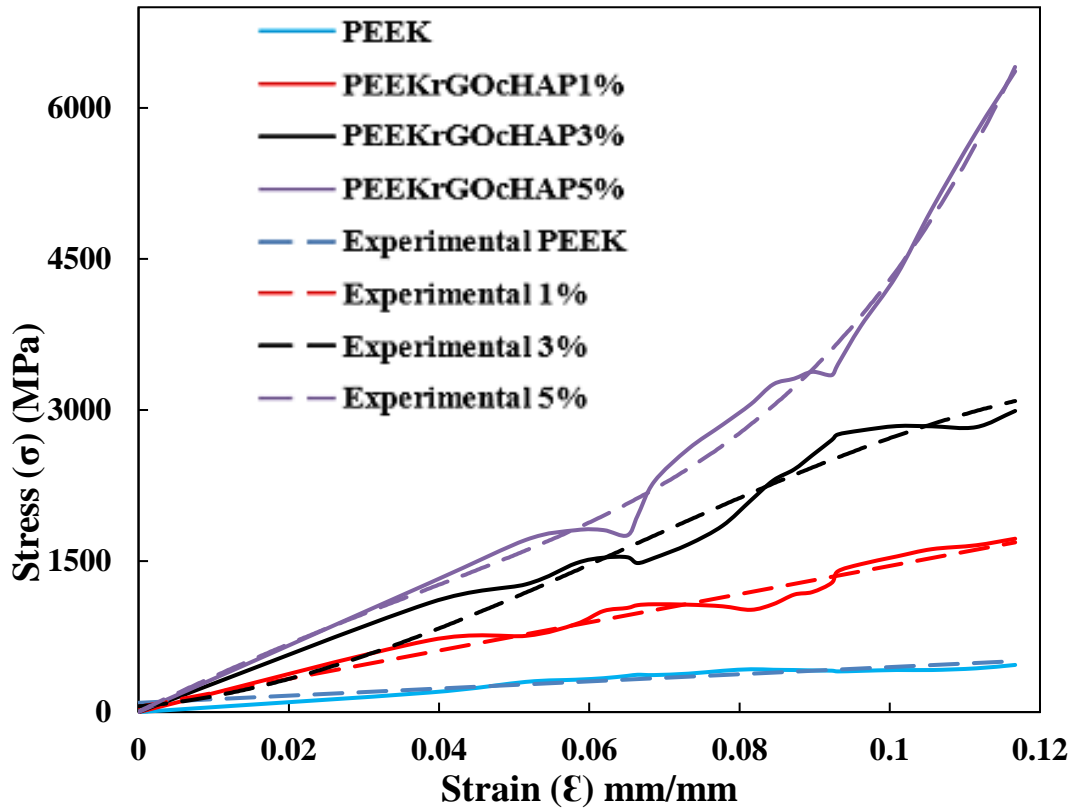
Figure 3.6 Comparison of TOC/Kelvin
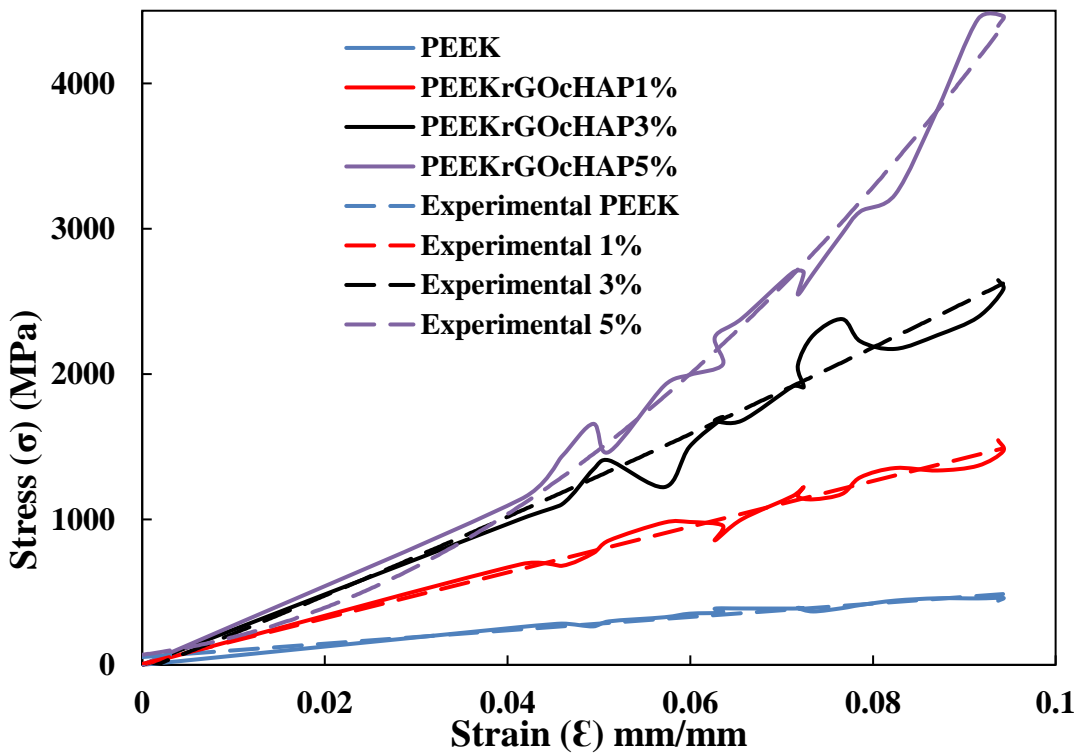
Figure 3.7 Comparison of face centre cubic FCCO.

3.4.   Model of femurs bone

The model was created more traditionally, beginning with a single unit cell, even if it may have been created using an equation-based modeller. It repeated it three times to get full-size cylinders. Figure 3.8 depicts the modelling approach, which includes the relevant measurements, a femur bone model with applied force and boundary conditions, and an iterative simulation programme for bone remodelling. The design selection was affected by manufacturing restrictions and the required pore size for sophisticated tissue engineering applications. Compression, performed on four samples from each structure, was the best and ideal choice for femur bone in terms of porosity and strength required for the four cells due to their strength. The reduction was parallel to the direction of the 3D printing building. The connections contacts have object contacts of zero. The Femurs bone model was analysed with a face overlap tolerance and cylindrical Faces, which helped search across model bodies [49,181]. The model was designed and analysed using associativity with no coordinate systems with advanced geometry options. Reader mode saves updated files in the software using smart CAD updates. An import facet quality source with a stitched surface is used in the 3D analysis in place of mixed import resolution, and disconnected geometry is processed with enclosure and symmetry.
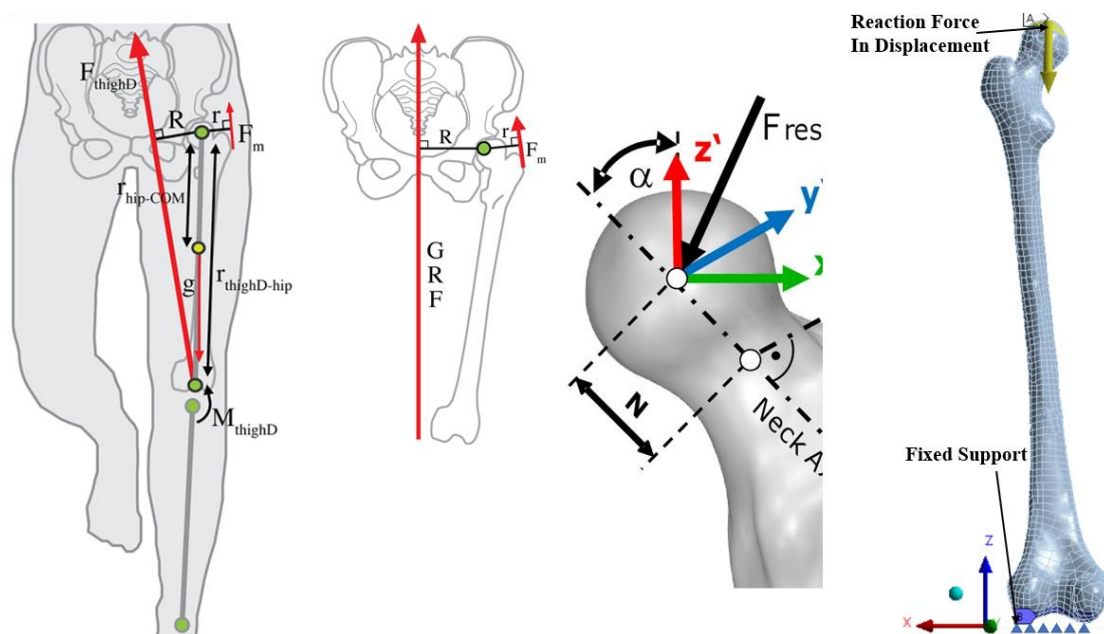
Figure 3.8 Model of femur Hip bone showing applied Force, boundary condition, and iterative femur bone geometry remodelling[50, 182].

Since the stiffness behaviour was adjustable with a coordinate system set at the default coordinate system, a reference temperature provided by the environment, and the reference frame Lagrange equation, the femurs bone model had 4444 nodes and 19772 elements. The volume of the bone is 282.91 mm^3, its mass is 3.6779 kg, and its centroid distances are 7.0653 mm, 15.055 mm, and 26.621 mm. The Moment of Inertia Ip1 is 7.59x10-3 kg/mm^2, the Moment of Inertia Ip2 is 7.61x10-3 kg/mm^2, and the Moment of Inertia Ip3 is $1.04x10^{-4}$ kg/mm^2. In the meshing analysis, the presentation style employs a geometry setting at the physics default of an explicit element order linear with a default element size. The centre of the original size seed has a coarse span angle. The enclosing box of the assembly has a diagonal of 43.16mm, a minimum edge length of 6.49x10-3mm, and an average surface area of 0.235 mm^2. The mesh quality check was accurate, with a high smoothing and no mesh metric inaccuracy of target quality default 0.05. The inflation does not use automatic inflation; instead, it grows at a rate of 1.2 at a transition ratio of 0.272 of the option's top five levels. The investigation was restricted to the inflation method without access to advanced settings. Figure 3.9 shows a Slipt, Lidinoid, Diamond and Gyroid lattice structure for the femur bone and a typical Force application on a unit cell for analysis. The number of central processing units for parallel part meshing was set to the program-controlled setting at straight-sided elements with rigid body behaviour and full mesh. The model employs program-controlled triangle surface meshes with topology verification and pinch tolerance while producing a pinch on refresh.
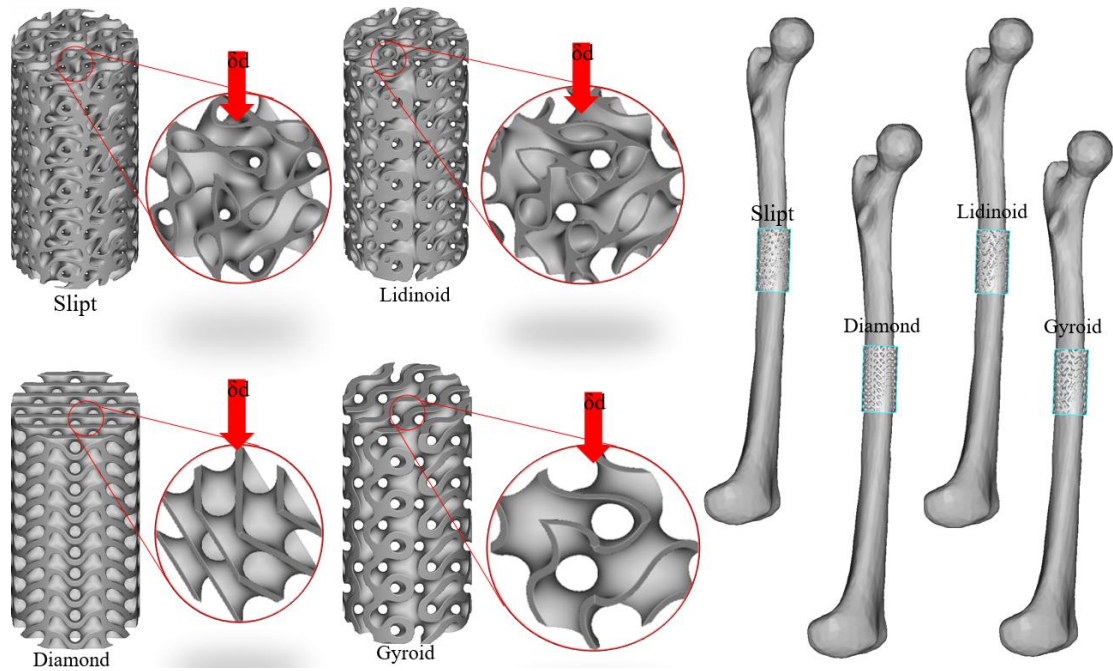
Figure 3.9 Lattice structure implant for femur bone and typical Force application on a unit cell for analysis.

3.5. Result of Femur Design and Analysis

PTC Creo 8.0 software Copyright © 2022 PTC Inc for design was used to generate the lattice and then updated in Ntopology. The Ansys workbench and the Ntopology software were used to model the excellent homogenisation of the methods. Selective electron beam melting was utilised on a preheated 10mm stainless steel beginning plate to construct bars with a 10mm supporting structure immediately on the starting plate after being heated to 330°C. High-purity helium gas was utilised as a controlling gas to keep the powder from charging throughout the process, allowing complete control of the vacuum. The powder recovery system was able to extract semi-sintered powder particles completely. Figure 3.10 depicts a von Mises stress of the femurs bone FEA of (a) PEEK, (b) PEEK-cHAp-rGO at 1wt% of rGO and 30 wt% of cHAp, (c) PEEK-cHAp-rGO of 2 wt% of rGO and 25 wt% of cHAp and (d) PEEK-cHAP-rGO of 3 wt% of rGO and 20 wt% cHAP, showing more comprehensive stress and Young's modulus. When polished parallel on compression surfaces, a maximum is 10 µm was achieved between the lattices. The mean areas of the system were 17.7, 32.9, and 21.1mm^2 for the three components.
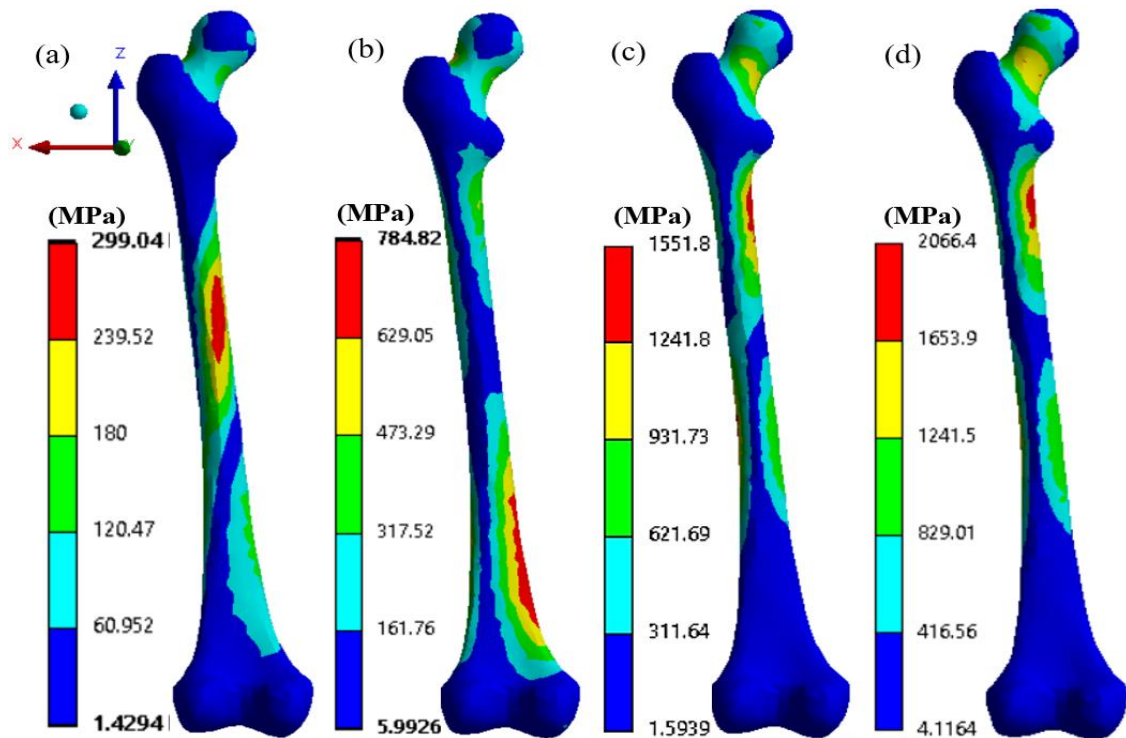
Figure 3.10 A von Mises stress of the femurs bone FEA of (a) PEEK (b)PEEK-cHAp-rGO of 1wt% of rGO and 30wt% of cHAp (c) PEEK-cHAp-rGO of 2wt% of rGO and 25wt% of cHAp (d) PEEK-cHAP-rGO of 3wt% of rGO and 20wt% cHAP

Fatigue, a failure, is caused by repeated mechanical stress in the traction, flexion, torsion, and compression directions. The materials are stressed below their yield stress limit when this failure occurs. Polymeric material manufacturing procedures, in particular, are more complicated. Polymer fracture initiation processes differ from metals and ceramics, even though crack propagation is the same in all materials. Because of the nonlinear viscoelastic behaviour of polymeric materials, the test frequency and other fatigue-specific features such as stress-strain levels and force application mode are critical factors to consider. Mechanical hysteresis and restricted thermal conductivity in polymers produce thermal failure when heated under cyclic stresses. Thermal softening failure occurs when the temperature rises to the glass transition temperature (Tg) of amorphous polymers or the melting point of semicrystalline polymers (Tm)[65,187]. Figure 3.11 shows the FEA of the different sectional views of Von Mises stress femur bone, which shows each composite's internal structure and stress analysis.
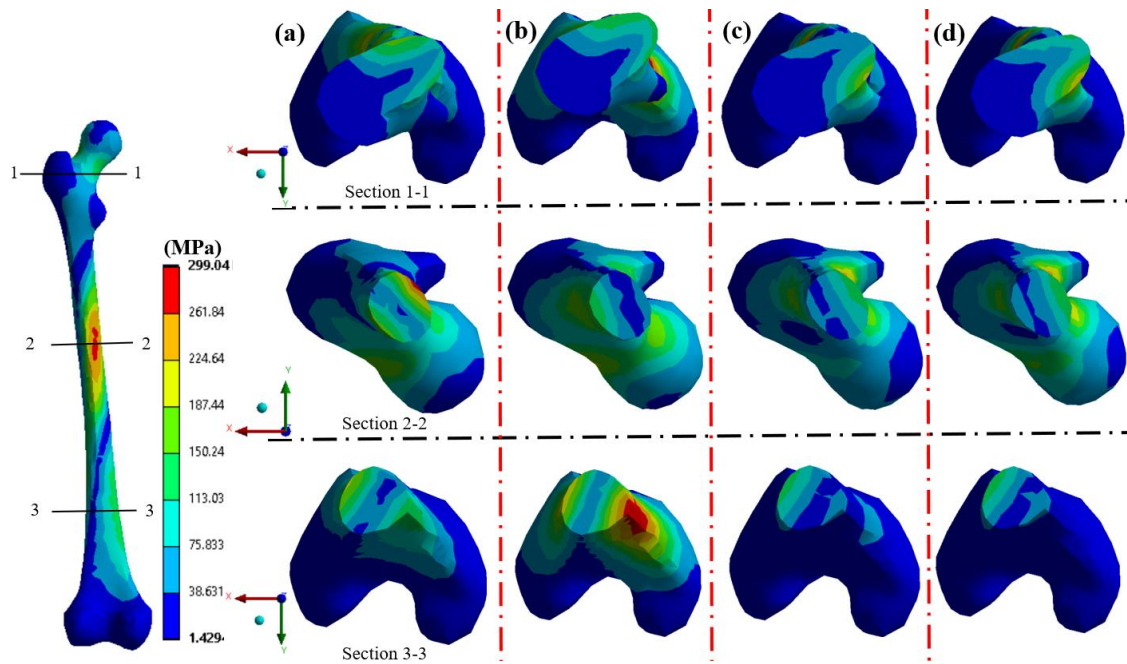
Figure 3.11 FEA of a sectional view of Von mises stresses femurs bone (a) PEEK (b)PEEK-cHAp-rGO of 1wt% of rGO and 30wt% of cHAp (c) PEEK-cHAp-rGO of 2wt% of rGO and 25wt% of cHAp (d) PEEK-cHAP-rGO of 3wt% of rGO and 20wt% cHAP.

Because of its high Tm of 343°C, thermal fatigue failure in PEEK is exceptional. Mechanical failure produced by fracture development is the most common type of failure. Defects are caused by the variability of materials and their microstructure. Particles beneath the surface of the cHAp-coated PEEK components produce heterogeneity. This results in macroscopic fractures due to complicated interactions between growth and defects. The FEA of a typical elastic strain femur bone. Cracks appear to propagate slowly at first, but they expand swiftly after a while. The fracture surface is frequently perpendicular to the applied force direction, indicating a failure process caused by damage propagation. Figure 3.12 shows the total deformation of femur bone FEA for the different composite ratios.
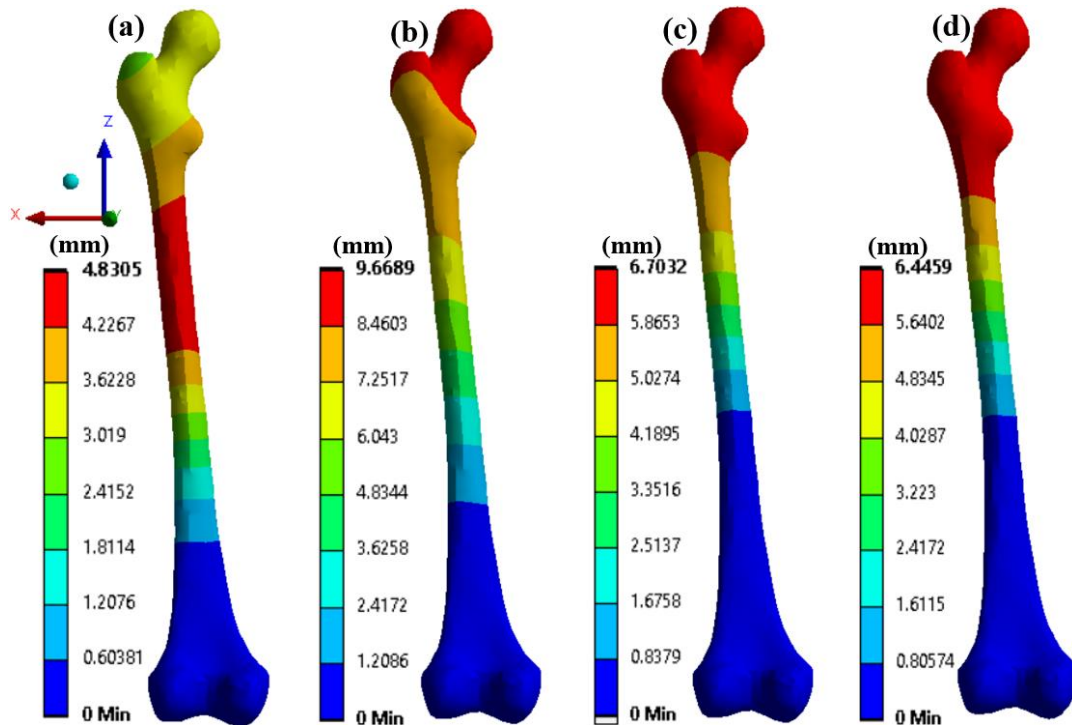
Figure 3.12 FEA of the deformation femur bone (a) PEEK (b)PEEK-cHAp-rGO of 1wt% of rGO and 30wt% of cHAp (c) PEEK-cHAp-rGO of 2wt% of rGO and 25wt% of cHAp (d) PEEK-cHAP-rGO of 3wt% of rGO and 20wt% cHAP.

An analysis of a tiny piece of heterogeneous media is required to identify the attributes of the medium, which is the basis for the homogenization technique and is suitable for analysing lattice unit cells. The representative volume element (RVE) represents samples of the whole region. The RVE includes the microstructure of appropriate materials and extends to the global domain where uniformly applied strain, or stress occurs with a boundary condition. When utilised in homogenization procedures, material properties such as relative density, defined as the density ratio of lattice material to solid, play an essential role in establishing a lattice's elastostatics. The lattice Hip implant design, homogenisation, elastic and modulus of elasticity are explained in the next section to show the application of another four different lattice cell structures selected from the ten, which is the combination of beam and formula lattice. In sections 3.6 and 3.7, the design of the lattice on the Hip implant, the flow process of hip design, and the Homogenisation of elastic Hip implant behaviour with the corresponding result of lattices cell applied to the hip implant were discussed.

3.6. Design of lattice on the Hip implant

The layer-by-layer production of items in 3D printing, also known as additive manufacturing (AM), allows the creation of structures that would be impossible to create with traditional removal techniques such as notching or milling. Ultra-thin 3D designs for bone transplants are constructed using composite materials. These components, too small to see with the naked eye, exhibit unique and often surprising properties when joined to form an ultra-lightweight biocomposite that will revert to its original structure following compression. The FDM was utilised to produce a more porous and capacious PEEK, as shown in Figure 3.14. Struts for hip implants with lattice cells. A lighter technique for 3D printing bone structures, producing large reticular structures with precisely regulated porosity, was used in the hip implant [48,176,190]. The usage of the five prosthetic Hip supports evaluated in this research is shown in Figure 3.13. In the case of PEEK compounds, their porous nature may increase body fluid penetration capacity. The geometric characteristics of the strut cells and the diameter evaluate the size of the pores.
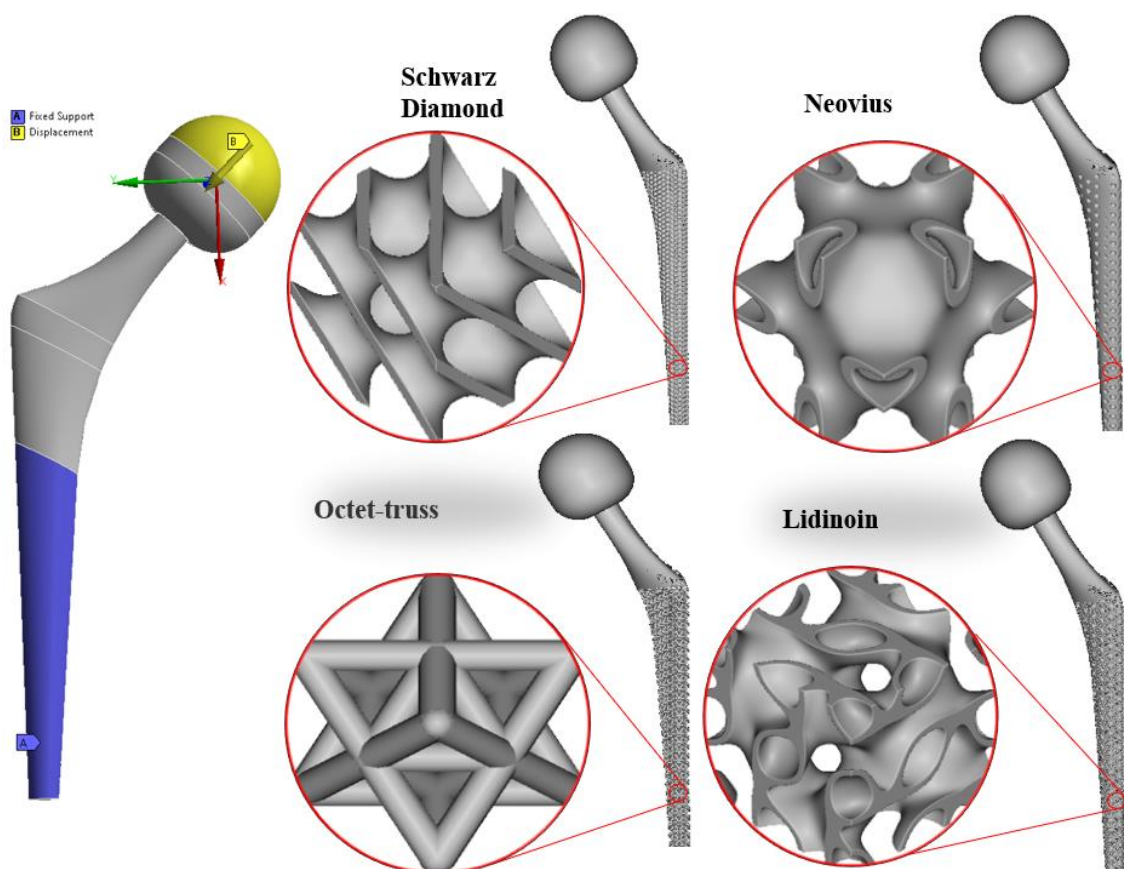
Figure 3.13. Struts for hip implants with lattice cells.

Porous hip bone implants created through FDM closely mimic natural bone lattice architecture and mechanical properties. Using homogenisation control techniques, PEEK with rGO and cHAp prints five isotropic lattice patterns. The effective module surface of five composite porous unit lattice designs is studied in three dimensions (3D). FEA investigated the connection between anisotropy, Young's modulus, and cell properties. The hip implant of PEEK and composites-controlled analysis of homogenisation and porosity to enhance cellular penetration and biological integration was designed to suit a broken femur bone. It is crucial to maintain that the unit cells will be homogenised. Hip implants are ultimately manufactured using isotropic. The network was built in Creo, updated, and simulated using the Ntopology programme. ANSYS Workbench and ntopology for FEA were used to determine homogenisation.

3.6.1. Flow process of hip design

Figure 3.14 depicts the experimental research in schematic form of the technique for making hip implants using composite PEEK. Figure 3.14 illustrates the extrusion printing technology, mechanical testing technique, and implantation. The method described for the direct fabrication of PEEK components for rapid implant production has the potential to usher in a revolution in medical technology and manufacturing procedures. They have pioneered the possibility of rapidly manufacturing implants with significant macro-dimensional compliance using cutting-edge technology.
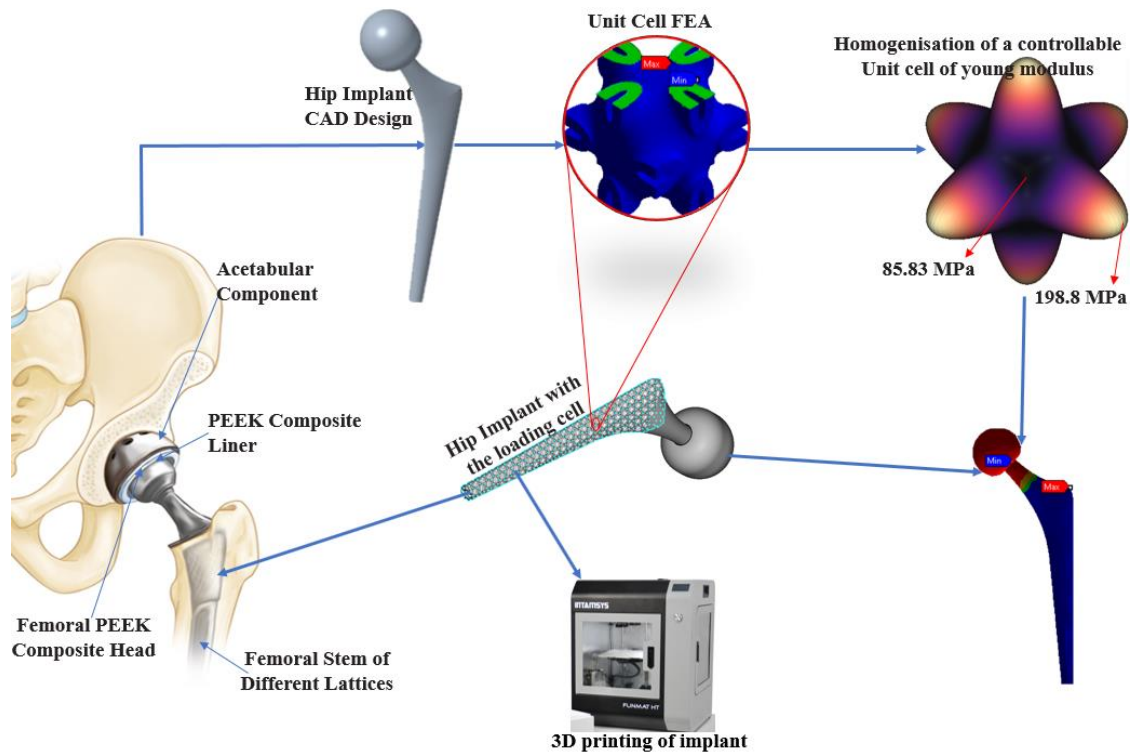
Figure 3.14. Schematic procedure of the experimental process of fabricating hip implants with PEEK composite.

3.6.2. Homogenisation elastic Hip implant

Homogenization methods for lattice structure and material design are briefly discussed. Elasticity, solid-state and data processing contributed to developing these approaches. A lattice material's behaviour is determined by its lattice category, relative density, cell shape, and element. A precise model for lattice structures in terms of parameters is thus critical. The dependent node position vector is produced by linearly multiplying the free node position vector by the period vector's entire product. All internal nodes are self-contained and always serve as agent nodes at the cell borders of the unit. Because of the macro-deformation displacement field, each micro-level rod receives internal stress. The bundle structure breaks when the inner tension in the tyre axle exceeds the material's elastic limit. Four of the ten lattice designs in this thesis were selected based on suitable strength and porosity for easy cell growth to apply to hip implants.

The approach begins by determining the node displacement vector's macroscopic stress field. Subtract the actual vector from the microscopic node's vector. The primary force vector is calculated via elemental balancing, considering cross-normal sections and shear

distributions. Three to two maximum distances between the cross-centre sections and halfway are used to determine initial stress. At the point of maximum slackness, the shear force to zero was set appropriately for the fixed point. However, the next phase uses maximum von Mises stress by using the fundamental shearing force at the centre. This procedure is also compatible with cell devices used in biomedical applications that need tiny scaffolds. Microdevices, which can be thought of as a kind of non-biological cell, also contributed to this endeavour. Because of the procedure's low weight and high capacity, the bone implant can be used on a larger scale. This study constructed and examined four lattice structures with cell sizes of 0.4 mm each: an octet-truss lattice, an FCCO lattice, and two Schwarz Primitive structures with 0.20 and 0.40 mm, which are applied to the hip implant.

3.7.   Result of lattices cell Apply to hip implant

3D printing produces porous PEEK with increased capacity and reduced weight. A novel technique for 3D manufacturing bone was designed by designing a PEEK composite with a porous lattice and a controlled microstructure. It is possible to increase the capacity of the bodily fluid to be carried; cells can enter virtually all bone formations via these sites. This result leads to very high utilisation and increased storage capacity for cells. A typical project consumes 10 and 30% of the entire compost volume. Increased Forcing rates and network design obtained via 3D printing provide a pathway for cells and fluids to be transported effectively inside the material.

A parametric study of the traditional homogeneous elastic limit has revealed the following results in Figure 3.15. Two different components may represent the internal tension of the connecting rod. The first concerns normal strength, while the second concerns bending cells in an extended unit of measurement. The seal properties have only a minor influence on the height of tall unit cells. The cubic cell results in Figure 3.16 demonstrate that the elastic limit entirely relies on the rod's diameter. The resistance of the cell is unaltered by the properties shared by all unit cells resulting in FCCO beam cells similar to those obtained for high-force joints in a cell. Low stiff joints affect perspective because the unit cell comprises a diagonal column of a straight line.

The lattice modelling in Figures 3.15 to 17 shows the composite and cell generated outcomes that were reliant on the standard features for the hip implant is to check the

mechanical strength. This trend is more complicated to monitor than the other two notable growing cells. In terms of solidity, the more the out-centricity, the greater the size of the elastic border. A shorter framework length leads to less bending time and a more external body structure than a more extended framework. Figure 3.17 and 3.20 shows the compressive stress of PEEK-cHAp composites and the principal elastic strain of PEEK-cHAp versus deformation, respectively.
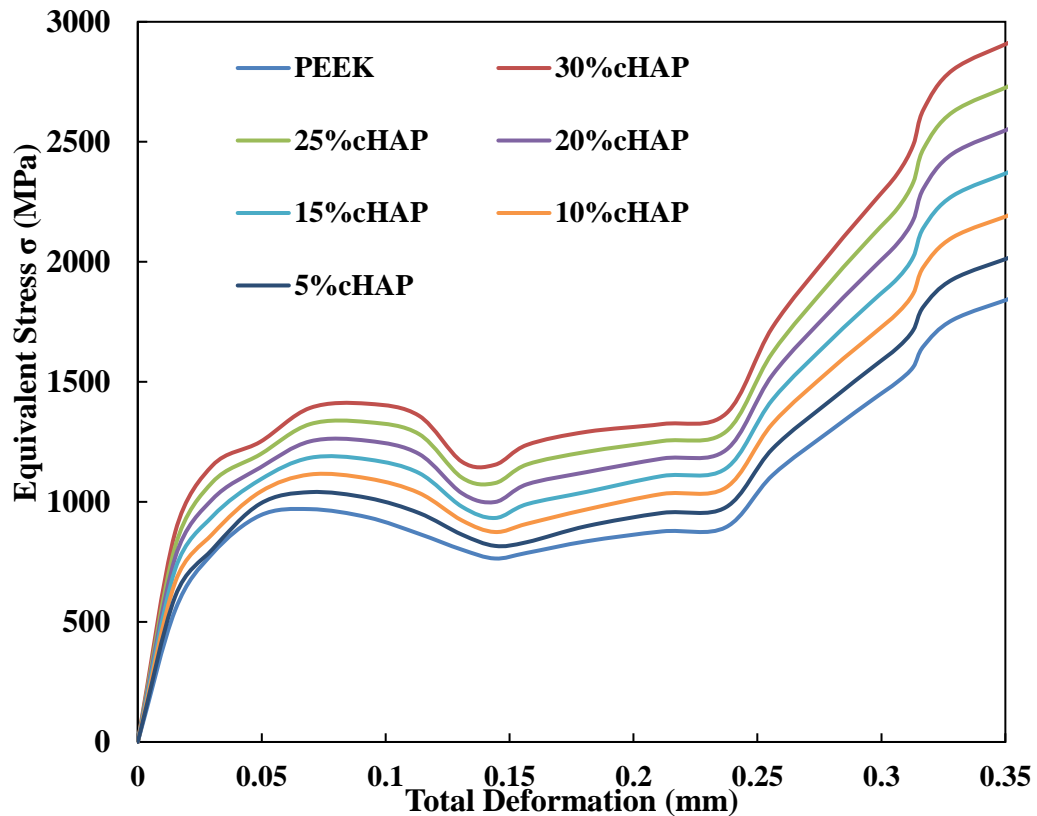
Figure 3.15 Compressive stress-deformation of PEEK-cHAp composites of a modelling result,
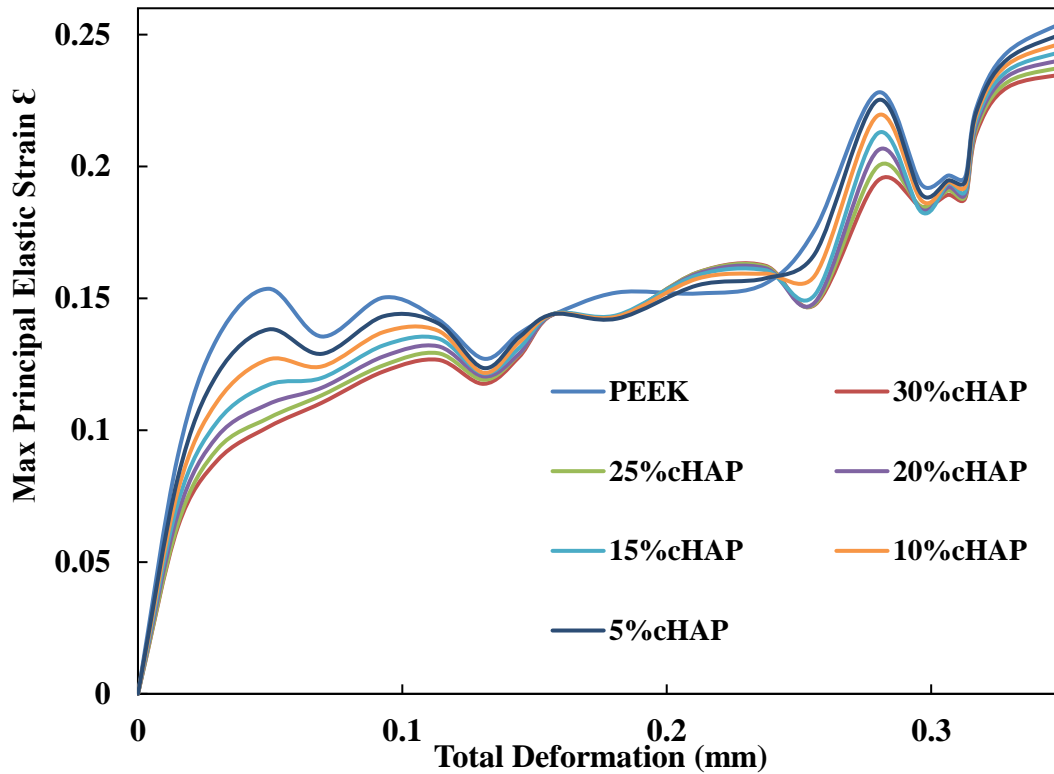
Figure 3.16 Compressive maximum principal elastic strain of PEEK-cHAp versus deformation.

Based on the geometry of the stress curve, the force frequently follows the same trend as the grid plateau force behind the elastic zone net, providing compression resistance to the elastic zone. The number following the highest and equivalent relative densities will collapse next. According to this study, PEEK-rGO-HAp with a weight ratio of PEEK-69, cHAp-30, and rGO-1 had Young's modulus and compressive strengths of around 60% and 50% higher, respectively. The wall materials have a higher inherent pressure resistance than the PEEK-78, cHAp-20, PEEK-87, cHAp-10, and rGO-3 materials. This is noteworthy because the diamond's hexagonal porosity did not affect its hardness or strength, and its structure did not suggest fundamental differences. Figure 3.21 depicts mechanical tests of PEEK and compounds in a range of cHAp ratios from 5% to 30% by weight, with corresponding PEEK values ranging from 95 to 95% by weight, at 5%-by-weight intervals, and structures 3D in a range of materials, from 5% to 70% by weight.
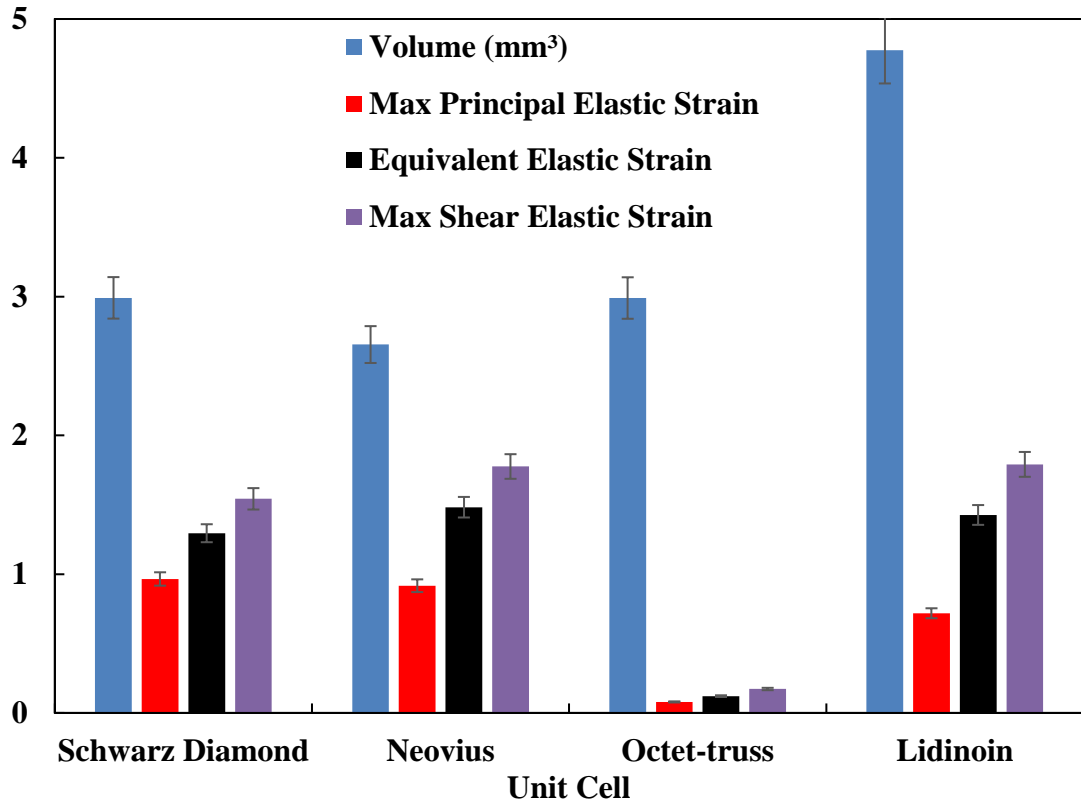
Figure 3.17. Strength of the various lattice structures
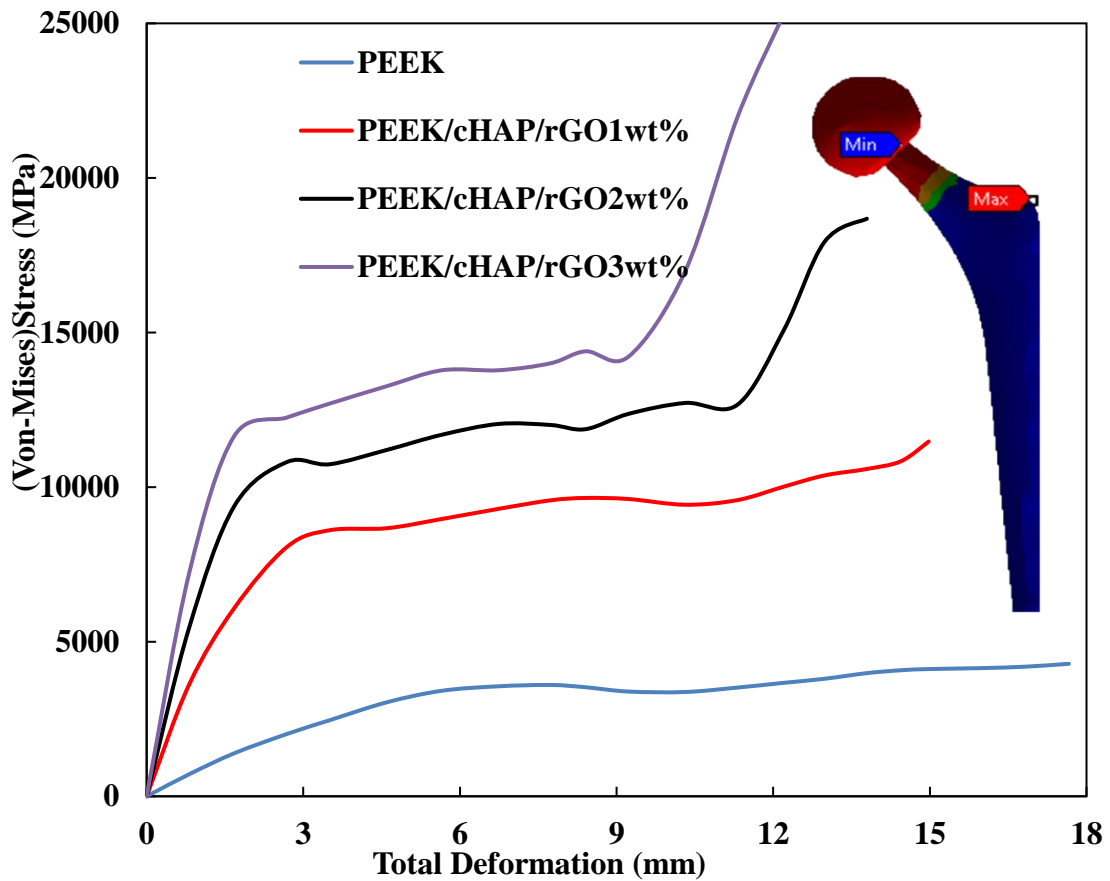
Figure 3.18 Von Mises Stress analysis of the deformation.

The findings of an FEA of a PEEK-rGO-cHAp composite hip implant with varied component ratios are shown in Figure 3.23 (a-d). PEEK-69, cHAp-30, rGO-1 (wt%), PEEK-78, cHAp-20, rGO-2, and PEEK-87, cHAp-10, rGO-3 were used under specified Force conditions, as were PEEK-69, cHAp-30, rGO-1 (wt%). Figure 3.19 Composite lattice structures, with red denoting the highest stress area after applying Force unit cell equivalent (von Mises) stress (MPa) and Von-Mises Stress findings for a PEEK and composite hip implant: Diamond (a), Neovius (b), Octet-truss (c), and Lidinoin (d). Figure 3.19 depicts the Von-Mises Stress results for a hip implant of (a) PEEK, (b) PEEK-69, cHAp-30, rGO-1, (c) PEEK-78, cHAp-20, rGO-2, and (d) PEEK-87, cHAp-10, rGO-3 (wt%).

The FEA setup features a simple force process with a completion time of 0.00001 and program-controlled starting time steps. The usual range safety factor is set to a minimum of 0.9 with a distinctive dimensional diagonal that is not scaled automatically. The safety factor was set to 1, and the carcass's hexagonal underlay was merged during printing. The shell shear correction factor was adjusted at 0.833, and the mean knot pressure test was used to determine the knot shell thickness. The program's control utilises Euler domain control to size the domain display accurately. All cell contents and domain resolution definitions have perfect bounds. When homogenisation and FEA findings are computed, the geometric scope technique produces time history and global coordinate systems. The average of the system's total results can be shown without computing the standard of the parts. To assess stress, stress, and all other safety considerations. The safety element supports PEEK-87, cHAp-10, and rGO-3% by weight due to its ability to sustain the tension of 25.32 GPa at the hip implant node with a minor deformation of 9.29 mm for PEEK with an uncertainty of 4.28 GPa and a deformation of 17.70 mm. Four-cell cubic samples were used to examine the effect of the angles chosen throughout the AM process. However, the address of the unit cell has been reversed. The features and homogeneous strength of about ten unit cell samples were simulated for better functionality in Figure 3.24. For instance, all Schwarz Primitive cells are identical in structure.

Lattice structures the highest strain area after applying Force cell equivalent elastic strain of diamond, Neovius, Octet-truss and Lidinoin. A parametric analysis was used to

determine the methods' effective structural parameters. Two mechanical properties are evaluated and compared with the test results: the elasticity module and the flow resistance. The normalisation of the data is performed using the most excellent and lowest modulus of elasticity recorded during the testing. For the octet-truss, kelvin, gyroid, and Schwarz primitives, the test produced 5790.7 MPa (413.9 MPa) and 165.3 MPa (110.4 MPa), 291.7 MPa (260 MPa), and 751.2 MPa (468.5 MPa), respectively. The proposed technique of comparing the modulus of elasticity at the most significant rotation angle results in an exact process. They are modifying the Euler structure, which results in tighter predictions. Figure 3.20 shows lattice structures of composites, with red representing the highest displace area after applying Force total displacement of each unit cell. Different thicknesses of cell lattice samples were used to calculate the average elasticity limit for octet-truss, diamond, Neovius, and Lidinoin lattice structures. Each of these thicknesses is associated with a unique mean and range. The octet-truss had a young's modulus of 496.8 MPa (165.8 MPa), whereas the kelvin, gyroid, and Schwarz primitive lattices had a young's modulus of 137.9 MPa (54.9 MPa), 275.8 MPa (31.7 MPa), and 609.8 MPa (282.7 MPa), respectively. The results show that the proposed homogenisation technique overvalues the elasticity module as a function of column diameter.

Additionally, the stiffness was overestimated by substituting Euler structural components for unitary primitive Schwarz cells. Due to the curved nature of the primitive Schwarz cell and the low taper percentage of the neck, the member of the Euler framework overestimates its stiffness by ignoring shear deformation. As previously mentioned, asymptomatic homogenisation leads to a more elastic module. For flexible limit estimation, estimates for various discrete homogenisation methods will be different. Because AM utilises the whole geometry, the process's effect cannot be included in the resource forecasting technique.
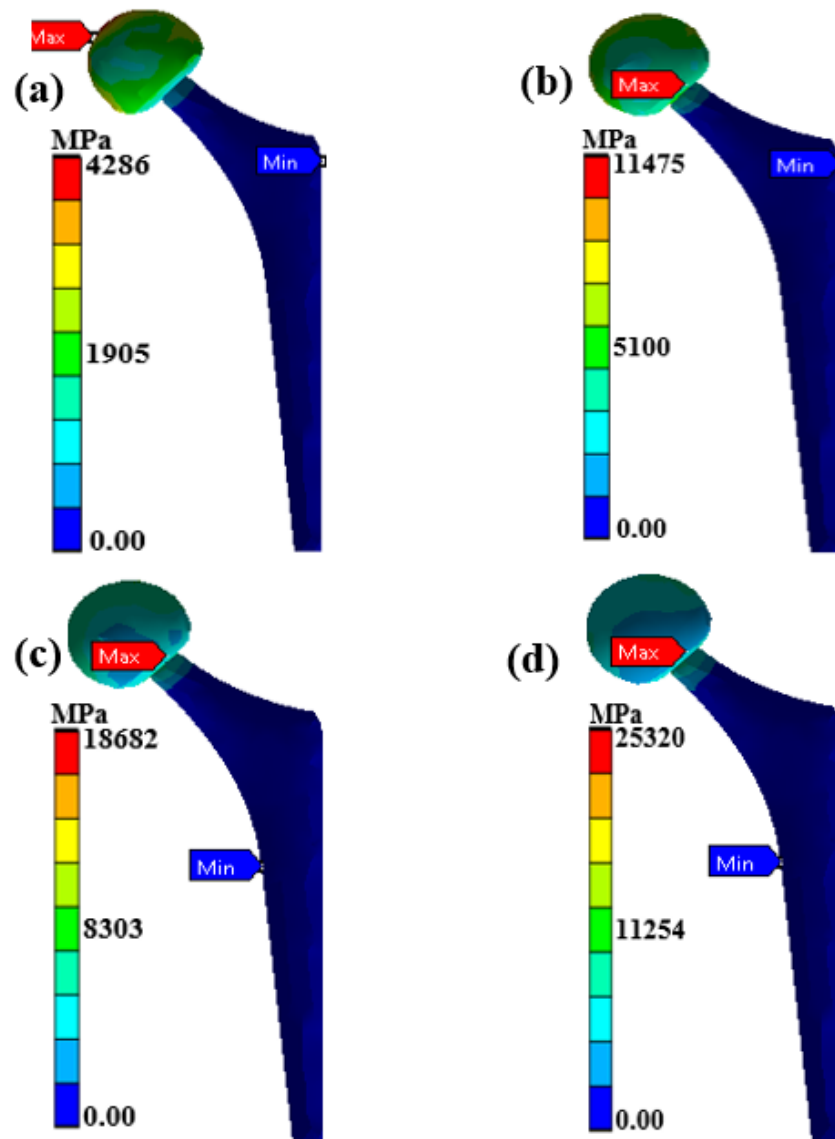
Figure 3.19 Von-Mises Stress results for a hip implant of (a) PEEK, (b) PEEK-69, cHAp-30, rGO-1, (c) PEEK-78, cHAp-20, rGO-2, and (d) PEEK-87, cHAp-10, rGO-3 (wt%).

Figures 3.21–3.23 illustrate the three-volume proportions of the PEEK compound. The stress distributions for three different mesh architectures are shown in Figure 3.24, as are the von Mises stress distributions for five different mesh configurations. 30 % cHAp and 1 % rGO were found in 69 % PEEK samples, 20 % cHAp and 2 % rGO were identified in 78 % PEEK samples, and 10 % cHAp and 3 % rGO were found in 87 % PEEK samples. Chemical reactions in PEEK are impossible in a solution containing organic and molecular linkages that bind to the substance to produce a polymer containing resin containing PEEK, such as the scaffolding utilised in the experiment. For a PEEK hip implant and a composite of PEEK, PEEK-69, cHAp-30, rGO-1, PEEK-78, cHAp-20,

rGO-2, and PEEK-87, cHAp-10, rGO-3, FEA results were collected (Figure 3.22-25). (weighted average)
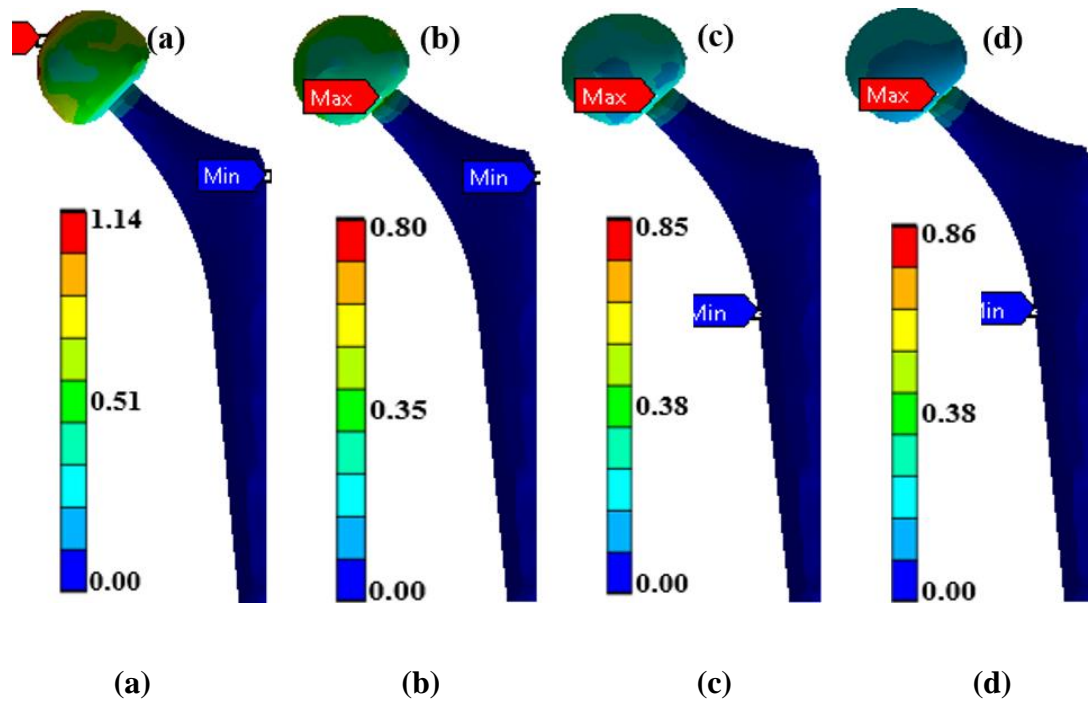
Figure 3.20 Elastic Strain of (a) PEEK, (b) PEEK-69, cHAp-30, rGO-1, (c) PEEK-78, cHAp-20, rGO-2, and (d) PEEK-87, cHAp-10, rGO-3 (wt%).
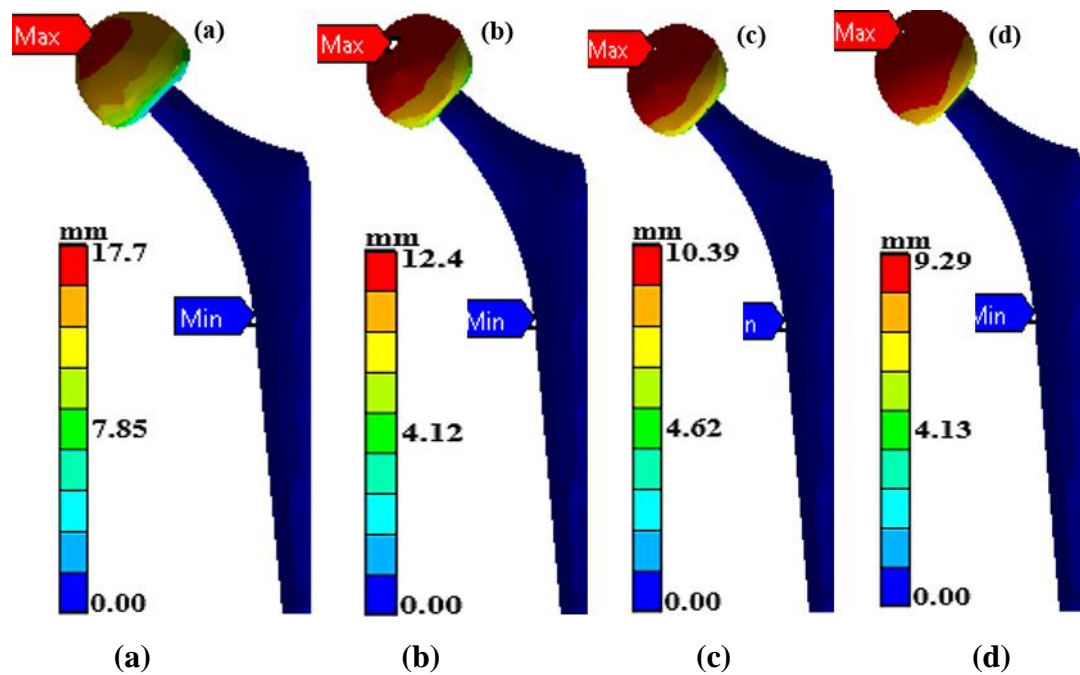
Figure 3.21 Total Deformation of (a) PEEK, (b) PEEK-69, cHAp-30, rGO-1, (c) PEEK-78, cHAp-20, rGO-2, and (d) PEEK-87, cHAp-10, rGO-3 (wt%).
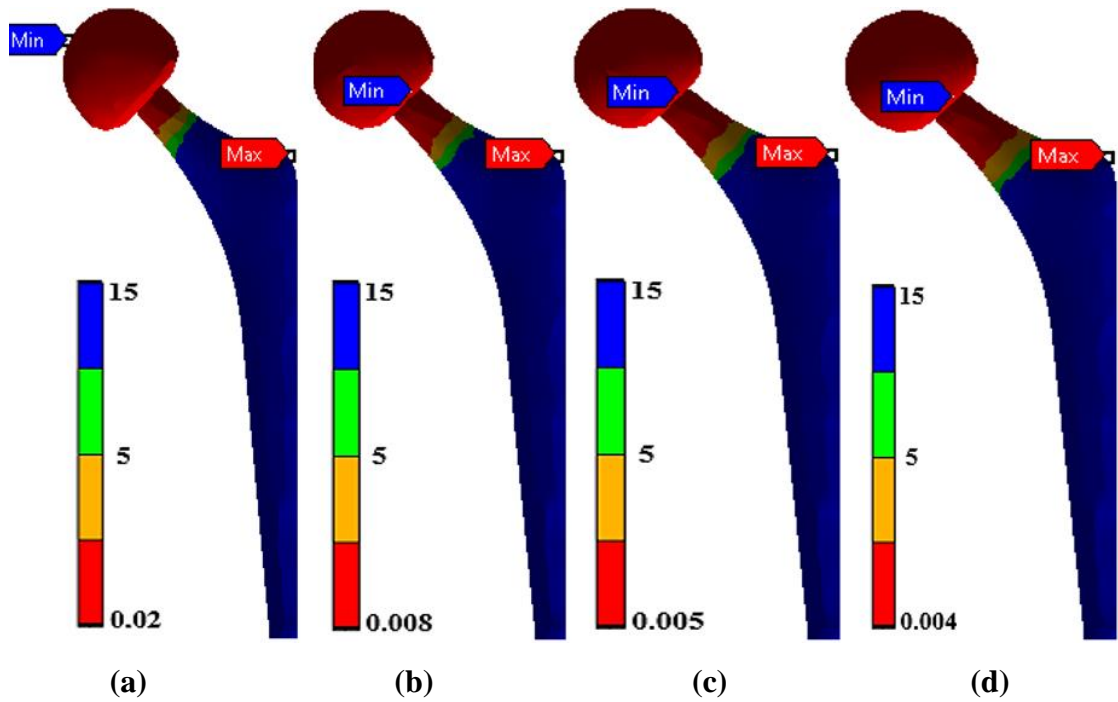
Figure 3.22 Stress Safety of Factor of (a) PEEK, (b) PEEK-69, cHAp-30, rGO-1, (c) PEEK-78, cHAp-20, rGO-2, and (d) PEEK-87, cHAp-10, rGO-3 (wt%).
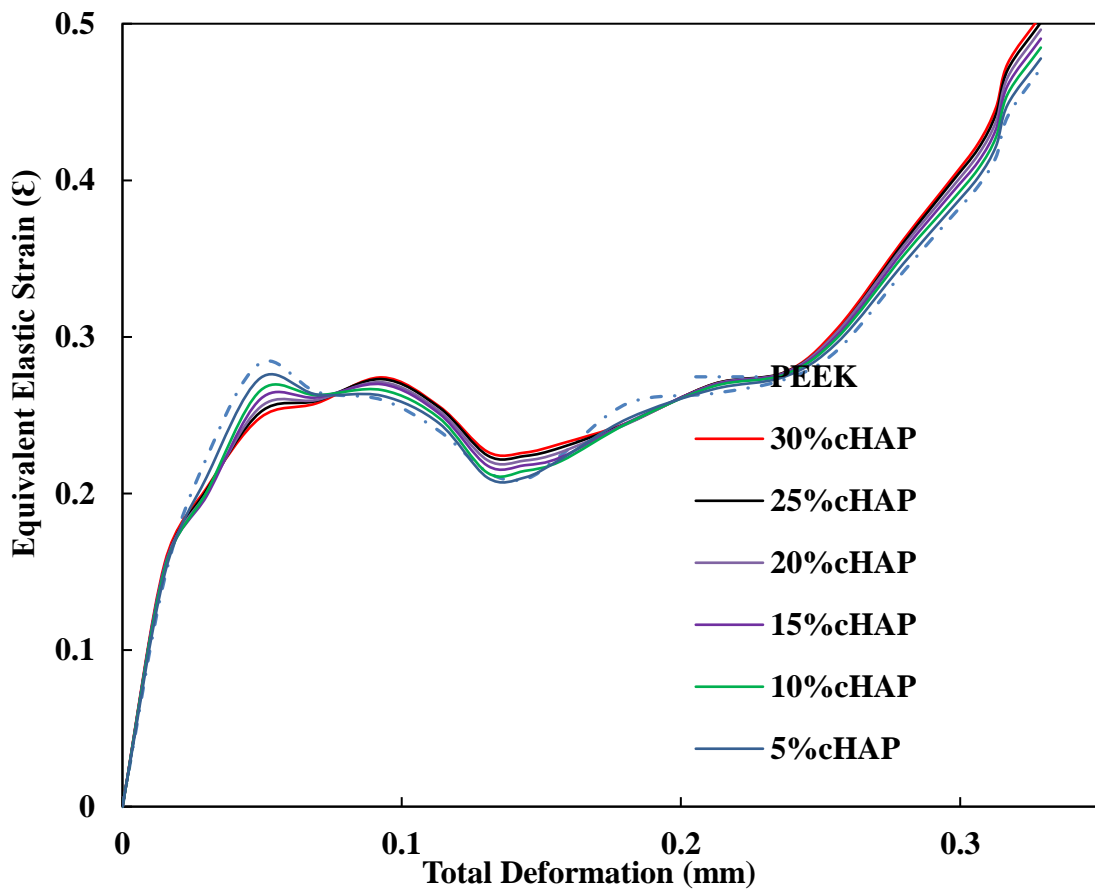
Figure 3.23 Compressive analysis of (a) equivalent elastic strain versus deformation,
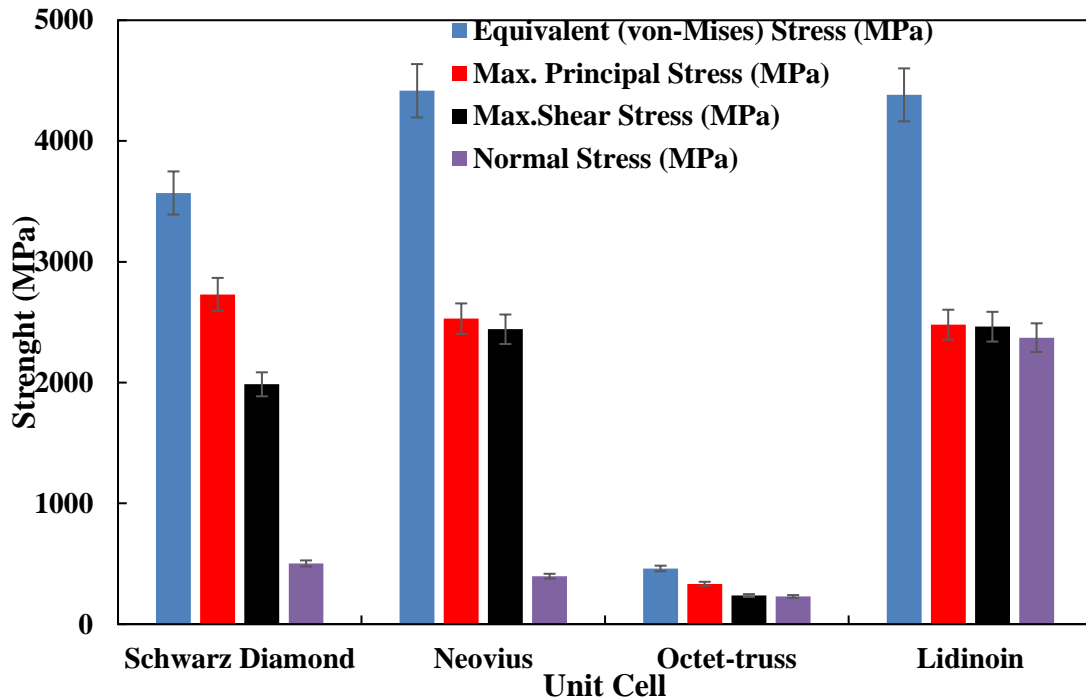
Figure 3.24 Compressive analysis of stress analysis of each unit cell by microstructure

3.8.   Conclusion

Porous structures have been studied using an FEA method called modular homogenisation, which was developed to exemplify the geographical circulation of young modules and the grade of anisotropy in the structures, which determine the primary characteristic of sound properties of bone materials which determine the mechanical strength of the hip femurs bone implants. Geometric characteristics and homogenisation coefficients were mapped to carry out homogenisation control procedures. Using a four-cell structure was analysed for each implant. Trabecular bone exhibited an elastic modulus equivalent to a diamond with the same porosity as diamond and gyroid cells. These components more closely resemble the hip bone than others. Compared with the custom mesh pore structures produced utilising 3D printing technology for hip implants, it demonstrates homogenisation between natural and porous materials. For weight-bearing porous hip implants to be successful, the ability of this implant to homogenise bone density and mimic the behaviour of femoral bone is critical.

The spatial distribution of moduli and anisotropy has been characterised using an effective numerical method for modular homogenisation, which has been developed. It was discovered that there is a relationship between geometric parameters and homogenisation coefficients, allowing control. This section presents five examples of lattice structures demonstrating solid materials' modulus spatial distribution response. A porous structure with identical porosity may indicate that the modulus of elasticity of trabecular bone is equivalent to that of two lattices, namely diamond and nervous. These structures are more similar to the hip bone than the others. The difference in homogenisation between bone and the porous structure was evaluated with the custom lattice pore structures produced using 3D printing technology for hip implants, which are not available commercially. The ability of weight-porous hip implants to induce bone and mimic the mechanical characteristics of the femur bone is critical to the efficacy of these implants in the long term.

Chapter 4

Materials selection and production of scaffold for bone implant

CHAPTER 4

4.0. MATERIALS AND METHODS

4.1. Introduction

PEEK implants machined or printed have been utilised in tissue engineering for people and animals without significant problems. Due to its excellent mechanical properties, chemical stability, and biocompatibility, this polymer has been of substantial interest. It has been subjected to various treatments, such as centrifugal coating, gas plasma treatment, electron beam accumulation, or immersion of cHAp ions in the plasma. Compared with [181-190] moulded PEEK, the monotonic tensile test revealed that the material had a strength of 73.9%. At 6 and 12 weeks, bone growth was detected inside the pore layer using microcomputer tomography technology and histological examination, indicating a substantial response[183-185]. Generally, the material enhances process formation while preserving structural integrity, allowing PEEK to be utilised as a support surface in arthroplasty procedures and other applications [1,191]. It was processed using a 3D printer to create a bespoke implant from customised geometry. It was possible to produce the bearing surfaces that satisfy current implant requirements established by ASTM and, most significantly, [185,192].

The bacterial endurance of PEEK implants made with random capillary spacing nanocolumns was tested. It was later compared with the bacterial persistence of copolymer. The PEEK biomaterial's excellent mechanical performance, machinability, and thermal stability should be combined with the main bone component (cHAp) to produce an attractive and efficient PEEK-cHAp bio-scaffolding composite are both attractive and efficient. The primary focus was on applications that used unique 3D printing and FDM technologies.
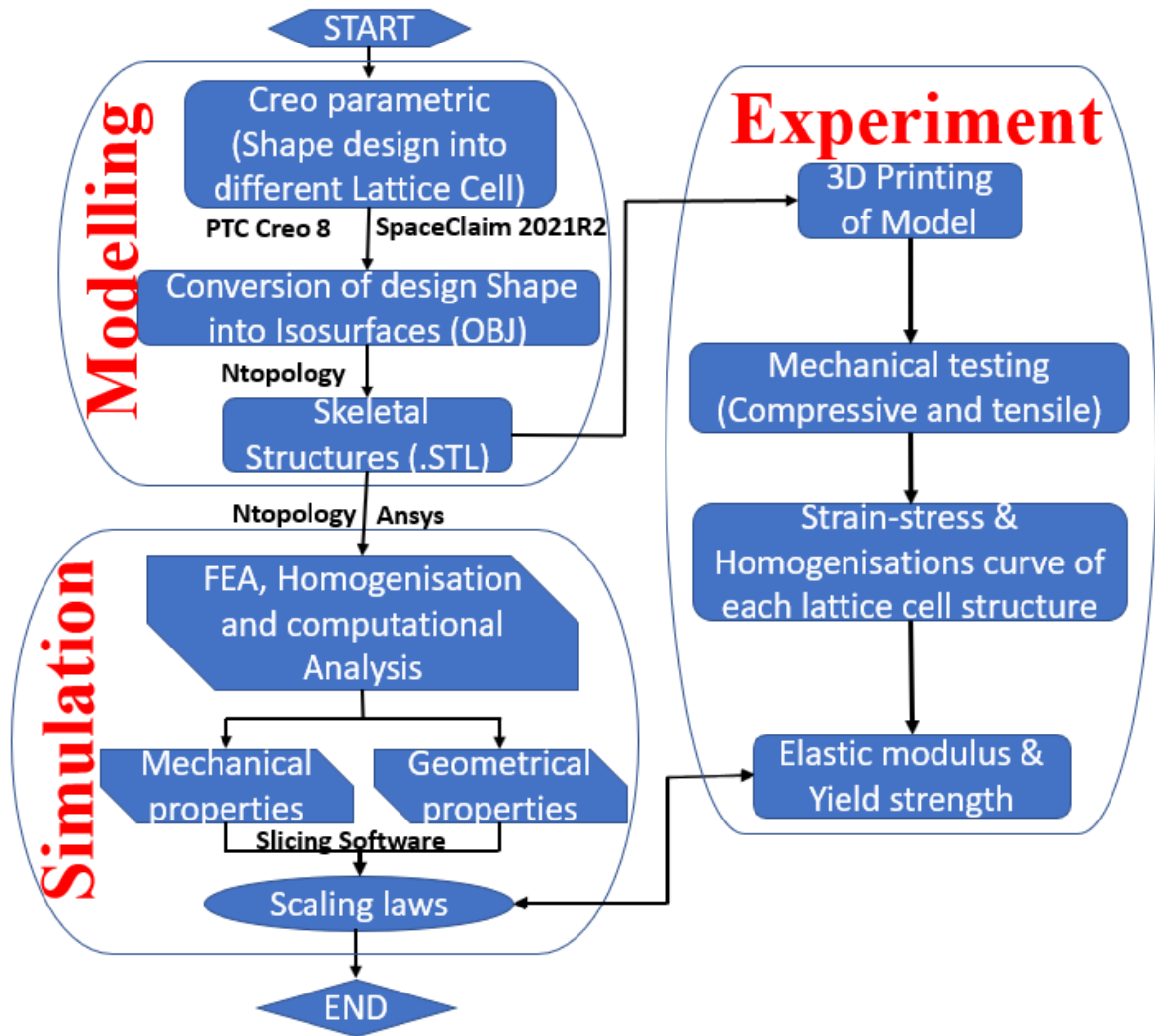
Figure 4.1 Flowchart for modelling, simulation, and experiment methodology of the hip femurs bone implant and the lattice structure application.

4.2. Material preparation

According to the manufacturer, the property of the used PEEK is as follows; the density matrix is 1301 kg/m3, and the flow rate is 3.6g/min (400°C/2.16 kg) [186-188]. The glass transition temperature is 147°C, and the crystal melting temperature is 343°C. The nano-hydroxyapatite (nHA) filler from Sigma is the preferred filler in this study. As a result of the sol-gel method, Aldrich nHA has an average particle size of less than 200 nm, a surface area of more than 9.4mn2/g, and the molecular formula [$Ca_5(OH)(PO_4)_3$]. It has a 1.30 grams per cubic centimetre density and 36 g/min of 400 ºC per 2.16kg. It has glass transition and crystal melting temperatures of 147 and 343ºC, respectively. It is made from hydroxyapatite with different chemical compositions and morphology. 1)

Nanohydroxyapatite (nHA), supplied by Sigma Aldrich, with a mean particle less than 200 nm, a surface area greater than $9.4 m^2/g$, and the molecular formula $Ca_5(OH)(PO_4)_3$ with a spherical particle geometry. 2) Nanohydroxyapatite (nHA) supplied by Sigma Aldrich, with a mean size less than 200nm and a surface area greater than 9.4 µm.

FDM is an AM method that specialises in producing PEEK components with very complex structures, which allows for more design freedom. The form and density of these particles contribute to their ability to mix, which is often advantageous and consistent [86,125,135]. In this research, the internal structure precisely controlled the phase dispersal of the bioactive chemicals inside the PEEK matrix, thus altering the final mixture quality and biological properties. The biocidal phase is linked to the PEEK matrix, better than the conventional microstructure design. This technique applies to various physiological agents, including bioglass; due to its biodegradability, it can be utilised at varying rates. 3D channels have been linked to enhancing the pace and spread of growth. Figure 4.2 shows the EDS-SEM setup for the materials EDX spectrum and mapping element of PEEK.

4.2.1. SEM mapping element of materials

This step is the mapping equivalent of the verify elements stage in the navigator's place to know the element present and observe if it can be bioactive. Instead of confirming the elements in a spectrum, it will ensure the element maps on a specimen. The mapping interface will have tools to add/delete maps, change the default X-ray line used to construct each element map, and even change the default energy windows used. While investigating the specimen, the spectra reconstruction from one point or area will give a quick idea of potential maps. Thus, the bone structure was established in PEEK *in-vivo*, substantially increasing the rate of implantation fixation when compared with the conventional methods (Figure 4.2). Figure 4.2, shows from the top blue component to the bottom green component elements. Examining compositional elements is a technique. Because of the high energy of the electron beam, electrons from the sample's inner atomic orbitals are evacuated. Vacancies are filled with electrons from higher energy shells, and the electrons' wasted energy is emitted as X-rays during these transitions. The significance of these modifications and the X-rays they produce are unique to each atomic species. The X-ray spectrum may be used to determine the constituents of a sample. It can detect concentration fluctuations as small as 0.5% to 1%. Like the backscattered

electrons, the observed X-rays emerge from a substantial subsurface interaction zone that may be on the micrometre scale. As a result, the spatial resolution of EDX in SEM is often decreased.
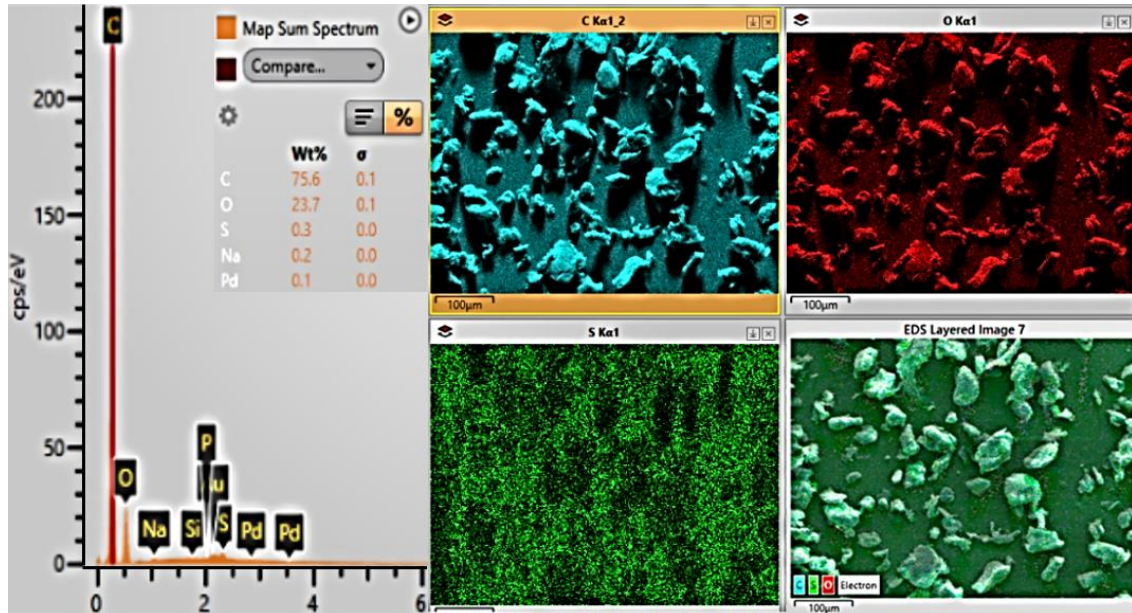
Figure 4.2 EDS-SEM setup for the materials EDX spectrum and mapping element of PEEK

However, when the spectra look more detailed, press the confirm elements link in the top right-hand corner of the Spectrum. It automatically relocated to the prove elements step of the point and navigator, and more advanced interrogation tools were used. When the mapping was finished, the map navigator was selected and returned to the Construct Maps step. A map was removed in a couple of different ways by deleting the map by forcing the delete icon in the corner of the map. The default venue is for X-ray lines and energy window width selection. Specifying the energy check box was checked to define the energy window's width manually. Lower Energy (keV) values were entered, and Upper Energy (keV), press the Update map with the change button. Also, the Specify Line Series check box was checked to manually select the X-ray line for mapping an element. The line from the Line series drop-down list was set. Then, the 'Update map with Changes' button was pressed. The next section describes the characteristics and elements of rGO, as a good biocomposite for PEEK and the high strength that can make PEEK stronger, similar to the bone structure.

4.2.2. Reduce graphene oxide (rGO)

When distributed, graphene oxide pH is critical for its quality. The graphene oxide solution produced by the Hummer technique is typically between 2 and 3 if the washing phase is omitted from the manufacturing process [181,187]. Unwashed graphene oxides' acidic nature (pH = 2-3) severely affects their characteristics. As a result, graphene oxide products must be regularly washed with significant quantities of distilled water. It is a novel graphene-based nanomaterial called rGO, a new graphene oxide dispersion 6-7. Due to its atomic thickness and other outstanding characteristics, it is a versatile material with many applications [193,194]. Chemical solvents or hot organic water are effective in dissolving it. Wet chemistry is economical, while rGO products are robust and widely accessible. The redesigned hummer combines water and methanol to create dispersion without surfactant. It is helpful for various applications, including ultrasonography, a vacuum chamber heated to 320°C. This temperature is less than 350°C but is sufficient to cause the PEEK organic material from the structure. This result implies that the size is decreased by 80% while maintaining the form and proportion. Figure 4.3 depicts fabrications of composite by cold modification of the PEEK Scaffold

Figure 4.3 Fabrications of composite by cold modification of PEEK scaffold.

The strong biomechanical characteristics of PEEK and related constituents make them useful in clinical dentistry. Compared with more conventional dental materials like

titanium, the researches in the literature show that PEEK has less stress. PEEK can be utilised in many dental applications because of its similar physical characteristics to bones. PEEK dental implant biological activity can be increased, but not because of its mechanical characteristics. In addition, PEEK is entirely safe since it is neither poisonous nor mutagenic and produces no significant inflammation. Manufacturing jaw teeth and facial devices is tricky, despite their tiny size, and must be thoroughly understood to use the existing technology fully. FDM and silicone moulding techniques were combined to create a hybrid manufacturing method. The implant was first made intraoperatively using a sterilised template [51,72].

4.2.3. cHAp and its application

Compared with synthetic cHAp, the biological products produced by HAp cells include several contaminants. Due to the apatite structure substituting for several ions in [194,195] the human body, like potassium and sodium, these impurities are evident. The FDA has approved the cHAp powder that is used in dental implants. The standard specifies that a minimum percentage of powder crystallinity of at least 95% must be achieved [57,195]. The calcium to phosphorus ratio is 1.65, reaching 1.82 when the trace element percentage is the greatest. As the specific rule demonstrates, coating techniques have the required powder characteristics, such as the Ca/P ratio and crystallinity, to achieve the desired results.

4.2.3.1. Thermomechanical behaviour of cHAp

Surface modification procedures often include temperatures plasma deposition processes of up to 590 °C in a torch. Thermal decomposition can alter the phase equilibrium in cHAp particles, altering many parameters, such as crystal composition and phase morphology. Three processes of water evaporation in cHAp are highly hygroscopic [13,67,81]. Due to initial changes during the heating of cHAP powder and evaporation of adsorbed water, as HAp gradually loses its hydroxyl group (-OH), dihydroxylation acts like water. As part of the apatite structure, decomposition occurs at a specific temperature. cHAp retains its crystalline structure during dihydroxylation and recovers during cooling. This result leads to calcium phosphates, like calcium tetraphosphate (TTCP), converted to calcium oxide. Figure 4.5 is shown EDX spectrum and mapping

element of cHAp. Also, Figure 4.6 depicts highly porous PEEK nanocomposites, including an electrostatically bound hydroxyapatite.

$Ca_{10}(PO_4)_6Ox \mathring{\downarrow}x \rightarrow 2Ca_3(PO4)_2 + Ca_4(PO_4)$ (Oxyapatite = Calcium triphosphate + Calcium tetraphosphate)

$Ca_3(PO_4)_2 \rightarrow 3CaO + P_2O_5$ (Calcium triphosphate→ Calcium oxide + Phosphorus pentoxide)

$Ca4(PO4)2O \rightarrow 4CaO + P2O5$ (Calcium tetraphosphate → Calcium oxide + Phosphorus pentoxide)
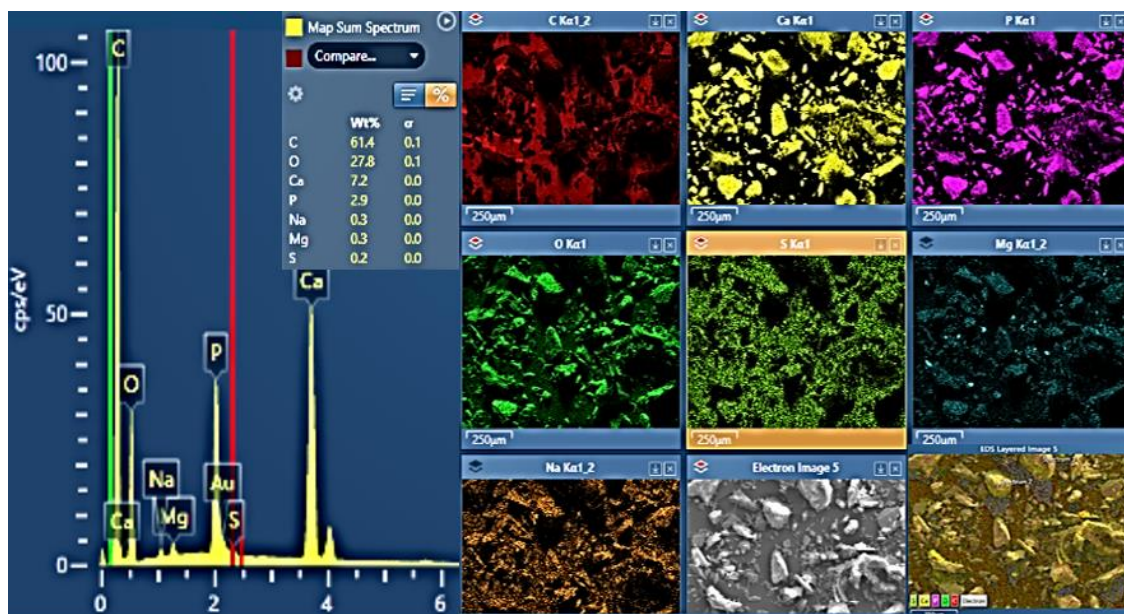
Figure 4.5 EDX spectrum and mapping element of cHAp.
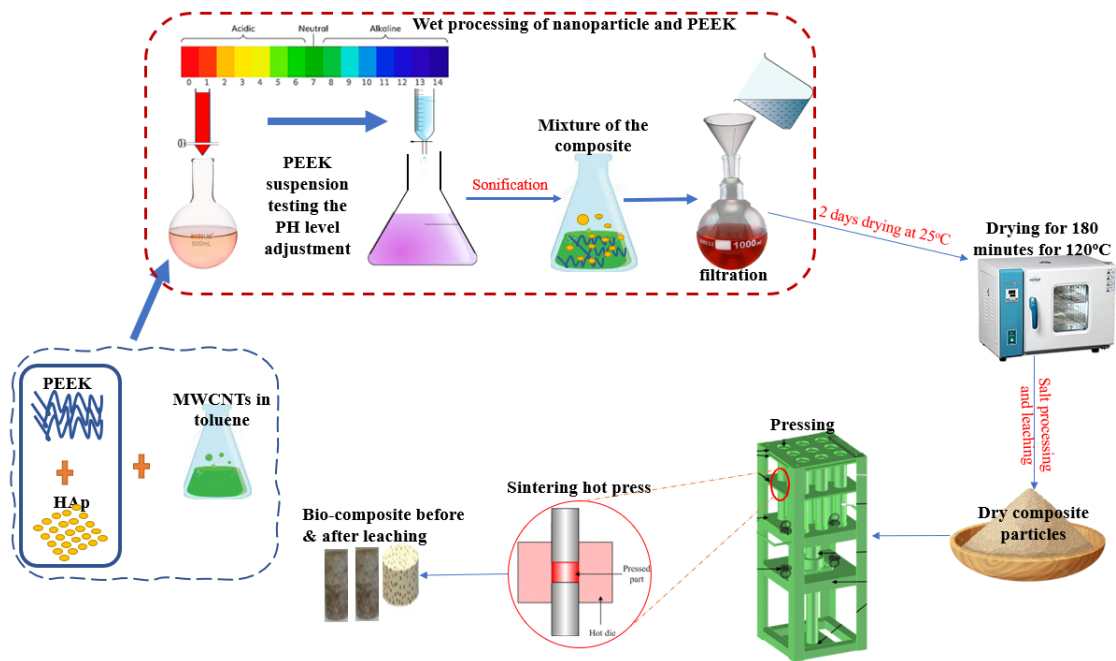
Figure 4.6. Highly porous PEEK nanocomposites, including an electrostatically bound cHAp.

For 72 hours, immerse the PEEK-cHAP composite in hydrochloric acid (HCl). After dissolving HA filaments in HCl, hollow passageways appropriate for cell adhesion, infiltration, and proliferation were formed. Good pore interconnectivity allows for cell infiltration and nutritional perfusion. Sufficient pore size was modelled to allow for vascularisation while maintaining appropriate mechanical strength, and channels aid cell alignment and differentiation. Extrusion free-forming allowed for precise pore size and interconnectivity required for bone ingrowth. Scaffolds are printed using FDM technology in this study. The extrusion temperature is set between 380 and 410°C, the print speed is 40 mm/s, the bead width of each print line is 0.4 mm, and the thickness of the PEEK filler layer is 0.2 mm. PEEK material's geometry and density determine their porosity following the ASTM F 2450-04 standard. Victrex® PEEK 450G has a density of 1.30 g/cm3. The sample mass, m, was determined using a Mettler Toledo AE240 digital dual-range analytical balance. This technology can fabricate various forms, sizes, and spatial distributions of scaffolds. Figure 4.7 shows the SEM micrographs showing the cHAp EDX spectrum and mapping. The next section describes the process and procedure of preparing graphene oxide as a composite. Figure 4.7 shows how a scanning electron microscope takes pictures of organic and inorganic materials that differ in structure or makeup. Standard components include energy-dispersive spectrometers, secondary electron detectors, and backscattered electron detectors. The secondary

electron detector can take pictures of a material's surface texture, while the backscattered sensor is best for catching changes in its composition.
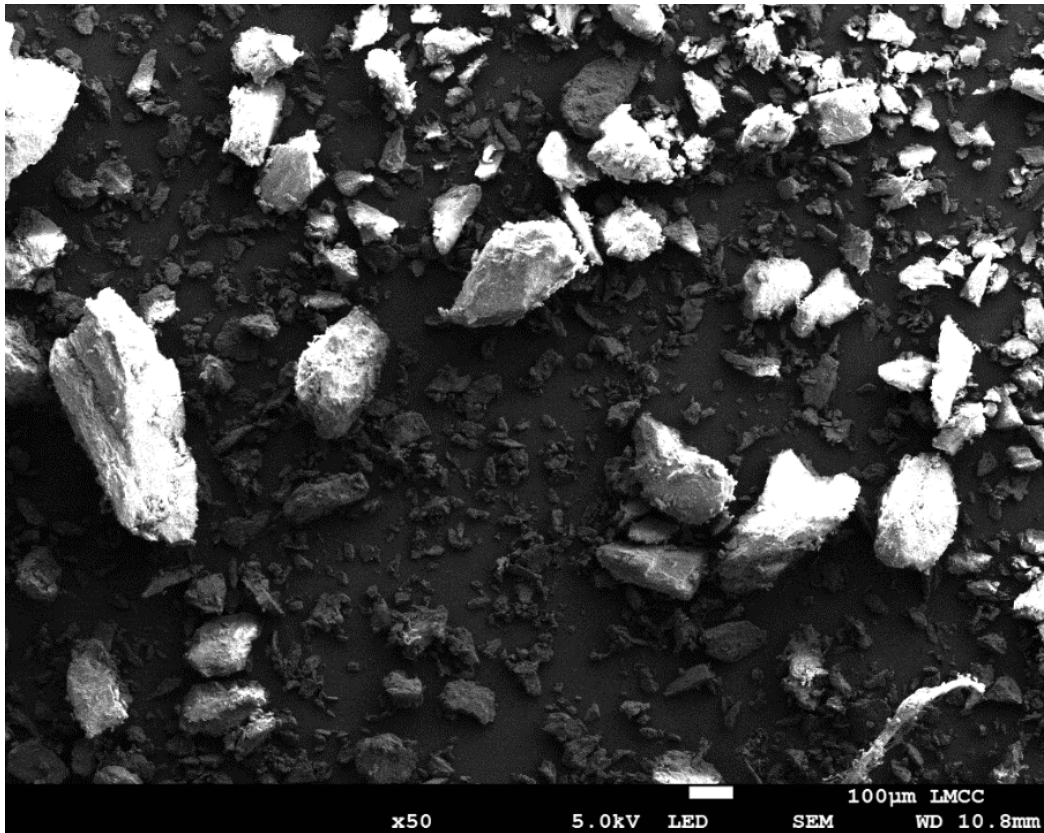
Figure 4.7 SEM micrographs showing cHAp EDX spectrum and mapping.

4.3.   Graphene oxide preparation

For over 150 years, [194,196] tried to determine its atomic weight by oxidising graphite compared with single-layer graphene, which is still considered a new material; otherwise, graphene oxide in the graphite oxide layer has been. Nitric acid content changed the body method to accelerate the production of graphite oxide under less severe conditions, such as a sodium mixture. The structure of rGO is controversial regarding its existence - functional distribution of oxygen groups and non-quantitative atomic composition [47,56]. Oxygen groups are essential in the mechanical and electrochemical properties of rGO when compared with graphene. It is much easier to disperse rGO in water and various solvents, making it possible to prepare polymer nanocomposites and scale processes to mass produce rGO. On the contrary, the available covalent oxygen in rGO creates a structural defect, affecting properties such as electrical conductivity and limiting rGO in conductive materials (Figure 4.8).
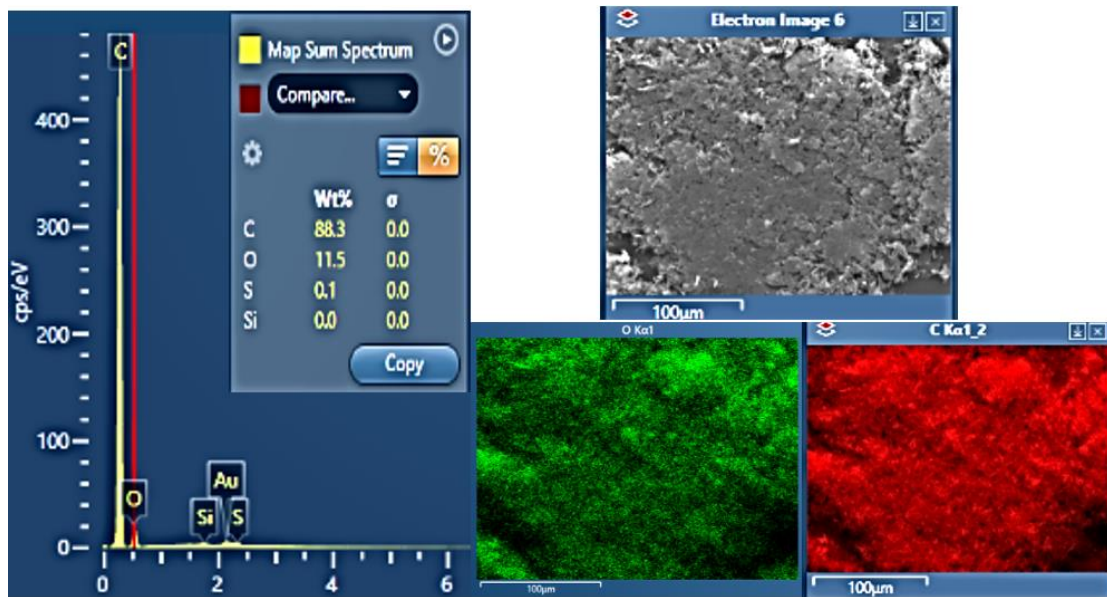
Figure 4.8 SEM micrographs showing rGO.

The rGO was synthesised chemically from Alexandria's graphene oxide (GO) monolayer [181]. rGO is not a semi-insulator; it exhibits excellent electrical conductivity and solubility. Simplifies the manufacturing of conductive nanocomposites by simplifying the processing of solutions. DMF is a colourless, transparent, hygroscopic liquid with a faint amine odour. Due to its high dielectric constant, the solvent characteristics of DMF are favoured. Characteristics of a wide range of liquid aprotic solvents with low volatility, the black-appearing rGO was developed by ultrasonic chemical reduction. Which is soluble in water ~0.24 mg/ml, ~0.8 mg/ml organic solvents like DMF and ~0.6mg/ml NMP Brunauer, Emmett and Teller specific surface area (BET) at 425-489.4 m^2/g is often used to estimate and produce gas adsorption data for a given surface area. Several standards associations such as ISO, USP and ASTM refer to this method. Leaf sizes range from several hundred nanometres to a few micrometres in the XY plane, with Atomic force microscopy (AFM) shapes at atomic ratios of more than 3:5. According to the company, the team also provided a Biophysical model directly from the biomaterial and fit the virtual model. Figure 4.9 shows current approaches for PEEK adjustment and bioactivity and the future perspective of CH_2. Combining oscillating integration and biomechanical properties develops implant panels with wide geometries, measurements, and spatial distribution. Direct implant technology can be migrated to non-invasive healthcare systems by integrating customised implants for training. In the next section,

the composite Engineering constants of the elastic properties of the materials are calculated.
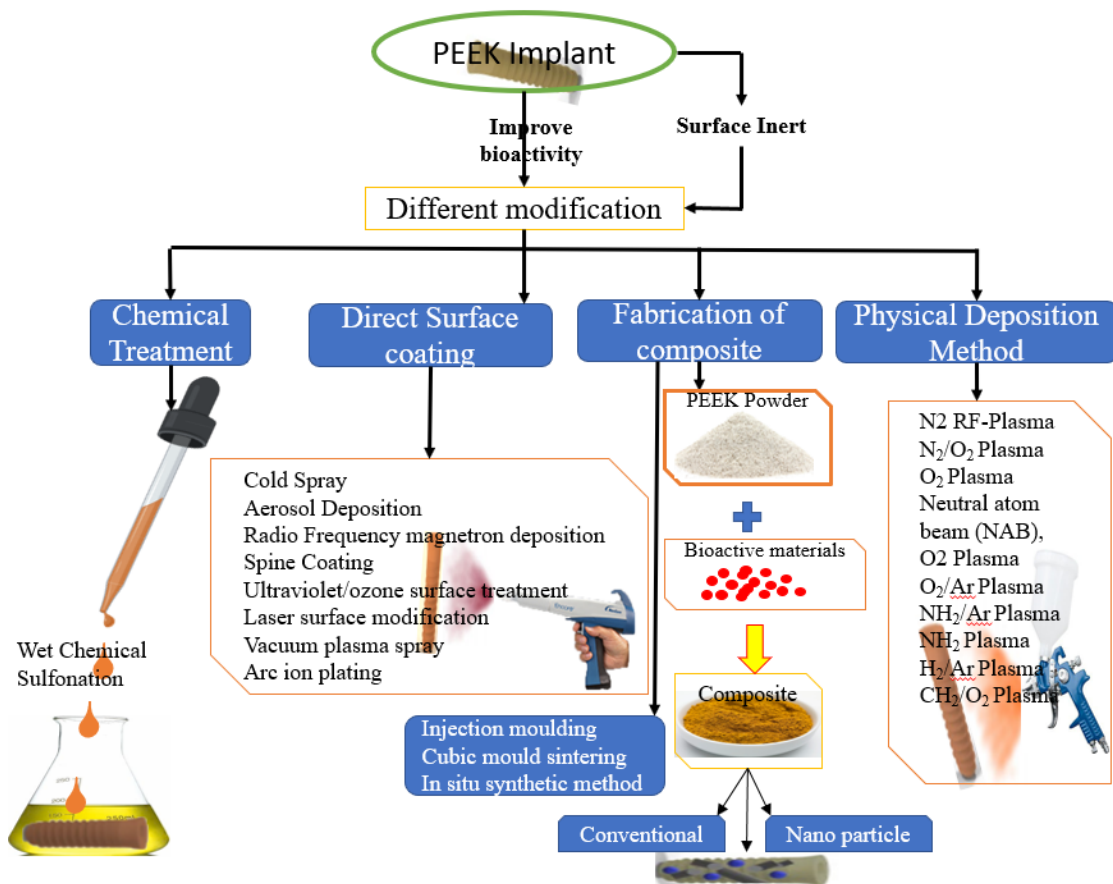
Figure 4.9 Schematic current strategies for PEEK modification and bioactivity state in osseointegration and future perspective of CH_2.

4.4. Calculation of composite

Mechanical and hygrothermal properties of composites are vital criteria to design and investigate. The Moduli and strength values essentially define a composite's mechanical qualities. The coefficient of expansion is caused by moisture diffusion and the coefficient of thermal expansion. Other criteria must be considered fibre form, size, distribution, misalignment and fibre-matrix interface qualities, void content, fibre fracture, and matrix cracking. Micro-models are employed in micromechanics studies since the sizes of fibres vary on a microscopic scale of 5-140 µm.

4.4.1. Engineering constants of elastic properties

The stress-strain connection is essential to interacting with a material and a structure. The stress-strain behaviour of a 1D isotropic elastic body is described by Hooke's law = E. The material constant E is the elastic modulus. Apart from E, the other well-known elastic modulus for a 2D or 3D isotropic body is Poisson's ratio v. G is not independent of E. Still, it is related to it, as $G = E/2(1+ v)$. Fundamentally, a composite material is heterogeneous. Where G is the modulus of rigidity, E is the young modulus, and v is the Poisson ratio

4.4.2. Particulate composites

The most fundamental mechanics of the material method calculates the elastic properties of anisotropic composites using conventional constant strain (Voigt) and constant stress (Reuss) models derived from the theory of constant strain and constant stress. The bulk modulus k and the modulus of rigidity G are given following the V_{oigt} model. The study of [197,198]revealed that $P = V_f\, P_f + V_m\, P_m$, where P=K,G and is the new composite, and

$$E = 9\ KG\ /\ (3K+G)$$

$$v = (3K-2G)\ /\ (6K+2G) \tag{4.1}$$

and with the Reuss model, the relations are

$$\frac{1}{P} = \frac{V_f}{P_f} + \frac{V_m}{P_m}\quad P = E, K, G \tag{4.2}$$

The characteristics anticipated by Voigt (the greatest) and Reuss (the lowest) oppose the qualities predicted by actual values. Many more accurate analytical models are known to exist [181,199]. The problem is that they are not readily available to users of traditional design programmes. The Halpin-Tsai model [200,201] is frequently used on a semi-pragmatic method because it gives upper and lowers bounds inside the Voigt and Reuss limits, which are otherwise. This research [134,201] shows that simple relations centred on an enhanced combination rule reasonably approximate anisotropic composite features. P_f is more than P_m, and V_f is less than 0.5; these are presented in the following.

$$P = \frac{P_m\left[1+\xi V_f\left\{\frac{(P_f-P_m)}{P_f+\xi P_m}\right\}\right]}{\left[1-V_f\left\{1+\frac{1}{2}(1-V_f^2)\right\}\{(P_f-P_m)/(P_f+\xi P_m)\}\right]} \tag{4.3}$$

with P = K, G.

For bulk modulus, K: $\xi = \dfrac{2(1-2V_m)}{1+V_m}$ (4.4)

and for shear modulus G: $\xi = \dfrac{7-5V_m}{8-10V_m}$ (4.5)

The modulus of elasticity E and Poisson's ratio v are then calculated from Eqs.4.6 and 4.7 with the help of Eqs.4.8 and 4.9.

The thermal expansion coefficient α is given by

$$\alpha = V_f\alpha_f + V_m\alpha_m + K_fK_m\left(\frac{\alpha_m-\alpha_f}{K_f-K_m}\right)\left(\frac{1}{K}-\frac{V_f}{K_f}-\frac{V_m}{K_m}\right) \tag{4.6}$$

where K is obtained using Equations.4.26 and 4.27.

The modulus of Elasticity [E] is $\dfrac{Stress}{Strain} = \dfrac{\sigma}{\varepsilon}$ (4.7)

$$E_c = E_pV_p + E_{cHAp}V_{cHAp} + E_{rGO}V_{rGO} \tag{4.8}$$

$$\sigma_c = \sigma_pV_p + \sigma_{cHAp}V_{cHAp} + \sigma_{rGO}V_{rGO} \tag{4.9}$$

The modulus of Elasticity [E] for the rGo is 1000Gpa [181], PEEK is 3.85Gpa [134], and cHAp is 10Gpa [202]. PEEK's most common use poison ratio is 0.4, from which another composite poison ratio is derived [177]. The density (ρ) of PEEK is 1310kg/m^3, cHAp ρ used is 3150 kg/m^3, and ρ of rGO is 1955 kg/m^3 [193] The modulus of rigidity or shear modulus (G) of PEEK is 1.375Gpa, cHAp is 3.943GPa, and rGO is 427.35GP, according to Equation (4.10).

$$G = \frac{E}{2(1-\vartheta)} \tag{4.10}$$

From Equation (4.8), 69 wt% of PEEK, 30 wt% of cHAp and 1 wt% of cHAp give the expression:

$$E_c = 3.85\text{Gpa x } 0.69 + 10\text{Gpa x } 0.3 + 1000\text{Gpa x } 0.01$$

$$E_c = (2.6565 + 3 + 10)\text{Gpa} = 15.6565\text{Gpa}$$

Table 4.1 Material property of PEEK-rGO-cHAP of different densities at 1310 kg/m^3 of PEEK density.

PEEK (wt%)	rGO (wt%)	cHAP (wt%)	Young Modulus (E)GPa	Shear Modulus (G) GPa	Poisson Ratio (ϑ)	Density ($\dot\rho$) kg/m3	Bulk Modulus (Gpa)	Relative Density
69.0	1.0	30.0	15.66	6.86	0.142	1868	7.287	0.7013
73.0	2.0	25.0	25.31	11.44	0.107	1782	10.72	0.7352
77.0	3.0	20.0	34.96	16.02	0.091	1696	14.26	0.7724
81.0	4.0	15.0	44.61	20.60	0.083	1610	17.84	0.8137
85.0	5.0	10.0	54.27	25.18	0.078	1524	21.42	0.8596

4.5. 3D printing machine

This work uses a Fumate HP 155/Gen 2 professional 3D printer to print PEEK filament with a product size of 225200200 mm and thermally insulating support in an insulated production environment. The diameter of the extruder is 0.4 mm. Before printing, the second layer of Dimafix® solution was added to a heated bed to improve the thermal layer adherence of the mesh. The X/Y axis extruder speed, often known as print speed, was consistent between cohorts, although the nozzle crossing speed was not. Four samples are printed at 1000 to 3000 mm/min rates with the PEEK-OPTIMATM LT1 filament. In FFF cohorts, print time and filament usage were measured. Control samples from the stretched PEEK-OPTIMATM LT1 jacket were treated alongside the printed batches. Before characterization, PEEK and nHA were dried in a vacuum oven at 150°C for at least four hours. Extrusion temperatures range between 380 and 410 degrees Celsius, and printing speeds range between 40 and 60 mm/s. Each printing line for the PEEK filler has a layer thickness of 0.2 mm and a bead width of 0.4 mm.

The primary goal is to replace current implants with specialised implants that mimic the solid mechanical qualities of the human femur. These implants are made from a virtual model built with the Mountain 8 Premium programme and then cast in PEEK. PEEK biomaterials are used as filaments and powders by the team. Apart from delivering high-fidelity natural biomaterial directly to virtual bio models, the manufacturer claims the team can create scaffolds with various shapes, sizes, and geographic distributions. After homogenising the unit cells, the final implant products should be built on anisotropic mesh Lattice structures generated in Creo software and simulated using the Ntopology tool to determine homogenisation. FEA was performed using ANSYS Workbench (FEA).

4.5.1. **3D printing settings**

The infill overlap percentage is the overlap between the infill and the walls expressed as a percentage of the infill line width. A little overlap allows the walls to be securely connected to the infill. The % infill, density, and pattern all impact the infill, with an infill line spacing of 0.4mm and an infill thickness of 0.1mm. The number of progressive infill steps is the number of times the infill density is reduced by half when approaching top surfaces set to zero. Because of the solidification and cooling process, the areas closer to the top surface of the scaffold have a higher density than the infill density. Layer height always influences layer thickness; a layer of infill materials set at 0.1mm will provide a flawless finish for a bone implant. This value is always a multiple of layer height and is rounded up. Figure 4.10 shows a 3D printing experimental setup, including printing layers, x-ray, and support for optimum fuse deposition modelling.
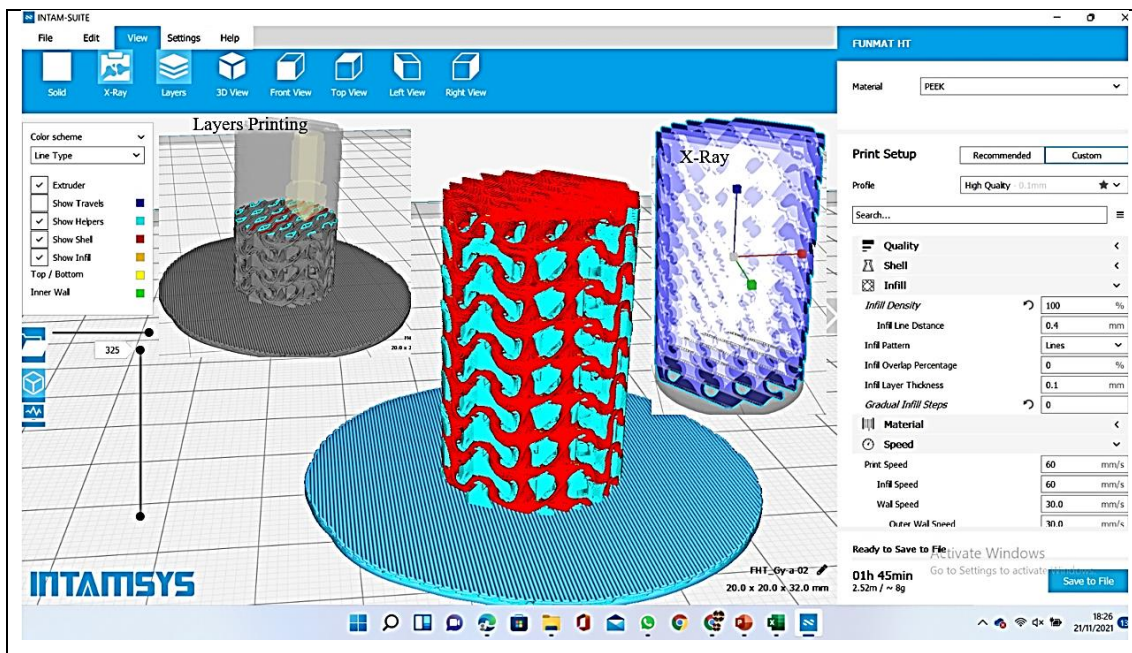
Figure 4.10 3D printing experimental setup showing the printing layers, x-ray, and the support for optimum fuse deposition modelling.

4.5.2. **Optimisation of printing machine**

Optimising the wall of a printing order reduces the number of retractions and distance travelled. Most will benefit from being enabled, but some will take longer than the projected printing time with and without optimization. Because the build plate adhesion type affects the printing, the initial layer is not optimised when picking the brim. The

outside wall option produces the scaffold's external walls at a rate of 30 mm/s. Printing the outside wall at a slower speed improves the final skin quality of the scaffold. A significant gap between the inner and outer wall speeds, on the other hand, harms quality and decreases the bridge wall speed. The standard surface mode was used in the scaffold printing process. It requires treating the model as a surface, a volume, or a volume with a loose surface. Only enclosed volumes are printed in the default print mode. A single wall painted in a surface mode without infill or top/bottom skin traces the mesh surface. Any remaining polygons are printed as surfaces, and both prints, as standard, include volumes. The outer contour was spiralized during printing to reduce the Z movement of the outer edge. Throughout the print, they will give a steady Z increase. Thanks to this functionality, a solid model becomes a single-walled print with a solid bottom.

This feature was made available because each layer has just one part. The print process involves printing each model in a single layer and waiting for one model to be finished before printing the next. All models are separated so the entire print head can travel between them. All models are printed in the one-at-a-time mode because they are smaller than the space between the nozzle and the X and Y axes. The structure was printed at a support speed of 60mm/s. Reduced printing time can be achieved by using faster printing support. The surface quality of the support structure is essential in this case since it remains after printing.

In this study, scaffolding is printed using FDM technology. The fastening surfaces of the printed lattices are parallel to a maximum of 10 mm. The extrusion temperature is between 340 and 450°C, the print speed is 40 mm/s, the bead width of each print line is 0.4 mm, and the PEEK filler layer thickness is 0.2 mm. Custom dental implants with the mechanical strength of a human femur are manufactured directly in PEEK using AM equipment based on a virtual model created in Mountain 9 Premium. The Premium Package states that the device is made of PEEK biomaterial in fibre and powder. Additionally, the company states that it enables high-precision direct physical modelling in biomaterials for virtual biological models. This technology can fabricate scaffolds with various forms, sizes, and spatial distributions (Figure 4.11).

Figure 4.11 Illustration of the Instrumentation or the experimental operation and fabrication o the scaffold.

According to a joint ASTM report [203–205], cache stereolithography (STL) files are generated from 3D models created using SolidWorks 2021 software packages. The samples were cut, 3D software generated the numeric code. All six cells were pressed with a heat leak multiple times, preventing the horizontal centre column from collapsing during printing. Before testing the mechanical or physical properties of the printed sample ISO-related standards, the printing parameters, packaging standards and their values are shown in Table 4.2. 3D-printed plastic granules were used to create this document. As a result, they were replaced with 5% cHAp and rGO 80-150 microns long and 7 microns in diameter.

Table 4.2 The properties of PEEK filament.

Description	Value PEEK	Test method
Melting Temperature	345 °C	---
Glass-transition temperature	143 ºC	---
Density	1.30 g/cm3	ISO 1183
Bulk Modulus	5.475-575 GPa	
Poisson's Ratio	0.38541	Computational

Young's modulus	3.76 GPa	ISO 527
Shear modulus	1.357 GPa	
Tensile strength	100 MPa	ISO 527
Impact strength notched Izod	55 kJ/m2	ISO 180/A

A lack of control over print speed could result in a geometric collapse while building scaffolds. The compressor's user handbook recommends 2 to 6 mm/s print rates for finely accurate lattice patterns and 8 to 16 mm/s for superb practices. By altering the pressure in the extrusion head, which changes the form of the scaffold, the volumetric flow rate and hence the material deposition rate may be changed. For example, by gradually increasing the amount of material deposited, the porosity of the structure can be reduced by checking the optimum porosity that mimics bone porosity according to [190-196]. Intracortical porosity was measured using tibial and femoral mid-diaphyses transverse sections (50micromter, thickness; N = 24) representing 52%-59% cortical bone porosity. The cross-sectional cortical area (mm2), total porous area (mm2), and several pores with a size greater than a detectable threshold of 11 m2 were all visually quantified using a Nikon Optiphot microscope and a Bioquant digitisation system. PEEK was injected at rates ranging from 5.2 to 23.2 cm^2/s to know how it affected its maximum degree of crystallinity and how much it fluctuated. Despite the variation in injection speeds, the thickness homogeneity is almost identical for high and low injection rates. On the other side, higher injection rates are somewhat beneficial. If this technique is used, PEEK mould crystallinity can be maintained uniformly throughout its thickness and length. PEEKs crystallinity and uniformity can be achieved at a mould temperature of 150 °C, which is somewhat higher than the PEEK. So the higher the mould temperature above the semicrystalline thermoplastics glass transition temperature. The shorter it takes to attain the necessary crystallinity and homogeneity throughout a PEEK printing component's thickness and length. Figure 4.12 shows the equipment for 3D printing the different lattice structures of femur bone at 2 x 2 x 2 mm cell structure to mimic the bone structure.
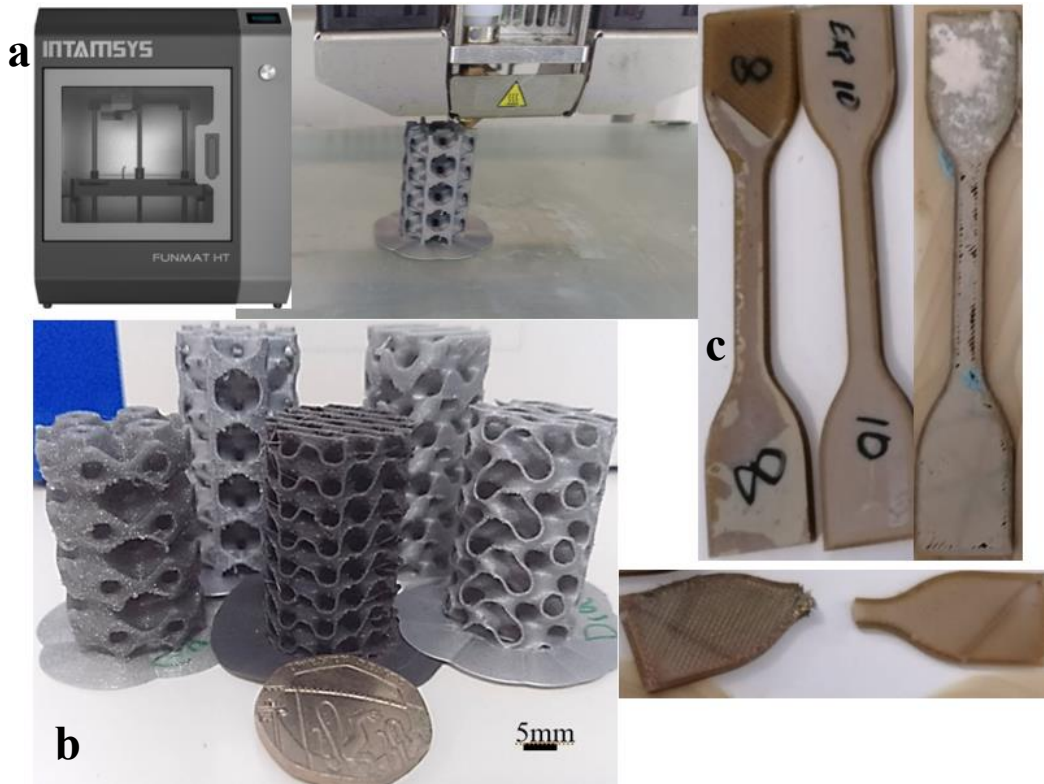
Figure 4.12 (a)Equipment set-up for the 3D printing of (b) the different lattice structure femur bone at 2 x 2 x 2 mm cell structure to mimic the bone structure (c) dog bone for tensile testing

When mould temperatures are low, a fast-cooling cycle can yield amorphous and transparent moulded components with very thin wall thicknesses. Under the same fast chilling conditions, pieces with transparent skin and an opaque crystalline core are formed as the cavity thickness increases. When cooled slowly and at temperatures up to 200oC, PEEK moulds exhibit good consistency in the degree of crystallinity throughout the thickness. The crystallinity of the skin and crumb remained virtually constant throughout the process. Figure 4.13 depicts the thermal process of coating cHAp onto PEEK in cells for a PEEK and cHAP 3D printing process with consistent melt processing temperatures of 400ºC, a mould temperature range of 20-200ºC, and injection speeds of 23.2 cm3/s as processing variables. Figure 4.13 depicts the construction of a three-dimensional scaffolding lattice (Table 4.3).

Table 4.3 Printing parameters of the FDM for PEEK-HAp.

Printing parameters	Technical specifications	Infill	Value
Nozzle diameter (mm)	0.4	Internal fill pattern	Rectilinear

Extrusion multiplier	0.78	External fill pattern	Rectilinear
Retraction distance (mm)	0.49	Interior fill percentage	100%
Retraction Speed (mm)	1750	Outline overlap	50%
Bed width	210 mm		
Layer thickness	0.1-0.2 mm	Infill extrusion width	90%
Printing speed	40-50 mm/s		
1st layer height (mm)	0.1	Minimum infill length (mm)	5
Top solid layer	3	Support	---
Raster angle	Longest edge		
Bottom solid layer	3	Support infill percentage	30%
Outline shells	3	Print support layers	1
1st layer height	170%	Bult Plate temperature	110-160ºC
1st layer width	95%	Nozzle temperature	340-415 ºC
1st layer speed	30%	Z-axis speed (mm/min)	1000
Additions (skirt/brim)		Filament diameter (mm)	1.75
Skirt layers	1	Ambient temperature	50 ºC
Skirt offset from part (mm)	0	Chamber Temperature	90 ºC
Skirt outlines	15%	----	---

The programme analyses melt level occurrences across whole components and offer extensive thermal history and microstructure data. Reproducing a single sphere allows for a quick assessment of the quantity and makeup of the resource pool. Furthermore, porosity was only partially controlled because of the step parameter set selection flaws. The experimental setup, sample preparation, and PEEK surface modification are then addressed in section 4.7.

4.6. Experiment

From the virtual 3D model, an STL is developed and then restored to a 3D printer, which produces an actual prototype that perfectly mimics the desired anatomy. When the solvent evaporates, the rich polymer phase becomes the matrix, while the weak polymer phase remains. The body's pores widen. Computer controls define the precise geometry of the intricate completed objects. Between 350 and 420ºC, extrusion occurs at a constant force rate of 40 mm/s. PEEK filler is a 3D-printed substance manufactured in the United Kingdom that consists of resins and filaments. cHAp and rGO with a content of 5% replaced composite materials with a length of 80-150 microns and a diameter of 7 µm. The computer oversees the ultimate complicated object's intended geometry. The extrusion temperature range for each print line is 380 to 410°C, the bead width is 0.4 mm, and the layer thickness is 0.2 mm. The output speed was 40 mm/s. Figure 4.13 depicts the system configuration for simulation, experiment, cell growth scaffold, and additional testing and coating media, such as Dulbecco's modified eagle's medium (DMEM) and

nutritional Agar solution (NAS), and mechanical testing of PEEK-rGO-chap strengths of scaffold samples. The PEEK filler material was also 3D printed and utilised in composite materials with fibre leftovers from the printed part of 5% cHAp and rGO granules with a 75–145 µm diameter and a length of 6.89 µm.
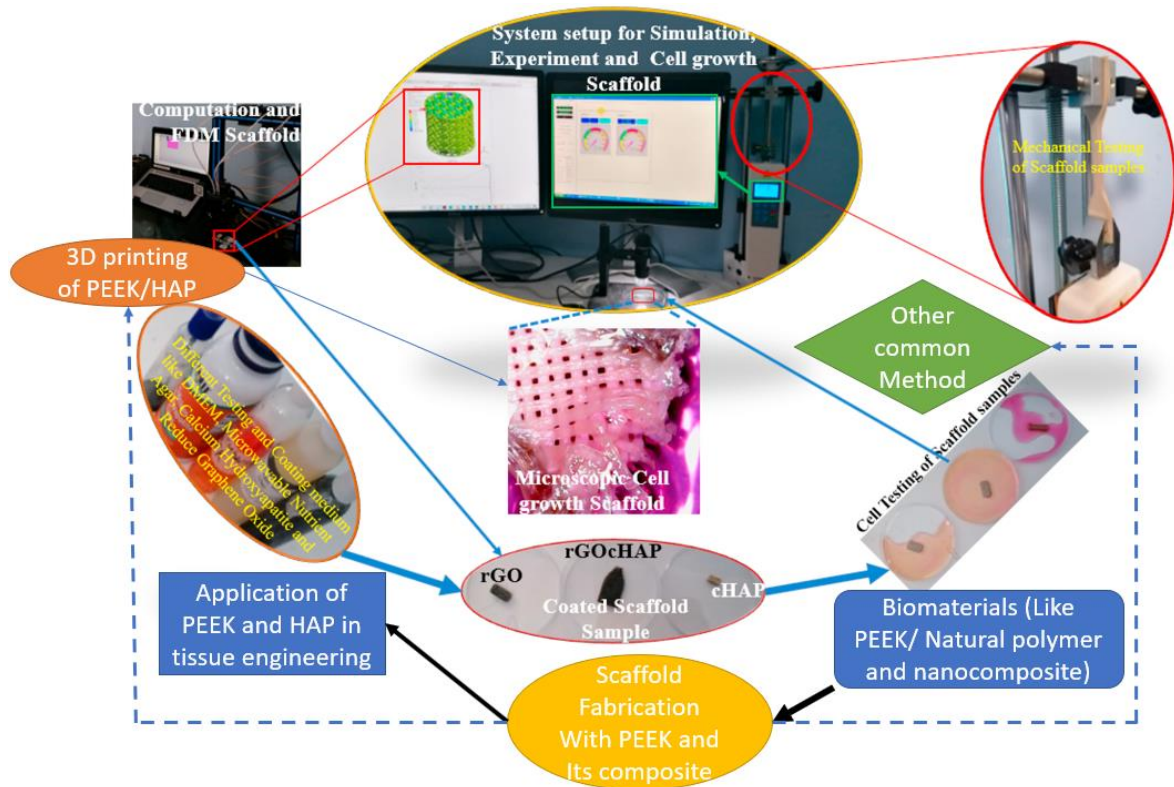
Figure 4.13. The setup for Simulation, Experiment, Cell Growth Scaffold, and Different Testing and Coating Media such as DMEM and NAS and Mechanical Testing of Scaffold samples PEEK-rGO-cHAp Strengths.

4.6.1. Sample preparation

This study applied medical-grade PEEK to 3D-printed samples of various sizes in real-time PCR testing. Cylindrical samples were applied parallel to the surface of 10mm-to-10mm samples *in vitro*, in 24-well tissue culture plates, and parallel samples from 20 mm x 20 mmx1mm in real-time. All models were polished on an almost flat side *in vitro* and purified in acetone, ethanol, and ultrapure water. Magnetic stirring with concentrated sulfuric acid (95%-98%) at room temperature was used to obtain a homogeneous porous structure in the sulfonation process. The sample was then immersed in deionised water for 5 minutes to remove surface debris. Figure 4.14. shows different printing bone scaffolds of the Structure Design of Gyroid, Schwarz Primitive, Diamond, Schwarz

Diamond, Neovius, Splitp and Lidinoin for PLA and PEEK after adding composite to mimic bone structures 25 printed samples scaffold. The samples were then subjected to hydrothermal treatment, and the sulphur concentration temperature was adjusted to room temperature. The sample was gently washed with deionised water and dried while the sample was sulfonate only. The reaction time at the given temperature depends on the sulphur content.
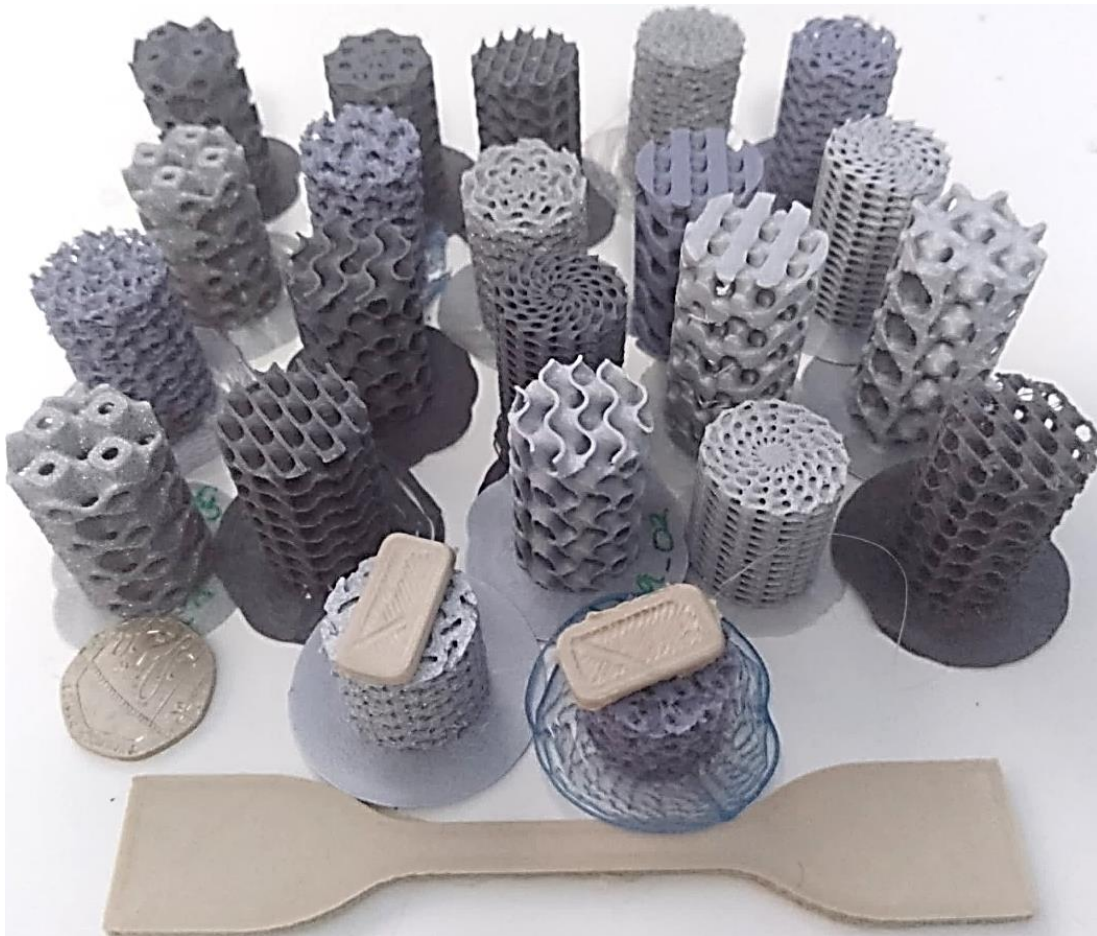
Figure 4.14. Different printing bone scaffolds of the structure design of gyroid, Schwarz Primitive, diamond, Schwarz diamond, Neovius, splitp and Lidinoin for PLA and PEEK after adding composite to mimic bone structures 25 printed samples scaffold.

The sulfuric acid used for the sulfonation of PEEK is 98% PA used for the rGO surface treatment is anhydrous acid. The glass powder of sulfuric acid, cHAP and rGO is treated with a PEEK surface. The citric acid increases the interfacial adhesion between the polymer matrix and the inorganic filler and facilitates PEEK [176,177]. The surface treatment of the cHAP glass powder was carried out with sulfonated PEEK. With 98%

sulfuric acid, 2 g of PEEK powder was first added to a 50 ml measuring flask containing sulfuric acid. PEEK was dissolved in a medium and then kept with magnetic stirring at room temperature. The temperature is raised and held at 50 °C for 90 minutes. Add 500 ml of cold distilled water with magnetic stirring to precipitate PEEK. Filtering and rinsing with distilled water several times with a pH-neutral PEEK was dried for seven days in processing steps in the following oven at 50 °C. After receiving PEEK containing sulfonates, Surface treatment of cHAP vitreous powder was performed with PEEK according to a process of 80 °C. Four hours of stirring was followed by evaporation at 120 °C in an oven, followed by chalcedony crushing. The surface treatment of rGO with citric acid was based on work. First, 0.5 g of citric acid was added to isopropyl alcohol. It was kept under magnetic stirring at room temperature 60 minutes later, and 10 g of rGO was added to the solution. It was kept stirring for 6 hours. Then, the solution was placed in a 60 °C oven to evaporate the solvent, and agate was used to grind the material.

4.6.2. Production of composite PEEK

Dry grinding is performed with a PEEK mixture with inorganic filling, a bowl and 50 dense zirconium balls with a diameter of 4 mm, grinding for 24 hours at a rotation speed of 180 rpm. Some of these materials were sent to atomisation inorganic charge with PEEK polymer. This procedure improves the filler dispersion in the polymer matrix and facilitates the next steps of powder compaction. The atomisation of the powder was carried out in the De Montfort University (DMU) laboratory by adding a PEEK powder filling cup water subjected to magnetic stirring after homogenisation of the suspension. The solid/liquid ratio was 25% m/v was suffocated and sprayed to dry. The atomisation control parameters previously used by the DMU laboratory were applied to the airflow of an atomising nozzle of 25-30 L/min with turbine airflow of 3.8 m^3/min and air temperature of 120 °C. Figure 4.15 depicts different printed scaffolds and nozzles of 0.2-0.4 for other bone implants.

Figure 4.15 Different printing Scaffold and Nozzle 0.2-0.4 of the different bone implants.

4.6.3. Surface modification of PEEK

The samples were made using the cold pressing technique with a hydraulic auxiliary press with a capacity of 10 tons for a square specimen 47 x 5 mm using a steel mould and a thickness used to 3 mm. The samples were incinerated for three hours. A sintering temperature of 350 °C was selected from dilatometry and subsequent tests. The thermal weight transformation analysis determined the sulfonation level of SPEEK. PEEK exhibited a single-pass mass loss consistent with sulfonation. Conversely, PEEK offers two stages of mass loss: the first step corresponds mainly to the loss of sulfonic groups. While the second stage corresponds to the deterioration of the PEEK backbone, suppose that the first stage of mass extinction corresponds only to the loss of sulfonic groups. Linear thermal shrinkage of PEEK-cHAP and PEEK-rGO blends was determined using a DMU laboratory photometer. A 3x3mm cylindrical mould sample was compressed to

a dilatometer and heated to 395°C at 10°C/min. It is probable to control the preliminary and concluding temperature of the condensation process of the material. This result makes it possible to determine the combustion cycle of the prepared material. Infrared analysis was performed using a Fourier transform spectrophotometer.

FTE analyses of PEEK and SPEEK were performed to determine the characteristic absorption bands of these polymers. The cHAP and rGO materials were analysed to confirm that the surface treatment of fibres and inorganic particles worked. All tests except SPEEK are interpreted as a membrane made of powder material. The direct surface modification method is a technique that changes the surface properties without placing a new layer of material on the surface. These techniques are characterised by the following. This approach alters the implant surface chemistry and affects surface bioactivity. Several studies report that PEEK bioactivity can be improved with a wet chemical treatment. PEEK sulfonate is available in two forms: sulfonated PEEK with subsequent dip and sulfonated PEEK with an extra drop of acetone. The schematic filament manufacturing process for 3D printing PEEK composites in biomedical scaffolds for tissue engineering and cell attachment creation on PEEK-rGO-HAp scaffolds with 500 m cubic pores on a composite bone is summarised (Figure 4.16).
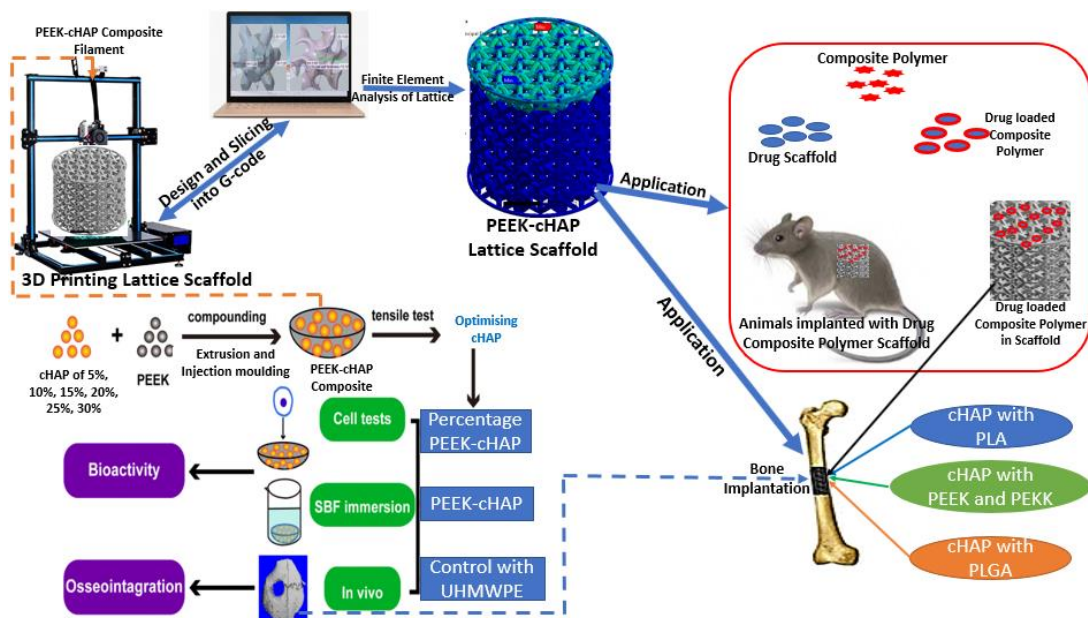
Figure 4.16. 3D printing of PEEK composite in biomedical scaffolds of cell proliferation and attachment process of a bone implant in FDM via in-vitro and its biological evaluation and application[184-186].

4.7. Conclusions

PEEK-cHAp-rGO bio-composite material for bone grafts is produced utilising a novel method including extrusion, extrusion, and free-forming. This novel technique allows for more precise control of the bioactive phase distribution than traditional 3D printing of 3D biopolymers at a constant pressure of 0.39 MPa, a residence period of 20 minutes, a temperature of 400 °C, and a pore size of 0.02 µm. There are over 200 intermediate shelves and cHAp, and the dimensions are $20 \, x \, 10 \, x \, 3$ mm, making them ideal for pressing moulds. It is a revision and extension of earlier work. The practical method enables the fabrication of perforated PEEK crimps in the connecting pipes. Adding cHAp and rGO particles to the PEEK enhanced the biological activity of PEEK when its tensile test and modulus characteristics were tested at concentrations ranging from 0 to 30% by weight samples in the next Chapter 5.

Chapter 5

ΔS

CG

ΔF
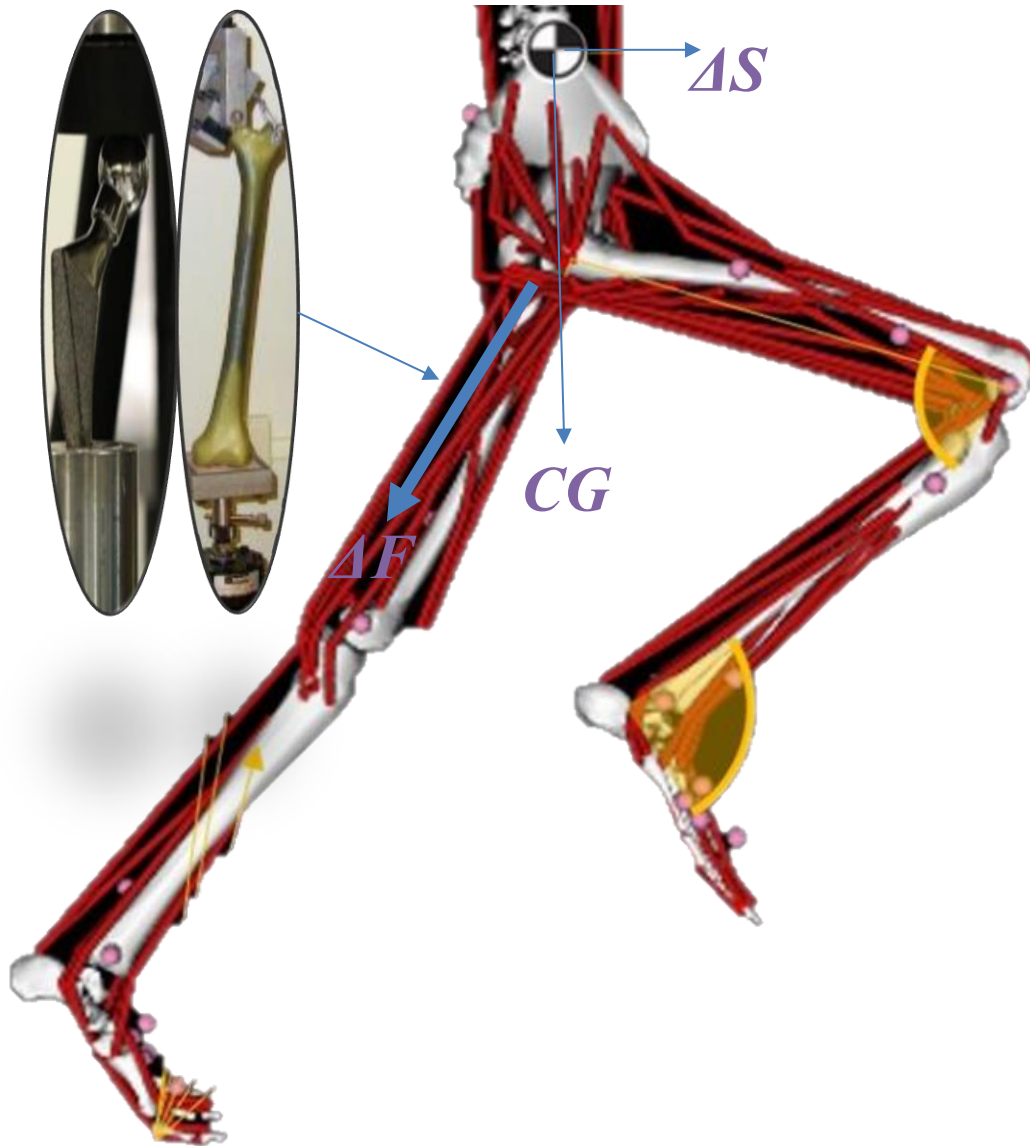
Mechanical strength testing on lattice scaffold to mimic bone implant

CHAPTER 5

5.0. MECHANICAL TEST

5.1. Introduction

The Sample materials designed in lattice were tested using an Instron machine model following the ASTM (American Society for Testing and Materials) D638 standard to analyse their mechanical properties. A 50 kN Force cell with a 5 mm/min claw speed was used to test about ten specimens. The MERLIN software generated the stress-strain curves and material property values. An extensometer was used in the 0.05 to 0.5 % deformation range for enhanced elastic modulus accuracy. Figure 5.1 depicts the dimensions of the ISO-527-2 standard's tensile specimen design. Using a compressive apparatus furnished with a video extensometer, the specimens were subjected to uniaxial compression testing to determine their mechanical characteristics. Compression testing was conducted at room temperature with a cross-head speed of 0.001 mm/s adjusted according to DIN 50106. Four samples were compressed from each structure. The direction of the drop was parallel to that of the FDM building (Figure 5.1). An extensometer with 0.05 to 0.5 % deformation was used to calculate the elastic module more precisely.
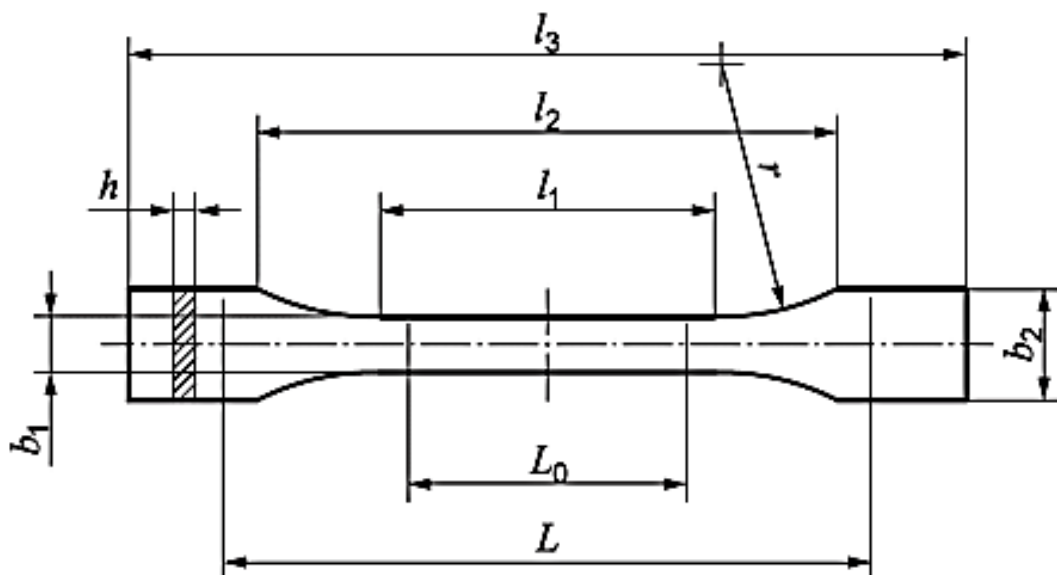
Figure 5.1. Tensile specimen design of ISO-527-2 standard.

Table 5.1 Dimension of tensile specimens.

Tensile test specimen	ISO-527-2(mm)	Printed (mm)
Overall Length (l_3)	≥ 75	76
Length of narrow parallel-sided (l_1)	30 ± 0.5	36
Distance between Shoulders (l_2)	58 ± 2	56
Radius (r)	≥ 30	30
Width at Center (b_1)	5 ± 0.5	10
Width at grip end (b_2)	10 ± 0.5	5
Thickness (h)	≥ 2	3
Gauge length (L_o)	25 ± 0.5	10 ± 0.2
The distance between clamps (L)	$l_{2\,0}^{+2}$	58

The specimens were printed before the tensile and compressive tests to equate bone strength. Ten samples were tested following ASTM D-256 guidelines. The dimensions of the specimens and the notches were fabricated. Tensile testing was done using an all-purpose Intron test at 1 mm/min and 25 °C. The Force rate was slowed to allow for comparisons with more flexible materials. The composite specimens' strain, tensile power, % elongation, and modulus were also determined using the Ansys and Creo software. The tensile test was conducted on rGO specimens weighing 1 to 5% of the total weight. Mountains MAP Premium 8.2 Surface Digitiser was used for virtual prototyping. Figure 5.2. shows the tensile and compressive test of the scaffolds; analysis of strengths.
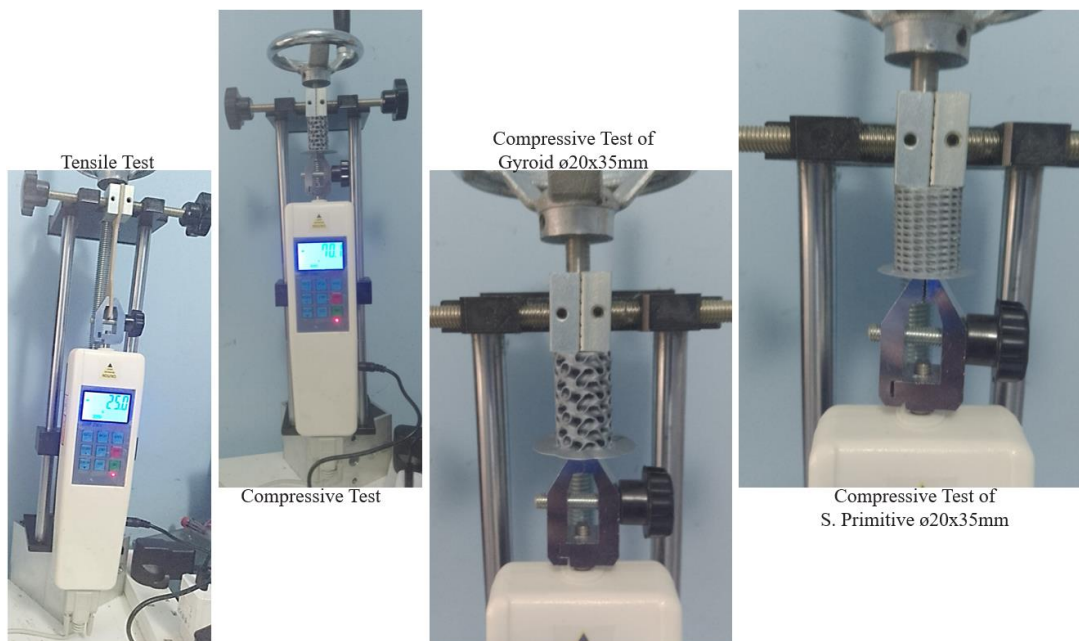
Figure 5.2. Tensile testing and compressive test of scaffolds Analysis of strength.

The fatigue tests were performed on an MTS Bionix Servo Hydraulic Test System equipment under controlled tension, at room temperature, and in traction-traction mode to get S-N curves. The trials used R = 0.1 and a frequency of 10 Hz. According to [142,206,207], The R-value was chosen to protect the specimens from compression forces and to prevent buckling. Tensile tests were utilised to determine the maximum stress values. For each sample, the selected values represented 30, 50, and 75% of the yield stress, respectively. It was agreed that if the sample did not divide up to 1 million cycles, it would not be considered fractured [23, 194-198]. Even if the exam had not failed, it was cut short. During the experiment, a Minima MT-350 infrared thermometer and a chrome-aluminium thermocouple were utilised to measure the temperature. Figure 5.3 depicts the design of several temperature-measuring methods.
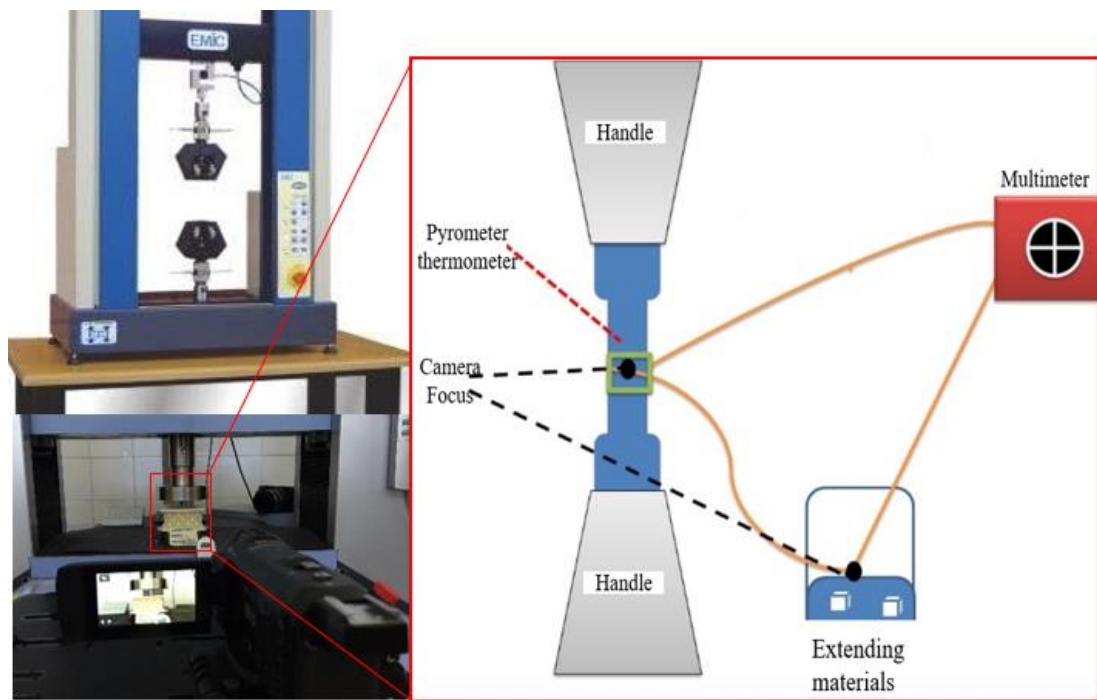
Figure 5.3 Detail the experimental configuration of the compression essay, and the Scheme show methods of obtaining the temperature of the scaffold.

The stress-strain responses of printed porous closed-cell samples were studied using the ASTM D695-02a standard compression test technique. At 100°C, we employed a porous hot plate with a maximum pore temperature of 4% and an average porosity of 38%. The samples were evaluated at 103 s^{-1} using 100kN Force cells on Instron testing equipment. The Instron test data were analysed using clever 6200 strain software; three samples were

taken. When big specimens were crushed, the PEEK flexible structure distorted. All species described in this study were subjected to direct pressure at the species' initial linear limit of compressive strength. The term "performance constraints" refers to compressive force strain (Table 5.2).

Table 5.2 Static tensile and static flexion test results of PEEK composite.

Properties	Flow tension (MPa)	Flow deformation (%)	Breaking stress (MPa)	Fracture deformation (%)	Modulus of elasticity(GPa)
Static tensile test					
Mean value	95.05	3.78	97.08	24.29	3.4
Standard deviation	0.98	0.15	0.80	1.57	0.08
Static flexion test					
Mean value	127.37	4.10	139.10		3.6
Standard deviation	1.82	0.059	4.95		0.059

The results were compared with the property of young modulus (E') following coating, the specimens were subjected same tests previously performed on coated cHAp and PEEK, and the results were reported. All analyses were performed in duplicate or triple, and the median curves were always shown. They were not taken into consideration in the event of outliers. A significant challenge has been the ability to 3D print structures of different materials ranging from ceramics to organic molecules. This method is especially true when structures are smaller than 50 µm long, approximately half the width of a human hair. The graph shows that this offered sufficient energy to solidify liquid polymers but not enough to fuse metals. PEEK does not have the same light-response characteristics as the polymeric resins utilised to fabricate nanoscale structures.

5.2. Determination of the Young Modulus

The elasticity module of the materials was evaluated non-destructively using Sonelastic® technology from the DMU laboratory. The modulus elasticity of each sample was measured three times before the flexion test. The microhardness of the samples was determined using a Shimadzu HMV Microhardness tester. The test was performed on scaffolds from each group previously polished with 1 mm and sanded at 1000 to 2500 meshes. The microhardness of each sample was determined by applying a force of 980.7 mN to five separate locations inside the sample for 15 seconds.

All specimens have been tested at an ambient temperature speed of 30mm/s, except for the 5 PLA probes tested at 3mm/s, which is the best and optimum test value. The comparison tests have been carried out on the AG-X universal testing machine, with a maximum Force of 50 kN - a compression of 100 mm in diameter with sufficient support area for testing purposes. The EMIC DL 2000 model machine was utilised to execute the mechanical compression test to characterise and confirm the strength of the printed scaffold. Figure 5.4 depicts the experiment's screen, showing the outcome or result as the compressive test was carried out from Figure 5.3.
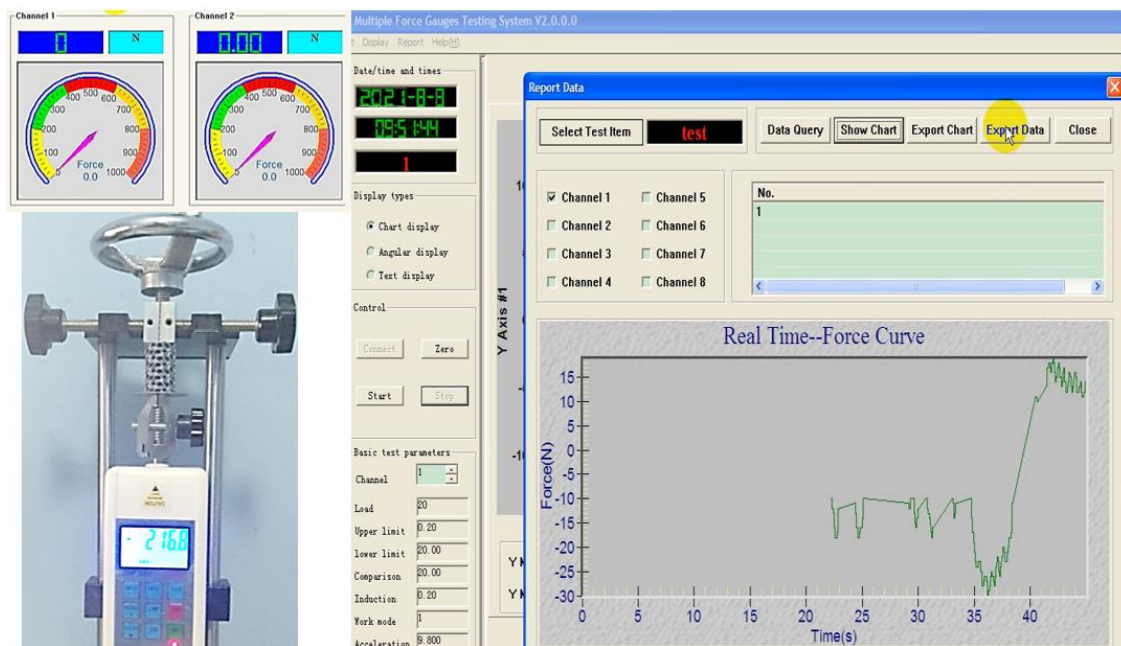
Figure 5.4 screen of the experiment showing the outcome and result as the compressive test has been carried out.

Thus, the proposed porosity calculation model can correctly predict the structure's porosity's magnitude according to [52-55]. The impact of joint hardening on the mechanical characteristics of joints is discussed in this section. I investigate parametric in three topologies of the cubic octet and the Schwarz Primitive cell, each with a different topology. The first two cells are dominated by tension, whereas the third is dominated by bending. Figure 5.5 depicts the Ntopology of the selected unit cell. Because of the periodic arrangement, duplicate edges are not included in a modified unit cell. Figure 5.6 shows three structural component characteristics, each with a 5mm unit cell starting point. PEEK is the material in issue. Figure 5.7 also depicts the results of tensile testing

of various lattice structures and the displacement of the composite and post-mechanical strength with time in microseconds. Figure 5.8 describe the relationship between maximum primary elastic strain and displacement.
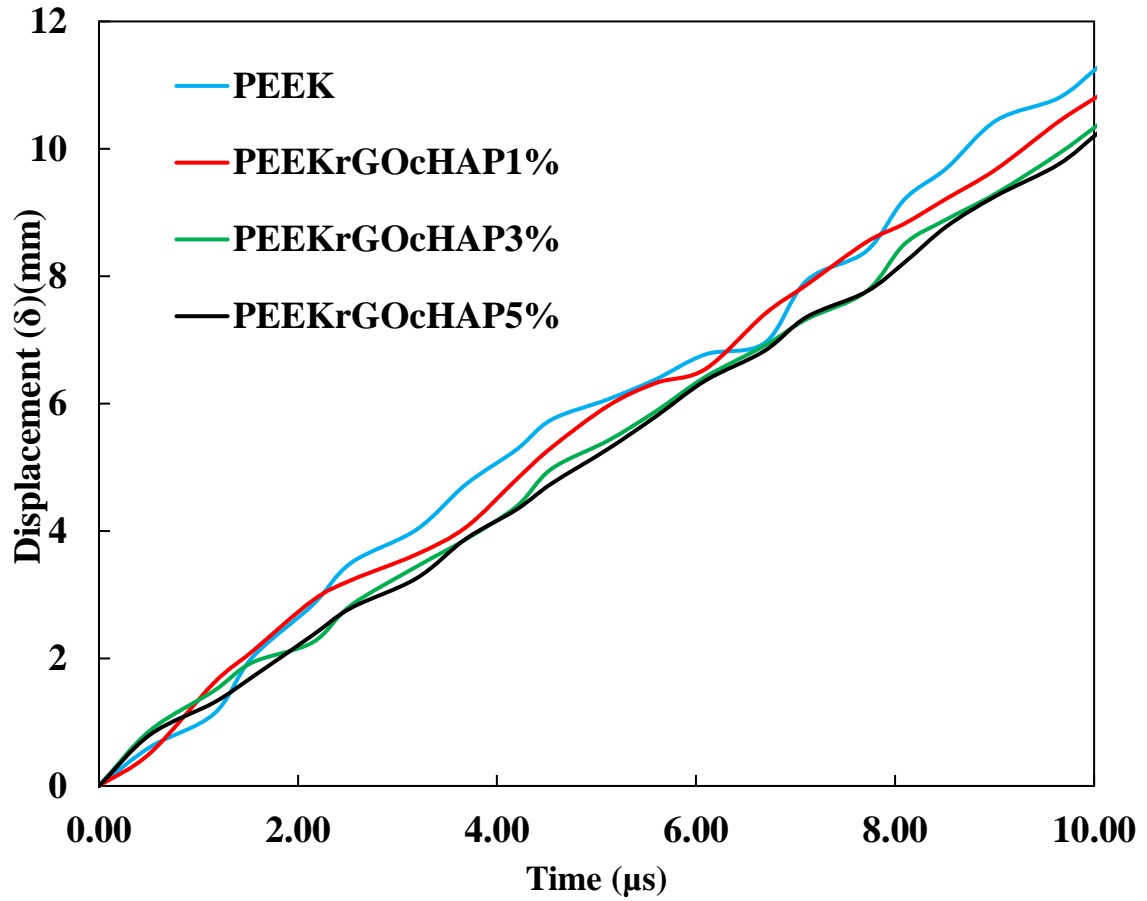
Figure 5.5 Results of tensile testing of different lattice structures and the composite and post mechanical strength displacement against time in microseconds
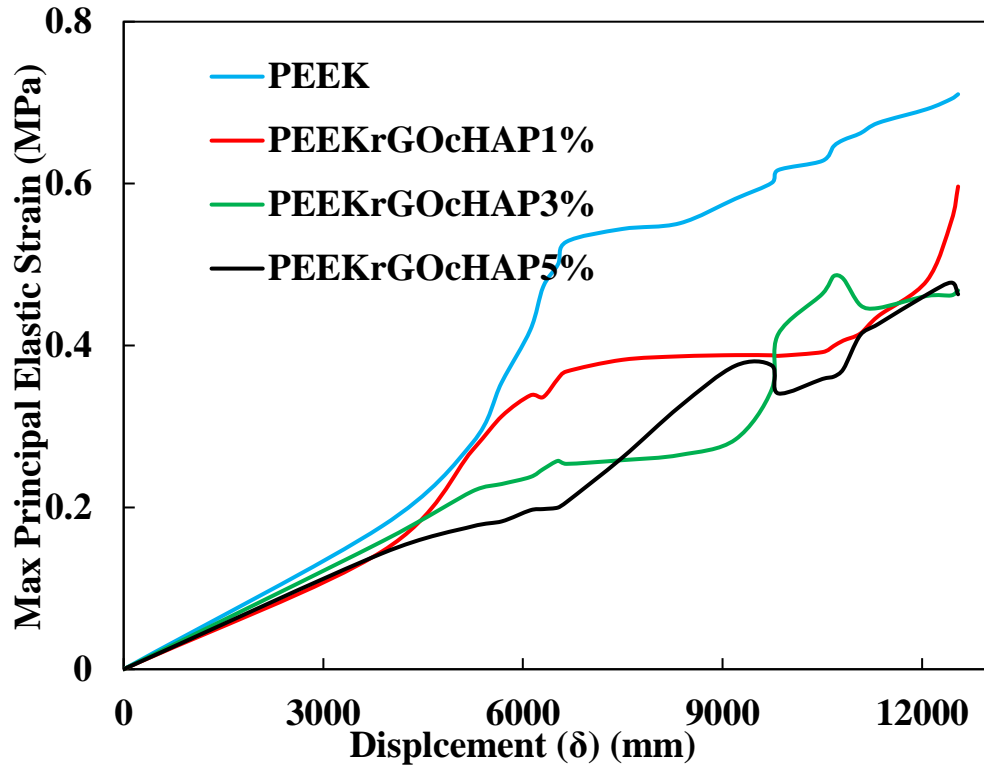
Figure 5.6 Relationship between maximum primary elastic strain and displacement.
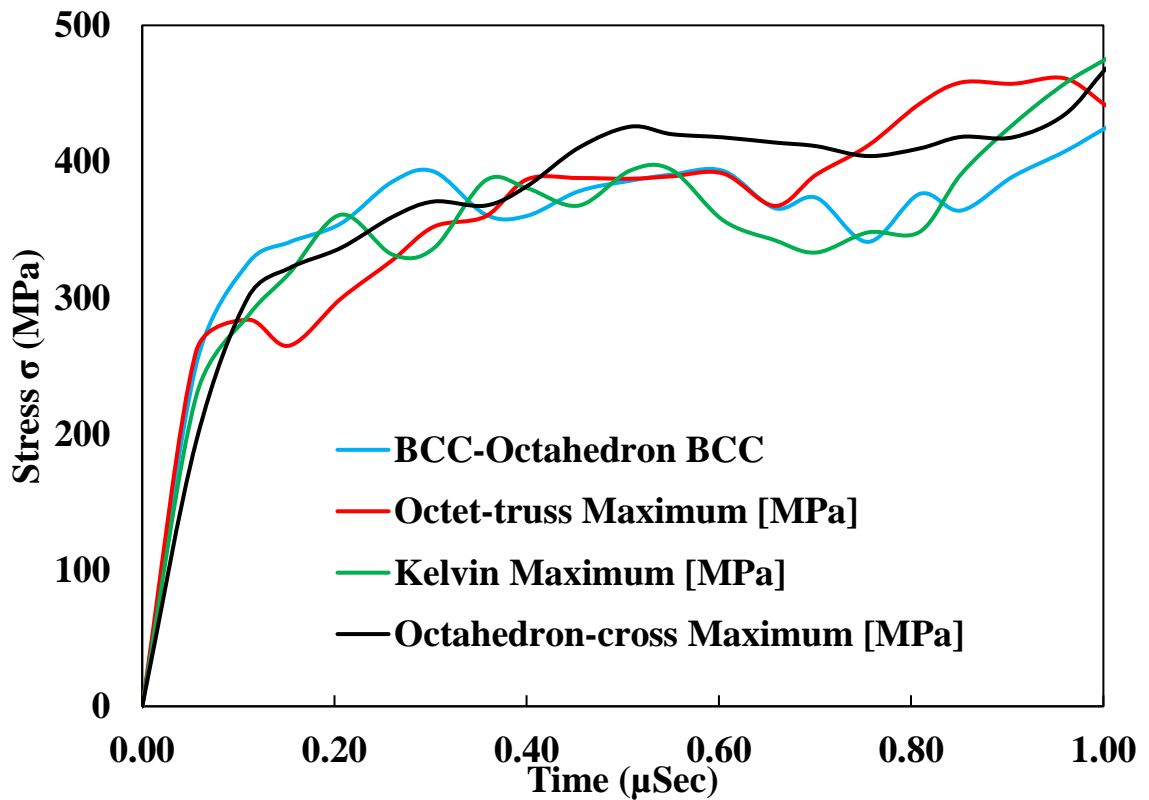
Figure 5.7 Comparison of the different lattice 3D printed scaffolds stress over a time of the unit cell
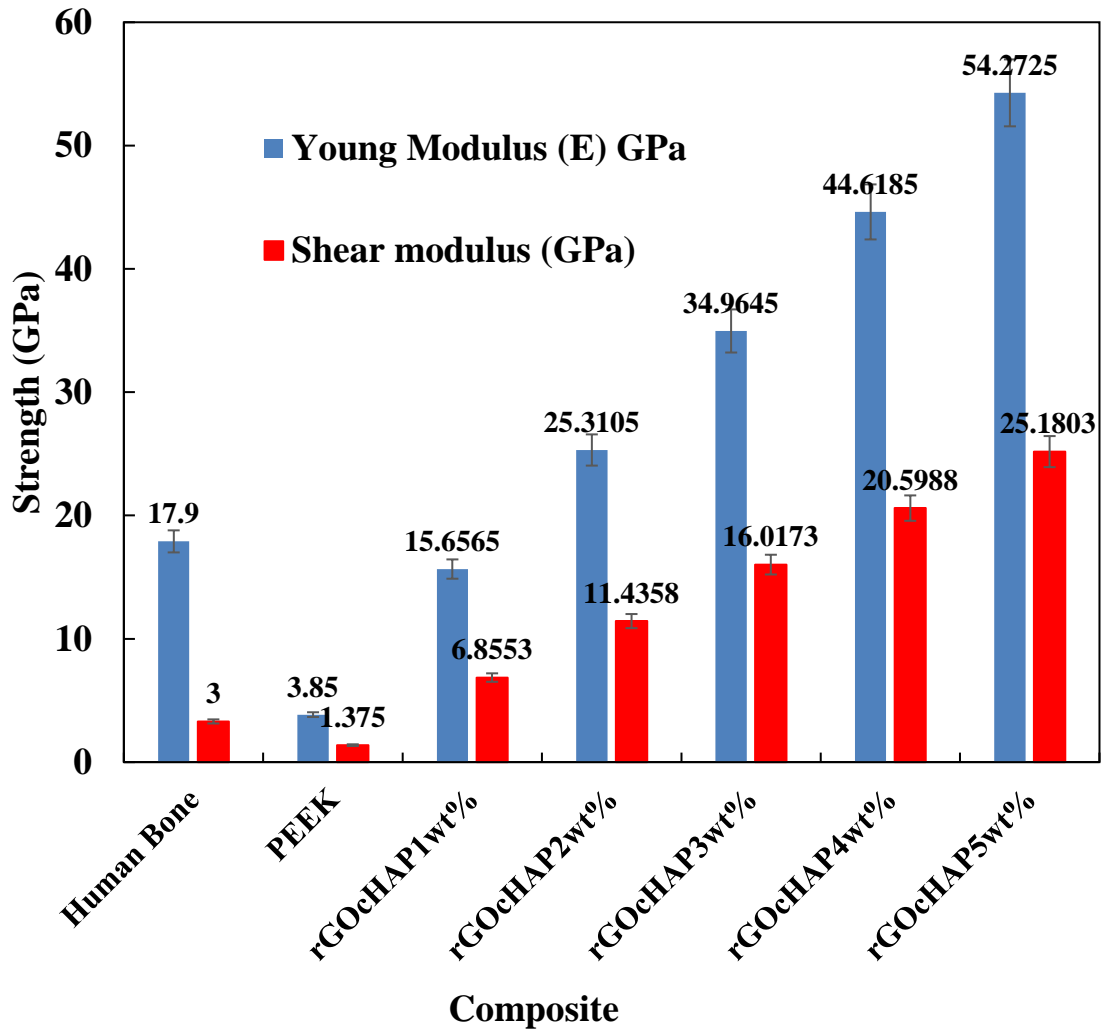
Figure 5.8 Scaffold compared with human femur bone of relative shear modulus versus composite relative density.

5.2.1. Tensile result of Scaffold Composite

Figure 5.9 depicts a general charge displacement curve for composite samples containing various quantities of cHAp and a specific charge displacement curve for composite samples. As the concentration of cHAp rose, the elongation decreased the composite effect of strengthening the PEEK. PEEK-cHAp showed a failure behaviour. The need for thermogravimetric analysis testing was also decreased because of this. The mechanical characteristics of the different specimens were determined via a slew of relevant experiments. A tensile test was performed on PEEK and composite materials to determine their strengths and weaknesses. Figure 5.10 shows the sample stress-strain curve at all temperatures tested (T_{amb}–250 °C); deformation remained constant in size. The deformation amplitude was increased to 60µm in a second instance to enhance the results'

resolution. Young's module (E') and loss module (E") curves have characteristics, as does the loss deformation and strain range for both the 20 and 60-micrometre levels of strain. According to the research [192-194], a tan (Tg) peak was found at temperatures between 150 and 160°C and E' temperature ranges. This means that amplitudes of 60 m can be used to obtain the greatest feasible resolution for future investigations.
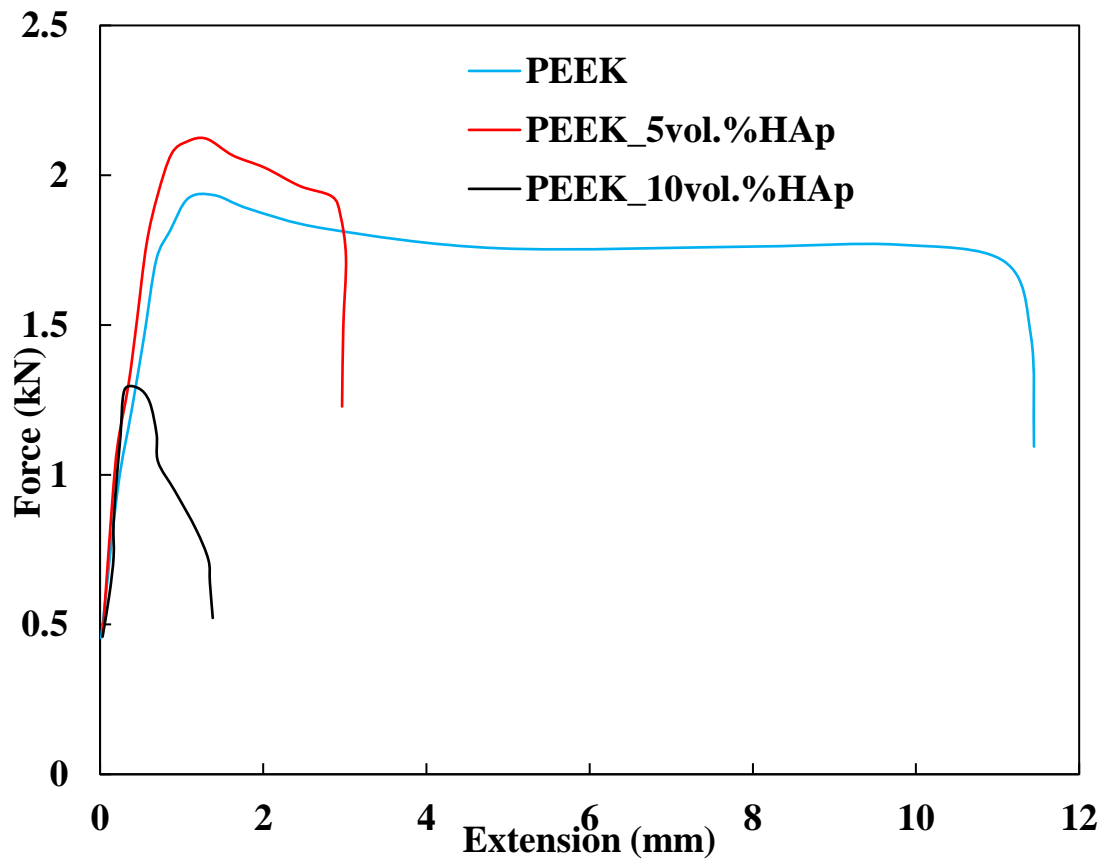
Figure 5.9 The force against extension curves of the PEEK–cHAp samples at different percentage volumes
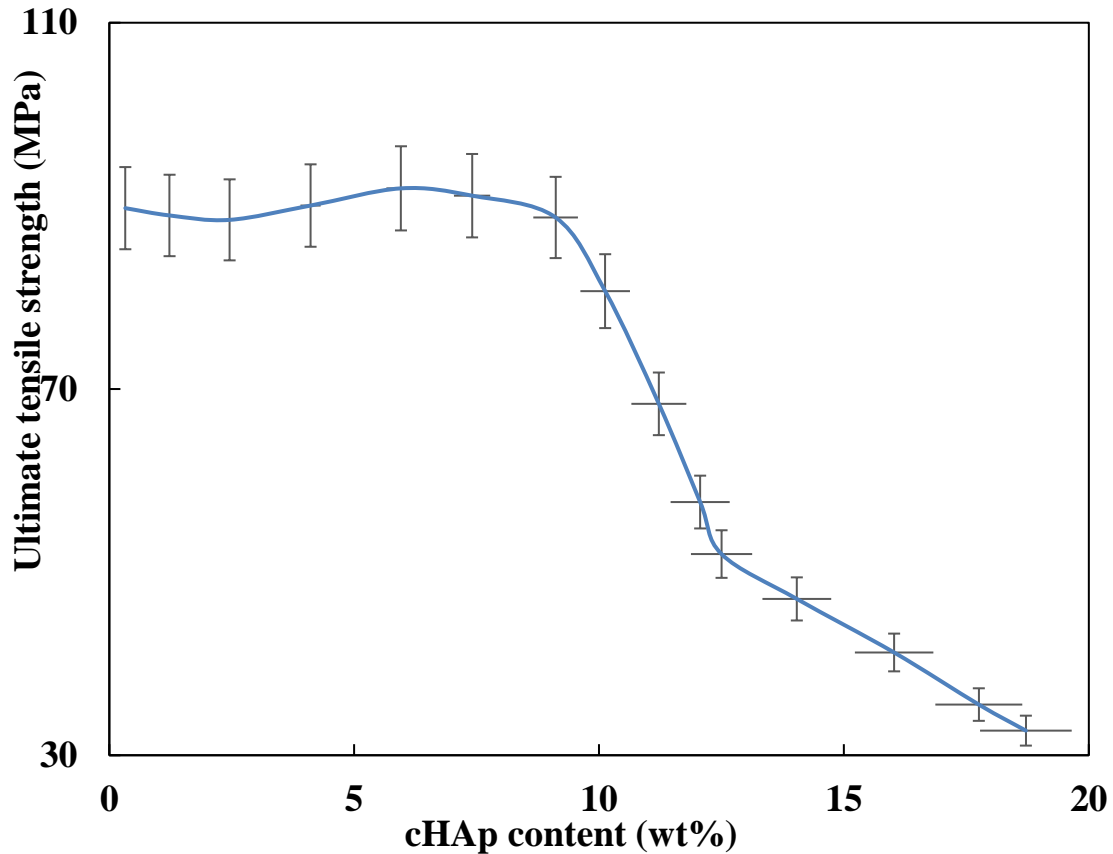
Figure 5.10 Variations of the ultimate tensile strength with percentage weight of the composite material of cHAp.

Table 5.3 compares the behaviour of samples exposed to the surface coating with cHAp to samples tested under the same conditions but without mechanical forces. PEEK is thermally robust and exhibits minimal mechanical stiffness loss when exposed to temperatures below 400ºC for long periods. Because the human body temperature is 37ºC, using PEEK in implants does not exceed this limit. In these applications, the materials' long-term mechanical stiffness behaviour remains unchanged in the vertical flow direction at 90ºC. The findings in Figures 5.11-12 pertain to the creep modules' behaviour under static mechanical Forcing. However, the mechanical forcing to which PEEK products are subjected under particular working conditions produces variations in mechanical strength with time. Dynamic fatigue resistance may always be lower than static fatigue resistance. The behaviour of coated sample pieces after 106 mechanical cycles differed significantly from that of models evaluated under similar conditions but without mechanical stress in DMA testing shown in Table 5.3.

Table 5.3. Results of the DMA test post mechanical cycling of the viscoelastic regime.

Sample	Max. temperature Tg (°C)	Intensity temperature
PEEK 106-cycle fatigue	161.7	0.207
cHAp	161.2	0.205
PEEK-cHAp 106-cycle fatigue	159.9	0.205
PEEK thermal shock	164.4	0.223
Fabricated properties	165.0	0.194

Greater thicknesses display more brittle fracture forms, showing the crazing and micro fibrillation phenomena around the fracture site. Smaller thicknesses are more prone to brittle and ductile fractures. The temperature range between 75 and 100°C has significantly changed fatigue behaviour. The results of this type of test are frequently represented on a graph, with the applied stress values in traction, flexion, compression, and torsion arranged on the coordinate axis and the log of the number of cycles (N) at which failure occurs for each specimen placed on the horizontal axis. Another term depicted on a durability graph is life under fatigue (Nf). It represents the number of cycles needed to attain failure. Data on the exhaustion of cHAp-rGO-coated PEEK components may be obtained from a few investigations, such as comparative traction findings between PEEK specimens with and without cHAp coating and results from sandblasted samples [1,190]. The static yield stress was reduced somewhat after coating, from 91 to 85 Mpa. PEEK was fatigue tested using sine waves at a frequency of 5 Hz. The findings indicated maximum stress of 77 Mpa and one million cycles of fatigue life. (See figures 11-12)
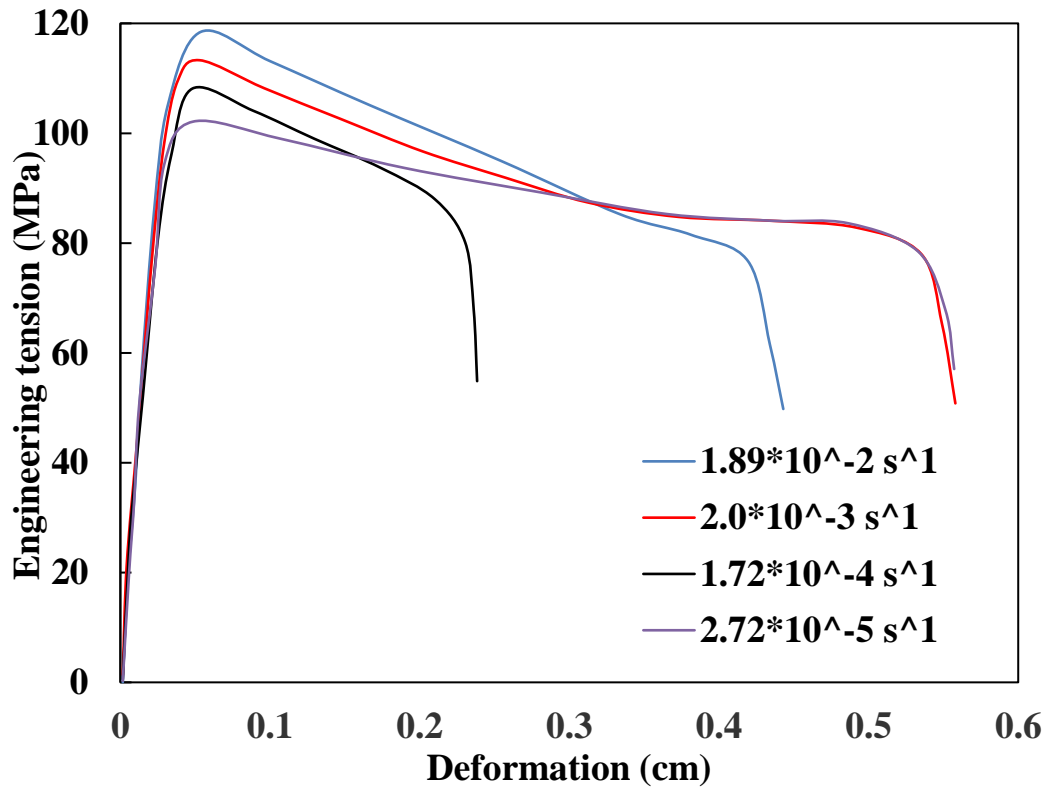
Figure 5.11 Stress-strain curve of PEEK in tension
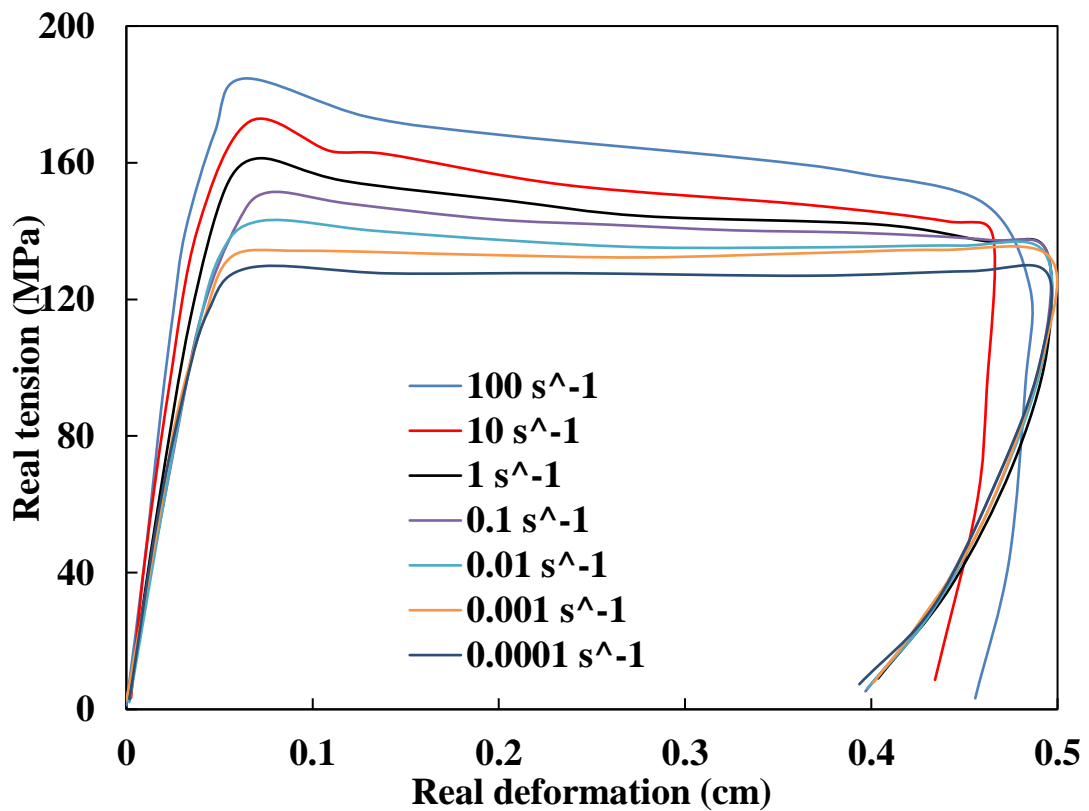
Figure 5.12 Compression for different strain rates

As a result of mechanical cycling, the E' values for all samples decreased consistently as the number of cycles conducted on each sample increased. After the mechanical fatigue test, the samples residual stress decreased, proving the presence of this effect. There was, however, a statistically considerable difference between the two groups when looking at the effects of tiredness on the E" property and the consequent effect on deformation. When the surface coat process's heat shock occurs on a sample, the deformation reduces, indicating a more elastic response. As the samples containing successfully coated cHAp aged, the importance of E" increased deformation, indicating that the samples had become more vicious. This behaviour showed that cHAp particles had been separated from the polymer surface. Therefore, the influence of mechanical hardening had been successfully removed. Because of this, the thermal-dynamic mechanical study found that the cHAp layer's adherence to the PEEK surface decreased as the temperature rose.

5.2.2. Fracture mechanics of PEEK under fatigue

Experiments on fracture formation in worn-out PEEK have been conducted, considering the effects of different variables on the materials' ageing process. In addition to a waveform, molecular weight and crystallinity must also be considered. According to studies[194-196] utilising the Paris Erdogan model on PEEK crack propagation, effects and molecule orientation do not influence the propagation of fractures in the material. Figures 5.13-14 show that materials with more excellent crystallinity and molecular weight exhibit less fracture propagation. The injecting PEEK at rates of 5.2 and 23.2 cm^3/s, with retention times of 1, 4 and 10mins at temperatures of 150°C, results in a more uniform distribution of crystallinity across the sample length while using retention times of 1, 4 and 10 mins. PEEK mouldings yield stress under strain as a function of mould temperature. A higher mould temperature combined with the same injection conditions results in more crystallinity. Figure 5.13 depicts how this leads to excellent crystallinity uniformity. PEEK injection moulds may achieve a 30 to 35% crystallinity by utilising slower cooling rates and 200°C. This results in perfect crystal homogeneity and slight crystallinity variation throughout the thickness and length of the mould. Given that the polymer glass transition temperature (Tg) is greater than the mould temperature ™, PEEK can be utilised in high-temperature applications.
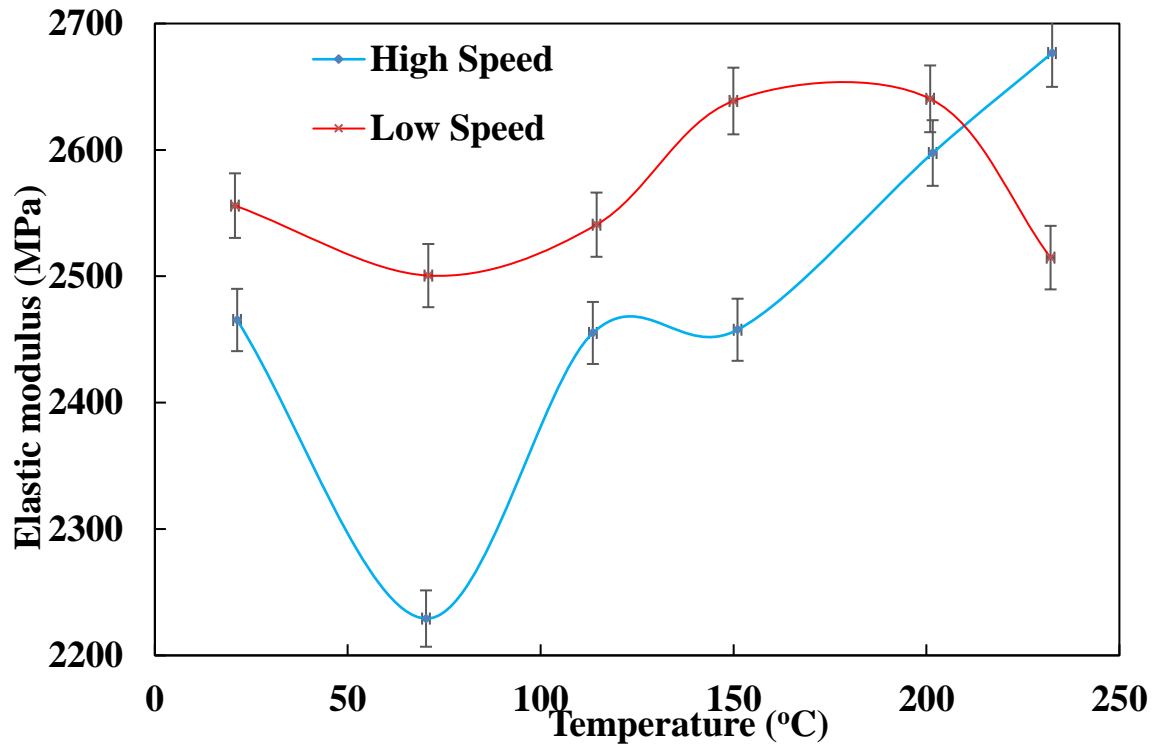
Figure 5.13 Effect times on the crystallinity variation along the length of PEEK samples elastic modulus yield stress under tension
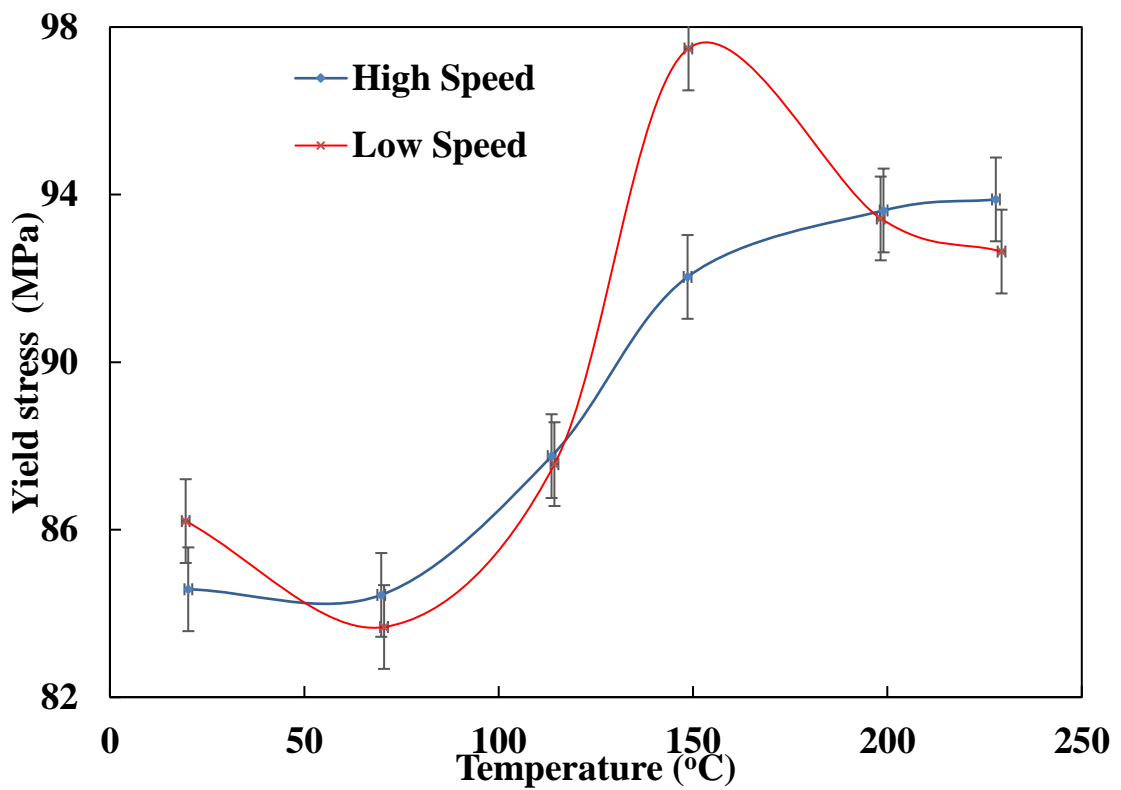
Figure 5.14 PEEK mouldings, depending on temperature injection speeds of PEEK 380Gpa.

5.3. Conclusion

PEEK-cHAp biocomposites were made using the FDM technique in the AM process. The PEEK improved the composite scaffolds' biological activities via cHAp particles. PEEK-cHAp composites with cHAp concentrations from 0% to 20% were tested for tensile properties, and elastic moduli of cHAp worked best at 15 wt%. Much research has gone into modifying PEEK to create derivatives with improved properties for creating tissue architectures. They could be distributed evenly in PEEK, and their compatibility with PEEK was improved to suit the demands of biomedical engineering applications. In the cHAp layer, mechanical cycling under fatigue showed stress release in PEEK at 1.58, less than PEEK-cHAp at 1.38 with this instruction. The coating interfacial adhesion degrades during mechanical fatigue, causing the most significant reductions in cHAp-coated PEEK. In tensile tests, the coating reduced PEEK-cHAp deformation. Finally, the limitations mentioned in this study relate to obtaining the fatigue life curves for the same material under more severe fatigue conditions. Parametric studies revealed that the curved grid is more responsive to standard features than the controlled elongation lattices. Finally, I compare the proposed technique's predictions to the traditional homogenisation method. The research found that the proposed method offered a more accurate mechanical material evaluation. The revised guidelines consider the effects of AM processes and joint stiffness

Chapter 6

Cell culture testing of scaffold for bone implant

CHAPTER SIX

6.0. CULTURE TEST (*In-vitro*)

6.1. Introduction

PEEK has physically and chemically stable properties. An orthopaedic replacement should be cytologically compatible with any biodegradable usage. Typically, bioactive materials must be improved to suit these needs. PEEK becomes sulfonated when submerged in concentrated sulfuric acid, resulting in geometric degradation. PEEK, titanium, and a chromium-cobalt-molybdenum alloy all showed binding adhesion plaques comparable in size and number and linked to cell development. Contradictory observations have called into question the link between PEEK and osteoblast growth in vitro and the ability of PEEK implants to produce bone. The mechanical stress is transferred to the implant without using human bone. Thus, the mechanical force given to adjacent bones decreases, resulting in osteopenia. As a result, they are a more attractive alternative than metallic ones in some materials. In the 1970s, Ultra-high molecular weight polyethene (UHMWPE) was utilised in implantable applications [68,189]. This polymer was selected for hip prostheses because of its higher wear resistance, especially in the sheared acetabular component. However, owing to high mechanical Forces in this region, UHMWPE was not used in the femoral component of the prosthesis. A potential PEEK-cHAp effect was observed since the PEEK-cHAp combination facilitated osteoblast development more than PEEK alone [177,208]. In general, the outcomes obtained using PEEK-based biomedical devices are contradictory. As a result, the successful extrusion of a PEEK structure using an extrusion system was coordinated to highlight crucial challenges, with an in-depth examination of process parameters included in our present work. Numerous mechanical properties from earlier literature show that platform injectors and ambient air temperatures are the most crucial thermal parameters for printing. Consequently, printed samples' mechanics and analysis were conducted at their highest possible temperature. A typical experimental setup for low-glucose DMEM culture conditions is shown in Figure 6.1.
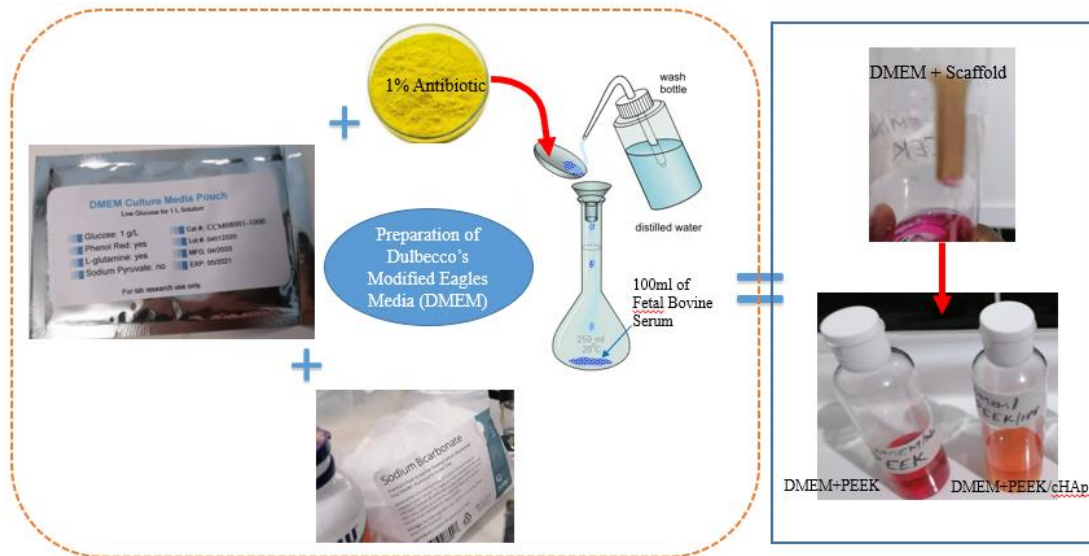
Figure 6.1 The experimental setup for the DMEM culture media of low glucose.

The cells are cultured in a Dulbecco's modified eagle's medium (DMEM) culture medium containing 10% foetal bovine serum. This medium is used to grow a variety of mammalian cells. The improved DMEM media has four times the amino acids and vitamins found in the original Eagle medium. The cells are cultured in CO_2 at 37°C and relative humidity of 5%. The culture of media is changed regularly. The ratio of powder to DMEM is 9.9 g per litre, supplemented with 3.7 g of sodium bicarbonate per litre. One bag of powder 15.25g is put into a container, followed by deionised water to boil the mixture to 450 ml and stir with a magnetic stirrer bar. An additional 0.5 L of deionised water is added, and the contents are heated to aid in the powder's dissolution. It is then autoclaved for 15 to 20 minutes at 121°C. The culture medium is composed of 125 ml of 3-chemical nutrient agar solution. It includes all the components required for most studies without adding additional fluid for cell growth. It is made in about 60 seconds in a microwave or hot water.

6.2. Methodology of Cell Culture

The cells in DMEM and low glucose 5-pack (Hyclone, Thermo USA) were then injected with 10% Fetal Bovine Serum to induce cell growth, and differentiation was cultured. Next, combine 1% Penicillin/Streptomycin (15140-122, Life Technologies Co., Carlsbad) with 1% GlutaMAX 0.5L deionised water in a sterile 75cm^3 cell culture flask. Then add the mixture to a 75cm^3 cell culture flask. After that, they were re-heated to fully

dissolve the powder before being steamed for 15-20 minutes. After that, the powder is dissolved in boiling water. Antibiotics are added to the solution once it has been re-heated, and sterile Petri plates are placed in the solution to culture. Cells were cultured at 37 degrees Celsius in a culture incubator with a 5% CO_2 atmosphere. The data in the DMEM was updated on a biweekly basis. Fusion Trypsin is activated when visible cells (GIBCO, Paisley, UK). DMEM cells were cultured at 37°C with an extracted volume for 24 hours and humidified with a 3 cm^2/ml sample area. The cells were pre-mixed simultaneously for a total of 24 hours. The L929 cells were cultivated in one 96-well plate at a density of 30 per cm^2 cells in 200 L of DMEM core temperature of 37°C. After each cell had extracted its medium, a separate 150ML sample was taken and changed the next day (Figure 6.2). Demonstrations are often tested *in-vitro,* using DMEM and created utilising parametric and generative design methods in scaffolds, often used in tissue engineering applications.

Figure 6.2 Materials for DMEM for animal cells and the scaffolds.

6.3. Cell culture with NAS

Microwaveable NAS 125 ml for Culture Medium Use on Agar Plates was purchased at Brian Taylor Office, Kent, UK. The most simple and affordable Culture Medium to verify and compare findings is 3-Chemical NAS 125 ml. It contains all the components needed for most investigations and does not need extra chemicals or biological fluids. According

to manufacturer instructions, it takes around 60 seconds in the microwave, but it may also be prepared in a hot water bath. The printed scaffold is placed in a Petri Dish on a 10-20 ml NAS of a container and includes detailed instructions for microwaving, culturing, and growing the cell. The drop-down box also contains a bundle of twenty sterile inoculation loops. With the Nutrient Agar for Petri Dishes culture and the Inoculating Loops, two extra one pk Petri Dishes (6 Dishes & 12 Loops) offer a complete project or activity package. Anti-bacterial UV radiation is used to sterilise Petri dishes that have been sealed in polythene according to Regulation (EC) 1272/2008; NAS 125ml is not hazardous A'Lab-Lemco' powder Yeast extract and Peptone Sodium chloride Agar are all present in the solution. It can be in a hot water bath or microwave for approximately 60 seconds. Figure 6.3 shows all of the Nutrient Agar scaffold solutions *in vitro* testing results and an explanatory remark.

The MG-63 and hBMSC cells were used to study cell responsiveness to scaffolds. It used 10% bovine foetal serum and 1% penicillin/streptomycin on a 12-wave platform at 37 °C and 5% humidity. Sterilising scaffolds (10% by 5 mm) in 70.1% ethanol for ten and twelve hours before adding cell semen was utilised. Adhesion and proliferation were achieved by planting 4-1105 cells/scaffold. After adhering to the 2-hectare scaffold, the cells were cultured for 1, 3, 5, and 7 days before adding a 2mL medium. To remove cells/scaffold structures, these were then rinsed three times with PBS and fixed overnight in 2.5% glutaraldehyde at pH 7.4 to remove the cells/scaffold structures. The specimens were rinsed with PBS and dried overnight with ethanol. SEM was used to analyse the morphology of the gold-sprayed specimens. The cell/scaffold was rinsed three times after culture with 4% paraformaldehyde to eliminate excess aldehyde. Living cells were given 30 minutes of calcein-AM, propidium Iodide, 4-diamidino-2-phenylindole treatment, and an Olympus fluorescent microscope. They were blue in the nucleus of live cells and green in dying cells.

Figure 6.3 Cell culture preparation with NAS and scaffold.

The MTT (3-(4, 5-dimethyl thiazolyl-2)-2, 5-diphenyltetrazolium bromide) assay test measured proliferation in control and scaffold cells after incubation at 1, 3, 5, and 7 days of each bowl received 150 L of MTT (5 mg/ml PBS). It was incubated for 4 hours at 37 °C to dissolve the formazan crystals; 150 L dimethyl sulfoxide was added to the top solvent of the spectrophotometer, and the optical density of 570 nm was measured p-nitrophenyl phosphate assays measured ALP activity after three and seven days of incubation. After gentle washing with PBS, the specimens were incubated for 10 minutes with a 1% Triton X-100 solution in Tris buffer. The lysate was then added to 12-well plates with 100 lp-nitrophenyl phosphate solution. The materials were dried in the air and stained under a microscope. Five samples of scaffolds were created and soaked in Tris-HCl solution. The scaffold was diluted with Tris-HCl to a volume ratio 0.1cm1, and the samples were kept at 37°C. A pH metre was used to determine the pH of each group after 1, 3, and 7 days. Three times the scaffold was cleaned with deionised water and anhydrous ethanol. The samples were washed at 60°C and weighed in an oven for 24 hours.

6.4. Characterisation SEM analysis

All experiments were carried out at a thermal evaluation facility at DMU Laboratory. They were carried out using TA Instruments DSC Q2000, digital differential calorimetry, and modulated differential calorimetry instruments. The Engineering Department's Materials Analysis was carried out on two separate occasions. To further improve the

reliability of the results, software analysis tools such as the DigitSurf gadget were used (Mountain 9 Premium). Using ASTM D638 as a guide, tensile tests were performed on PEEK samples coated or left uncoated with rGO and cHAp. As previously noted, the HAp layer affects the material's tensile strength. Following the fracturing of the model, the fixed tensile test for the PEEK sample was deemed inconclusive. The model was deformed but did not break during the bend test preventing this from being detected. As a result, using static tensile testing, it is possible to evaluate the effect of the coating process on the tensile, elasticity, and fracture toughness properties of the steel (Figure 6.4).
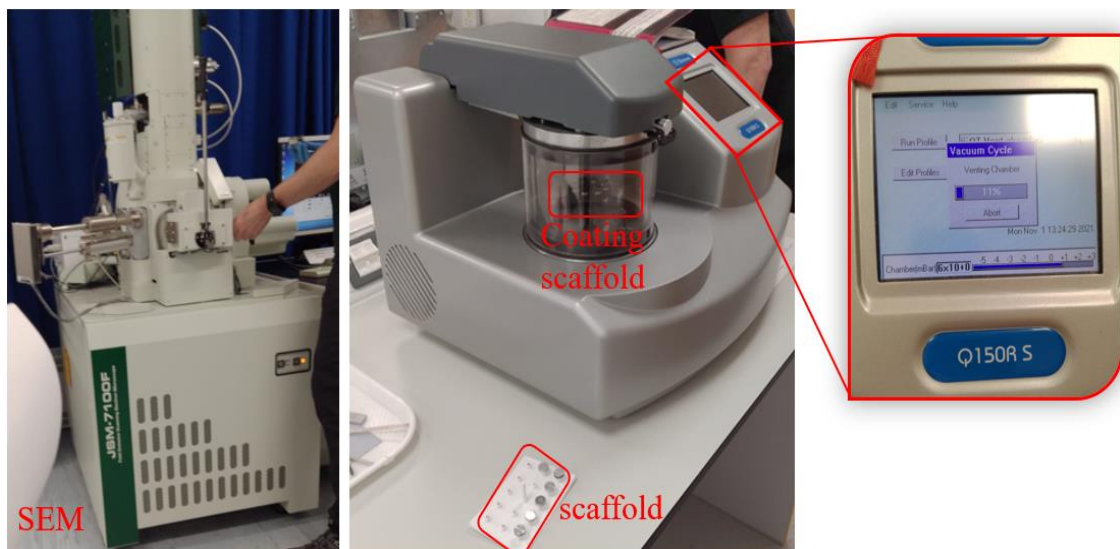
Figure 6.4 Characterisation SEM analysis, showing the coating of the scaffold**.**

6.5.   **EDS-SEM test**

This study used a Hitachi S416 scanning electron microscope to examine the dispersion and adherence of nano rGO flakes on cracked mortar surfaces (SEM) (Figure 6.5). The samples are incubated for 28 days after analysis. The body is broken into 1054 mm parts of a 3 nm platinum coating to improve its conductivity. The crystalline phase of the cement matrix is determined using X-ray diffraction (XRD). The internal standard XRD technique quantifies the crystalline hydrate cement phases. Bruker's X-ray diffusion metre is used to determine crystal distances. In addition to CuK radiation, the system has 0.02 °/s scanning in the 24–70° range, 40 kV and 30 mA acceleration current. The waist depth and width of each model are 0.5 mm accurate. The model is Forced into a tensile tester with a 5–6.4 mm/min crosshead speed.

A 37°C incubator with 4.98% CO_2 maintained the cells warm. The DMEM culture medium was changed every four days. It was next necessary to transfer 9.98% of all cells into a new container, which required Fusion Trypsin. This research used the ISO 10993-5 extraction method to extract PEEK and PEEK reinforced with cHAP. The DMEM cell was used at 37 °C, and the cell was produced by gradually increasing the moisture content of the material. In this case, 3 cm^2/mL sample surface area to extraction volume. During this time, the cells were pre-mixed. In a 95.79 well plate, L929 had 3,000 cells per centimetre square in 200 L of DMEM. A sample of 145 L was added to each cell after 1 day.
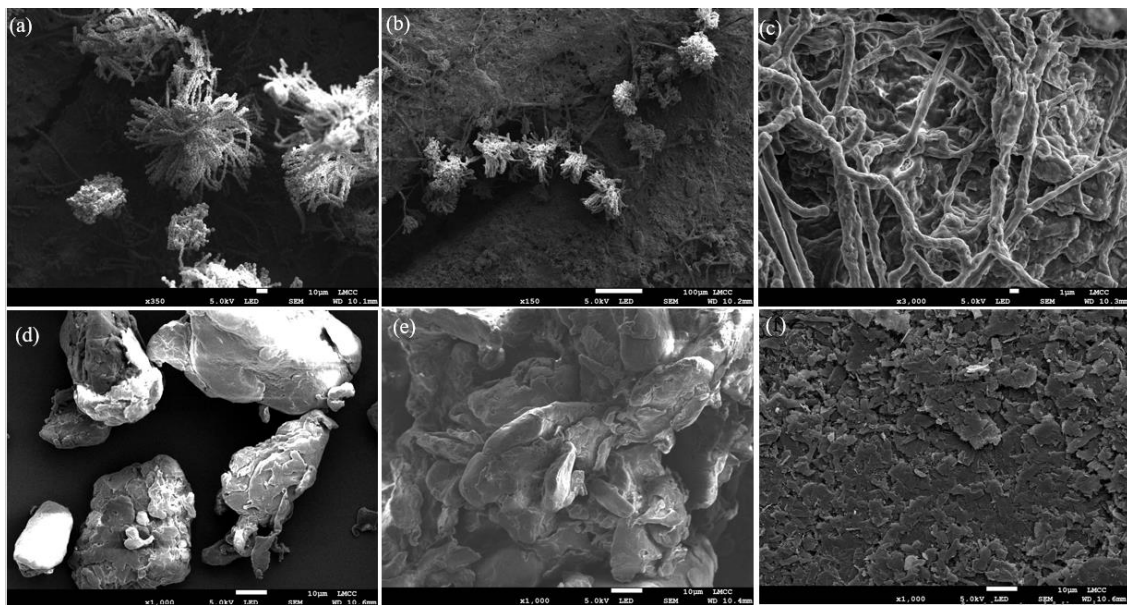
Figure 6.5. SEM structures of (a-c) PEEK-cHAp-rGO culture scaffold, (d) PEEK, (e) cHAp and (f) rGO.

6.5.1. Surface imaging characterisation

81 to 135 µm pores were generated in all cohorts with the relationship between printing speed and average pore size (PCC = 0.37; p = 0.08). Conclusions: The average pore size was zero, significantly lower than the average pore size for all groups at p = 0.01 for the actual test, indicating that the average pore size was zero. SEM images obtained at a 3000 mm/min speed were used to identify tiny cracks in the print layer caused by faults in the printing process. Regardless of the stress conditions they were printed, the fracture surface morphology was the same for all groups; it started parallel to the layers, changed direction, and eventually turned perpendicular to the layers. Figure 6.6 depicts the phase map produced by Energy Dispersive Spectroscopy (EDS) using the microstructures

discussed above. The carbon K1 phase is easily distinguishable because it contrasts with the oxygen K1 phase, which has green microstructures, as shown in Figures 6.6 and 6.7, respectively, and therefore is easily distinguished.

(a)   (b)
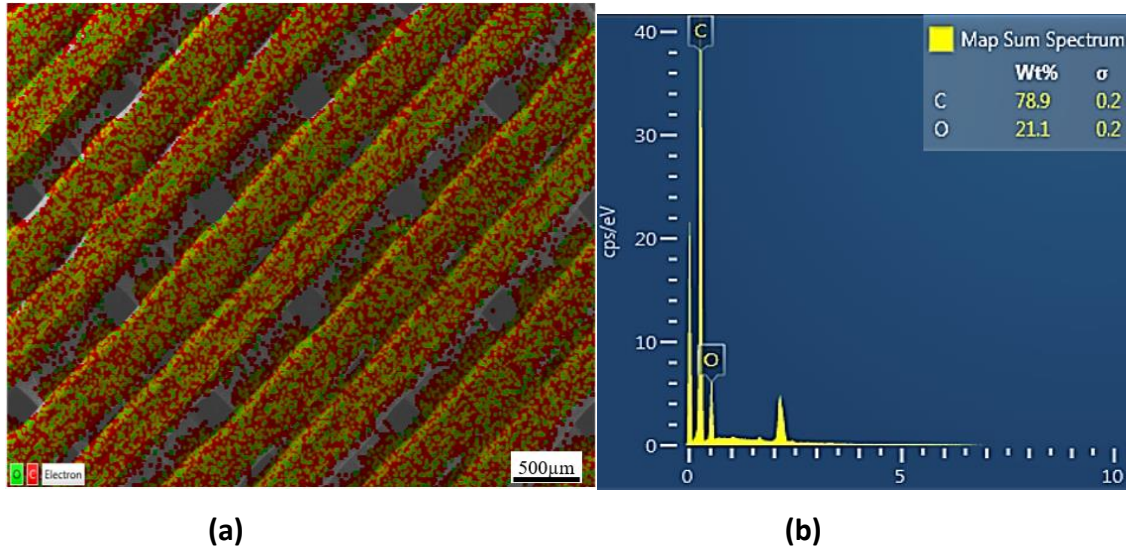
Figure 6.6 Characterisation of microstructures, showing the (a) elemental mapping for elemental microstructure mapping for PEEK in 2 layers of EDS of Carbon 78.9wt% (b) the elemental mapping for the EDS spectrum for PEEK.

(a)   (b)
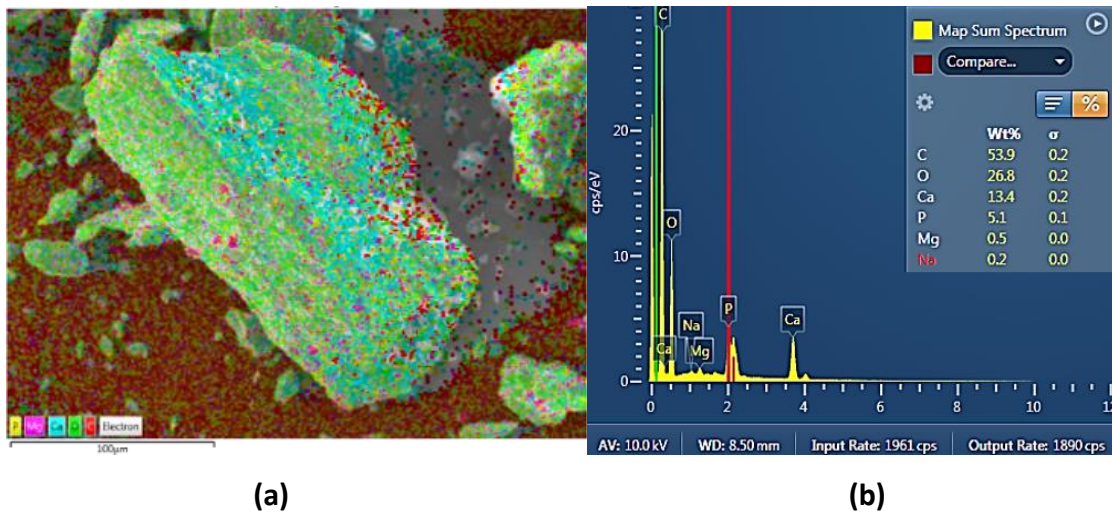
Figure 6.7 Characterisation of microstructures, showing the elemental mapping for EDS of cHAp at 100 μm.

Figure 6.8 shows a typical PEEK X-ray diffraction spectrum. The PEEK-cHAp opposing side 0.1 sample has a grain size of 7.3 mg, obtained using a ramp method. There was a 2% crystallinity difference between the exposed and unexposed skin after the cHAp surface coating process. The slight shift indicated that the surface coat procedure had

altered the crystallinity. After being subjected to the thermal shock method connected with the surface coat process, the research was performed only on the PEEK specimen, and the results are as follows. PEEK samples had a crystalline fusion temperature (Tm) of 340°C and a crystallinity level of 28.6%, respectively. Before testing, the cHAp was subjected to a 341°C melting temperature, a 30.5% crystallisation level, and a thermal shock at 338 °C. The crystallinity of samples produced from the layers subjected to the surface coating procedure increased by roughly 2% and 10%, relative. There was also a difference in crystallinity between samples coated with cHAp and those just subjected to the thermal shock associated with the coating process. It revealed no impact from possible CHAp particles in the gathered samples, which aligned with the research methodology. Figure 6.8 shows a microscopic view of PEEK (a) 500 micrometre, (b) 25 micrometre and (c) profile intensity.
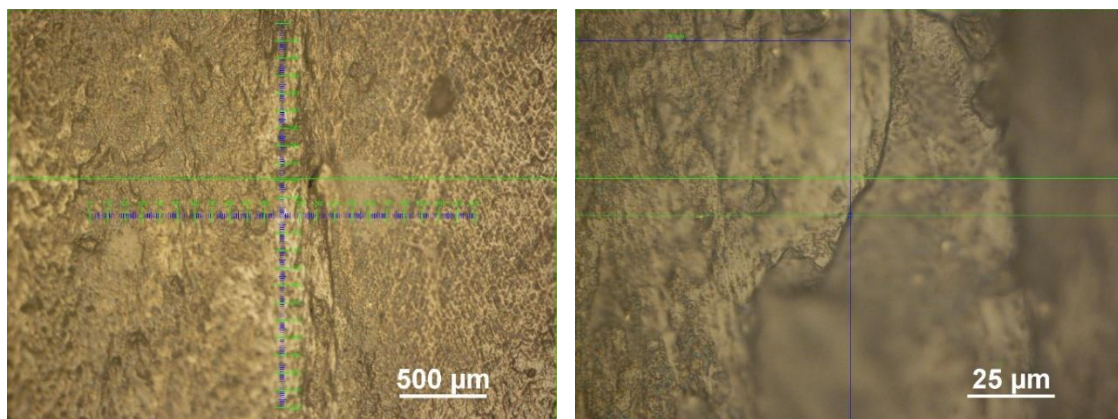
(a)

(b)
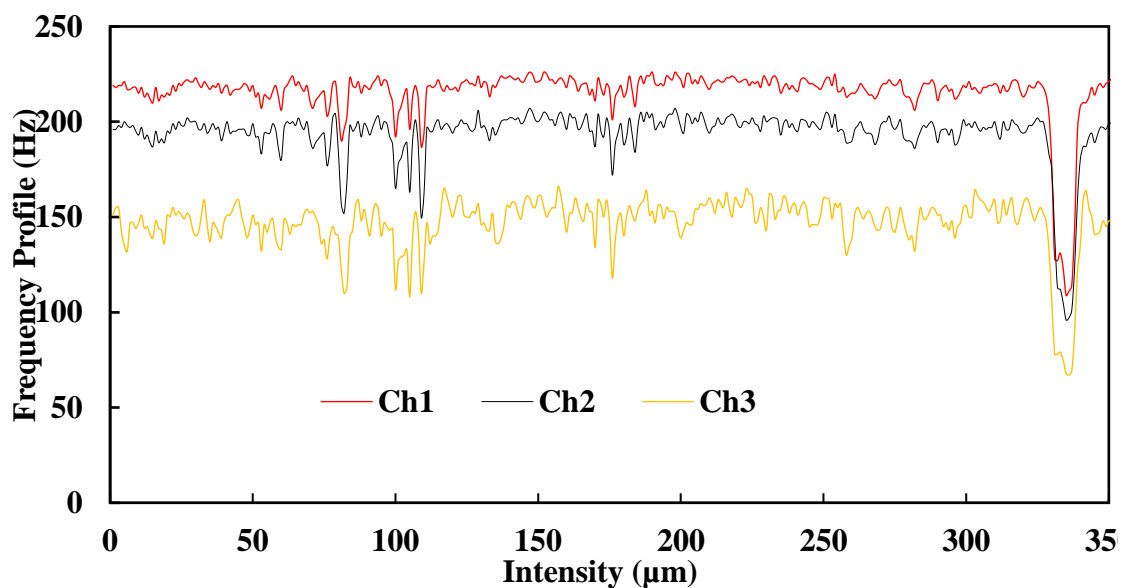
(c)

Figure 6.8 A microscopic view of PEEK (a) 500micrometer (b) 25micrometer (c) of Profile intensity.

6.5.2. In-vitro cytotoxicity

For continuous printing without clogging the polymer's main factor, the experiments proved the necessity of central heating, PEEK head extrusion design, nozzle or high-temperature printing, and environmental management [68]. Although the plate considers the adhesion and curvature reduction of the printed component syringe design on the extruded head base, heat on PEEK could not achieve adequate control. The essential components from the PEEK syringe were delivered into the needle, which avoided thermal breakdown viscosity and aided in vitro control. Additionally, the syringe method was selected in line with the testing limitations on the number of printed components that can be tested. Because the initial results of the heat buffer on glass, as determined by temperature, changed throughout the printing process, the three-level PEEK jetty print was done with an extrusion syringe. The alkaline phosphatase-staining spots on the blue PEEK-cHAp combination were consistently denser than those on the PEEK surfaces in the previous experiment [69]. On day 14, cells grown in the PEEK-cHAp combination showed much higher relative alkaline phosphatase activity than cells cultured in PEEK, with a p-value of 0.005, indicating a significant difference between the two groups. These *in vitro* samples (Figs. 6.9a-f) are similar to those reported in [53-55] and are shown here as an example. Actin filaments were more prominent in PEEK-cHAp cells than in adjacent bound cells in this study. The cell nuclei on the PEEK-cHAp surfaces were more densely packed than those on the PEEK surfaces, indicating that the combination was more effective.
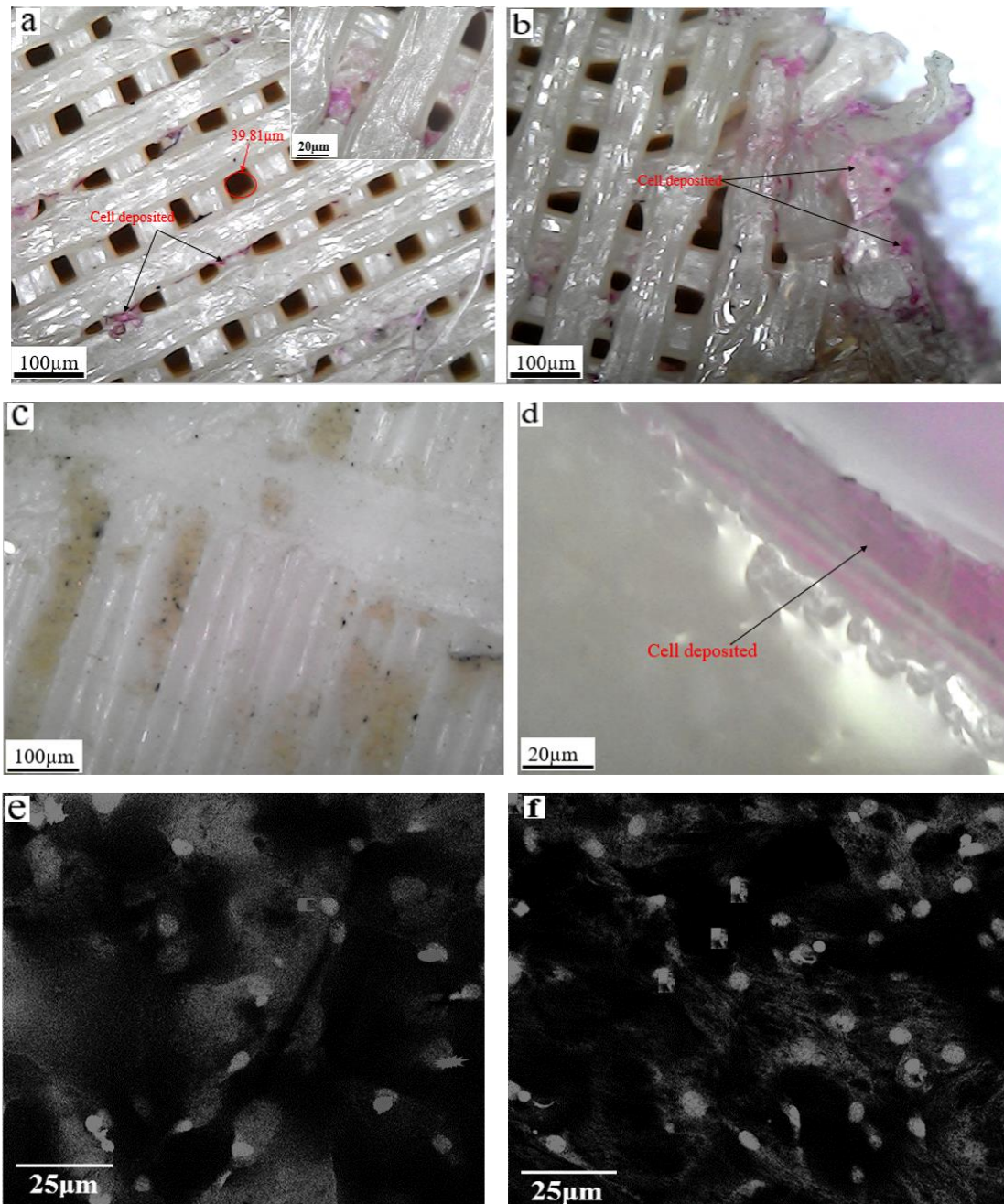
Figure 6.9 The cells adhere to FDM 3D printed PEEK composite sample surfaces after pink culture: (a) 100 µm magnification of PEEK with 20µm, (b) 100 m magnification of fractured PEEK, (c-d) spreading cell activity of cells after days of PEEK-cHap labelling at various magnifications and (e-f) after days of morphological nuclei staining with 4, 6-diamidino-2-phenylindole 0.1 g/mL in the white spot of PEEK and PEEK-cHAp, the filamentous activity of the cytoskeleton was determined using SEM.

6.6.   Result of cell culture of DMEM

Cells were grown in 75 cm3 sterile cell culture flasks bought in the GlutaMAX, USA, using DMEM pouches (low glucose, 5 per pack) supplemented with 10% foetal bovine serum, 1% penicillin/streptomycin. Mammalian cells of various types were able to grow

in the medium. Adding DMEM to the original eagle medium increased the concentration of amino acids and vitamins by four. The low-cost DMEM powder also included Phenol Red L-glutamine and low glucose levels of 1 g/L and little to no $NaHCO_3$. A humidified atmosphere containing 4.98 per cent carbon dioxide raised the cells to 37°C. Every day they have brought a new form of cultural expression with it. 9 g powder to 1 mL DMEM media was used in the experiment. In compensation for the absence of carbon dioxide, 3.7 g sodium bicarbonate was added to each DMEM medium before 450 mL of deionised water was added to the mixture. A magnetic stirrer bar was used to mix. The total volume of the mixture was 15.25 g of powder. After adding 0.5 L of deionised water, this solution was boiled to help dissolve the powder. After that, it was sterilised in an autoclave for 15–20 minutes at 121 °C. Antibiotics were added, and the liquid was pipetted onto sterile Petri plates after a short chilling time to allow the fluid to reheat to body temperature.

Figures 6.10 (a-d) depict accumulating cells in the surface grooves of PEEK-HAp composite cells grouped while the PEEK cells are dispersed across the device. PEEK-rGO-actin cHAp filaments are more prominent than other cells due to a strong connection. PEEK-HAp alkaline cell phosphatase showed a statistically significant difference from PEEK on day 14 (p = 0.005.5A-F) relative behaviour. Actin filaments in PEEK-HAp can be more prominent than in PEEK-HAp since it is linked to nearby cells. To top it all off, the PEEK-HAp layer outside the cell nucleus is thicker than the one within. Cells adhering to the FDM 3D-printed PEEK composite sample surfaces were stained to determine whether they were alive or dead (Figure 6.10). After the samples have been grown in the NAS for a day, this is observed at 50 µm of PEEK and PEEK-rGO-cHAp. Significantly, live-cell growth is observed at ten microns of PEEK-rGO-cHAp. This development is further increased at twenty microns. PEEK-rGO-cHAp cells grow to form a ring around tiny dead cells after seven days and 14 days when exposed to the same PEEK-rGO-cHAp cells.
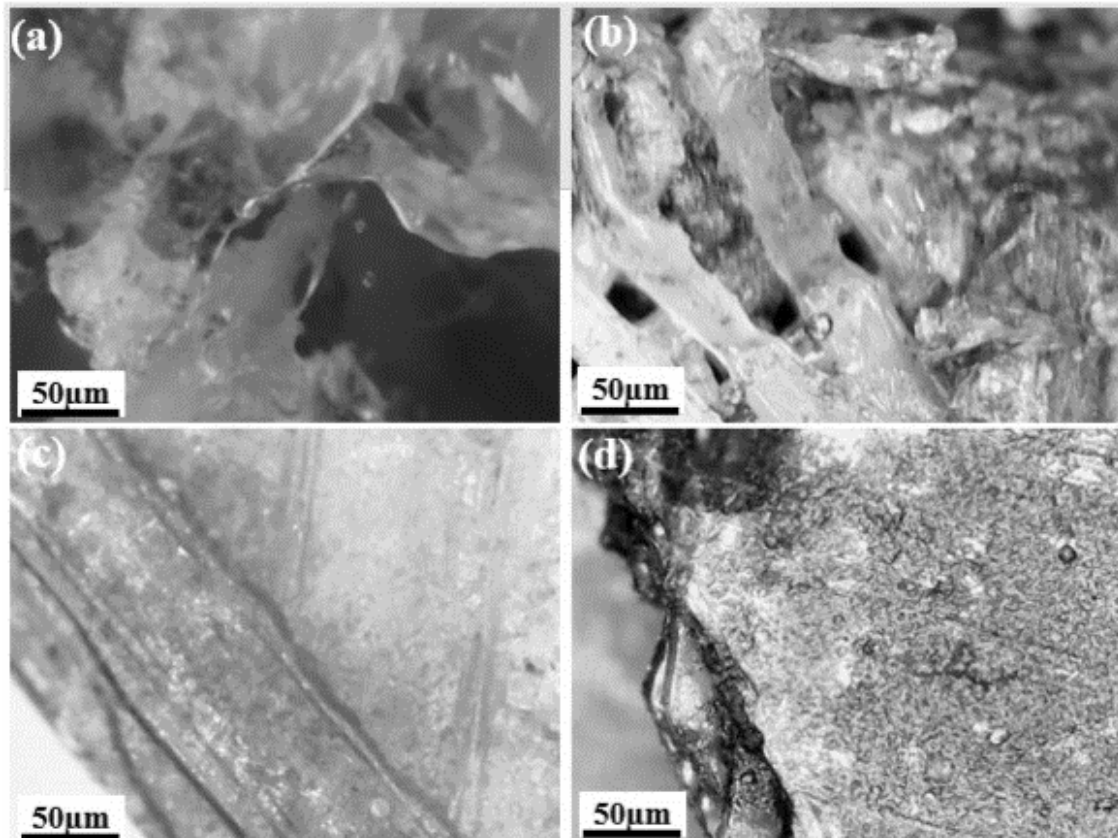
Figure 6.10 Cells adhered to sample scaffold surfaces for days using DMEM medium: (a) 50 µm of PEEK after 24 hours, (b) 50 µm of PEEK-rGO-cHAp composite scaffold after 24 hours, (c) 50 µm of PEEK after three days, and (d) corresponding magnification of 50 µm of cell deposition of PEEK-rGO-cHAp composite scaffold after three days.

This result shows that the cHAP and rGO coating procedures impact PEEK's surface crystallisation and an elastic response in the studied regime. The use of glass improves the polymer's resistance to frost stress. An anchoring effect of the cHAP layer is obtained when the glass transition temperature is reached. The sample coated with rGO and cHAp had a much lower tan value than the sample subjected to heat shock. Only heat shock samples were examined, followed by PEEK-rGO-cHAp non-mechanical samples. The results obtained for elastic modulus confirm this, and a mathematical method is used to determine the viscoelastic phase's peak E after bending. The bare minimum values for this attribute can be found in the static collection. A higher crystallinity was observed in samples exposed to heat, shock, and cHAP and rGO treatments, showing these factors' significance on behaviour. Figure 6.11 (a–f) shows cells adhered to sample surfaces after days of culture in DMEM, demonstrating 50µm of PEEK after over 24h and 50µm of PEEK after three days. Increased alkaline phosphatase activity spread in cells after seven

days of PEEK culture 50μm of PEEK-rGO-cHAP scaffold after 24 hours. The equivalent magnification of 50 µm of PEEK-rGO-cHAP cell deposition and more robust adhesion of living cells to the PEEK-rGO-cHAP scaffold. Figure 6.11 (g–l) shows that after culture with NAS, live/dead cells adhered to FDM 3D-printed PEEK composite surfaces. Increased cell activity on the third day in 50 µm PEEK 50m of PEEK cell spreading with few dead cells on the seventh day and 50 µm PEEK for 24 hours. Also (j-l) shows 50 µm of PEEK-rGO-cHAP for 24 hours, 50 µm of PEEK-rGO-cHAP on the third day, and PEEK-rGO-cHAP cell growing to spread with few dead cells on the seventh day.
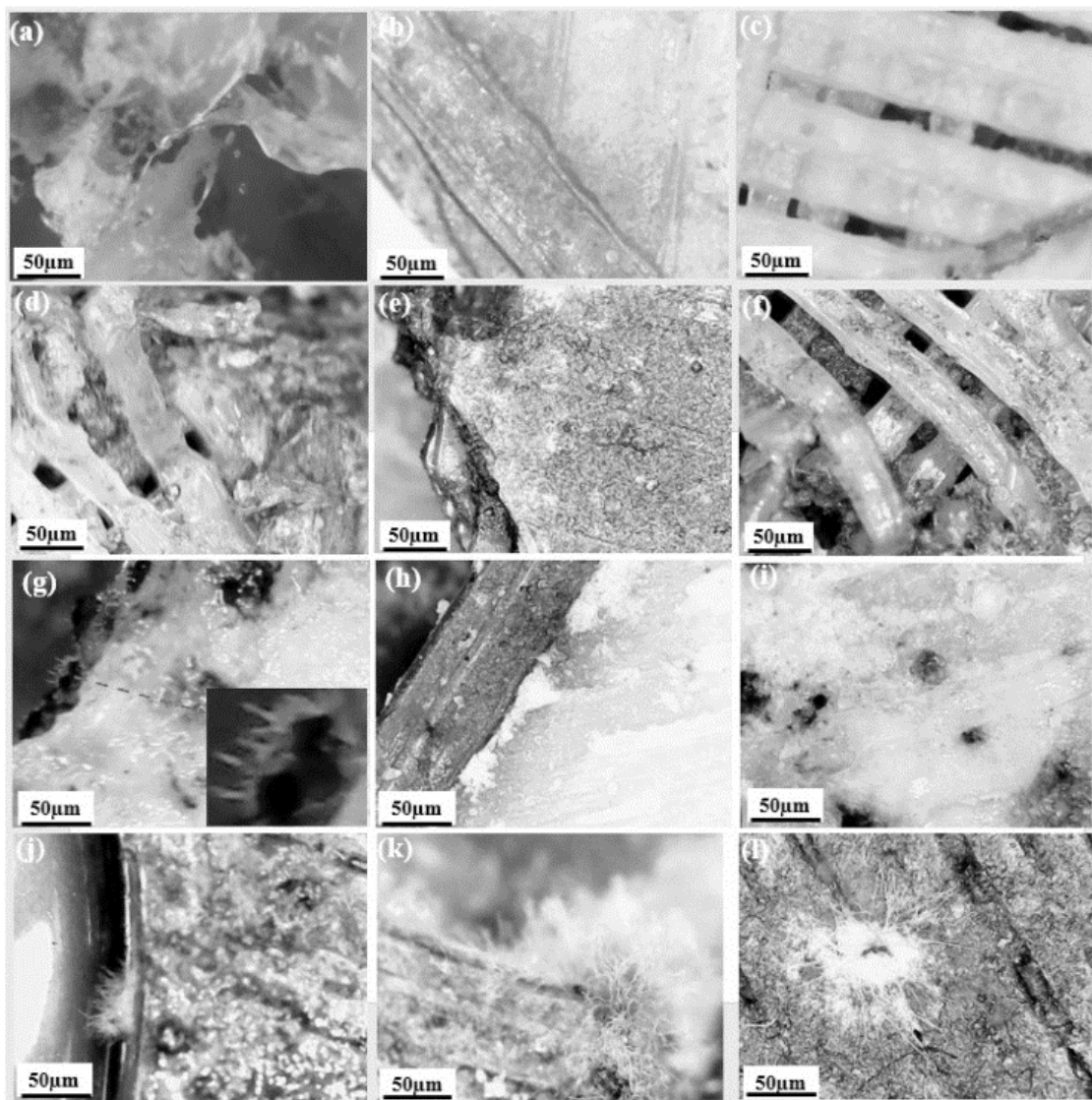
Figure 6.11 (a–f) Cells adhered to sample scaffold surfaces after days of culture in DMEM, demonstrating (a) 50 µm of PEEK after over 24 h and (b) 50 µm of PEEK after three days. (b) Increased spreading of alkaline phosphatase activity in cells after seven days of PEEK culture (d) 50 µm of PEEK-rGO-cHAP composite scaffold after 24 hours, (e) the equivalent magnification of 50 µm of PEEK-rGO-cHAP cell deposition. (f) A more robust adhesion of living cells to the PEEK-rGO-cHAP composite

scaffold. (g–l) After culture with Nutrient Agar Solution, live/dead staining of cells adhered to FDM 3D-printed PEEK composite sample surfaces. (g) 50 µm PEEK for 24 hours (h) Increased cell activity on the third day in 50 µm PEEK I 50m of PEEK cell spreading with few dead cells on the seventh day (j) 50 µm of PEEK-rGO-cHAP for 24 hours (k) 50 µm of PEEK-rGO-cHAP on the third day (l) PEEK-rGO-cHAP cell growing to spread with few dead cells on the seventh day.

6.7. Cell Culture with NAS Result

Figure 6.12 shows the aggregation of cells in the surface grooves due to the manufacturing process deposition patterns. Incorporation and cluster formation were of the PEEK-rGO-cHAP cell lines. Actin cells predominated in the PEEK-rGO-cHAP composite over bond cells. The PEEK-rGO-cHAP composite cell nuclei are denser than those on the PEEK surface. Figure 6.12 depicts the body's qualitative and quantitative effects of alkaline phosphatase activity. It is shown in Figure 6.12(a–g) that cells are attached for over 24 hours to a sample scaffold after DMEM crop medium treatment and that 50 metres of a composite scaffold are treated for 24 hours with DMEM crop media. After three days of 50 m magnification of PEEK-rGO-cHAP cell deposition, Figure 6.12(c–d) depicts 50 m of PEEK. Figure 6.12 (e–f) demonstrates better PEEK-rGO-cHAP live-cell adhesion after seven days of PEEK culture with higher cell alkaline phosphatase activity. Figure 6.11 depicts the live/dead cell labelling in FDM 3D following culture with NAS on the composite PEEK sample surfaces. Figure 6.12a-c shows the live-cell growth of 10 m after 24 hours, whereas the picture displays 50 m PEEK after 24 hours and 50 m.

Figure 6.12 show cell activity at 50mm PEEK on the third day, PEEK-rGO-cHAP on the third day, and cell growth at 20mm on the third day. Figure 6.12 (a–f) shows the distribution of 50 m and the presence of PEEK-rGO-cHAP in the circles with small dead cells on the seventh day. However, the strength of various young modules was significantly varied in age, and thus the tanning effect was regulated. The derived youthful modulus value decreased together with the skin tone. Replace the smaller sample with a larger one. A complete response was provided for the surface subjected to thermal stress throughout the coating process. The SEM picture shows that the polymer is heated on a shattered, ice-covered ledge throughout the coating process. In samples with effectively coated HAp, the modulus of elasticity and tan increased with age, indicating a more sterile performance. This behaviour proposed that mechanical cycle deformation

had caused the rGO and cHAp particles to separate from the polymeric substrate 7.3 mg of grain was used in the PEEK-cHAp sample. Starting with an opposing concentration of Surface-coated skin exposed to cHAp had a 2% higher crystallinity than skin not exposed to it. It was a little but telling sign that the crystallinity of the surface coating was changing.
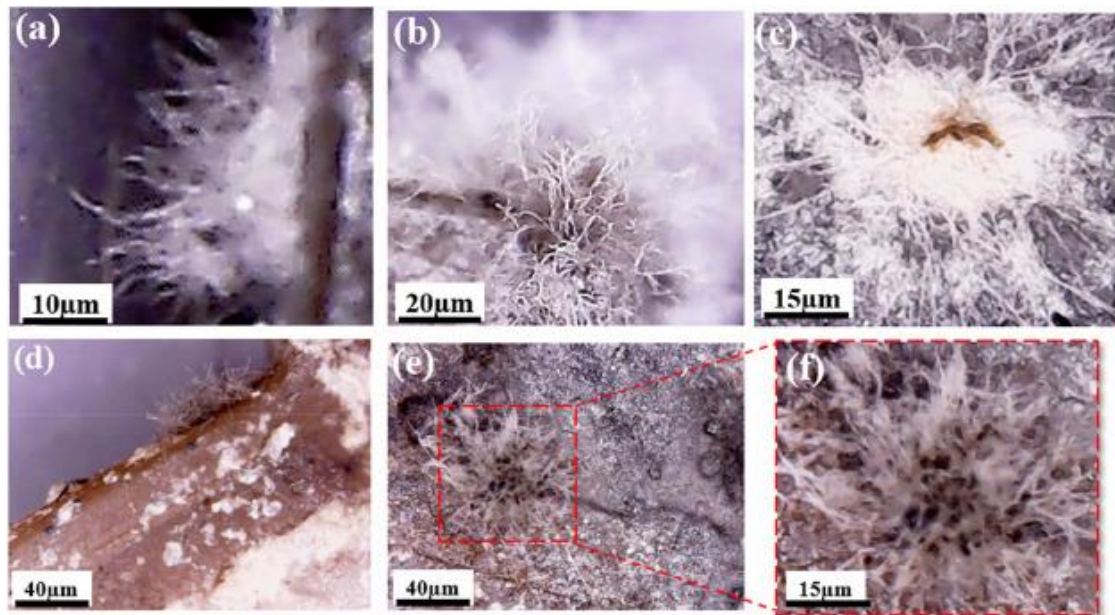
Figure 6.12 After culturing with NAS, live/dead staining of cells adhered to FDM 3D-printed PEEK composite sample surfaces: (a) 10 µm of PEEK-rGO-cHAp demonstrating live cell growth after 24 h, (b) cell spreading and alkaline phosphatase activity on PEEK-rGO-cHAp at 20 µm on the third day, and (c) 10µm of PEEK cell spreading with small dead cells on PEEK-rGO-cHAp on the seventh day. (d) PEEK cell spreads rapidly on the fourteenth day, and (e–f) PEEK-rGO-cHAp with a dead cell on the fourteenth day.

The crystallinity of layer samples treated with the surface coating approach increased by 2% in absolute terms and 10% in relative ones. The crystallinity of a cHAp-lacquered model was only subjected to a heated air shock during the surface coating process. The samples analysed using these methods found no interaction with cHAp particles. Microwavable NAS 125 ml was delivered by Brian Taylor Offices 2 in the UK as a culture media for Agar Plates. The NAS Culture media made from the 3-Chemical NAS is the quickest and most adaptable. No extra chemicals or biological fluids are required since they contain everything needed for most investigations. It was prepared by placing a microwave bottle filled with hot water for 60 seconds. The printed scaffold is placed gently on a prepared NAS in a standard Petri dish. The bottle came with instructions on

microwaving it, obtaining cultures, and developing the cell, all in great detail. A package of twenty sterile inoculation loops is available through the drop-down box.

6.8.   SEM analysis results

SEM was used for image processing at a life science laboratory at DMU. Using the ASTM D790 standard for examining cross-sections of the manufactured specimen, the covered layer morphology was analysed before and after mechanical cycling and its thickness, morphology, fractures, roughness and porosity. cHAp tensile and extensive testing was used to create the specimen, which flows deformed to 90% following static bending. The surface coat technique was evaluated using X-ray diffraction to determine whether the generated layer matched the needed and expected for use as an osteoconductive layer. X-ray diffraction analysis was used to compare experimental results to published literature findings. The results were found to agree. Based on an evaluation of the thermal shock that PEEK specimens were exposed to during the coating process, estimate the thermal shock effect on polymer crystallinity. This experiment aimed to know whether the exposure altered PEEK matrix crystallinity. Studies on specimen surface layers were conducted since they are more susceptible to change due to the procedures' high thermo-mechanical impact. Mass was removed from PEEK samples coated with cHAp to ensure no cHAp particles interfered with the research. The research was carried out at the materials engineering department's DMU polymer division using DMU Instruments, differential scanning calorimetry, and modulated DSC. There were two rounds of analysis. Software analyses such as Digit Surf (Mountain 8 Premium) Instrument were used to verify the results correctness. As previously reported, a cHAp layer was applied on PEEK specimens and tested for its impact on mechanical strength under stress using tensile testing.

Static tensile testing on PEEK specimens was halted after one of the samples broke. During the flexion test, the specimen flexed without breaking. As a result, this was not an issue. While performing a static tensile test, it was possible to evaluate how the coating technique affected the tensile strength characteristics, resilience, and fracture toughness. Figure 6.13 shows nanoparticle thresholds ranging from 60.89 to 39.12 nm for PEEK-HAp employing a Daubechies waviness high-pass filter image and a solid Gaussian filter at 285 nanoparticles. The watershed detection approach uses 1336 nanoparticles with a mean projected area of 37.48 m2, equivalent diameter of 5.837 nm, height of 14.36 nm, roundness, compatibility, and pitch of 0.5803, 0.7573, and 7.323 nm, respectively. The

roughness analysis in the Daubechies wavelet filter and the scaled sample profile analysis in the 0.8 mm Gaussian filter demonstrates the nanoparticles slice luminance conversion and the frequency luminance spectrum conversion of the micro-nano particles.
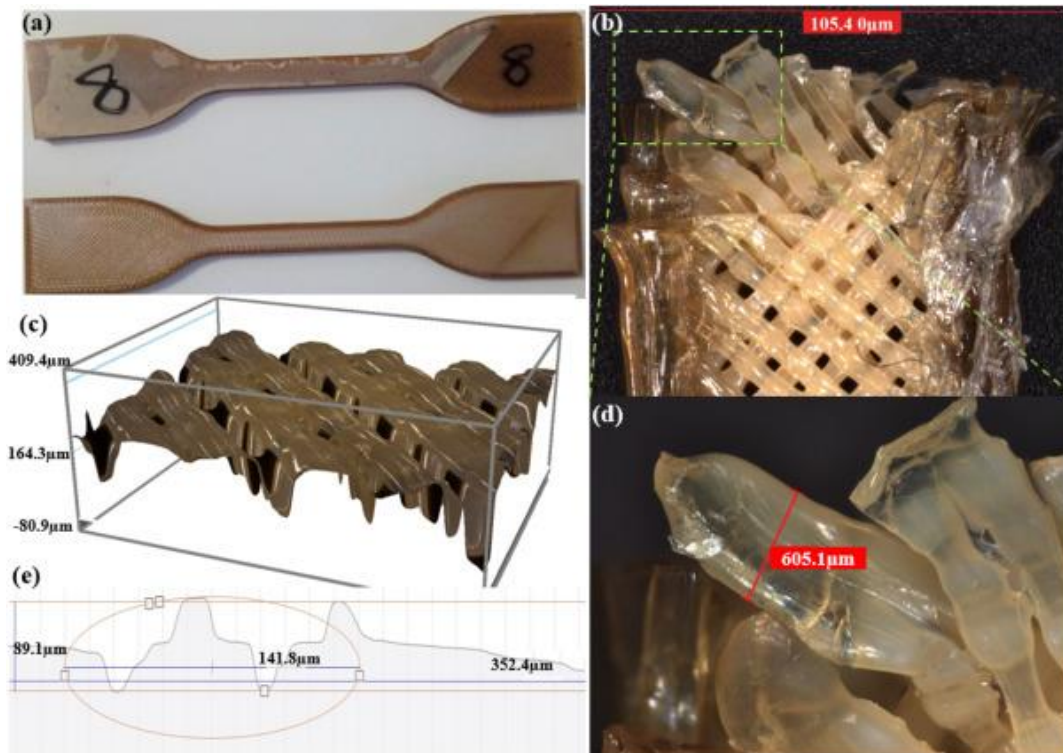
Figure 6.13 (a) A 3D-printed PEEK tensile reference sample, (b) a sample with 105 m porosity after tensile fracture, (c) a microscopic profile of the 3D model, (d) a 500 x of a 605 µm fibre, and (e) a profile graph of the 3D with pixels of 1.2872 ms and an of 0.2225 m/pixel.

PEEK scaffolds with various fill sizes were used for the FDM of the scaffold, which was created via 3D printing. During the extrusion process, I used multiple points to produce PEEK-cHAp compounds with a static Force and keep air out of the composite mould. It was steel and had a 25 mm bore accessed via a 0.5 mm vent hole on the bottom surface. The optimal temperature formation was 400°C, and external construction with dimensions of 10 x 10 x 3 mm^3 was moulded and tested at a pressure of about 0.39 MPa. The filler/porous cHAp sizes used in evaluating the mould were varied. Heating a mould to 250°C and progressively increasing the weight and pressure until the temperature reached 400°C was used to achieve static charging of the mould (Figure 6.14).
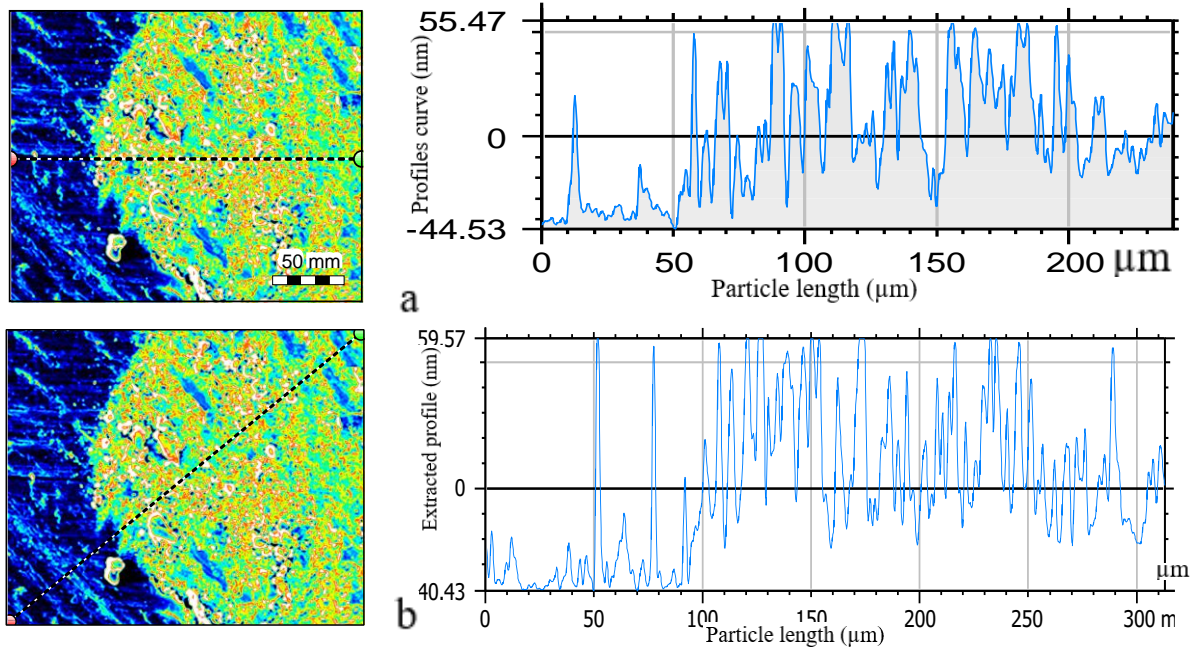
Figure 6.14. The PEEK-cHAp composite's parameter values are shown in (a) the curve retrieved profile with a length ranging from 144 to 159 µm and (b) the filtered extracted waviness profile using Gaussian filter settings and a cut-off of 2.50 µm.

The PEEK crystallised and solidified when forced to cool in the mould under pressure. In the first cHAp platform, the surface hardness of individual cHAp fibres was measured. The surface hardness of the PEEK lines that penetrated the absorbed PEEK was also determined. The average surface hardness value of each of the three investigated sites was recorded.

Figure 6.15 shows the four XRD zoom factors, which are not 180° smoothing for the 180^0 angle profile. The coating maintains good adhesion to PEEK substrates even after high static deformation. It can be observed by comparison—3D depiction of the binarised grain evaluation results for PEEK-HAp. DAPI (4′,6-diamidino-2-phenylindole) to stain the nuclei of adhering cells throughout the composite material demonstrates the extensive presence of adhering cells throughout the composite material. The high level of scaffold green-channel autofluorescence interferes with the green signal from the cell tracker, reducing the experiment's effectiveness significantly. The watershed detection method uses 1336 nanoparticles with a mean projected area of 37.48 m2, an equivalent diameter of 5.837 nm, a height of 14.36 nm, and roundness, compatibility, and pitch values of 0.5803, 0.7573, and 7.323 nm, respectively. The roughness analysis in the Daubechies wavelet filter and the scaled sample profile analysis in the 0.8 mm Gaussian filter

demonstrates the micro-nano particles' frequency luminance spectrum conversion and the scaled sample profile analysis in the 0.8 mm Gaussian filter.
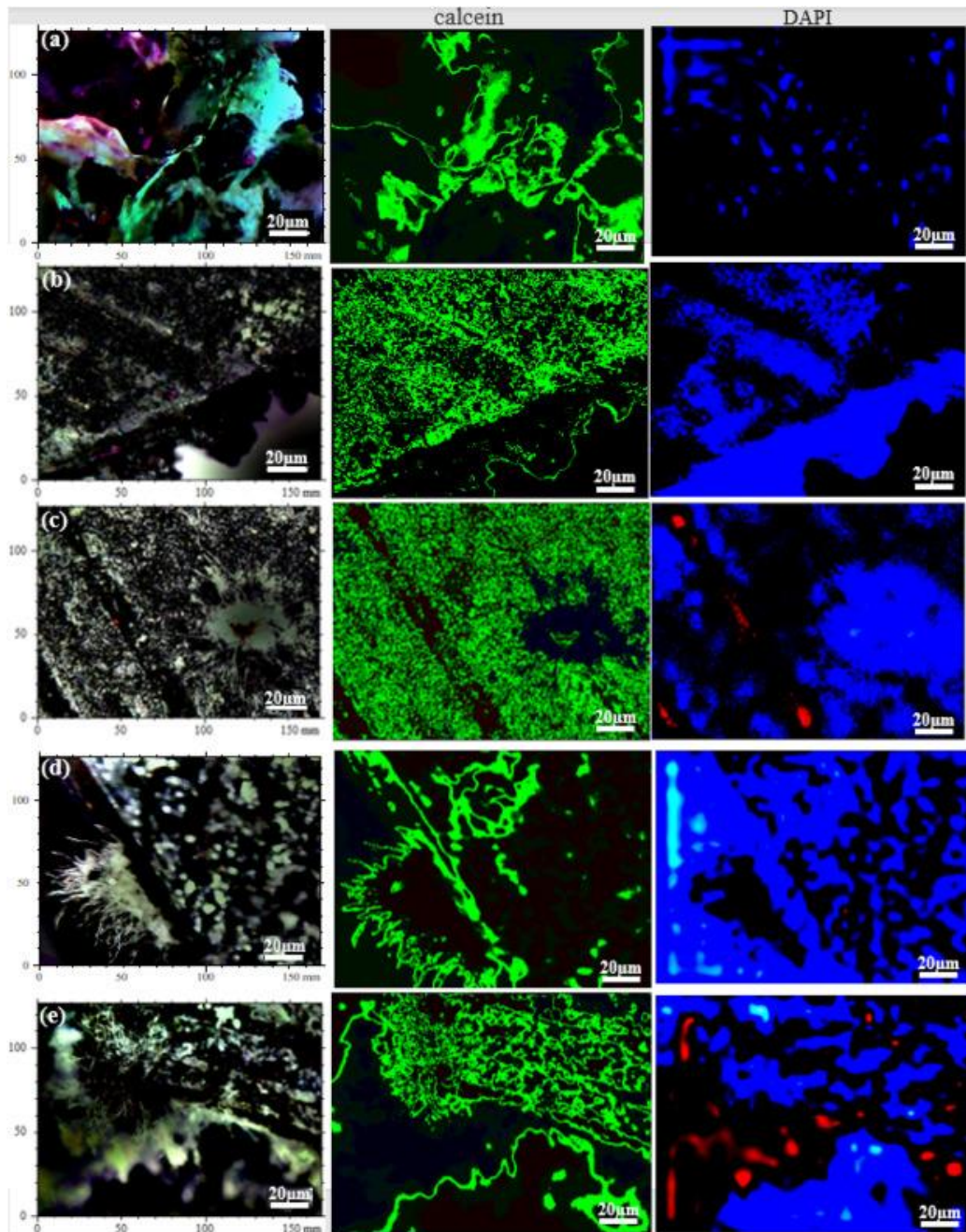
Figure 6.15 (a) PEEK tested with DMEM, (b) PEEK-rGO-cHAp tested with DMEM, (c) PEEK tested with NASand (d–e) PEEK-rGO-cHAp tested with NAS on different days.

6.8.1. Nanostructure of PEEK-cHAp biocomposite

To limit the utilisation of biocomposite structures, PEEK can be utilised. The evisceration of 3D-PEEK implants was studied using microscopic and porosity measures. Porosity

was 14% and 31% in samples with 100% and 80% fill rates, respectively. With a 100% fill rate, the material had a porosity of 14% due to air spaces between the fibres; due to the inherent limitations of the technique, airbags accumulated on the ground in layers. The loading fibres' form also restricted each segment's filling, resulting in unwanted gaps between the sheets and the loading fibres. When the workpiece was attached to the base material, these air channels were more likely to form than later. A commercial Ultem 9085/Stratasys FDM machine was used with a lasting material and a 420 °C nozzle temperature for the required applications. A wavelet filter roughness of 10 was found in the PEEK-HAp biocomposite, as was a scatter compatibility control chart of height motifs analysis and a histogram of compactness from a volume island study of 33 points. Figure 6.16 shows the composite wavelength at 30.73 nm, with an amplitude of 5.89 nm, and composite amplitude at 5.892 nm, with a dominating wavelength of 24.93 nm and a maximum amplitude of 12.50nm of the root-mean-square gradient (Sdq).

| (a) | (b) |
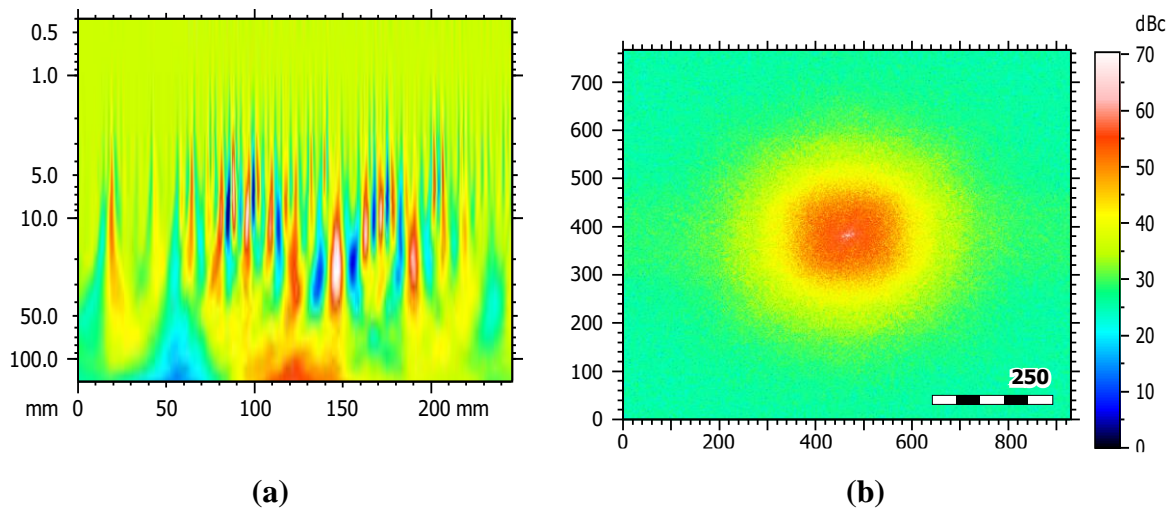
Figure 6.16 Parameters for the PEEK-HAp biocomposite, showing (a) the roughness of the continuous wavelength decomposition of a Daubechies wavelet filter of 10 and (b) the scatter compatibility of the investigated surface-generated fast Fourier transform (FFT) spectrum.

The related Slope and R2 equations were, for example, -2.65 and 0.9965 on the first day, -2.47 and 0.9998 on the third day, and -2.55 and 0.9997 on the seventh day when applied to actual units with fractal dimensions of 2.66, 2.47 and 2.55. When using PEEK-HAp with a Gaussian filter set to 0.8 millimetres roughness amplitude, the following results were obtained: texture direction of the converted luminance analysis of PEEK nanoparticles, scatter plot of the Sq height parameter of the nanoparticle in ISO25178 standard, and microstructure failure analysis (Figure 6.17).
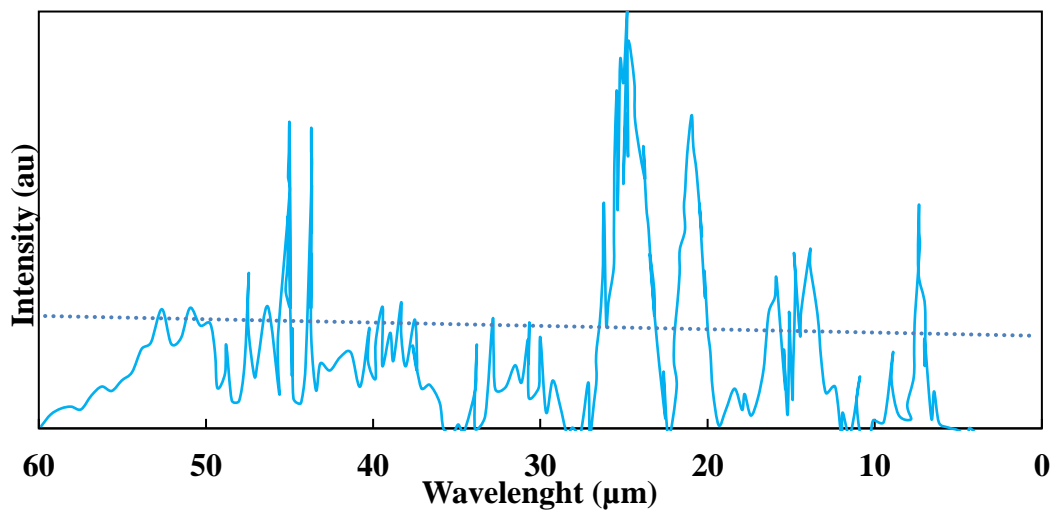
Figure 6.17 The PEEK-HAp biocomposite's X-ray diffraction (XRD) pattern analysis of the average power spectrum density patterns.

This control is specified in the descriptions of porosity and, therefore, the ultimate mechanical characteristics of the scaffolding when the Force is applied using bonded sintering powder. Powder supply methods are mature and must be enhanced to meet the needs of the new AM technology. The result required lower laser spot widths and powder particles with smaller particle sizes. However, given the rapid advancement of lasers and powders, these criteria did not represent an impassable barrier. With the development of nanotechnology, nanopowder may enhance the functionality of implants, such as the regulated release of medicines. Thus, technical resources for AM applications in the biometric industry seem accessible since the equipment required appears minimal. Along with microfabrication, AM used in the biomedical sector will soon offer stimuli resulting in what is referred to as high precision. In the case of scaffolds, AM or rapid prototyping of microphones will allow replicating of bone trabecular structure (Figure 6.18).
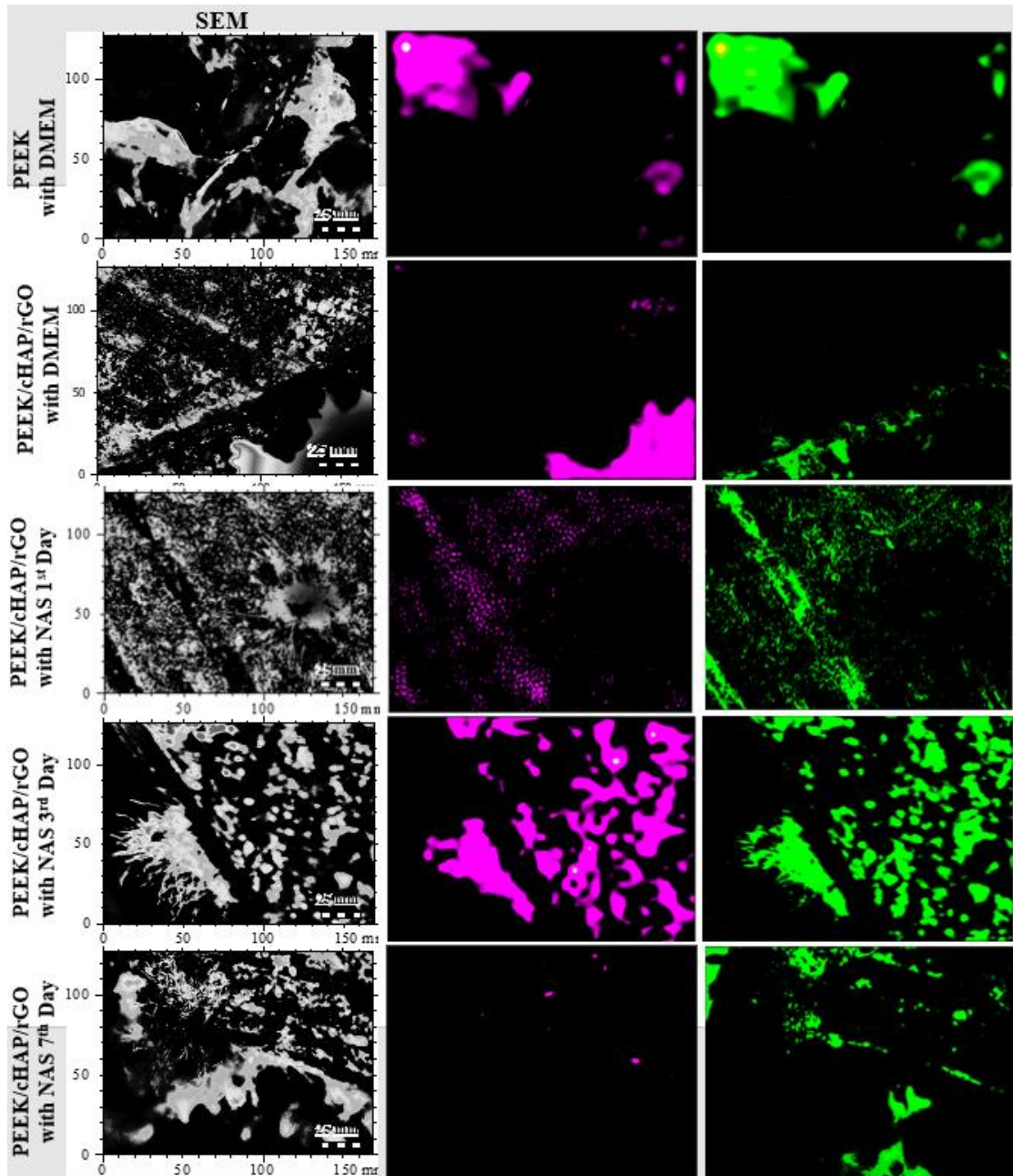
Figure 6.18 Computational view of the PEEK-cHAp-rGO scaffold in DMEM and NAS changes in time.

6.8.2. Computational and Microstructural analysis

Impure residues may remain even after removing binders, putting cHAp biocompatibility at risk by creating *in-vivo* agents that promote inflammation. Composites of HAp and biocompatible polymers often combine rGO-HAp with PEEK to produce scaffolds. The composites were made via the use of heat. Thus, AM technology was ideal for directly synthesising composite materials due to its unique polymer melting temperature compared with other AM methods. Figure 6.19 shows a

computational analysis of the nanostructure of Scaffolds in a change in time using mountain premium digital surf software
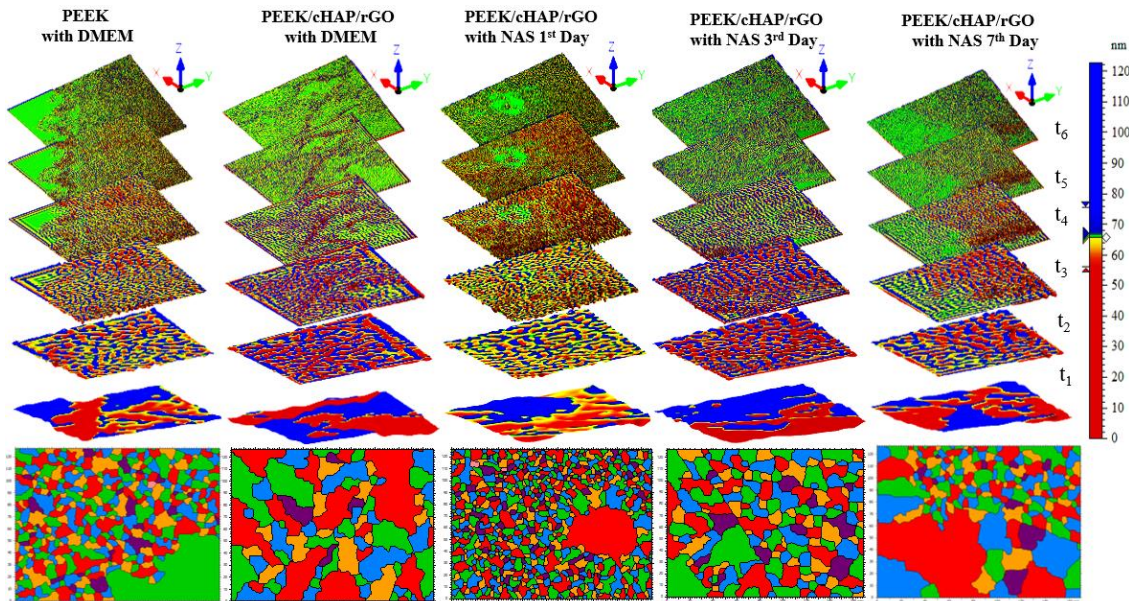
Figure 6.19 Computational analysis of nanostructure of Scaffolds in a change in time

The concepts and features of ISO 4287 outlined the influencing variables in tissue engineering 3D printing with converted scaffolding brightness. The average height of the elements in the raw profile (Rc) with ISO 4287 amendment 2 was 2.94, compared to 13.8 for the total rawness (Rt) profile and 1.04 for the roughness profile (Ra). The divergence in the root-mean-square (RMS) of the 1.22 roughness profile was fixed at 0.0718 throughout the study. To obtain an accurate result, the (Rsk) skewness was set to 0, and the (Rku) skew was set to 1.82. Additional *in vitro* test findings using DMEM were included in Figure 6.20 with a brief caption. Complete valley profile roughness (Rv) was 120maximum peak profile roughness (Rp) was 1.22, and complete ruggedness profile (Rh) was 2.41, according to the study findings. The investigation was carried out. On PEEK-rGO-cHAp grooves, tissue engineering cells adhere and develop for several test days, as shown in Figure 6.20. The sample profile is inscribed using the Gaussian 0.8 mm filter on the analytical scale. It has taken several days to generate the sampled amplitude roughness profile. PEEK-HAp particle brightness with reduced valley depth (Sck) frequency spectrum and tolerance limit test results are presented in Figure 6.20. There was a phase angle of 135.6^o and an angular value of -44.49^o for a light wavelength equal 0.535 µm.
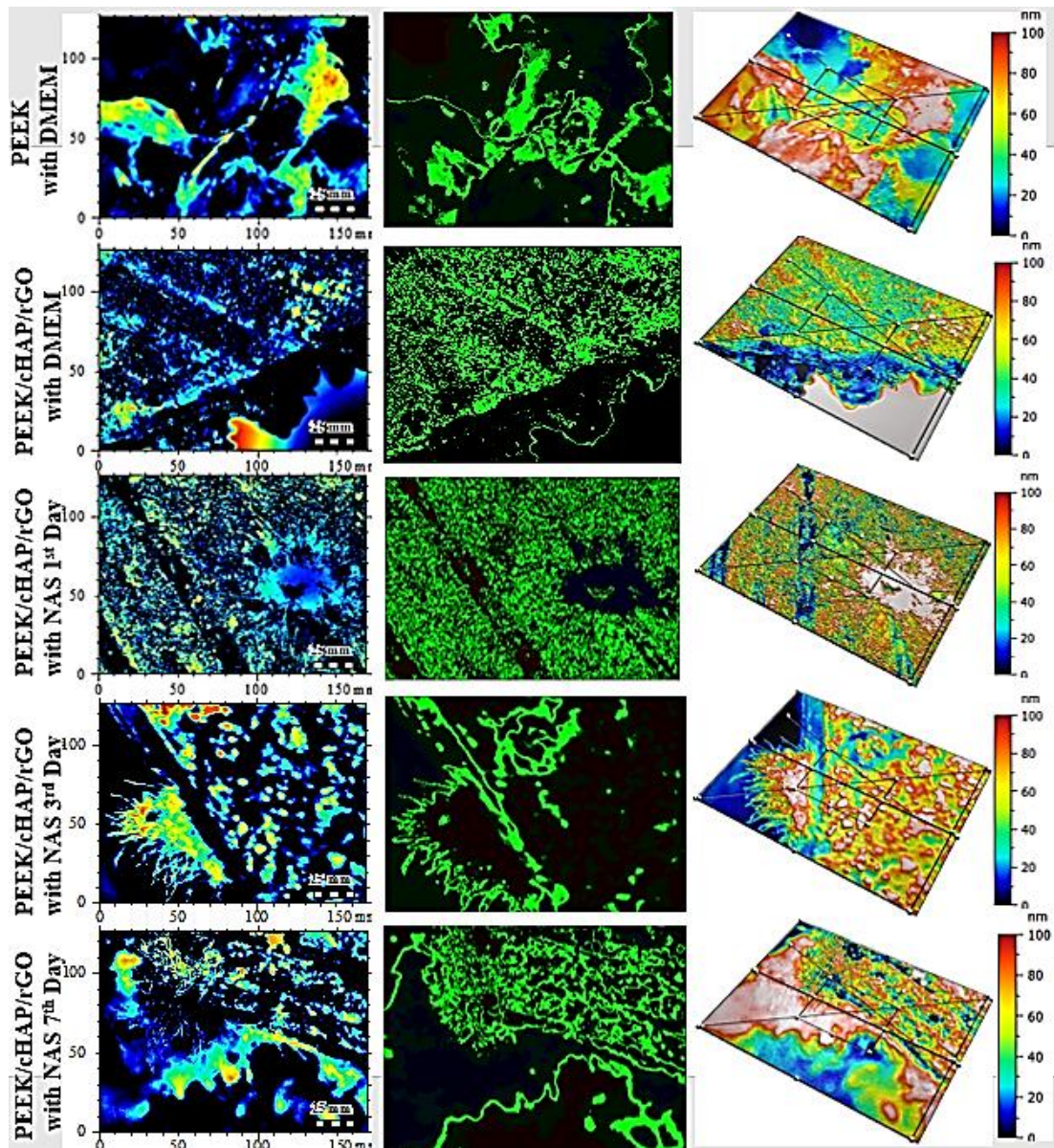
Figure 6.20 Computational view of the PEEK-cHAp-rGO scaffold in DMEM and NAS with a change in time and the 3D view of the nanostructure

6.9.   Summary and conclusion

Adding cHAp and rGO particles to PEEK during the FDM manufacturing process increases the biological activity of the material. The mechanical properties and elastic moduli of PEEK-rGO-HAp composites containing PEEK-69, cHAp-30, and rGO-1 (wt %), PEEK-78, cHAp-20, and rGO-2 (wt %), and PEEK-87, cHAp-10, and rGO-3 (wt %) have been determined, as well as the mechanical properties and elastic moduli of PEEK-rGO-HAp composite when compared to the other composite ratios, and they have the minor displacement of 9.29 m. After 14 days of immersion in DMEM-simulated

physiological fluid, the PEEK-rGO-HAp composite was discovered to trigger apatite production. The data indicate that cHAp and rGO significantly boost PEEK biological activity and osteogenesis. According to the experiments, the PEEK-cHAp composite showed better adhesion, proliferation, and cell activity when tested *in vitro* using the DMEM culture medium compared with the pure PEEK. PEEK and cHAp composites together resulted in excellent cell clotting results. Because of the composite addition, a slight reduction in mechanical properties was not significant. This research undoubtedly established a framework for biomedical bone-implant compatibility novel material products. Future development may provide preliminary proof for effective 3D printing of medical-grade PEEK using an independent extrusion method while providing a framework for future growth.

6.10. Conclusion

The PEEK-cHAp composite outperformed pure PEEK in adhesion, proliferation, dispersion, and alkaline phosphatase activity. The PEEK-cHAp composite produced apatite after 14 days of immersion in DMEM-simulated physiological fluid. The PEEK-cHAp composite exhibited a higher osseointegration activity than PEEK alone, according to *in-vivo* results. According to these results, cHAp absorption significantly increased PEEK biological activity and osteogenesis. The cHAp and rGO particles are added to PEEK during FDM production to increase their biological activity. PEEK-rGO-HAp composites with PEEK-69, cHAp-30, rGO-1 (wt%), PEEK-78, cHAp-20, and rGO-2, and PEEK-87, cHAp-10, and rGO-3, are investigated for their mechanical properties and elastic moduli. PEEK-87, cHAp-10, and rGO-3 (wt%) composites produced the most significant stress of 25.32 GPa and the lowest displacement of 9.29 mm compared with the others. It takes 14 days for the PEEK-rGO-HAp composite to stimulate apatite formation after immersion in DMEM-simulated physiological fluid. According to all the research, PEEK and osteogenesis, biological activity is significantly increased following absorption of cHAp and rGO. Moulds for bioactive PEEK-HAp composites may also be compressed using it. rGO and cHAp are consistently distributed in PEEK after being modified to provide significant derivatives with improved tissue scaffold engineering properties. Enhancing rGO-HAp compatibility with PEEK is required for biomedical engineering applications.

Chapter 7
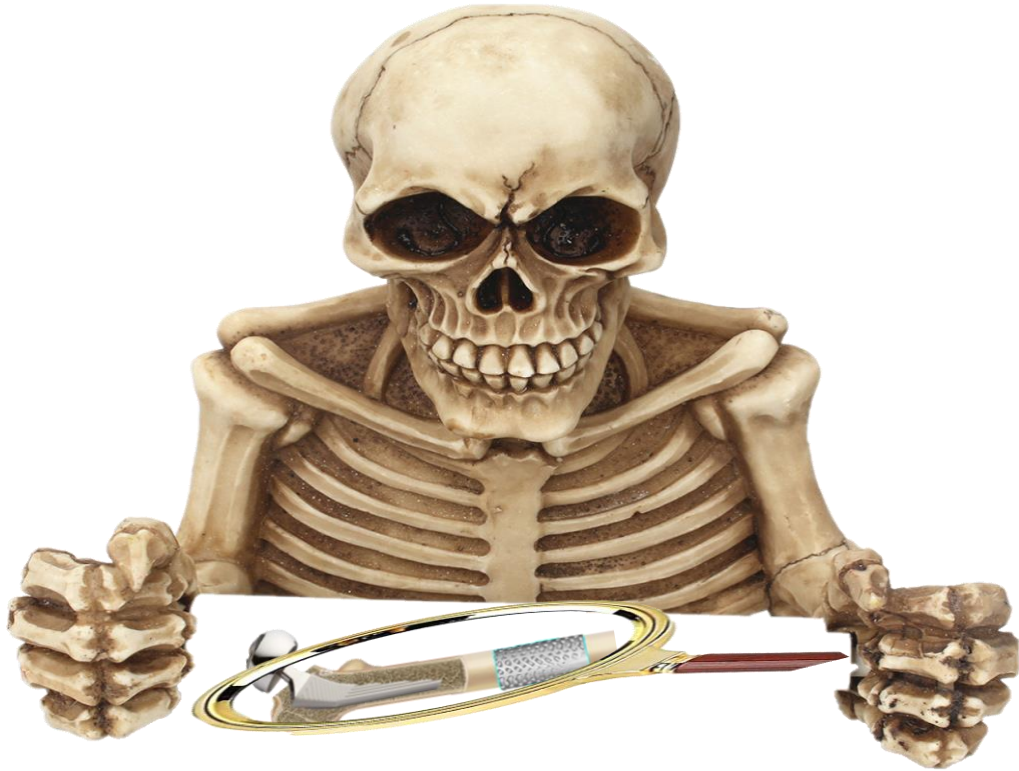
Conclusion and Ssummary on bone implant

CHAPTER 7

7.0. CONCLUSIONS

7.1.   Achievements

The design of a new bone medical implant was introduced and reviewed in the first two chapters of this thesis. The other chapters include the original work on designing and developing a bone implant, using PEEK materials with some compositions, such as cHAp and rGO, to produce a set of new composites. The key achievements of this work on bone implants are subsequently summarised:

i. A new PEEK and PEEK-rGO-cHAp biocomposites were designed and created using the FDM technique, with different proportions of composite, such as 1% wt to 5%wt of rGO and cHAp, and applied to different bone medical implants.

ii. The addition of rGO and cHAp nanoparticles to the PEEK matrix increased the biological activity of the composite structure. Various cHAp concentrations were used to determine the tensile and elastic modulus of PEEK-rGO-cHAp compounds.

iii. The presence of rGO at concentrations of 3 and 5% by weight implied a higher mechanical strength of the modulus of elasticity. A strength of 3.85 GPa was obtained with this product. The adhesion and diffusion of PEEK-rGO /cHAP were studied in *in-vitro* experiments.

iv. PEEK-rGO-cHAp composite caused apatite production in DMEM and NAS medium after 14 days of adding the compounds. The *in-vivo* findings revealed that the aggregation activity of PEEK-rGO-cHAp was much higher than that of PEEK alone.

v. Design and implement a new ten different lattice structure in the bone-implant application of PEEK-rGO-cHAp.

vi. According to these findings, rGO and cHAp significantly impacted biological activity in the body. Bone formation was substantially improved because of the verified PEEK behaviour. An accurate baseline of each door frame was produced and then simulated to replicate the skeletal structure of the pillars accurately mesh structure based on the BCC-octahedron. Mechanical strength was much higher than that of other mesh samples designed, such as gyroid and diamond, to imitate the porosity and strength of the bone structure.

7.2. General Conclusions

In conclusion, after this innovative study, it is feasible to infer that, owing to the intricacy of biological tissue imitation of PEEK and the composite. Mixing materials using coating composites was best rather than extruding the multilayer structures combination method. Surface treatment is another option for improving the characteristics of the support system and promoting bone regeneration in the patient. The findings were evaluated both *in-vitro* and *in-vivo* by utilising tissue-specific imprint structures created by different AM-based techniques to rebuild complicated tissues to recreate complex tissues. The treatment of surfaces was based on plasma activity and bioactive coatings. Stem cells aimed to enhance cell surface affinity and differentiation ability to maximise their potential for stem cells. PEEK-cHAp, biocompatible polymers and their constituents have been thoroughly investigated. It is still the most appropriate biomaterial for inorganic components, such as bones and is also the least expensive.

Also, the cHAp-PEEK interface ensured that the implant adhered to the bone optimally to restore bone function via a biologically functional and biocompatible interface. PEEK's capacity to create cells resulted in an evenly flexible structure. Because of its chemical composition and surface structure, the structure enabled cell development at the PEEK-HAp interface. It depended on the interface's interaction with the surrounding biological environment. Accumulate cHAp in PEEK, and several different techniques have been devised. Bio growth is one of the most promising of these approaches. Because it generated HAp as PEEK-cHAp physiologically in bones and enabled improved resorption of porous implants, cell adhesion, migration and proliferation were highly affected by pre-absorbed proteins during the resorption process. Therefore, it created HAp fusion interfaces attached to proteins, such as fibrin, which promotes cell proliferation and adhesion in many ways.

Moving forward, the activation of PEEK-based composites and the surface treatment of the same material were investigated in this research. This substance was selected for its potential for bone tissue regeneration and its ability to promote bone regeneration. The benefits of AM methods over other traditional manufacturing techniques to produce porous tissue were obtained in this study. The investigation showed significant discoveries on how the HAp-PEEK interface affected bodily fluids. Future studies may substantially enhance the current experimental techniques for generating and analysing

functional fusion linkages of cHAp and polymeric nanoceramics, which are currently being used. Also, these investigations contributed to a better understanding of the interaction between nanomaterials.

PEEK and cHAp can be combined in various ways, including coating with composite material, extrusion and multilayer constructions. Surface treatment is another option for enhancing the characteristics of systems that stimulate bone regeneration, which can be employed in conjunction with other methods. The production parameters for injection moulding and coating were compared using information from the literature. This study also examined the mechanical features of static and dynamic testing and the effects of these qualities on the mechanical properties of PEEK filaments following the cHAp coating process. The coating and particle dispersion quality features, morphological examination of the granulometry, depth of penetration, cHAp layer status following static and dynamic mechanical Forces, and their broad applications have been well elucidated. This critical research revealed that the thermal process successfully formed a cHAp layer with properties suitable for osteointegration. This study determined whether the thermal process successfully created a cHAp layer with properties ideal for osteointegration.

Besides, PEEK and cHAp can be utilised to repair and replace bone in hard tissues for improved support strength. Interfacial biological macromolecular cellular investigations of cHAp embedded in PEEK and other polymers will benefit biomedical application research in the future. Cellular cHAp combined with a soft polymer, such as PEEK fabric, helps to retain the functional characteristics of skin tissues that need flexibility. Long-term blood vessels or catheters must satisfy current scientific difficulties regarding tendon regeneration and cartilage replacement. Additionally, interactions at nano-bio material interfaces must be investigated. It is necessary to know cellular behaviour when exposed to implanted PEEK and cHAp scaffolds. Tissue engineering methods must consider cell adhesion characteristics, whether for surface augmentation via absorption or the insertion of specialised binding proteins. Investigating biological cellular interfaces of hybrid autonomous cells and bone material has significant potential to create biomaterials.

In addition, composite constructions can combine PEEK and cHAP in various configurations. Extrusion or a layered structure are two options. Surface treatment is another method for improving the structural characteristics of the bone used to promote

bone regeneration. Production parameters for injection moulding and coating were compared with those found in the literature [48,190]. In addition, the mechanical properties of static and dynamic tests and the effects of cHAP coating on the mechanical properties of PEEK filament, coating quality characteristics and particle dispersion were investigated in this study. Particle size was analysed morphologically. Clarification has been provided on the penetration depth, the condition of the cHAp layer after static and dynamic mechanical stresses, and the general application of the technique. This research demonstrated that the X-ray diffraction characteristics of cHAp revealed that the heat treatment results in a cHAp layer were suitable for oscillatory integration, with values at technical and international standards established to safeguard it.

Molecular-level intercellular biology studies of cHAp incorporated into PEEK and other polymers will be carried out in the future, as well as other polymers. Biomedical applications research will profit from this study since PEEK and cHAp can be utilised to repair and replace bone in complex tissues, resulting in increased strength. Cellular cHAps made of soft polymers, such as PLA textiles, aid in healing skin tissues and have functional characteristics that need flexibility. Tendon repair and cartilage replacement need a catheter or a long-term vascular system. It is necessary to investigate interactions at nanomaterial interfaces. It is critical to have a thorough knowledge of cellular behaviour when exposed to implanted PEEK and cHAp structures to create safe new methods for detecting biomolecular interactions. Tissue engineering methods must consider cell adhesion characteristics to improve surface enhancement via the adsorption or implantation of specific binding proteins. A significant deal of promise exists for researching cell biology interfaces between independent hybrid cells and bone materials to aid in creating new biomaterials.

7.3.   Summary

The adhesion and diffusion of PEEK-rGO-cHAP were shown in *in-vitro* experiments. Bone formation was substantially improved because of the verified PEEK behaviour. PEEK-rGO-cHAP compounds caused apatite production in DMEM and NAS medium after 14 days of adding the compounds. According to these findings, rGO and cHAp significantly impacted biological activity in the body. The presence of rGO at concentrations of 5 and 3% by weight implied a higher mechanical strength of the modulus of elasticity. The intricacy of biological tissue imitation was so complex that

mixing materials were best. PEEK-cHAp, biocompatible polymers and their constituents have been investigated both *in-vitro* and *in-vivo*. The cHAp-PEEK interface ensured that the implant adhered to the bone in the most optimum manner. Bio growth was a technique that generated HAp as PEEK-cHAp physiologically in bones and enabled improved resorption of porous implants that accumulated cHAp in PEEK; some methods were devised. The activation of PEEK-based composites and the surface treatment of the same material were investigated within the scope of this research. The effect of thermal shock caused by cHAp on PEEK and its thermomechanical characteristics was addressed. This study also examined the mechanical features of static and dynamic testing and their effects on the mechanical properties of PEEK filaments following the cHAp coating process. When the thermal process successfully formed a cHAp layer suitable for osteointegration, it determined whether it created properties suitable for complemented bone regeneration.

Significantly, PEEK and cHAp can repair and replace bone in hard tissues for improved support strength. Interfacial biological macromolecular cellular investigations of cHAp embedded in PEEK and other polymers will benefit biomedical application research in the future. Creating new safe methods for detecting biomolecular interactions is necessary to know cellular behaviour when exposed to implanted PEEK and cHAp scaffolds. The PEEK effects of thermal shock from cHAp crystallisation processes and the thermal-mechanical properties of the crystallisation products have been discussed. Production parameters for injection moulding and coating were compared with those obtained in the literature. In addition, the mechanical properties of static and dynamic tests and the effects of cHAP coating on the mechanical properties of PEEK filament, coating quality characteristics and particle dispersion were investigated in this study. Molecular-level intercellular biology studies of cHAP incorporated into PEEK and other polymers will be carried out in the future, as well as other relevant polymers. Biomedical applications research will profit from this novel study since PEEK can be utilised to repair and replace bone in complex tissues, resulting in increased strength. Lastly, when investigating the cHAP and PEEK structures, it is essential to have a comprehensive knowledge of cellular behaviour. A significant deal of promise exists for researching cell biology interfaces between hybrid cells and bone materials to aid in creating new biomaterials. Particle size was investigated morphologically. This study demonstrated

that the heat treatment resulted in a suitable cHAp layer for oscillatory integration, with values within technical and international standards.

7.4. Implications and Applications

The findings and outcomes of this research study on enhancing biocompatibility and structural integrity of hip and femur implants through PEEK composites and FDM techniques have several implications and applications in orthopaedics and biomaterials. The successful development and characterization of functional PEEK composites for bone implants open up new possibilities and advancements in the design and manufacturing of implant materials. One of the key implications of this research is the potential improvement in the performance and biocompatibility of PEEK materials for bone implantation. PEEK composites incorporating biocompatible additives like calcium hydroxyapatite (cHAp) and reduced graphene oxide (rGO) have enhanced mechanical strength, bioactivity, and cell adhesion properties. These improvements address the limitations of PEEK materials in replicating natural bone strength and biological properties. The developed PEEK composites have the potential to provide better compatibility with the human body, reducing the risk of adverse reactions and improving the long-term performance of hip and femur implants.

The application of fused deposition modelling (FDM) techniques in manufacturing porous hip and femur bone implants with homogenization lattice structures is another significant implication of this research. FDM allows for the precise control of scaffold geometry, porosity, and interconnectivity, crucial factors for successful bone tissue regeneration. The lattice structures designed to mimic the bone structure within the composite provide a more realistic and biomimetic implant, promoting better integration with the surrounding bone tissue. This approach opens up possibilities for patient-specific implant designs, allowing for customization and optimization of the implant properties to suit individual patient requirements.

Developing a novel lattice structure for bone implants using PEEK composites also has important implications for implant manufacturing industries. The lattice structure offers advantages such as reduced weight, improved osseointegration, and enhanced mechanical properties, making the implants more efficient and functional. Using lattice structures can potentially reduce the stress shielding effect, which occurs when the

implant bears a significant portion of the load instead of the surrounding bone. This can lead to improved long-term implant stability and longevity. The findings of this research study also have implications for the broader field of biomaterials and tissue engineering. The successful incorporation of cHAp and rGO into PEEK composites improves the mechanical properties and enhances the materials' bioactivity and cell growth potential. The developed PEEK-hydroxyapatite (HAp) composite with micropores and nanostructures provides an environment conducive to bone tissue regeneration. This bioactive composite can potentially be applied in other orthopaedic and dental applications where bone regeneration is required.

Furthermore, this study's research methodology and techniques, including extrusion, spraying, and coating deposition methods, can be applied to other polymer-based biomaterials for different implant applications. Process optimization and material characterization techniques can guide future research and development in biomaterials and implant design. The implications of this research extend beyond the academic realm to practical applications in the healthcare industry. The result of biocompatible and structurally-integrated PEEK composites for hip and femur implants can potentially improve the quality of life for patients suffering from bone defects and degenerative bone diseases. Using customized and patient-specific implants can lead to better clinical outcomes, reduced complications, and enhanced patient satisfaction. Moreover, adopting these advanced biomaterials and manufacturing techniques can contribute to the growth and advancement of the medical device industry, stimulating innovation and economic development.

In conclusion, the implications and applications of this research study are far-reaching and have significant potential to advance the field of orthopaedics and biomaterials. Developing functional PEEK composites, utilising FDM techniques for scaffold fabrication, and incorporating novel lattice structures in bone implants provide valuable contributions to the scientific and industrial communities. The improved biocompatibility, structural integrity, and performance of the developed PEEK composites pave the way for developing more advanced and patient-specific implant materials, ultimately benefiting individuals needing hip and femur implantation.

7.5. Limitations of the Study

While this research study has made significant contributions to enhancing the biocompatibility and structural integrity of hip and femur implants through PEEK composites and FDM techniques, it is vital to acknowledge the study's limitations. These limitations provide insights into areas that could be further explored and improved in future research.

i. **Limited sample size:** One of the limitations of this study is the relatively small sample size used for experimental testing and characterization. While the samples used in the study provided valuable data and insights, a larger sample size would allow for a more robust statistical analysis and a better representation of the overall performance of the PEEK composites. Additionally, a larger sample size would help account for potential variations and provide more confidence in the results obtained.

ii. **Simplified loading conditions:** The mechanical testing conducted in this study focused on compressive and tensile tests to evaluate the mechanical properties of the PEEK composites. However, the loading conditions applied in these tests were simplified and may not fully replicate the complex biomechanical forces experienced by hip and femur implants in vivo. Future research could consider incorporating more realistic loading conditions, such as cyclic, to assess the durability and fatigue resistance of the implants.

iii. **Lack of long-term assessment:** This study's evaluation of the PEEK composites and lattice structures was primarily focused on short-term performance and biocompatibility. While the initial findings are promising, long-term assessment, like fatigue analysis, is essential to determine the implants' durability, stability, and long-term biocompatibility. Future research should consider conducting long-term in vivo studies and monitoring the implants over extended periods to assess their performance over time.

iv. **Simplified in-vitro testing:** The in-vitro biocompatibility testing conducted in this study provided valuable preliminary data on the cytotoxicity and cell adhesion properties of the PEEK composites. However, it is essential to note that in-vitro testing cannot fully replicate the complex biological interactions that occur in vivo. Further studies should include more comprehensive in-vitro testing, such as cell proliferation assays and differentiation studies, to better understand the biological response to the PEEK composites.

v.   **Limited clinical validation:** While the developed PEEK composites and lattice structures show promise for hip and femur implants, it is essential to acknowledge that their clinical validation was beyond the scope of this study. Clinical proof, including rigorous testing in human subjects, is necessary to assess the implants' safety, efficacy, and long-term performance in real-world scenarios. Collaboration with orthopaedic surgeons and conducting clinical trials would provide valuable insights into the clinical feasibility and applicability of the developed implants.

vi.   **Manufacturing considerations:** The FDM technique used in this study for scaffold fabrication has certain limitations, such as limited resolution and the potential for porosity in the printed structures. While the FDM technique is suitable for research and prototyping purposes, additional optimization and validation are required to ensure the scalability and commercial viability of the manufacturing process. Exploring other additive manufacturing techniques or optimizing the FDM parameters for large-scale production would benefit future research.

vii.   **Surface modification limitations**: While surface modifications were considered in this study to enhance the properties of the PEEK composites, the methods used, such as extrusion and coating deposition, have limitations. Further research could explore alternative surface modification techniques, such as plasma treatment or chemical functionalization, to better control surface properties and improve the interaction between the implants and surrounding tissues.

viii.   **Lack of comparative studies:** This study focused on developing and characterising PEEK composites and lattice structures. However, comparative studies with existing materials and implant designs were not conducted. Comparative studies would provide valuable insights into the performance and advantages of the developed PEEK composites compared to traditional materials and other biomaterials for bone implants.

ix.   **Regulatory and approval considerations:** While this research study focused on the material development and characterization aspects of PEEK composites, it is essential to note that regulatory and support processes are crucial in translating these materials into clinical practice. Future research should consider the regulatory requirements and work towards obtaining the necessary approvals and certifications for the developed implants.

In summary, while this research study has significantly enhanced hip and femur implants' biocompatibility and structural integrity through PEEK composites and FDM techniques, several limitations should be acknowledged. Addressing these limitations in future research will help further improve the understanding and application of PEEK composites for bone implantation and contribute to developing safer, more effective, and long-lasting implant solutions for patients in need.

7.6. Recommendations for Future Research

This research study has provided valuable insights into developing and characterising PEEK composites for hip and femur implants. Building upon the findings and limitations of this study, several recommendations for future research can be made to advance further the field of biocompatible and structurally enhanced bone implants. These recommendations include material optimization, manufacturing techniques, biocompatibility assessment, and clinical implementation.

i. **Exploration of alternative composite materials:** While this study focused on PEEK composites, a wide range of alternative biomaterials and composite combinations could be explored for bone implant applications. Future research should investigate using different polymers, ceramics, metals, and their composites to optimize the implants' mechanical properties, bioactivity, and biocompatibility. Comparative studies between other composite materials can provide valuable insights into the optimal material composition for specific implant applications.

ii. **Advanced lattice structures and design optimization:** The lattice structures used in this study were relatively simple and limited in complexity. Future research should focus on developing more advanced lattice structures that closely mimic natural bone's hierarchical architecture and properties. Utilizing computational modelling and optimization techniques can aid in the design of optimized lattice structures that offer improved mechanical strength, osseointegration, and bone regeneration potential.

iii. **Integration of bioactive agents:** To further enhance the bioactivity and cellular response of the PEEK composites, future research should explore the integration of bioactive agents, such as growth factors, peptides, and proteins. Incorporating these bioactive agents into the composite matrix can promote enhanced bone formation,

angiogenesis, and tissue integration, improving implant performance and long-term stability.

iv. **Advanced manufacturing techniques:** While FDM was used in this study for scaffold fabrication, other additive manufacturing techniques could be explored for polymers like PLA. Techniques such as selective laser sintering (SLS), stereolithography (SLA), and inkjet 3D printing offer different advantages regarding resolution, porosity control, and material compatibility. Investigating these alternative manufacturing techniques can provide further opportunities for optimizing the fabrication process and improving the mechanical properties of the implants.

v. **In-vivo studies and long-term assessment:** This study primarily focused on in-vitro biocompatibility testing and short-term evaluation of the PEEK composites. Future research should conduct comprehensive in-vivo studies using animal models to assess the implants' long-term performance, biocompatibility, and tissue integration. Long-term assessment should include evaluating factors such as implant stability, bone ingrowth, mechanical durability, and potential adverse reactions to ensure the safety and efficacy of the developed implants.

vi. **Clinical validation and patient outcomes:** Collaboration with orthopaedic surgeons and conducting clinical trials are crucial to clinically validating the developed PEEK composites. Future research should aim to establish partnerships with medical institutions and initiate clinical studies to evaluate the performance of the implants in real patient scenarios. Long-term monitoring of patients with PEEK composite implants can provide valuable data on patient outcomes, implant survivorship, and overall clinical efficacy.

vii. **Surface modification techniques:** While surface modifications were explored in this study, there is still room for further research on advanced surface modification techniques for PEEK composites. Investigating methods such as plasma treatment, chemical functionalization, or nanocoatings can enhance the surface properties of the implants, promoting improved tissue integration, reduced bacterial adhesion, and enhanced biocompatibility.

viii. **Multidisciplinary collaborations:** Future research should encourage multidisciplinary collaborations between materials scientists, engineers, biologists, clinicians, and regulatory experts. Collaboration across different fields can foster a

comprehensive understanding of the complex requirements and challenges of developing and implementing PEEK composites for other bone implants like dentistry, spine, and skull. This interdisciplinary approach will contribute to translating research findings into clinical practice more effectively.

In conclusion, the recommendations above outline potential areas for future research to further advance the field of PEEK composites for bone implantation. By exploring alternative materials, optimizing manufacturing techniques, conducting in-vivo studies, and fostering clinical collaborations, researchers can continue improving hip and femur implants' biocompatibility, mechanical properties, and long-term performance. These advancements have the potential to significantly impact patient outcomes and contribute to the development of safer and more effective implant solutions in orthopaedic surgery.

REFERENCES

[1]   Oladapo BI, Ismail SO, Zahedi M, Khan A, Usman H. 3D printing and morphological characterisation of polymeric composite scaffolds. Engineering Structures 2020;216:110752. https://doi.org/10.1016/j.engstruct.2020.110752.

[2]   Correia TR, Figueira DR, Int J Biol Macromol 2016;93:1432–45. https://doi.org/10.1016/j.ijbiomac.2016.06.004.

[3]   Das M, Balla VK. Additive Manufacturing in Materials Innovation. In: Bandyopadhyay A, Bose S, editors. Additive Manufacturing. 2nd ed., CRC Press; 2020, p. 377–420. https://doi.org/10.1201/9780429466236-12.

[4]   Pollack S, Venkatesh C, Neff M, Healy AV, Hu G, Fuenmayor EA, et al. Polymer-Based Additive Manufacturing: Historical Developments, Process Types and Material Considerations. Polymer-Based Additive Manufacturing, Cham: Springer International Publishing; 2019, p. 1–22. https://doi.org/10.1007/978-3-030-24532-0_1.

[5]   Tong A, Pham QL, Abatemarco P, Mathew A, Gupta D, Iyer S, et al. Review of Low-Cost 3D Bioprinters: State of the Market and Observed Future Trends. SLAS TECHNOLOGY: Translating Life Sciences Innovation 2021;26:333–66. https://doi.org/10.1177/24726303211020297.

[6]   Fazlollahi M, Pooshidani Y, Eskandari M. Additive Manufacturing in Bone Tissue Engineering. 3D Printing in Biomedical Engineering, Singapore: Springer Singapore; 2020, p. 95–125. https://doi.org/10.1007/978-981-15-5424-7_5.

[7]   Vaezi M, Yang S. Extrusion-based additive manufacturing of PEEK for biomedical applications. Virtual and Physical Prototyping 2015;10:123–35. https://doi.org/10.1080/17452759.2015.1097053.

[8]   Lunenfeld B, Stratton P. The clinical consequences of an ageing world and preventive strategies. Best Pract Res Clin Obstet Gynaecol 2013;27:643–59. https://doi.org/10.1016/j.bpobgyn.2013.02.005.

[9]   future-of-an-ageing-population.pdf n.d.

[10]   Gautam G, Kumar S, Kumar K. Processing of biomaterials for bone tissue engineering: State of the art. Materials Today: Proceedings 2021. https://doi.org/10.1016/j.matpr.2021.09.459.

[11] Navarro M, Michiardi A, Castaño O, Planell JA. Biomaterials in orthopaedics. J R Soc Interface 2008;5:1137–58. https://doi.org/10.1098/rsif.2008.0151.

[12] Golafshan N, Vorndran E, Zaharievski S, Brommer H, Kadumudi FB, Dolatshahi-Pirouz A, et al. Tough magnesium phosphate-based 3D-printed implants induce bone regeneration in an equine defect model. Biomaterials 2020;261:120302. https://doi.org/10.1016/j.biomaterials.2020.120302.

[13] Volkov AV, Muraev AA, Zharkova II, Voinova VV, Akoulina EA, Zhuikov VA, et al. Poly(3-hydroxybutyrate)/hydroxyapatite/alginate scaffolds seeded with mesenchymal stem cells enhance the regeneration of critical-sized bone defect. Mater Sci Eng C Mater Biol Appl 2020;114:110991. https://doi.org/10.1016/j.msec.2020.110991.

[14] Anandkumar R, Babu SR. FDM filaments with unique segmentation since evolution: a critical review. Progress in Additive Manufacturing 2019;4:185–93. https://doi.org/10.1007/s40964-018-0069-8.

[15] Hulsart-Billström G, Dawson JI, Hofmann S, Müller R, Stoddart MJ, Alini M, et al. A surprisingly poor correlation between in vitro and *in-vivo* testing of biomaterials for bone regeneration: results of a multicentre analysis. 2016. https://doi.org/10.22203/ecm.v031a20.

[16] Partridge K, Yang X, Clarke NMP, Okubo Y, Bessho K, Sebald W, et al. Adenoviral BMP-2 Gene Transfer in Mesenchymal Stem Cells: I*n-vitro* and *in-vivo* Bone Formation on Biodegradable Polymer Scaffolds. Biochemical and Biophysical Research Communications 2002;292:144–52. https://doi.org/10.1006/bbrc.2002.6623.

[17] Seebach E, Kubatzky KF. Chronic Implant-Related Bone Infections—Can Immune Modulation be a Therapeutic Strategy? Frontiers in Immunology 2019;10:1724. https://doi.org/10.3389/fimmu.2019.01724.

[18] Ribeiro M, Monteiro FJ, Ferraz MP. Infection of orthopedic implants with emphasis on bacterial adhesion process and techniques used in studying bacterial-material interactions. Biomatter 2012;2:176–94. https://doi.org/10.4161/biom.22905.

[19] Hanssen AD, Spangehl MJ. Treatment of the Infected Hip Replacement. Clinical Orthopaedics and Related Research® 2004;420:63–71.

[20] Zheng Z, Eglin D, Alini M, Richards GR, Qin L, Lai Y. Visible Light-Induced 3D Bioprinting Technologies and Corresponding Bioink Materials for Tissue Engineering: A Review. Engineering 2021;7:966–78. https://doi.org/10.1016/j.eng.2020.05.021.

[21] Chen F-M, Liu X. Advancing biomaterials of human origin for tissue engineering. Progress in Polymer Science 2016;53:86–168. https://doi.org/10.1016/j.progpolymsci.2015.02.004.

[22] Kumar N, Ramakrishnan SA, Lopez KG, Madhu S, Ramos MRD, Fuh JYH, et al. Can Polyether Ether Ketone Dethrone Titanium as the Choice Implant Material for Metastatic Spine Tumor Surgery? World Neurosurgery 2021;148:94–109. https://doi.org/10.1016/j.wneu.2021.01.059.

[23] Sam J, Franco B, Ma J, Karaman I, Elwany A, Mabe JH. Tensile actuation response of additively manufactured nickel-titanium shape memory alloys. Scripta Materialia 2018;146:164–8. https://doi.org/10.1016/j.scriptamat.2017.11.013.

[24] Gonzalez-Gutierrez J, Cano S, Schuschnigg S, Kukla C, Sapkota J, Holzer C. Additive Manufacturing of Metallic and Ceramic Components by the Material Extrusion of Highly-Filled Polymers: A Review and Future Perspectives. Materials 2018;11:840. https://doi.org/10.3390/ma11050840.

[25] Mohammed AS, Irfan Fareed M. Surface Modification of Polyether Ether Ketone (PEEK) with a Thin Coating of UHMWPE for Better Tribological Properties. Tribology Transactions 2017;60:881–7. https://doi.org/10.1080/10402004.2016.1225876.

[26] Seal S, Singh S, Crawford K, Brisbois E, Coathup M. NOVEL POLYMERS FOR USE IN TOTAL JOINT ARTHROPLASTY: Advanced Materials & Processes 2018;176:30–4.

[27] Merola M, Affatato S. Materials for Hip Prostheses: A Review of Wear and Forceing Considerations. Materials 2019;12:495. https://doi.org/10.3390/ma12030495.

[28] Hadjidakis DJ, Androulakis II. Bone Remodeling. Annals of the New York Academy of Sciences 2006;1092:385–96. https://doi.org/10.1196/annals.1365.035.

[29] 33-JMES-363-2013-Verma.pdf n.d.

[30] Jiang S, Agarwal S, Greiner A. Low-Density Open Cellular Sponges as Functional Materials. Angewandte Chemie International Edition 2017;56:15520–38. https://doi.org/10.1002/anie.201700684.

[31] 802467.pdf n.d.

[32] 1-s2.0-S2351978915000359-main.pdf n.d.

[33] Geng P, Zhao J, Wu W, Ye W, Wang Y, Wang S, et al. Effects of extrusion speed and printing speed on the 3D printing stability of extruded PEEK filament. Journal of Manufacturing Processes 2019;37:266–73. https://doi.org/10.1016/j.jmapro.2018.11.023.

[34] Souza JCM, Correia MST, Henriques B, Novaes de Oliveira AP, Silva FS, Gomes JR. Micro-scale abrasion wear of novel biomedical PEEK-matrix composites for restorative dentistry. Surface Topography Metrology and Properties 2019;7:15019. https://doi.org/10.1088/2051-672X/ab0324.

[35] Liu D, Zhu Z, Zhou J, Zhao H, Chen J, Bai R, et al. Preparation and biocompatibility of Fe50Ni50p/HAP/PEEK biocomposites with weak magnetic properties. RSC Advances 2019;9:181–19. https://doi.org/10.1039/c9ra00719a.

[36] Panayotov IV, Orti V, Cuisinier F, Yachouh J. Polyetheretherketone (PEEK) for medical applications. Journal of Materials Science Materials in Medicine 2016;27:1–11. https://doi.org/10.1007/s10856-016-5731-4.

[37] Kizuki T, Matsushita T, Kokubo T. Apatite-forming PEEK with TiO2 surface layer coating. Journal of Materials Science Materials in Medicine 2015;26:1–9. https://doi.org/10.1007/s10856-014-5359-1.

[38] Merenda A, Ligneris E des, Sears K, Chaffraix T, Magniez K, Cornu D, et al. Assessing the temporal stability of surface functional groups introduced by plasma treatments on the outer shells of carbon nanotubes. Sci Rep 2016;6:31565. https://doi.org/10.1038/srep31565.

[39] Desmet T, Morent R, De Geyter N, Leys C, Schacht E, Dubruel P. Nonthermal Plasma Technology as a Versatile Strategy for Polymeric Biomaterials Surface Modification: A Review. Biomacromolecules 2009;10:2351–78. https://doi.org/10.1021/bm900186s.

[40] Chen C-T, Gu GX. Machine learning for composite materials. MRS Communications 2019;9:556–66. https://doi.org/10.1557/mrc.2019.32.

[41] Full Text PDF n.d.

[42] Sionkowska A. Current research on the blends of natural and synthetic polymers as new biomaterials: Review. Progress in Polymer Science 2011;36:1254–76. https://doi.org/10.1016/j.progpolymsci.2011.05.003.

[43] Lee SJ, Yoo JJ, Atala A. Biomaterials and Tissue Engineering. In: Kim BW, editor. Clinical Regenerative Medicine in Urology, Singapore: Springer; 2018, p. 17–51. https://doi.org/10.1007/978-981-10-2723-9_2.

[44] Khan F, Ahmad SR. Bioactive Polymers and Nanobiomaterials Composites for Bone Tissue Engineering. In: Ramalingam M, Wang X, Chen G, Ma P, Cui F, editors. Biomimetics, Hoboken, NJ, USA: John Wiley & Sons, Inc; 2013, p. 91–117. https://doi.org/10.1002/9781118810408.ch5.

[45] Almasi D, Iqbal N, Sadeghi M, Sudin I, Abdul Kadir MR, Kamarul T. Preparation Methods for Improving PEEK's Bioactivity for Orthopedic and Dental Application: A Review. International Journal of Biomaterials 2016;2016:e8202653. https://doi.org/10.1155/2016/8202653.

[46] Hetemi D, Pinson J. Functionalization of Polymers by Hydrolysis, Aminolysis, Reduction, Oxidation, and Some Related Reactions. Surface Modification of Polymers, John Wiley & Sons, Ltd; 2019, p. 211–40. https://doi.org/10.1002/9783527819249.ch8.

[47] Feng P, Jia J, Peng S, Yang W, Bin S, Shuai C. Graphene oxide-driven interfacial coupling in laser 3D printed PEEK-PVA scaffolds for bone regeneration. Virtual and Physical Prototyping 2020;15:211–26. https://doi.org/10.1080/17452759.2020.1719457.

[48] Oladapo BI, Zahedi SA, Ismail SO. Mechanical performances of hip implant design and fabrication with PEEK composite. Polymer 2021.

[49] Oladapo BI, Zahedi SA. Improving bioactivity and strength of PEEK composite polymer for bone application. Materials Chemistry and Physics 2021;266:124485.

[50] Anguiano-Sanchez J, Martinez-Romero O, Siller HR, Diaz-Elizondo JA, Flores-Villalba E, Rodriguez CA. Influence of PEEK Coating on Hip Implant Stress Shielding: A Finite Element Analysis. Computational and Mathematical Methods in Medicine 2016;2016:6183679–10. https://doi.org/10.1155/2016/6183679.

[51] Zheng J, Zhao H, Dong E, Kang J, Liu C, Sun C, et al. Additively-manufactured PEEK-HA porous scaffolds with highly-controllable mechanical properties and excellent biocompatibility. Mater Sci Eng C Mater Biol Appl 2021;128:112333. https://doi.org/10.1016/j.msec.2021.112333.

[52] Polley C, Distler T, Detsch R, Lund H, Springer A, Boccaccini AR, et al. 3D Printing of Piezoelectric Barium Titanate-Hydroxyapatite Scaffolds with Interconnected Porosity for Bone Tissue Engineering. Materials (Basel) 2020;13:E1773. https://doi.org/10.3390/ma13071773.

[53] Chakravarty J, Rabbi MF, Chalivendra V, Ferreira T, Brigham CJ. Mechanical and biological properties of chitin/polylactide (PLA)/hydroxyapatite (HAP) composites cast using ionic liquid solutions. International Journal of Biological Macromolecules 2020;151:1213–23. https://doi.org/10.1016/j.ijbiomac.2019.10.168.

[54] Li W, Kang J, Yuan Y, Xiao F, Yao H, Liu S, et al. Preparation and characterization of PVA-PEEK-PVA-β-TCP bilayered hydrogels for articular cartilage tissue repair. Composites Science and Technology 2016;128:58–64. https://doi.org/10.1016/j.compscitech.2016.03.013.

[55] Saravanan S, Leena RS, Selvamurugan N. Chitosan based biocomposite scaffolds for bone tissue engineering. International Journal of Biological Macromolecules 2016;93:1354–65. https://doi.org/10.1016/j.ijbiomac.2016.01.112.

[56] Eivazzadeh-Keihan R, Maleki A, de la Guardia M, Bani MS, Chenab KK, Pashazadeh-Panahi P, et al. Carbon based nanomaterials for tissue engineering of bone: Building new bone on small black scaffolds: A review. Journal of Advanced Research 2019;18:185–201. https://doi.org/10.1016/j.jare.2019.03.011.

[57] Rajan M, Sumathra M. et al., Polymer Nanocomposites in Biomedical Engineering, Cham: Springer International Publishing; 2019, p. 167–204. https://doi.org/10.1007/978-3-030-04741-2_6.

[58] Baştan FE.. Journal of Biomedical Materials Research Part B: Applied Biomaterials 2020;108:2513–27. https://doi.org/10.1002/jbm.b.34583.

[59] Barkarmo S, Wennerberg A, Hoffman M, Kjellin P, Breding K, Handa P, et al. Nano-hydroxyapatite-coated PEEK implants: A pilot study in rabbit bone. Journal of Biomedical Materials Research Part A 2013;101A:465–71. https://doi.org/10.1002/jbm.a.34358.

[60] Wang Y, Shen J, Yan M, Tian X.. Materials & Design 2021;201:109510. https://doi.org/10.1016/j.matdes.2021.109510.

[61] Dayan Ç, Bural C, Geçkili O. Clinical Implant Dentistry and Related Research 2019;21:42–5. https://doi.org/10.1111/cid.12689.

[62] Hwangbo H, Lee H, Roh EJ, Kim W, Joshi HP, Kwon SY, et al.. Applied Physics Reviews 2021;8:021403.

[63] Chen S, Shi Y, Luo Y, Ma J.. Colloids Surf B Biointerfaces 2019;179:121–7. https://doi.org/10.1016/j.colsurfb.2019.03.063.

[64] Oladapo BI, Zahedi SA, Omigbodun FT. A systematic review of polymer composite in biomedical engineering. European Polymer Journal 2021;154:110534. https://doi.org/10.1016/j.eurpolymj.2021.110534.

[65] Oladapo BI, Ismail SO, Adebiyi AV, Omigbodun FT, Olawumi MA, Olawade DB. . Colloids and Surfaces A, Physicochemical and Engineering Aspects 2021;627. https://doi.org/10.1016/j.colsurfa.2021.127190.

[66] Volyanski I, Volchkov S, Shishkovsky I. Cytotoxicity and apoptotic effects of polymer coated copper oxide nanoparticles synthesized via SLM in mesenchymal stem cells. Optical and Quantum Electronics 2017;49:1–10. https://doi.org/10.1007/s11082-017-0957-z.

[67] Galindo TGP, Chai Y, Tagaya M. Hydroxyapatite Nanoparticle Coating on Polymer for Constructing Effective Biointeractive Interfaces. Journal of Nanomaterials 2019;2019:e6495239. https://doi.org/10.1155/2019/6495239.

[68] Sagomonyants KB, Jarman-Smith ML, Devine JN, Aronow MS, Gronowicz GA. The in vitro response of human osteoblasts to polyetheretherketone (PEEK) substrates compared to commercially pure titanium. Biomaterials 2008;29:1563–72. https://doi.org/10.1016/j.biomaterials.2007.12.001.

[69] Khuu N. Biomimetic Extracellular Matrices for in Vitro Cancer Models and Tissue Engineering Platforms. PhD Thesis. University of Toronto (Canada), 2021.

[70] Sargin F, Erdogan G, Kanbur K, Turk A. Investigation of in vitro behavior of plasma sprayed Ti, TiO2 and HA coatings on PEEK. Surface and Coatings Technology 2021;411:126965. https://doi.org/10.1016/j.surfcoat.2021.126965.

[71] Kurtz SM, Devine JN. PEEK biomaterials in trauma, orthopedic, and spinal implants. Biomaterials 2007;28:4845–69. https://doi.org/10.1016/j.biomaterials.2007.07.013.

[72] Kurtz SM, Books24x7 I. PEEK biomaterials handbook. 1st;1st; Waltham, MA;Oxford UK; William Andrew; 2012.

[73] Oladapo BI, Zahedi SA, Ismail SO, Omigbodun FT. 3D printing of PEEK and its composite to increase biointerfaces as a biomedical material- A review. Colloids Surf B Biointerfaces 2021;203:111726. https://doi.org/10.1016/j.colsurfb.2021.111726.

[74] Anil S, Al-Sulaimani A, E B A, Chalisserry E, Varma H, Al Amri M. Drug Delivery Systems and Bone Regeneration in implant Dentistry, 2015, p. 1–27. https://doi.org/10.13140/2.1.1850.1921.

[75] Chaudhari AA, Vig K, Baganizi DR, Sahu R, Dixit S, Dennis V, et al. Future Prospects for Scaffolding Methods and Biomaterials in Skin Tissue Engineering: A Review. International Journal of Molecular Sciences 2016;17:1974. https://doi.org/10.3390/ijms17121974.

[76] Bessa PC, Casal M, Reis RL. Bone morphogenetic proteins in tissue engineering: the road from laboratory to clinic, part II (BMP delivery). Journal of Tissue Engineering and Regenerative Medicine 2008;2:81–96. https://doi.org/10.1002/term.74.

[77] Cunniffe GM, Gonzalez-Fernandez T, Daly A, Sathy BN, Jeon O, Alsberg E, et al. * Three-Dimensional Bioprinting of Polycaprolactone Reinforced Gene Activated

Bioinks for Bone Tissue Engineering. Tissue Eng Part A 2017;23:891–900. https://doi.org/10.1089/ten.tea.2016.0498.

[78] Neufurth M, Wang X, Wang S, Steffen R, Ackermann M, Haep ND, et al. 3D printing of hybrid biomaterials for bone tissue engineering: Calcium-polyphosphate microparticles encapsulated by polycaprolactone. Acta Biomater 2017;64:377–88. https://doi.org/10.1016/j.actbio.2017.09.031.

[79] Alizadeh-Osgouei M, Li Y, Wen C. A comprehensive review of biodegradable synthetic polymer-ceramic composites and their manufacture for biomedical applications. Bioactive Materials 2019;4:22–36. https://doi.org/10.1016/j.bioactmat.2018.11.003.

[80] Researchers from Engineering Department Report Details of New Studies and Findings in Sustainability Research (Recent Advances In Biopolymeric Composite Materials: Future Sustainability of Bone-implant). Health & Medicine Week 2021:434.

[81] Ma R, Yu Z, Tang S, Pan Y, Wei J, Tang T. Osseointegration of nanohydroxyapatite- or nano-calcium silicate-incorporated polyetheretherketone bioactive composites *in-vivo*. International Journal of Nanomedicine 2016;11:6023–33. https://doi.org/10.2147/IJN.S115286.

[82] Boudeau N, Liksonov D, Barriere T, Maslov L, Gelin J-C. C. Materials in Engineering 2012;40:148–56. https://doi.org/10.1016/j.matdes.2012.03.028.

[83] Flanagan M, Grogan DM, Goggins J, Appel S, Doyle K, Leen SB, et al. Permeability of carbon fibre PEEK composites for cryogenic storage tanks of future space launchers. Composites Part A, Applied Science and Manufacturing 2017;101:173–84. https://doi.org/10.1016/j.compositesa.2017.06.013.

[84] Singh S, Prakash C, Ramakrishna S. 3D printing of polyether-ether-ketone for biomedical applications. European Polymer Journal 2019;114:234–48. https://doi.org/10.1016/j.eurpolymj.2019.02.035.

[85] Machining ULTEM: A Plastics Guide. AIP Precision Machining 2018. https://aipprecision.com/machining-ultem-plastics-guide/ (accessed November 13, 2021).

[86] Guo C, Liu X, Liu G. Surface Finishing of FDM-Fabricated Amorphous Polyetheretherketone and Its Carbon-Fiber-Reinforced Composite by Dry Milling. Polymers 2021;13:2175. https://doi.org/10.3390/polym13132175.

[87] Heimer S, Schmidlin PR, Stawarczyk B. Discoloration of PMMA, composite, and PEEK. Clinical Oral Investigations 2017;21:1191–200. https://doi.org/10.1007/s00784-016-1892-2.

[88] Lacerda PSS, Gama N, Freire CSR, Silvestre AJD,. Polymers 2020;12:1867. https://doi.org/10.3390/polym12091867.

[89] Corni I, Cannio M, Romagnoli M, Boccaccini AR.. Materials Research Bulletin 2009;44:1494–501. https://doi.org/10.1016/j.materresbull.2009.02.011.

[90] Pace N MD, Marinelli M MD, Spurio S MD. The Journal of Arthroplasty 2008;23:151–5. https://doi.org/10.1016/j.arth.2006.07.012.

[91] Ehmaida MM.. University of Bradford, 2012.

[92] Hausberger A, Stiller T, Kappl C, Hensgen L, Grün F.. Lubricants 2021;9:91. https://doi.org/10.3390/lubricants9090091.

[93] Peng C, Li X. The Mechanical Properties of PEEK-CF Composites Reinforced With ZrO2 Nanoparticles. Mech Compos Mater 2014;49:679–84. https://doi.org/10.1007/s11029-013-9384-9.

[94] Gao G, Gong J, Qi Y, Ren J, Wang H, Yang D, et al. Tribological Behavior of PTFE Composites Filled with PEEK and Nano-ZrO2. Tribology Transactions 2020;63:296–304. https://doi.org/10.1080/10402004.2019.1687796.

[95] McCook NL, Hamilton MA, Burris DL, Sawyer WG. Tribological results of PEEK nanocomposites in dry sliding against 440C in various gas environments. Wear 2007;262:1511–5. https://doi.org/10.1016/j.wear.2007.01.036.

[96] Zalaznik M, Kalin M, Novak S, Jakša G. Effect of the type, size and concentration of solid lubricants on the tribological properties of the polymer PEEK. Wear 2016;364–365:31–9. https://doi.org/10.1016/j.wear.2016.06.013.

[97] Li S, Wen F, Sun C, Wang Z, Chen R, He Q, et al.. Journal of Applied Polymer Science 2021;138:50720-n/a. https://doi.org/10.1002/app.50720.

[98] Alam F, Varadarajan KM, Koo JH, Wardle BL, Kumar S. A Advanced Engineering Materials 2020;22:2000483-n/a. https://doi.org/10.1002/adem.202000483.

[99] Lin L, Han Y, Zhao X, Wang Y, Zhang H, Jiang Z, et al. High Performance Polymers 2019;31:875–84. https://doi.org/10.1177/0954008318804045.

[100] Hassan EAM, Ge D, Zhu S, Yang L, Zhou J, Yu M. . Composites Part A, Applied Science and Manufacturing 2019;127:105613. https://doi.org/10.1016/j.compositesa.2019.105613.

[101] Costa MM, Dantas TA, Bartolomeu F, Alves N, Silva FS, Miranda G, et al. Transactions of Nonferrous Metals Society of China 2019;29:2523–33. https://doi.org/10.1016/S1003-6326(19)65160-5.

[102] Liu Y, Zhai X, Deng Y, Wu D.. Tribology Transactions 2019;62:962–70. https://doi.org/10.1080/10402004.2019.1635671.

[103] Vail JR, Krick BA, Marchman KR, Sawyer WG.. Wear 2011;270:737–41. https://doi.org/10.1016/j.wear.2010.12.003.

[104] Slonov A, Musov I, Zhansitov A, Rzhevskaya E, Khakulova D, Khashirova S. The Effect of Modification on the Properties of Polyetherimide and Its Carbon-Filled Composite. Polymers 2020;12:1056. https://doi.org/10.3390/polym12051056.

[105] Pandelidi C, Bateman S, Piegert S, Hoehner R, Kelbassa I, Brandt M. International Journal of Advanced Manufacturing Technology 2021;113:3057–77. https://doi.org/10.1007/s00170-021-06837-6.

[106] Yan J-H, Wang C-H, Li K-W, Zhang Q, Yang M, Di-Wu W-L, et al.. International Journal of Nanomedicine 2018;13:3425–40. https://doi.org/10.2147/IJN.S160030.

[107] Zeller-Plumhoff B, Malich C, Krüger D, Campbell G, Wiese B, Galli S, et al. Acta Biomaterialia 2020;101:637–45. https://doi.org/10.1016/j.actbio.2019.11.030.

[108] Ma R, Tang T.. International Journal of Molecular Sciences 2014;15:5426–45. https://doi.org/10.3390/ijms15045426.

[109] Wang S, Yang Y, Mu Y, Shi J, Cong X, Luan J, et al. Composites Science and Technology 2021;203. https://doi.org/10.1016/j.compscitech.2020.108562.

[110] Fu Q, Gabriel M, Schmidt F, Müller W-D, Schwitalla AD. Dental Materials 2021;37:e15–22. https://doi.org/10.1016/j.dental.2020.09.020.

[111] Ishizaki C, Yabutsuka T, Takai S. Coatings (Basel) 2020;10:191. https://doi.org/10.3390/coatings10020191.

[112] Kruse HV, McKenzie DR, Clark JR, Suchowerska N. Plasma Processes and Polymers 2021;18:2000219-n/a. https://doi.org/10.1002/ppap.202000219.

[113] 1000Hour_Steam_Resistance.pdf n.d.

[114] PEEK_OPTIMA_Effects_GammaSterl.pdf n.d.

[115] Naffakh M, Díez-Pascual AM, Gómez-Fatou MA. J Mater Chem 2011;21:7425–33. https://doi.org/10.1039/C1JM10441A.

[116] Zhang G, Schlarb AK, Tria S, Elkedim O. Composites Science and Technology 2008;68:3073–80. https://doi.org/10.1016/j.compscitech.2008.06.027.

[117] Chan KW, Liao CZ, Wong HM, Kwok Yeung KW, Tjong SC. RSC Advances 2016;6:19417–29. https://doi.org/10.1039/c5ra22134j.

[118] Liu G, Zhang L, Li G, Zhao F, Che Q, Wang C, et al. Acta Biomaterialia 2019;87:285–95. https://doi.org/10.1016/j.actbio.2019.01.038.

[119] Melčová V, Svoradová K, Menčík P, Kontárová S, Rampichová M, Hedvičáková V, et al. Polymers 2020;12:2806. https://doi.org/10.3390/polym12122806.

[120] Ursini C, Collini L. Materials 2021;14:5645. https://doi.org/10.3390/ma14195645.

[121] Puppala AK, Sonnati V, Gangapuram S. Journal of Physics Conference Series 2020;1495:12021. https://doi.org/10.1088/1742-6596/1495/1/012021.

[122] Pravdivtseva MS, Peschke E, Lindner T, Wodarg F, Hensler J, Gabbert D, et al. Medical Physics (Lancaster) 2021;48:1469–84. https://doi.org/10.1002/mp.14714.

[123] Januszewicz R, Tumbleston JR, Quintanilla AL, Mecham SJ, DeSimone JM. Layerless fabrication with continuous liquid interface production. PNAS 2016;113:11703–8. https://doi.org/10.1073/pnas.1605271113.

[124] Camargo JC, Machado ÁR, Almeida EC, Silva EFMS. International Journal of Advanced Manufacturing Technology 2019;103:2423–43. https://doi.org/10.1007/s00170-019-03532-5.

[125] Jayaraghul TK, Karthik K, Yaswanth A, Venkatesan M. Materials Today : Proceedings 2021;44:2963–7. https://doi.org/10.1016/j.matpr.2021.02.004.

[126] Chatham CA, Long TE, Williams CB. Progress in Polymer Science 2019;93:68–95. https://doi.org/10.1016/j.progpolymsci.2019.03.003.

[127] Han X, Yang D, Yang C, Spintzyk S, Scheideler L, Li P, et al. Journal of Clinical Medicine 2019;8:240. https://doi.org/10.3390/jcm8020240.

[128] Zhang Y, Cheung V, Westland S, Beverley KJ. Colour management of a low-cost four-colour ink-jet printing system on textiles. Coloration Technology 2009;125:29–35. https://doi.org/10.1111/j.1478-4408.2008.00172.x.

[129] Thompson R. Printing materials: science and technology. Leatherhead, UK: Pira International; 2004.

[130] Kan CW, Yuen CWM, Tsoi WY. U. Cellulose 2011;18:827–39. https://doi.org/10.1007/s10570-011-9522-2.

[131] Hassanin H, Abena A, Elsayed MA, Essa K. 4D Printing of NiTi Auxetic Structure with Improved Ballistic Performance. Micromachines (Basel) 2020;11:745. https://doi.org/10.3390/mi11080745.

[132] Pradeepkumar C, Karthikeyan S, Rajini N, Budholiya S, Aravind Raj S. A contemporary review on additive manufactured biomedical implants. Materials Today : Proceedings 2021;46:8812–6. https://doi.org/10.1016/j.matpr.2021.04.184.

[133] Buj-Corral I, Tejo-Otero A, Fenollosa-Artés F. Development of AM Technologies for Metals in the Sector of Medical Implants. Metals (Basel) 2020;10:686. https://doi.org/10.3390/met10050686.

[134] Oladapo BI, Zahedi SA, Ismail SO, Olawade DB. Recent advances in biopolymeric composite materials: Future sustainability of bone-implant. Renewable and Sustainable Energy Reviews 2021;150:111505. https://doi.org/10.1016/j.rser.2021.111505.

[135] Wang P, Zou B, Ding S, Huang C, Shi Z, Ma Y, et al. Preparation of short CF/GF reinforced PEEK composite filaments and their comprehensive properties evaluation for FDM-3D printing. Composites Part B, Engineering 2020;198:108175. https://doi.org/10.1016/j.compositesb.2020.108175.

[136] Sharma N, Welker D, Aghlmandi S, Maintz M, Zeilhofer H-F, Honigmann P, et al. A Multi-Criteria Assessment Strategy for 3D Printed Porous Polyetheretherketone (PEEK) Patient-Specific Implants for Orbital Wall Reconstruction. Journal of Clinical Medicine 2021;10:3563. https://doi.org/10.3390/jcm10163563.

[137] Verma S, Sharma N, Kango S, Sharma S. Developments of PEEK (Polyetheretherketone) as a biomedical material: A focused review. European Polymer Journal 2021;147:110295. https://doi.org/10.1016/j.eurpolymj.2021.110295.

[138] Han C-M, Jang T-S, Kim H-E, Koh Y-H. Creation of nanoporous TiO2 surface onto polyetheretherketone for effective immobilization and delivery of bone morphogenetic protein. Journal of Biomedical Materials Research Part A 2014;102:793–800. https://doi.org/10.1002/jbm.a.34748.

[139] Ghodsi S, Zeighami S, Meisami Azad M. Comparing Retention and Internal Adaptation of Different Implant-Supported, Metal-Free Frameworks. The International Journal of Prosthodontics 2018;31:475–7. https://doi.org/10.11607/ijp.5800.

[140] Elawadly T, Radi IAW, El Khadem A, Osman RB. Can PEEK Be an Implant Material? Evaluation of Surface Topography and Wettability of Filled Versus Unfilled PEEK With Different Surface Roughness. The Journal of Oral Implantology 2017;43:456–61. https://doi.org/10.1563/aaid-joi-D-17-00144.

[141] Lecocq M, Bernard C, Felix MS, Linares J-M, Chaves-Jacob J, Decherchi P, et al. Biocompatibility of Four Common Orthopedic Biomaterials Following a High-Salt Diet: An *In-vivo* Study. International Journal of Molecular Sciences 2017;18:1489. https://doi.org/10.3390/ijms18071489.

[142] Maharaj G, Bleser S, Albert K, Lambert R, Jani S, Jamison R. Characterization of wear in composite material orthopaedic implants. Part I: The composite trunnion/ceramic head interface. Bio-Medical Materials and Engineering 1994;4:193–8. https://doi.org/10.3233/BME-1994-4307.

[143] Nakahara I, Takao M, Bandoh S, Bertollo N, Walsh WR, Sugano N. *In-vivo* implant fixation of carbon fiber-reinforced PEEK hip prostheses in an ovine

model. Journal of Orthopaedic Research 2013;31:485–92. https://doi.org/10.1002/jor.22251.

[144] Stepashkin AA, Chukov DI, Senatov FS, Salimon AI, Korsunsky AM, Kaloshkin SD. 3D-printed PEEK-carbon fiber (CF) composites: Structure and thermal properties. Composites Science and Technology 2018;164:319–26. https://doi.org/10.1016/j.compscitech.2018.05.032.

[145] Morrison C, Macnair R, MacDonald C, Wykman A, Goldie I, Grant MH. In vitro biocompatibility testing of polymers for orthopaedic implants using cultured fibroblasts and osteoblasts. Biomaterials 1995;16:987–92. https://doi.org/10.1016/0142-9612(95)94906-2.

[146] Karthikeyan L, Sudhi S, Bhatt TS, Ganesan M, Soumyamol PB, Thankarajan J, et al. Poly(ether ether ketone)s processed through extrusion-machining and 3D printing: A comparative study on mechanical, thermal and fracture properties at ambient and cryogenic environments. Journal of Elastomers and Plastics 2021;53:672–83. https://doi.org/10.1177/0095244320961830.

[147] van de Werken N, Koirala P, Ghorbani J, Doyle D, Tehrani M. Investigating the hot isostatic pressing of an additively manufactured continuous carbon fiber reinforced PEEK composite. Additive Manufacturing 2021;37:101634. https://doi.org/10.1016/j.addma.2020.101634.

[148] Honigmann P, Sharma N, Okolo B, Popp U, Msallem B, Thieringer FM. Patient-Specific Surgical Implants Made of 3D Printed PEEK: Material, Technology, and Scope of Surgical Application. BioMed Research International 2018;2018:4520636–8. https://doi.org/10.1155/2018/4520636.

[149] Kumar A. Self Assemblies of Poly(ether ether ketone) Block Copolymers for Biomedical Applications. ChemistrySelect (Weinheim) 2021;6:9060–8. https://doi.org/10.1002/slct.202102238.

[150] Ng ZY, Nawaz I. Computer-designed PEEK implants: a peek into the future of cranioplasty? The Journal of Craniofacial Surgery 2014;25:e55–8. https://doi.org/10.1097/SCS.0b013e3182a2f7b6.

[151] Persson J, Helgason B, Engqvist H, Ferguson SJ, Persson C, Institute of Clinical Sciences D of B, et al. Stiffness and strength of cranioplastic implant systems in

comparison to cranial bone. Journal of Cranio-Maxillo-Facial Surgery 2018;46:418–23. https://doi.org/10.1016/j.jcms.2017.11.025.

[152] Pipola V, Boriani S, Ghermandi R, Tedesco G, Evangelisti G, Girolami M, et al. Composite PEEK-carbon fiber pre-shaped rods and sublaminar bands for posterior stabilization of cervico-thoracic junction: A novel technique. Journal of Clinical Neuroscience 2020;72:429–33. https://doi.org/10.1016/j.jocn.2019.12.035.

[153] Liu D, Fu J, Fan H, Li D, Dong E, Xiao X, et al. Application of 3D-printed PEEK scapula prosthesis in the treatment of scapular benign fibrous histiocytoma: A case report. Journal of Bone Oncology 2018;12:78–82. https://doi.org/10.1016/j.jbo.2018.07.012.

[154] Roskies M, Jordan JO, Fang D, Abdallah M-N, Hier MP, Mlynarek A, et al. Improving PEEK bioactivity for craniofacial reconstruction using a 3D printed scaffold embedded with mesenchymal stem cells. Journal of Biomaterials Applications 2016;31:132–9. https://doi.org/10.1177/0885328216638636.

[155] Kelsey DJ, Springer GS, Goodman SB. Composite Implant for Bone Replacement. Journal of Composite Materials 1997;31:1593–632. https://doi.org/10.1177/002199839703101603.

[156] de Ruiter L, Rankin K, Browne M, Briscoe A, Janssen D, Verdonschot N. Decreased stress shielding with a PEEK femoral total knee prosthesis measured in validated computational models. Journal of Biomechanics 2021;118:110270–110270. https://doi.org/10.1016/j.jbiomech.2021.110270.

[157] Zach L, Kunčická L, Růžička P, Kocich R. Design, analysis and verification of a knee joint oncological prosthesis finite element model. Computers in Biology and Medicine 2014;54:53–60. https://doi.org/10.1016/j.compbiomed.2014.08.021.

[158] Böhler C, Kolbitsch P, Schuh R, Lass R, Kubista B, Giurea A. Midterm Results of a New Rotating Hinge Knee Implant: A 5-Year Follow-Up. BioMed Research International 2017;2017:7532745–7. https://doi.org/10.1155/2017/7532745.

[159] Gao X, Wang H, Zhang X, Gu X, Liu Y, Zhou G, et al. Preparation of Amorphous Poly(aryl ether nitrile ketone) and Its Composites with Nano Hydroxyapatite for 3D Artificial Bone Printing. ACS Applied Bio Materials 2020;3:7930–40. https://doi.org/10.1021/acsabm.0c01044.

[160] Tretto PHW, dos Santos MBF, Spazzin AO, Pereira GKR, Bacchi A. Assessment of stress/strain in dental implants and abutments of alternative materials compared to conventional titanium alloy-3D non-linear finite element analysis. Computer Methods in Biomechanics and Biomedical Engineering 2020;23:372–83. https://doi.org/10.1080/10255842.2020.1731481.

[161] Kraft M PhD, MSc, Koch DK MBA, Bushelow M MSc. An investigation into PEEK-on-PEEK as a bearing surface candidate for cervical total disc replacement. The Spine Journal 2012;12:603–11. https://doi.org/10.1016/j.spinee.2012.07.009.

[162] Schwitalla A, Müller W-D. PEEK dental implants: a review of the literature. The Journal of Oral Implantology 2013;39:743–9. https://doi.org/10.1563/AAID-JOI-D-11-00002.

[163] Oladapo BI, Ismail SO, Bowoto OK, Omigbodun FT, Olawumi MA, Muhammad MA. Lattice design and 3D-printing of PEEK with $Ca_{10}(OH)(PO_4)_3$ and *in-vitro* bio-composite for bone implant. International Journal of Biological Macromolecules 2020;165:50–62. https://doi.org/10.1016/j.ijbiomac.2020.09.175.

[164] Xiong J, Mines R, Ghosh R, Vaziri A, Ma L, Ohrndorf A, et al. Advanced Micro-Lattice Materials. Advanced Engineering Materials 2015;17:1253–64. https://doi.org/10.1002/adem.201400471.

[165] Braun M, Aranda-Ruiz J, Fernández-Sáez J. Mixed Mode Crack Propagation in Polymers Using a Discrete Lattice Method. Polymers 2021;13:1290. https://doi.org/10.3390/polym13081290.

[166] Jiang D, Sun D, Xiang N, Chen K, Yi H, Ni Z. Lattice Boltzmann numerical simulation and experimental research of dynamic flow in an expansion-contraction microchannel. Biomicrofluidics 2013;7:34113–34113. https://doi.org/10.1063/1.4812456.

[167] Wang P, Li X, Jiang Y, Nai MLS, Ding J, Wei J. Electron beam melted heterogeneously porous microlattices for metallic bone applications: Design and investigations of boundary and edge effects. Additive Manufacturing 2020;36:101566. https://doi.org/10.1016/j.addma.2020.101566.

[168] Epasto G, Palomba G, Andrea DD, Di Bella S, Mineo R, Guglielmino E, et al. Experimental investigation of rhombic dodecahedron micro-lattice structures manufactured by Electron Beam Melting. Materials Today: Proceedings 2019;7:578–85. https://doi.org/10.1016/j.matpr.2018.12.011.

[169] Liu F, Zhang DZ, Zhang P, Zhao M, Jafar S. Mechanical Properties of Optimized Diamond Lattice Structure for Bone Scaffolds Fabricated via Selective Laser Melting. Materials 2018;11:374. https://doi.org/10.3390/ma11030374.

[170] Benedetti M, du Plessis A, Ritchie RO, Dallago M, Razavi SMJ, Berto F. Architected cellular materials: A review on their mechanical properties towards fatigue-tolerant design and fabrication. Materials Science and Engineering: R: Reports 2021;144:100606. https://doi.org/10.1016/j.mser.2021.100606.

[171] Smith BH, Szyniszewski S, Hajjar JF, Schafer BW, Arwade SR. Steel foam for structures: A review of applications, manufacturing and material properties. Journal of Constructional Steel Research 2012;71:1–10. https://doi.org/10.1016/j.jcsr.2011.10.028.

[172] Du Plessis A, Yadroitsava I, Yadroitsev I, Roux S, Blaine D. Numerical comparison of lattice unit cell designs for medical implants by additive manufacturing. Virtual and Physical Prototyping 2018;13:1–16. https://doi.org/10.1080/17452759.2018.1491713.

[173] Mahmoud D, Elbestawi MA. Lattice Structures and Functionally Graded Materials Applications in Additive Manufacturing of Orthopedic Implants: A Review. Journal of Manufacturing and Materials Processing 2017;1:13. https://doi.org/10.3390/jmmp1020013.

[174] Feng J, Liu B, Lin Z, Fu J. Isotropic octet-truss lattice structure design and anisotropy control strategies for implant application. Materials & Design 2021;203:109595. https://doi.org/10.1016/j.matdes.2021.109595.

[175] Chen Y, Zheng B-B, Fu M-H, Lan L-H, Zhang W-Z. Doubly unusual 3D lattice honeycomb displaying simultaneous negative and zero Poisson's ratio properties. Smart Materials and Structures 2018;27:45003. https://doi.org/10.1088/1361-665X/aaae2b.

[176] Oladapo BI, Obisesan OB, Oluwole B, Adebiyi VA, Usman H, Khan A. Mechanical characterization of a polymeric scaffold for bone implant. Journal of Materials Science 2020;55:9057–69.

[177] Oladapo BI, Zahedi SA, Ismail SO. Assessing 3D printing of Poly (ether-ether-ketone) and cellular cHAp to increase biointerfaces as a biomedical material. Colloids and Surfaces B: Biointerfaces 2021:111726.

[178] Kang J, Dong E, Li D, Dong S, Zhang C, Wang L. Anisotropy characteristics of microstructures for bone substitutes and porous implants with application of additive manufacturing in orthopaedic. Materials & Design 2020;191:108608. https://doi.org/10.1016/j.matdes.2020.108608.

[179] Feng J, Liu B, Lin Z, Fu J. Isotropic porous structure design methods based on triply periodic minimal surfaces. Materials & Design 2021;210:110050. https://doi.org/10.1016/j.matdes.2021.110050.

[180] Matassi F, Botti A, Sirleo L, Carulli C, Innocenti M. Porous metal for orthopedics implants. Clin Cases Miner Bone Metab 2013;10:111–5.

[181] Oladapo BI, Ismail SO, Ikumapayi OM, Kayode JF. Impact of rGO-coated PEEK and lattice on bone implant. Colloids and Surfaces B: Biointerfaces 2022:112583.

[182] Chen Z, Xie YM, Wu X, Wang Z, Li Q, Zhou S. On hybrid cellular materials based on triply periodic minimal surfaces with extreme mechanical properties. Materials & Design 2019;183:108109. https://doi.org/10.1016/j.matdes.2019.108109.

[183] Ni S, Zhong Z, Huang J, Wang W, Guo X. Field-Aligned and Lattice-Guided Tetrahedral Meshing. Computer Graphics Forum 2018;37:161–72. https://doi.org/10.1111/cgf.13499.

[184] Riester O, Borgolte M, Csuk R, Deigner H-P. Challenges in Bone Tissue Regeneration: Stem Cell Therapy, Biofunctionality and Antimicrobial Properties of Novel Materials and Its Evolution. Int J Mol Sci 2020;22:192. https://doi.org/10.3390/ijms22010192.

[185] Oladapo BI, Zahedi SA, Vahidnia F, Ikumapayi OM, Farooq MU. Three-dimensional finite element analysis of a porcelain crowned tooth. Beni-Suef University Journal of Basic and Applied Sciences 2018;7:461–4.

[186] Fisher SA, Tam RY, Shoichet MS. Tissue mimetics: engineered hydrogel matrices provide biomimetic environments for cell growth. Tissue Engineering Part A 2014;20:895–8.

[187] Oladapo BI, Zahedi SA, Balogun VA, Ismail SO, Samad YA. Overview of additive manufacturing biopolymer composites 2021.

[188] Peek hip implant encourages useful stem cell growth. High Performance Plastics 2012:7.

[189] Du Y-W, Zhang L-N, Ye X, Nie H-M, Hou Z-T, Zeng T-H, et al. *In-vitro* and *in-vivo* evaluation of bone morphogenetic protein-2 (BMP-2) immobilized collagen-coated polyetheretherketone (PEEK). Frontiers of Materials Science 2015;9:38–50. https://doi.org/10.1007/s11706-015-0276-x.

[190] Oladapo BI, Zahedi SA, Ismail SO, Omigbodun FT, Bowoto OK, Olawumi MA, et al. 3D printing of PEEK–cHAp scaffold for medical bone implant. Bio-Design and Manufacturing 2021;4:44–59.

[191] Oladapo BI, Adebiyi AV, Elemure EI. Microstructural 4D printing investigation of ultra-sonication biocomposite polymer. Journal of King Saud University-Engineering Sciences 2021;33:54–60.

[192] Oladapo BI, Adeoye AOM, Ismail M. Analytical optimization of a nanoparticle of microstructural fused deposition of resins for additive manufacturing. Composites Part B: Engineering 2018;150:248–54. https://doi.org/10.1016/j.compositesb.2018.05.041.

[193] Smith AT, LaChance AM, Zeng S, Liu B, Sun L. Synthesis, properties, and applications of graphene oxide/reduced graphene oxide and their nanocomposites. Nano Materials Science 2019;1:31–47.

[194] Wang S, Liu N, Su J, Li L, Long F, Zou Z, et al. Highly stretchable and self-healable supercapacitor with reduced graphene oxide based fiber springs. Acs Nano 2017;11:2066–74.

[195] Nemmani A, Mutra RR, Balamurali G. Static structural analysis of hip joint with various profiles by finite element method. IOP Conference Series Materials Science and Engineering 2021;1123:12054. https://doi.org/10.1088/1757-899X/1123/1/012054.

[196] Singh A, Banerjee SL, Dhiman V, Bhadada SK, Sarkar P, Khamrai M, et al. Fabrication of calcium hydroxyapatite incorporated polyurethane-graphene oxide nanocomposite porous scaffolds from poly (ethylene terephthalate) waste: A green route toward bone tissue engineering. Polymer 2020;195:122436. https://doi.org/10.1016/j.polymer.2020.122436.

[197] Shokrieh MM, Mazloomi MS. A new analytical model for calculation of stiffness of three-dimensional four-directional braided composites. Composite Structures 2012;94:1005–15. https://doi.org/10.1016/j.compstruct.2011.09.010.

[198] Berger H, Kari S, Gabbert U, Rodriguez-Ramos R, Bravo-Castillero J, Guinovart-Diaz R, et al. Unit cell models of piezoelectric fiber composites for numerical and analytical calculation of effective properties. Smart Mater Struct 2006;15:451–8. https://doi.org/10.1088/0964-1726/15/2/026.

[199] Alvarez-Gayosso C, Barceló-Santana F, Guerrero-Ibarra J, Sáez-Espínola G, Canseco-Martínez MA. Calculation of contraction rates due to shrinkage in light-cured composites. Dental Materials 2004;20:228–35. https://doi.org/10.1016/S0109-5641(03)00097-6.

[200] Osoka E, Onukwuli O. A Modified Halpin-Tsai Model for Estimating the Modulus of Natural Fiber Reinforced Composites 1* 2018;7:63–70.

[201] Shokrieh MM, Moshrefzadeh-Sani H. On the constant parameters of Halpin-Tsai equation. Polymer 2016;106:14–20. https://doi.org/10.1016/j.polymer.2016.10.049.

[202] Oladapo BI, Kayode JF, Karagiannidis P, Naveed N, Mehrabi HA, Ogundipe KO. Materials Chemistry and Physics 2022:126454. https://doi.org/10.1016/j.matchemphys.2022.126454.

[203] Siskey R, Ciccarelli L, Lui MKC, Kurtz SM. Clinical Orthopaedics and Related Research 2016;474:2428–40. https://doi.org/10.1007/s11999-016-5041-7.

[204] Borruto A. A new material for hip prosthesis without considerable debris release. Medical Engineering & Physics 2010;32:908–13. https://doi.org/10.1016/j.medengphy.2010.06.007.

[205] Baykal D, Siskey RS, Underwood RJ, Briscoe A, Kurtz SM. T Clinical Orthopaedics and Related Research 2016;474:2384–93. https://doi.org/10.1007/s11999-016-4989-7.

[206] Darwich A, Nazha H, Daoud M. Effect of Coating Materials on the Fatigue Behavior of Hip Implants: A Three-dimensional Finite Element Analysis. Journal of Applied and Computational Mechanics 2020;6:284–95. https://doi.org/10.22055/jacm.2019.30017.1659.

[207] Xin H, Shepherd D, Dearn K. PEEK (Polyether-ether-ketone) Based Cervical Total Disc Arthroplasty: Contact Stress and Lubrication Analysis. The Open Biomedical Engineering Journal 2012;6:73–9. https://doi.org/10.2174/1874230001206010073.

[208] Grau M, Matena J, Teske M, Petersen S, Aliuos P, Roland L, et al. In Vitro Evaluation of PCL and P(3HB) as Coating Materials for Selective Laser Melted Porous Titanium Implants. Materials 2017;10:1344. https://doi.org/10.3390/ma10121344.